ISSN 0387-6144

BULLETIN OF THE

RESEARCH LABORATORY FOR NUCLEAR REACTORS

VOL. 34 2010

RESEARCH LABORATORY FOR NUCLEAR REACTORS
TOKYO INSTITUTE OF TECHNOLOGY

BULLETIN OF THE RESEARCH LABORATORY FOR NUCLEAR REACTORS

BULL. RES. LAB. NUCL. REACTOR, Vol.34, 2010

CONTENTS

B. Mass Transmutation Engineering

C. System and Safety Engineering

Research staffs of
RESEARCH LABORATORY FOR NUCLEAR REACTORS,
TOKYO INSTITUTE OF TECHONOGY

Director

Masanori ARITOMI	Professor

Energy Engineering Division

Hisashi NINOKATA	Professor
Masanori ARITOMI	Professor
Masayuki IGASHIRA	Professor
Hiroshi AKATSUKA	Associate Professor
Minoru TAKAHASHI	Associate Professor
Yoshiyuki OGURI	Associate Professor
Yukitaka KATO	Associate Professor
Takatoshi TAKEMOTO	Visiting Associate Professor
Tetsuo SAWADA	Assistant Professor
Jun HASEGAWA	Assistant Professor
Junichi RYU	Assistant Professor

Mass Transmutation Engineering Division

Hiroshi SEKIMOTO	Professor
Toshiyuki HATTORI	Professor
Toyohiko YANO	Professor
Kenji TAKESHITA	Professor
Yoshihisa MATSUMOTO	Associate Professor
Jun ONOE	Associate Professor
Tatsuya SUZUKI	Associate Professor
Noriyosu HAYASHIZAKI	Associate Professor
Eiichi ASANO	Visiting Associate Professor
Masao NOMURA	Assistant Professor
Haruaki MATSUURA	Assistant Professor
Katsumi YOSHIDA	Assistant Professor
Tatsuya KATABUCHI	Assistant Professor
Masayuki HARADA	Assistant Professor
Takehiko TSUKAHARA	Assistant Professor

System and Safety Engineering Division

Ryuichi SHIMADA	Professor
Masaki SAITO	Professor
Yasuhisa IKEDA	Professor
Yoshihiro YAMANE	Visiting Professor
Matovic BRANKO	Visiting Professor
Fumiaki KAWAKAMI	Visiting Professor
Shunji IIO	Associate Professor
Toru OBARA	Associate Professor
Hiroshige KIKURA	Associate Professor
Hiroaki TSUTSUI	Assistant Professor
Hiroshi SAGARA	Assistant Professor
Etsuko KOIZUMI	Assistant Professor

Technical Staffs

Mitsuo MATSUZAKI	Senior Technical Specialist
Atsushi NEZU	Senior Technical Specialist
Hitoshi FUKUDA	Senior Technical Specialist
Masamitsu IMAI	Senior Technical Specialist
Ken-ichi TOSAKA	Senior Technical Specialist
Keizo MATSUMURA	Senior Technical Specialist

Common Staffs

Motoharu MIZUMOTO	Professor
Noriyuki WATANABE	Assistant Professor

Ⅰ.1 Some Main Research Works Performed by H. Sekimoto from 1976 to 2010

Hiroshi SEKIMOTO

INTRODUCTION

Since this article is for Celebration of 65th birthday, I will try to make a summary of my research activities. Though my research activities had already started earlier before I came to Tokyo Institute of Technology (TokyoTech), this summary covers only my activities performed in Tokyo Tech since it appears in the Bulletin of the Research Laboratory for Nuclear Reactors.

When I came to TokyoTech, I started my research on fusion neutronics. This study was performed as a key member of Special Research Project on Nuclear Fusion supported by the Grand-in-Aid for Fusion Research by the Ministry of Education, Science and Culture. This study continued during 1976-1982, while my position was a research associate. We employed the unfolding method to obtain neutron energy spectrum from measured pulse height distribution of liquid scintillation counter. Unfolding method was studied not only for pulse height distribution but also activation analyses.

When I became an associate professor, I changed my research area from fusion energy to fission energy, and started this research with development of a new calculation method for pebble-bed type high-temperature gas reactor. Later I proposed several innovative reactors with my students including high flux reactor and pulse reactor by using similar technologies developed in the high-temperature gas reactor studies.

In 1987 I started with my students the study on nuclear equilibrium society in the future where separation and transmutation of spent fuel are the main problem. The timing is coincident with the Omega Project promoted by JAERI, and this study was performed intensively for long period. This study won the AESJ Award for Scholastic Accomplishment in 2004.

In 1989 I started small long-life reactor design study with one of my foreign students from Indonesia. We chose fast reactors with metal and nitride for fuel and lead and lead-bismuth eutectic (LBE) as coolant. It stimulated Russian project on lead-bismuth cooled small fast reactor. Soon the Generation IV International Forum (GIF) was established and lead (including LBE) cooled fast reactor (LFR) was selected one of six Generation IV reactors. I signed MOU for Collaboration on LFR Nuclear Energy System.

I was wondering about the possibility of CANDLE burning for many years. In 1999 my student Mr. Ryu and I found it is possible for a large LBE cooled metallic fuel fast reactor. The principle of CANDLE burning is similar to the principle of Travelling Wave Reactor later developed by TerraPower which is supported by Bill Gates, and our research attracted interests of the mass media.

In this article I will make brief descriptions on the following topics:

1. fusion neutronics
2. unfoldings
3. graphite moderated reactors
4. equilibrium nuclear systems
5. small long-life fast reactors
6. CANDLE burning

In the references I will list only papers published in technical journals widely distributed in the nuclear engineering community and books easily obtainable. Otherwise the number of papers will be too many for this bulletin. They are listed chronologically.

FUSION NEUTRONICS [1-14, 17-19, 25, 28, 36, 45]

A miniature spectrometer was designed to measure the neutron spectrum inside an assembly. A small spherical container filled with NE213 liquid scintillator is inserted in the assembly and a light guide is used to transmit the scintillation light from the scintillator to a photomultiplier outside the assembly. A light coupler of parabolic shape is inserted between the scintillator and light guide, so that the light in the guide may reflect totally on its side surface.

Scalar neutron spectra were measured with this spectrometer at several positions in water, graphite and lithium fluoride assemblies, which were irradiated with D-T neurons. The n-γ discrimination was executed at each pulse height. The pulse height spectrum was unfolded to an energy spectrum with a modified FERDOR code.

The measured spectrum was compared with a calculated spectrum using the MOESE-GG Monte Carlo code with the GICXFNS group cross-section set processed from the ENDF/B-IV and –V libraries. A continuous-energy Monte Carlo code was developed and used to investigate the accuracy of multi-group approximation used in the MOESE-GG Monte Carlo code.

The measured spectrum in the graphite assembly showed fine structure, and each peak and valley corresponds to a level-inelastic scattering and total cross-section resonance peak. The measured spectrum in the lithium-fluoride assembly might contain considerable error and oscillation of the unfolded spectrum became substantial.

UNFOLDINGS [1, 3, 6, 19, 140, 141, 143]

The minimization of the functional defined by the prior knowledge and integral data of a neutron spectrum can be the basis of many unfolding methods. The form of these functionals classifies the widely used methods: FERDOR, SPECTRA, RFSP, CRYSTAL BALL, SAND-II, STAYSL and others. The methods were systematically derived and theoretically compared to each other. Their relations to the function expansion method were discussed, and several

cases of estimated spectra were studied. Treatments of response function errors were also investigated.

A new unfolding method has been developed to minimize an objective function by adjusting the logarithm of the spectrum. This method gives a positive solution over the whole energy region. The solution oscillates much less than conventional solutions using the linear least-squares method, such as FERDOR, even without an oscillation damping term.

Another new unfolding code based on quadratic programming has been developed for precise treatment of the non-negativity constraint of the neutron spectrum. This code does not require any initial guess and enables a global optimum solution to be derived.

GRAPHITE MODERATED REACTORS [15, 16, 20-22, 24, 27, 30-33, 35, 37, 39, 40, 42, 48, 51, 59, 67, 122, 129]

A new computer code PREC was developed to solve neutron and nuclide density distributions at the equilibrium cycle of pebble bed reactors. The PREC code has the following special advantages:

(1) To provide a direct solution of the equilibrium cycle
(2) To fix the effective neutron multiplication factor as an input
(3) To treat continuous fuel movement
(4) To treat *r-z* two-dimensional geometry, leading in turn to the following special advantages:
  (4-1) Ability to treat the cavity at the top of the core
  (4-2) Ability to treat the curved fuel stream-lines

A feasibility design study of the graphite moderated gas-cooled reactor as a high flux reactor has been performed. The core of the reactor is equipped with two graphite reflectors, i.e. the inner reflector and the outer reflector. The highest value of the thermal neutron flux is expected to be achieved in the inner reflector region, and a moderately high thermal neutron flux is also expected to be obtained in the outer reflector region. By choosing optional values of the core-reflector geometrical parameters and moderator-to-fuel atomic density, a high thermal neutron flux can be obtained. Because of the thermal design constraint, however, this design will produce a relatively large core volume (about 10^7 cm^3) and consequently a higher reactor power (100 MWt). Preliminary calculation results show that with an average power density of 10 W/cm^3, a maximum thermal neutron flux of 10^{15} $cm^{-2}s^{-1}$ can be achieved in the inner reflector. Pulsed neutron reactors were also investigated using graphite moderator. The graphite is a good heat source for this reactor where coolant cannot be relied on.

Here it is better to add another high thermal neutron flux reactor concept using a fast reactor core. Reactor configurations were investigated to obtain high thermal flux under design constraints on the total reactor power and peak power density. Graphite and heavy water were compared as the reflector material, and oxide and metallic fuels were also compared. The power density necessary for a maximum thermal flux of 10^{16} $cm^{-2}s^{-1}$ was obtained in a reasonable range for all cases.

EQUILIBRIUM NUCLEAR SYSTEMS [23, 26, 29, 38, 46, 52-58, 65, 69-73, 76-82, 88, 90, 91, 93, 94, 99, 104, 105, 112, 114, 119, 123, 126, 131-134, 136, 139, 144, 149, 151]

The nuclear equilibrium society has been investigated by the author, where the radioactive toxicity discharged from a nuclear centre is less than the level of natural uranium supplied to the centre. Enough neutrons necessary for transmuting toxic nuclides to harmless ones can be supplied in hard spectrum fast reactors. However, extremely high decontamination factor is required for the separation technology of toxic nuclides from harmless ones and is too difficult to be realized considering to the present technology level. The present separation technology does not satisfy this criterion, and extremely high performing storage system like underground disposal is employed for the present fuel cycle system instead. The reprocessing plant has several difficult problems in addition to this problem. At present once-through fuel cycle may be one option, and at the same time intensive studies to improve separation technology should be promoted for the future use.

Theory on nuclide importance was developed during this study. Conventional methods for evaluating some characteristic values of nuclides relating to burnup in a given neutron spectrum had been reviewed using a mathematically systematic way, and a new method based on the importance theory was proposed. This method is derived from the fact that these characteristic values of a nuclide are equivalent to the importances of the nuclide. By solving the equation adjoint to the steady-state burnup equation with a properly chosen source term, the importances for all nuclides are obtained simultaneously. The fission number importance, net neutron importance, fission neutron importance and absorbed neutron importance have been evaluated and discussed. The net neutron importance is a measure directly estimating neutron economy, and can be evaluated simply by calculating the fission neutron importance minus absorbed neutron importance, where the fission neutron importance does not depend on the fission product, and only the absorbed neutron importance depends on it. Sensitivity studies on these importances were also performed.

The nuclear equilibrium analysis was performed not only for future nuclear equilibrium system but also for evaluation of some new nuclear system such as thorium reactors.

SMALL LONG-LIFE FAST REACTORS [34, 41, 43, 44, 47, 49, 50, 84-86, 92, 95, 97, 98, 101, 103, 107-112, 116, 117, 121, 124, 126, 135, 148]

Lead bismuth eutectic (LBE) is a good coolant for fast reactor especially from safety point of view, and shows a good performance especially for small reactor. I proposed a concept of long-life small reactor by employing LBE cooled fast reactor. It is the world first trial of LBE coolant to long-life small fast reactor. Since then this reactor concept has been studied continuously. We named this reactor LBE-cooled Long-Life Safe Simple Small Portable

Proliferation-Resistant Reactor (LSPR) to distinguish it from reactors proposed by the other institutes.

This reactor does not require any high level infrastructures available now in developed countries, shows nuclear proliferation resistance, satisfies the safety criteria equivalent to ones for modern LWRs without any actions by personnel or machinery.

LSPR is built in a developed country, and shipped to a developing country, and set it there. The steam and water pipes are connected at operation site. It is operated for 10 to 30 years, and replaced by a new one, if necessary. Old one is shipped back to the developed country. The reactor vessel cannot be opened for refueling at the operation site. It is good for nuclear proliferation resistance. The Polonium, which is an alpha emitter, is produced from neutron capture reaction by bismuth in coolant and works efficiently for physical protection.

The total power of the typical design is 150 MWt (53MWe). The height and width of the reactor vessel for this power level are 15.2m and 5.2m, respectively. The artist view of reactor vessel is shown in Fig. 1.

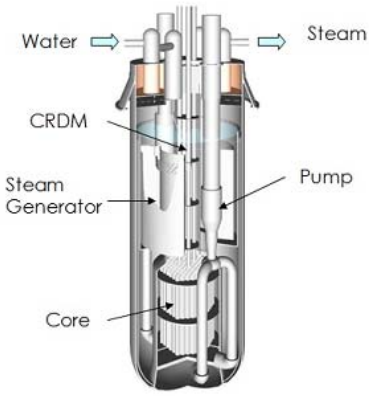

Fig.1 Artist view of LSPR

The excess reactivity required for burnup is very low. Our previous study shows that the 12 years operation requires only less than 0.1% Δk. It makes UTOP accident inherently safe. LSPR confirms negative coolant dilatation coefficient over whole reactor life. This characteristic together with some other characteristics makes ULOF accident inherently safe. This reactor can survive even simultaneous UTOP ULOF and ULOHS accident without the help of an operator or active device. Here we employ two mechanical pumps for the primary circuit for expecting coast-down of coolant flow at ULOF. The replacement of impeller is simple, but performed by regularly visiting maintenance crew from the developed country. In addition to the mechanical pump, the use of magnetic pumps, lift-up pumps and natural circulation can be the alternatives for their performances at either normal or accidental conditions.

CANDLE BURNING [61, 66, 68, 74, 83, 96, 100, 102, 106, 109, 112, 113, 115, 118, 120, 122, 125-128, 130, 137, 138, 142, 146, 147, 150, 152]

In conventional reactors, control rods inserted at the start-up of operation are gradually extracted along fuel burning in order to maintain the reactor critical. On the other hand, CANDLE (Constant Axial shape of Neutron flux, nuclide densities and power shape During Life of Energy production) reactors do not need this kind of control rods. Their burning region moves along the direction of the core axis, at a speed proportionate to the power output, without changing the spatial distribution of the nuclide densities, neutron flux and power density as shown in Fig. 2. We can use either natural uranium or depleted uranium for the fresh fuel. The same idea is employed in Travelling Wave Reactor, whose design study was stared recently by the support of Bill Gates.

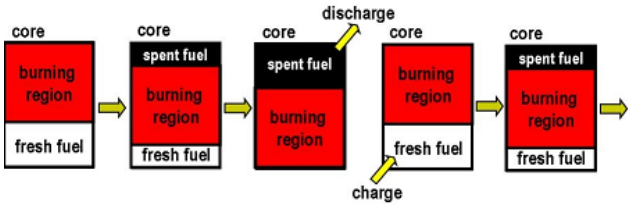

Fig. 2 CANDLE burning and fuel management

Very high neutron economy is required to realize CANDLE burning for the fast reactor case. From our previous studies fast reactors with metallic fuel and some others with very hard neutron spectrum can realize this burning. However, once it is realized, natural or depleted uranium can be used for replacing fuels and 40% (400 MWd/tHM) of it can burn up.

The nuclear energy has the resource problem, if we operate only light water cooled reactors (LWR). It has also inherent difficult problems caused by radioactive materials produced in it and by employed materials and technologies tightly relating to nuclear bombs. The radioactive materials cause the problem of accident during reactor operation, and the problem of radioactive wastes after reactor operation. Any proposed reactors should satisfy technical feasibility, of course. Finally reasonable price is usually an important requirement to energy. Thus the necessary and sufficient conditions for nuclear energy utilization as primary energy in the future are considered to satisfy six requirements for 1) resource, 2) safety, 3) waste, 4) bomb, 5) technical feasibility, and 6) economy:

1) Resource

The burn-up of the spent fuel is about 40%. This value is competitive to the value of the presently expected fast reactor system with reprocessing plant. The 40% of natural uranium burns up without enrichment or reprocessing.

The present once-through fuel cycle of 4% enriched uranium in LWR performs the burn-up of about 4% of the inserted fuel, and it corresponds to the utilization of about 0.7% of natural uranium depending on the enrichment of

depleted uranium. For this case about 87% of the original natural uranium is left as depleted uranium. If this depleted uranium is utilized as the fuel for CANDLE reactor, 35% (=0.87x0.4) of the original natural uranium is utilized. Therefore, if the LWR has already produced energy of X Joules, the CANDLE reactor can produce about 50X Joules from the depleted uranium stored at the enrichment facility for the LWR fuel.

If LWRs have already produced energy sufficient for full 40 years and the nuclear energy production rate will not change in the future, we can produce the energy for 2000 years by using the CANDLE reactors as shown in Fig. 3. We need not mine any uranium ore, and do not need reprocessing facility.

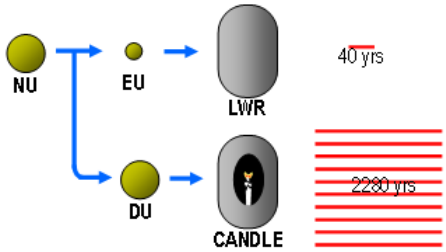

Fig. 3 CANDLE reactor operation after LWR operation

2) Safety

There are so many kinds of events and accidents for nuclear reactor that the best way for increasing safety features of nuclear reactor is considered to reduce both frequency of undesired events and consequence of the most severe accident.

The frequency of undesired events for CANDLE reactor is reduced by many ways as follows. Firstly the burn-up reactivity control mechanism is not required for CANDLE burning. The reactor control becomes simple and easy. The excess burn-up reactivity becomes zero, and the reactor becomes free from reactivity-induced accidents at operating condition. Secondly the number density distribution of each nuclide does not change with burning in the burning region. Therefore, the reactor characteristics such as power peaking and power coefficient of reactivity do not change with burning. The estimation of core condition becomes very reliable. The reactor operation strategy remains un-changed for different burning stage. Thirdly since the radial power profile does not change with burning, the required flow rate for each coolant channel does not change. Therefore, the orifice control along burning is not required. The operational mistakes are avoided. Furthermore, fresh fuel charged after the second cycle is depleted uranium or natural uranium. The transportation and storage of fresh fuels become simple and safe.

Recriticality accidents occurring after core disruptive accidents are considered the most secure accident of fast reactors. CANDLE reactors considerably reduce the possibility and consequences of recriticality accidents since control rods are not inserted in the core and only a little coolant in the core.

3) Waste

The present LWR performs the burn-up of about 4% of the inserted fuel of 4% enriched uranium. On the other hand the burn-up of the spent fuel for CANDLE reactor is about 40%. It is ten times as high as for LWR. Therefore, the spent fuel amount per produced energy is reduced to be one-tenth of once-through cycle of LWR.

Separation of spent fuel and vitrification may reduce the volume of high level wastes, but the total volume of radioactive wastes increases. The once-through fuel cycle of CANDLE reactor system reduces the total volume of radioactive wastes.

The amount of actinides is decreased since they are stored in the core much longer than conventional reactors and fissioned in a considerable amount during this period.

We can use the depleted uranium. The wastes from uranium mining do not appear.

4) Bomb

The enrichment and reprocessing are the most important key technologies for bomb-making. CANDLE reactor can be operated without enrichment or reprocessing forever, once it starts, if only natural or depleted uranium is available. Therefore, CANDLE reactor shows excellent features on physical protection and non-proliferation.

5) Technical feasibility

When we use conventional cladding materials, the burnup of 40% is too much and we should employ recladding. Once we employ this process, frequency of it becomes an optional parameter. The recladding process is a purely dry process and its cost is much cheaper than conventional reprocessing. If the burnup for one-cycle is small enough, the recladding becomes very easy and the separation of cladding from meat becomes rigid.

The start-up of the initial core can be easily performed by enriched uranium.

Now we do not have any severe technical difficulties.

6) Economy

The cost of nuclear reactor consists of capital, fuel, and O& M (operation and maintenance).

We can expect low O&M cost, since CANDLE reactor is simple.

We can also expect low fuel cycle cost, since the reprocessing of discharged fuel is not required.

Since coolant channel space is smaller than conventional reactors, the core cooling performance is poor. It may result in lower average power density. Low average power density deteriorates strongly its economical performance. However, this deterioration may be reduced considerably by the designs without blanket, short core height and radially flat power distribution. The short core and radially flat power distribution can be realized by employing radially multi-region core and MOTTO fuel cycle.

REFERENCES

[1] H. Sekimoto, "A Direct Technique for Unfolding Neutron Spectra from Activation Data", *Nucl. Sci. Eng*., **68**, 351-356(1978).

[2] H. Sekimoto, M. Ohtsuka and N. Yamamuro, "A Miniature Fast-Neutron Spectrometer for Scalar Spectrum Measurement", *Nucl. Instr. Meth*., **189**, 469-476(1981).

[3] H. Sekimoto and N. Yamamuro, "Unfolding Methods with the Prior Knowledge and Integral Data of Neutron Spectrum", *Nucl. Sci. Eng.*, **80**, 101-112(1982).

[4] H. Sekimoto, M. Ohtsuka and N. Yamamuro, "The Perturbation Produced in the Neutron Spectrum of an Assembly by a Spectrometer", *Nucl. Sci. Eng*., **80,** 407-411(1982).

[5] H. Sekimoto, K. Oishi, K. Hojo and T. Hojo, "Some Characteristics of a Miniature Neutron Spectrometer", *Nucl. Instr. Meth*., **227**, 146-149(1984).

[6] H. Sekimoto, "An Unfolding Method Leading to a Positive Solution Only", *Nucl. Instr. Meth*., **228**, 129-132(1984).

[7] D. Lee, H. Sekimoto and N. Yamamuro, "Fast Neutron Spectrum in Lithium Fluoride Pile with D-T Neutron Source", *J. Nucl. Sci. Techno*l., **22**, 28-37(1985).

[8] H. Sekimoto, K. Hojo and T. Hojo, "Fast Neutron Spectrum Generated in Graphite Pile with D-T Neutron Source", *J. Nucl. Sci. Technol*., **22**, 174-182(1985).

[9] H. Sekimoto, K. Hojo, T. Hojo and K. Oishi, "A Simple Facility to Measure the Scalar Neutron Spectrum in an Assembly", *Nucl. Instr. Meth*., **A234**, 148-151(1985).

[10] K. Sugiyama, K. Kanda, S. Iwasaki, M. Nakazawa, H. Hashikura, T. Iguchi, H. Sekimoto, S. Itoh, K. Sumita, A. Takahashi and J. Yamamoto, "Integral Experiment in a 120-cm Lithium Sphere", *Fusion Technol.*, **8,** 1491-1494(1985).

[11] H. Sekimoto, D. Lee, K. Hojo, T. Hojo, K. Oishi, T. Noura, M. Ohtsuka and N. Yamamuro, "Measurement and Calculation of Fast-Neutron Spectrum in Water, Graphite and Lithium Fluoride Assemblies with a D-T Neutron Source", *J. Nucl. Mater*., **133**, 882-886(1985).

[12] H. Sekimoto, K. Oishi, T. Hojo and K. Hojo, "Fast Neutron Spectrum in Water with a Deuterium-Tritium Neutron Source", *Nucl. Sci. Eng.*, **91**, 359-367(1985).

[13] H. Sekimoto and D. Lee, "Scalar Fast Neutron Spectra in Graphite-Reflected Lithium Fluoride Pile with D-T Neutron Source", *J. Nucl. Sci. Technol.*, **23**, 381-386(1986).

[14] H. Sekimoto, "Spectral Covariance Associated with the Monte Carlo Method", *Nucl. Sci. Eng*., **94**, 277-281(1986).

[15] H. Sekimoto, T. Obara, S. Yukinori and E. Suetomi, "New Method to Analyze Equilibrium Cycle of Pebble-Bed Reactors", *J. Nucl. Sci. Technol*., **24,** 765-772(1987).

[16] E. Suetomi and H. Sekimoto, "Application of Preconditioned Conjugate Gradient Method to Eigenvalue Problems for One-Group Neutron Diffusion Equation", *J. Nucl. Sci. Technol*., **25**, 100-103(1988).

[17] H. Sekimoto, K. Watanabe, E. Suetomi, K. Yosikawa, M. Okamoto, T. Suzuki, B. G. Logan and C. Maninger, "Conceptual Design of the Blanket and Superheater in Compact Fusion Advanced Rankine Cycle", *Fusion Engin. Design*, **9**, 445-449(1989).

[18] Y. Oka, T. Ida, S. Ohno, M. Aoki, M. Yokozawa, K. Shin, J. Yamamoto, A. Takahashi, H. Sekimoto and S. Sakamoto, "Fusion Neutron Streaming Benchmark Experiments and the Analysis by the Three-Dimensional Transport Calculation Code, TRISTAN", *Fusion Engin. Design*, **10**, 127-132(1989).

[19] T. Onoda and H. Sekimoto, "A Neutron Spectrometry Unfolding Code Based on Quadratic Programming", *Nucl. Instr. Meth.*, **A272**, 844-846(1988).

[20] P. Liem, H. Sekimoto and E. Suetomi, "Design Study of Graphite Moderated Gas-Cooled High Flux Reactor", *Nucl. Instr. Meth.*, **A274**, 579-583(1988).

[21] Y. Hirose, P. Liem, E. Suetomi, T. Obara and H. Sekimoto, "Fuel Management Effects on Inherent Safety of Modular High Temperature Reactor", *J. Nucl. Sci. Technol*., **26**, 647-654(1989).

[22] E. Suetomi and H. Sekimoto, "Conjugate Gradient Like Methods and Their Application to Fixed Source Neutron Diffusion Problems", *J. Nucl. Sci. Technol.*, **26**, 913-926(1989).

[23] N. Takagi, H. Sekimoto and T. Nakagawa, "Evaluation of Neutron Nuclear Data for Z>88 Minor Nuclides", *J. Nucl. Sci. Technol.*, **27**, 853-861(1990).

[24] E. Suetomi and H. Sekimoto, "Conjugate Gradient Like Methods and Their Application to Eigenvalue Problems for Neutron Diffusion Equation", *Ann. Nucl. Energy*, **18**, 205-228(1991).

[25] H. Sekimoto, K. Watanabe and D. Lee, "A Design Study of Detectors for Low-Level Neutrons", *Nucl. Instr. Meth*., **A302,** 150-157(1991).

[26] H. Sekimoto and N. Takagi, "Preliminary Study on Future Society in Nuclear Quasi-Equilibrium", *J. Nucl. Sci. Technol.*, **28**, 941-946(1991).

[27] T. Obara and H. Sekimoto, "New Numerical Method for Equilibrium Cycle of High Conversion Pebble Bed Reactors", *J. Nucl. Sci. Technol*., **28**, 947-957(1991).

[28] K. Yoshikawa, D. Shimohiro, Y. Yamamoto, H. Toku, Y. Inui, M. Ishikawa, J. Umoto, N. Miki, A. Fukuyama, O. Mitarai, M. Okamoto, H. Sekimoto, Y. Fujii, H. Kim, K. Watanabe, T. Ishii, T. Takagi, T. Suzuki, I. Mutoh, K. Miyazaki, M. Saitoh, B. G. Logan, W. L. Barr, M. A. Hoffman and R. B. Campbell, "A D-T Tokamak Fusion Reactor with Advanced Blanket Using Compact Fusion Advanced Rankine (CFAR) Cycle", *Fusion Engin. Design*, **18**, 239-248(1991).

[29] N. Takagi and H. Sekimoto, "Feasibility of Fast Fission System Confining Long-Lived Nuclides", *J. Nucl. Sci. Technol*., **29**, 276-283(1992).

[30] H. Sekimoto and Y. Anmo, "A Neutronic Study on the Concept of Using a Fast Reactor Core for High Flux Reactors", *Ann. Nucl. Energy*, **19**, 431-439(1992).

[31] P. Liem and H. Sekimoto, "Neutronic Modeling for Modular High Temperature Pebble Bed Reactor during Reactivity Accident", *J. Nucl. Sci. Technol.*, **29**, 805-812(1992).

[32] P. Liem and H. Sekimoto, "Neutronic and Thermal Hydraulic Design of the Graphite Moderated Helium-Cooled High Flux Reactor", *Nucl. Engin. Design*, **139**, 221-233(1993).

[33] E. Suetomi and H. Sekimoto, "Derivation of Anisotropic Diffusion Coefficients in a Large Annular Cavity", *Nucl. Sci. Eng.*, **114**, 168-175(1993).

[34] Zaki S. and H. Sekimoto, "Preliminary Design Study of the Ultra Long Life Fast Reactor", *Nucl. Engin. Design*, **140**, 251-260(1993).

[35] P. Liem and H. Sekimoto, "Core Safety Characteristics of High Flux Safe Reactor (HFSR)", *J. Nucl. Sci. Technol*., **30**, 648-663(1993).

[36] K. Yoshikawa, M. Ohnishi, Y. Yamamoto, H. Toku, I. Kataoka, Y. Inui, M. Ishikawa, U. Umoto, A. Fukuyama, O. Mitarai, M. Okamoto, H. Sekimoto, and M. Nagatsu, "A

Preliminary Study of a D-T Tokamak Fusion Reactor with Advanced Blanket Using Compact Fusion Advanced Brayton (CFAB) Cycle", *Fusion Engin. Design*, **29**, 78-88(1995).

[37] T.Obara and H. Sekimoto, "Zero Temperature Coefficient Thermal Core with Diluted Fuel", *Trans. Amer. Nucl. Soc.*, **71**, 495-496(1994).

[38] H. Sekimoto and V. V. Kuznetsov, "Lead-Cooled Fast Reactor Use in Future Equilibrium Energy Production", *Trans. Amer. Nucl. Soc.*, **71**, 496-497(1994).

[39] M. Takahashi, M. Kotaka and H. Sekimoto, "Burn-off and Production of CO and CO_2 in the Oxidation of Nuclear Reactor-Grade Graphites in a Flow System", *J. Nucl. Sci. Technol*., **31**, 1275-1286(1994).

[40] T. Obara and H. Sekimoto, "Feasibility of Zero Temperature Coefficient Core with Highly Diluted Fuel and Graphite Moderator", *Ann. Nucl. Energy*, **22**, 331-337(1995).

[41] H. Sekimoto and Zaki S., "Design Study of Lead- and Lead-Bismuth-Cooled Small Long-Life Nuclear Power Reactors Using Metallic and Nitride Fuel", *Nucl. Technol.*, **109**, 307-313(1995).

[42] V. V. Kuznetsov and H. Sekimoto, "Radioactive Waste Transmutation and Safety Potentials of the Lead-Cooled Fast Reactor in the Equilibrium State", *J. Nucl. Sci. Technol.*, **32**, 507-516(1995).

[43] Zaki S. and H. Sekimoto, "Safety Aspect of Long-Life Small Safe Power Reactors", *Ann. Nucl. Energy*, **22,** 711-722(1995).

[44] Zaki S. and H. Sekimoto, "Design and Safety Aspect of Lead and Lead-Bismuth Cooled Long-Life Small Safe Fast Reactors for Various Core Configurations", *J. Nucl. Sci. Technol*., **32,** 834-845(1995).

[45] K. Yoshikawa, M. Ohnishi, Y. Yamamoto, H. Toku, I. Kataoka, Y. Inui, M. Ishikawa, U. Umoto, A. Fukuyama, O. Mitarai, M. Okamoto, H. Sekimoto, and M. Nagatsu, "A Preliminary Study of a D-T Tokamak Fusion Reactor with Advanced Blanket Using Compact Fusion Advanced Brayton (CFAB) Cycle", *Fusion Engin. Design*, **29**, 78-88(1995).

[46] H. Sekimoto, H. Nakamura and N. Takagi, "Toxicity of Radioactive Waste Discharged from Nuclear Energy Center in the Future Equilibrium State", *Ann. Nucl. Energy*, **23**, 663-668(1996).

[47] Zaki S. and H. Sekimoto, "Accident Analysis of Lead or Lead-Bismuth Cooled Small Safe Long-Life Fast Reactor Using Metallic and Nitride Fuel", *Nucl. Engin. Design*, **162**, 205-222(1996).

[48] T. Obara and H. Sekimoto, "Design Concept of Fast Spectrum Pulse Reactor with Packed Core of Coated Dilute Fuel Particles", *J. Nucl. Sci. Technol.*, **33**, 547-554(1996).

[49] A. Mizutani and H. Sekimoto, "Calculational Method of One-Group Nuclear Constants in Nuclear Equilibrium State", *J. Nucl. Sci. Technol.*, **34,** 596-602(1997).

[50] T. Seino, H. Sekimoto and Y. Ando, "A New Estimation Method for Nuclide Number Densities in Equilibrium Cycle", *J. Nucl. Sci. Technol*., **34**, 745-754(1997).

[51] T. Obara and H. Sekimoto, "Concept and Basic Performance of an In-pile Experimental Reactor for Fast Breeder Reactors Using Fast Driver Core", *Ann. Nucl. Energy*, **24**, 1491-1513(1997).

[52] H. Sekimoto, H. Nakamura and A. Mizutani, "Sensitivities of Some Characteristics of Nuclear Equilibrium State to One-Group Constants", *J. Nucl. Sci. Technol.*, **34**, 1039-1046(1997).

[53] N. Takaki, R. Takagi and H. Sekimoto, "Effect of Decontamination Factor of Recycled Actinide and FP on the Characteristics of SCNES", *Progress in Nucl. Energy*, **32**, 441-447(1998).

[54] A. Mizutani and H. Sekimoto, "Cell Geometry Effect on Equilibrium State of Nuclear Reactors", *Progress in Nucl. Energy*, **32,** 713-720(1998).

[55] T. Seino and H. Sekimoto, "A Study on the Criticality Search of Transuranium Recycling BWR Core by Adjusting Supplied Fuel Composition in Equilibrium State", *Ann. Nucl. Energy*, **25**, 223-236(1998).

[56] A. Mizutani and H. Sekimoto, "Cell Geometry Effects on Nuclear Characteristics in Equilibrium State", *Ann. Nucl. Energy*, **25**, 623-638(1998).

[57] H. Sekimoto and K. Kanai, "Trade-off between Neutron Excess and Long-Term Toxicity Reduction by Employing LLFP Incineration", *Ann. Nucl. Energy*, **25**, 793-799(1998).

[58] A. Mizutani and H. Sekimoto, "Core Performance of Equilibrium Fast Reactors for Different Coolant Materials and Fuel Types", *Ann. Nucl. Energy*, **25**, 1011-1020(1998).

[59] T. Obara and H. Sekimoto, "Effect of Low Energy Resonance Absorber on Positive Neutron Temperature Coefficient of Dilute Plutonium-Water Solution", *Nucl. Sci. Eng*., **130**, 386-390(1998).

[60] V. Toshinsky, H. Sekimoto and G. Toshinsky, "A Method to Avoid Spatial Treatment in Xenon Poisoning Calculation While Providing Conservative Reactivity Estimates", *Ann. Nucl. Energy*, **26,** 373-385(1999).

[61] V. Toshinsky, H. Sekimoto and G. Toshinsky, "Multiobjective Fuel Management Optimization for Self-Fuel-Providing LMFBR Using Genetic Algorithms", *Ann. Nucl. Energy*, **26**, 783-802(1999).

[62] H. Sekimoto and A. Nemoto, "Sensitivities of Nuclide Importance for Neutron Economy to One-Group Data", *Trans. Amer. Nucl. Soc*., **80**, 54-55 (1999).

[63] K. Ryu and H. Sekimoto, "Basic Study of Concentrically Zoned Fast Reactor Using Natural Uranium Highly Efficiently without Fuel Reprocessing", *Ann. Nucl. Energy*, **27**, 93-98 (1999).

[64] H. Sekimoto, V. Toshinsky and G. Toshinsky, "Fuel Management Optimization for SFPR Using Multi-objective Genetic Algorithm", *Trans. Amer. Nucl. Soc*., **81**, 296-298 (1999).

[65] H. Tachihara and H. Sekimoto, "Exact Error Estimation for Solutions of Nuclide Chain Equations", *J. Nucl. Sci. Technol*., **36**, 1176-1185 (1999).

[66] V. Toshinsky, H. Sekimoto and G. Toshinsky, "A Method to Improve Multiobjective Genetic Algorithm Optimization of a Self-Fuel-Providing LMFBR by Niche Induction among Nondominated Solutions", *Ann. Nucl. Energy*, **27**, 397-410 (2000).

[67] K. Ryu and H. Sekimoto, "A Possibility of Highly Efficient Uranium Utilization with a Pebble Bed Fast Reactor", *Ann. Nucl. Energy*, **27**, 1139-1145 (2000).

[68] H. Sekimoto and K. Ryu, "Feasibility Study on the CANDLE New Burnup Strategy", *Trans. Amer. Nucl. Soc*., **82**, 207-208 (2000).

[69] H. Sekimoto and A. Nemoto, "Nuclide Importance and the Steady-State Burnup Equation", *Nucl. Sci. Engin*., **135**, 84-102 (2000).

[70] A. Shelley, H. Akie, H. Takano and H. Sekimoto, "Parametric Studies on Plutonium Transmutation Using Uranium-free Fuels in Light Water Reactors", *Nucl. Technol*., **131**, 197-209 (2000).

[71] H. Sekimoto, "Sustainability of Fission Energy in Future Equilibrium Society", *Prog. Nucl. Energy*, **40**, 441-448(2002).
[72] K. Fujimura, T. Sanda, S. Moro, M. Saito and H. Sekimoto, "Feasibility Study of Large MOX Fueled FBR Core Aimed at the Self-Consistent Nuclear Energy System", *Prog. Nucl. Energy*, **40**, 587-596(2002).
[73] K. Suzuki, H. Sekimoto and N. Ishigure, "Sensitivity Analysis of Dose Coefficients for ^{239}Pu to Transfer Rates", *Radiation Protection Dosimetry*, **88**, 197-206 (2000).
[74] H. Sekimoto and K. Ryu, "Demonstrating the Feasibility of the CANDLE Burnup Scheme for Fast Reactors", *Trans. Amer. Nucl. Soc*., **83**, 45 (2000).
[75] Y. Tahara, T. Kanagawa and H. Sekimoto, "Two-Dimensional Baffle/Reflector Constants for Nodal Code in PWR Core Design", *J. Nucl. Sci. Technol.*, **37**, 986-995 (2000).
[76] A. Waris and H. Sekimoto, "Basic Study on Characteristics of Some Important Equilibrium Fuel Cycles of PWR", *Ann. Nucl. Energy*, **28**, 153-167 (2001).
[77] A. Shelley, H. Akie, H. Takano and H. Sekimoto, "Comparison of the Burnup Characteristics and Radiotoxicity Hazards of Rock-like Oxide Fuel with Different Types of Additives", *J. Nucl. Sci. Technol*., **38**, 134-142 (2001).
[78] K. Suzuki, H. Sekimoto and N. Ishigure, "Dependence of Dose Coefficients for Inhaled ^{239}Pu on Absorption Parameters", *Radiation Protection Dosimetry*, **93**, 267-269 (2001).
[79] A. Shelley, H. Akie, H. Takano and H. Sekimoto, "Radiotoxicity Hazard of Inert Matrix Fuels after Burning Minor Actinides in Light Water Reactors", *Prog. Nucl. Energy*, **38**, 439-442 (2001).
[80] H. Sekimoto and A. Waris, "Analysis of Equilibrium Fuel Cycles of PWR Using Nuclide Importance", *Trans. Amer. Nucl. Soc.*, **84**, 355-356 (2001).
[81] H. Sekimoto, A. Nemoto and Y. Yoshimura, "Sensitivity Analysis of Nuclide Importance to One-Group Neutron Cross Sections", *Nucl. Sci. Engin.*, **138**, 279-294 (2001).
[82] A. Waris and H. Sekimoto, "Characteristics of Several Equilibrium Fuel Cycles of PWR", *J. Nucl. Sci. Technol.*, **38**, 517-526 (2001).
[83] H. Sekimoto, K. Ryu and Y. Yoshimura, "CANDLE: The New Burnup Strategy", *Nucl. Sci. Engin.*, **139**, 306-317 (2001).
[84] H. Sekimoto, S. Makino, K. Nakamura, Y. Kamishima and T. Kawakita, "Some Characteristics of LBE-Cooled Long-Life Small Fast Reactor LSPR", *Trans. Amer. Nucl. Soc*., **85**, 43-44 (2001).
[85] T. Obara, Y. Fujita, Y. Ando and H. Sekimoto, "Removal of Polonium Contamination on Quartz Glass by Baking", *Trans. Amer. Nucl. Soc*., **85**, 49 (2001).
[86] M. Takahashi, T. Suzuki and H. Sekimoto, "Corrosion of Steels in a Flowing Nonisothermal Pb-Bi", *Trans. Amer. Nucl. Soc*., **85**, 300 (2001).
[87] P. Liem, T. Taswanda, M. S. Tagor, H. Sekimoto, Y. Naito, "Study on the control rod interaction effect in RSG gas multipurpose reactor (MPR-30)", *Annals of Nuclear Energy* **29**, 701–716 (2002)
[88] H. Sekimoto and A. Waris, "Influence of Moderation Ratio on Several Equilibrium Fuel Cycles of PWR", *Trans. Amer. Nucl. Soc*., **86**, 301-302 (2002).
[89] Y. Tahara and H. Sekimoto, "Transport Equivalent Diffusion Constants for Reflector Region in PWRs", *J. Nucl. Sci. Technol.*, **39**, 716-728 (2002).
[90] K. Suzuki, H. Sekimoto and N. Ishigure, "Effect of Uncertainty in Transfer Rates for the ICRP Publication 67 Biokinetic Model on Dose Estimation of ^{239}Pu", *Radiation Protection Dosimetry*, **102**, 383-341(2002).
[91] H. Sekimoto and K. Tanaka, "Application of CANDLE Burnup Strategy to Small Reactors", *Trans. Amer. Nucl. Soc*., **87** (CD) (2002).
[92] T. Obara, T. Miura, Y. Fujita, H. Sekimoto, "Removing Effect of Polonium Contamination by LBE in Various Baking Conditions", *Trans. Amer. Nucl. Soc*., **87** (CD) (2002).
[93] T. Kawakita, K. Ikeda, S. Moro, M. Saito, and H. Sekimoto, "Feasibility study on nitride fuel core and recycling system toward self-consistent nuclear energy system", *Prog. Nucl. Energy*, **40**, 587-596(2002).
[94] K. Arie, M. Suzuki, M. Kawashima, S. Moro, M. Saito and H. Sekimoto, "A metal fuel fast reactor core for the self-consistent nuclear energy system", *Prog. Nucl. Energy*, **40,** 587-596(2002).
[95] T. Obara, T. Miura, Y. Fujita, Y. Ando and H. Sekimoto, "Preliminary study of the removal of polonium contamination by neutron-irradiated lead-bismuth eutectic", *Ann. Nucl. Energy*, .**30**, 497-502 [2003].
[96] Y. Ohoka and H. Sekimoto, "Application of CANDLE Burnup to Block-type High Temperature Gas Cooled Reactor", *Nucl. Engin. Design*, **229,** 15-23 (2004).
[97] K. Saito, M. Igashira, J. Kawakami, T. Ohsaki, T. Obara and H. Sekimoto, "Measurement of keV-Neutron Capture Cross Sections and Capture Gamma-Ray Spectra of ^{209}Bi", *J. Nucl. Sci. Technol*., **41**, 406-412 (2004).
[98] T. Obara, T. Mirua and H. Sekimoto, "Updated NRC Research Plan for Digital System Safety in Nuclear Polonium Distribution Analysis by Alpha-Ray Spectrum Unfolding Method", *Trans. Amer. Nucl. Soc*., **91** (CD) (2004).
[99] K. Iwanaga and H. Sekimoto, "Treatments of Kinetic Equation of Fast Sub Critical Assembly", *Trans. Amer. Nucl. Soc*., **92** (CD) (2004).
[100] Y. Ohoka and H. Sekimoto, "Simulation Study on CANDLE Burnup of High Temperature Gas Reactor", *Trans. Amer. Nucl. Soc.*, **92** (CD) (2004).
[101] T. Obara, T. Miura and H. Sekimoto, "Polonium Contamination Removal from Stainless Steel by Baking Method", *Trans. Amer. Nucl. Soc*., **92** (CD) (2004).
[102] H. Sekimoto, "Effect of Neutron Spectra and Fuel Burnup on CANDLE Calculation", *Trans. Amer. Nucl. Soc*., **92** (CD) (2004).
[103] T. Miura, T. Obara and H. Sekimoto, "Unfolding of Polonium Distribution in Depth of Irradiated Lead-Bismuth Eutectic from alpha-particle Pulse-height distribution", *Appl. Rad. Isotopes*, **61** 1307-1311 (2004).
[104] K. Hibi and H. Sekimoto, "Investigation of Neutron Reaction Behavior in Water-cooled FBR with (Pu,U)O2 Fuel", *J. Nucl. Sci. Technol*., **42**, 153-160 (2005).
[105] K. Iwanaga and H. Sekimoto, "Study on Kinetics of Subcritical System - Contribution of Delayed Neutrons to the Transition after a Reactivity Insertion", *Ann. Nucl. Energy*, **32**, 1953-1962(2005).
[106] H. Sekimoto and Y. Udagawa, "Shut-down and Restart Simulation of CANDLE Fast Reactors", *Trans. Amer. Nucl. Soc*., **93** (CD) (2005).
[107] T. Miura, T. Obara and H. Sekimoto, "Chemical Form of Polonium in Lead-Bismuth Eutectic", *Trans. Amer. Nucl. Soc*., **93** (CD) (2005).

[108]T. Obara, T. Miura and H. Sekimoto, "Polonium Release Experiment in Direct Contact of Lead-Bismuth Eutectic with Water", *Trans. Amer. Nucl. Soc*., **93** (CD) (2005).
[109]E. Greenspan, P. Hejzlar and H. Sekimoto, G. Toshinsky and D. Wade, "New Fuel Cycle and Fuel Management Options in Heavy Liquid Metal-Cooled Reactors", *Nucl. Technol*., **151**, 177-191 (2005).
[110]T. Obara, T. Miura and H. Sekimoto, "Fundamental Study of Polonium Contamination by Neutron Irradiated Lead-Bismuth Eutectic", *J. Nucl. Materials*, **343**, 297-301 (2005).
[111]M. Kondo, M. Takahashi, T. Suzuki, K. Ishikawa, K. Hata, S. Qiu and H. Sekimoto, "Metallurgical Study on Erosion and Corrosion Behaviors of Steels Exposed to Liquid Lead-Bismuth Flow", *J. Nucl. Materials*, **343**, 349-359 (2005).
[112]H. Sekimoto, "The 21st Century COE Program : COE-INES", *Progress in Nucl. Energy*, 47, 9-15(2005).
[113]H. Sekimoto, "Application of CANDLE Burnup Strategy for Future Nuclear Energy Utilization", *Progress in Nucl. Energy*, **47**, 91-98(2005).
[114]K. Iwanaga and H. Sekimoto, "Study on Kinetics of fast Subcritical Assembly - Contribution of Delayed Neutrons to the Transition after Reactivity Insertion in a Subcritical System", *Progress in Nucl. Energy*, **47**, 163-170(2005).
[115]Y. Ohoka, T. Watanabe and H. Sekimoto, "Simulation Study on CANDLE Burnup Applied To Block-Type High Temperature Gas Cooled Reactor", *Progress in Nucl. Energy*, **47**, 292-299(2005).
[116]T. Obara, T. Miura and H. Sekimoto, "Development of Polonium Surface Contamination Measure in Lead-Bismuth Eutectic Coolant", *Progress in Nucl. Energy*, **47**, 577-585(2005).
[117]T. Miura, T. Obara and H. Sekimoto, "Removal of Polonium from Stainless Steel Surface Contaminated by Neutron Irradiated Lead-Bismuth Eutectic", *Progress in Nucl. Energy*, **47**, 624-631(2005).
[118]H. Sekimoto and Y. Udagawa, "Effects of Fuel and Coolant Temperatures and Neutron Fluence on CANDLE Burnup Calculation", *J. Nucl. Sci. Technol.*, **43**[2], 189-197 (2006)
[119]Sidik P., N. Takaki and H. Sekimoto, "Impact of Different Moderator Ratios with Light and Heavy Water Cooled Reactors in Equilibrium States", *Ann. Nucl. Energy*, **33**, 561-572 (2006).
[120]H. Sekimoto and S. Miyashita, "Startup of "Candle" Burnup in Fast Reactor from Enriched Uranium Core", *Energy Conv. Manag*., **47**, 2772-2780 (2006).
[121]T. Miura, T. Obara and H. Sekimoto, "Investigation of Polonium Decontamination from Stainless Steel Surfaces Using the Baking Method", *Nucl. Technol*., **155,** 78-89 (2006).
[122]Ismail, Y. Ohoka, P. Liem and H. Sekimoto, "Long Life Small CANDLE-HTGRs with Thorium", *Ann. Nucl. Energy*, **34**, 120-129 (2007).
[123]Sidik P., N. Takaki and H. Sekimoto, "Feasible Region of Design Parameters for Water Cooled Thorium Breeder Reactor", *J. Nucl. Sci. Technol*., **44**, 946-957, (2007).
[124]T. Miura, T. Obara and H. Sekimoto, "Experimental verification of thermal decomposition of lead polonide", *Ann. Nucl. Energy*, **34**, 926-930 (2007).
[125]M. Yan and H. Sekimoto, "Design research of small long life CANDLE fast reactor", *Ann. Nucl. Energy*, **35**, 18–36(2008).
[126]H. Sekimoto, "Progress in COE-INES'', *Prog. Nucl. Energy*, **50**, 71-74(2008).
[127]H. Sekimoto and A. Nagata, "CANDLE burnup regime after LWR regime", *Prog. Nucl. Energy*, **50**, 109-113(2008).
[128]N. Takaki and H. Sekimoto, "Potential of CANDLE reactor on sustainable development and strengthened proliferation resistance", *Prog. Nucl. Energy*, **50**, 114-118(2008).
[129]P. Liem, Ismail and H. Sekimoto, "Small high temperature gas-cooled reactors with innovative nuclear burning", *Prog. Nucl. Energy*, **50**, 251-256(2008).
[130]M. Yan and H. Sekimoto, "Study on small long-life LBE cooled fast reactor with CANDLE burn-up – Part I: Steady state research", *Prog. Nucl. Energy* **50**, 286-289(2008).
[131]Ismail, P. Liem, N. Takaki and H. Sekimoto, "Performance of natural uranium- and thorium-fueled fast breeder reactors (FBRs) for 233U fissile production", *Prog. Nucl. Energy* **50**, 290-294(2008).
[132]A. Waris, Z. Su'ud, S. Permana and H. Sekimoto, "Influence of void fraction change on plutonium and minor actinides recycling in BWR with equilibrium burnup", *Prog. Nucl. Energy* **50**, 295-298(2008).
[133]Sidik P., N. Takaki and H. Sekimoto, "Power density effect on feasibility of water cooled thorium breeder reactor", *Prog. Nucl. Energy* **50**, 308-313(2008).
[134]Sidik P., N. Takaki and H. Sekimoto, "Preliminary study on feasibility of large and small water cooled thorium breeder reactor in equilibrium states", *Prog. Nucl. Energy* **50**, 320-324(2008).
[135]T. Obara, T. Koga, T. Miura and H. Sekimoto, "Polonium evaporation and adhesion experiments for the development of polonium filter in lead–bismuth cooled reactors", *Prog. Nucl. Energy* **50**, 556-559(2008).
[136]Sidik P., N. Takaki and H. Sekimoto, "Breeding Capability and Void Reactivity Analysis of Heavy-Water-Cooled Thorium Reactor", *J. Nucl. Sci. Technol*., **45**, 589-600 (2008).
[137]M. Yan and H. Sekimoto, "Safety analysis of small long life CANDLE fast reactor", *Ann. Nucl. Energy*, **35**, 813–828 (2008)
[138]H. Sekimoto and M. Yan, "Design study on small CANDLE reactor", *Energy Conversion and Management*, **49**, 1868-1872 (2008)
[139]K. Iwanaga, H. Sekimoto and T. Mori, "Application of Monte Carlo Method to Solve the Neutron Kinetics Equation for a Subcritical Assembly", *J. Nucl. Sci. Technol*., **45**, 1099-1107 (2008)
[140]K. Kumar and H. Sekimoto, "Maximization of representativity factors for experimental planning of cross-section measurements: An information theoretic approach", *Ann. Nucl. Energy*, **35**, 2243–2248 (2008).
[141]K. Kumar and H. Sekimoto, "An information theory approach to minimize correlated systematic uncertainty in modeling resonance parameters", *Appl. Rad. Isotopes*, **67**, 329–333 (2009)
[142]A. Nagata, N. Takaki and H. Sekimoto, "A feasible core design of lead bismuth eutectic cooled CANDLE fast reactor", *Ann. Nucl. Energy*, **36**, 562-566 (2009)
[143]K. Kumar and H. Sekimoto, "Reduction of systematic uncertainty in the transmission measurement of iron using entropy based mutual information", *Radiation Measurements*, **44**, 168-172 (2009).
[144]Ismail, P. Liem, Sidik P., N. Takaki and H. Sekimoto, "Symbiotic systems consisting of large-FBR and small water-cooled thorium reactors (WTR)", *Ann. Nucl. Energy*, **36**, 1076-1085 (2009).
[145]K. Kumar and H. Sekimoto, "Simulation of optical model parameters with reduced model deficiency 3 by D-optimal criterion", *Ann. Nucl. Energy*, **36**, 1208-1210 (2009).

[146]H. Sekimoto and A. Nagata, "Core Height Shortening of CANDLE Reactor by Employing MOTTO Cycle", *Trans. Amer. Nucl. Soc*., **101** (CD) (2009).
[147]H. Sekimoto, "CANDLE Reactor: An option for simple, safe, high nuclear proliferation resistant, small waste and efficient fuel use reactor", *Nuclear Power and Energy Security* (ed. S. Apikyan and D. J. Diamond), pp. 197- 204, Springer (2009).
[148]Zaki S. and H. Sekimoto, "Local blockage analysis of lead-cooled next-generation nuclear power reactors", *Int. J. Nuclear Energy Science and Technology*, **5**, 162-170 (2010).
[149]S. Ishida and H. Sekimoto, "Applicability of Dynamic Programming to the Accelerator Driven System (ADS) Fuel Cycle Shuffling Scheme for Minor Actinide (MA) Transmutation", *Ann. Nucl. Energy*, **37**, 406-411 (2010).
[150]T. Okawa and H. Sekimoto, "A Design Study on Pb-208 Cooled Compact Candle Burning Reactor for Future Nuclear Energy Supply", *Ann. Nucl. Energy*, **37**, 1620-1625 (2010).
[151]S. Ishida and H. Sekimoto, "Finding the best fuel assemblies shuffling scheme of ADS for MA transmutation using Dynamic Programming", *Nucl. Engin. Design*, **240**, 3645-3653 (2010).
[152]H. Sekimoto, "Light a CANDLE", CRINES, Tokyo Tech (2010).

Ⅰ.2 APF-IH Liner Accelerator of A Heavy Ion Implanter

Toshiyuki HATTORI

1. Introduction

A major aim of current works is the design and fabrication of a new generation heavy ion implanter for the semiconductor industry. The reason for choosing the IH structure in the design process is that it has an extremely high shunt impedance value resulting in enhanced power efficiency and acceleration efficiency in the low-to-middle energy region compared to other linear accelerators [1]. The beam focus was performed using a self-focusing method, the APF method [2], using the rf focusing force generated by the high-frequency phase to focus the accelerating particles. Furthermore, the cell length and the total cavity length can be shortened when using the APF method.

This new heavy ion linac can accelerate $^{11}B^{+}$ and $^{31}P^{2+}$ ions; where He^{+} ions were used in the CW test experiment. The experiment showed that measured parameters, including the operation frequency, the Q value, the axial electric distribution, and the consumed power for acceleration, are well within the design limits. In particular, the measured operation frequency was 99.95% of the design specification of 60MHz. An important design feature is the variability of the linac output energy spectrum peak, which can be varied by changing the feeding power, desirable in the semiconductor fabrication process.

2. Design Procedure

In the past it was difficult to evaluate the high frequency electric field distribution and cavity resonant frequency for the IH linac. In this work the design process was based on CAD design software: SolidWorks [3], and an advanced computer simulation technology: 3-D electromagnetic solver Microwave Studio [4]. These softwares were utilized to perform simulations of the cavity electromagnetic distribution. The orbit calculation was simulated using PARMILA [5] and PMLOC (Pi Mode Linac Orbit Calculation), a program based on the thin lens principle, developed by our group.

This IH-DT linac design consisted of 8 drift tubes and 9 cells. Firstly, the drift tube table including drift tube lengths, gap lengths, phase and energy on each cell were created using PMLOC. Then PARMILA was used to evaluate the transit-time-factor and the energy distribution. The profile of the last cell of the PARMILA simulation is shown in Fig. 1.

Secondly, these drift tubes, based on the PMLOC calculation and an appropriate cavity based on experience, were sketched and assembled in SolidWorks. Next, the resonance frequency and the axial electric field distribution of the cavity were solved using Microwave Studio. Finally, based on the results of the Microwave Studio simulation, the cavity was adjusted to an optimal structure, where the resonance frequency and axial electric field distribution were correctly fitted to design limits. The simulation results of the electric field distribution were used to simulate further the beam orbit. The final parameters of the cavity are outlined in table 1.

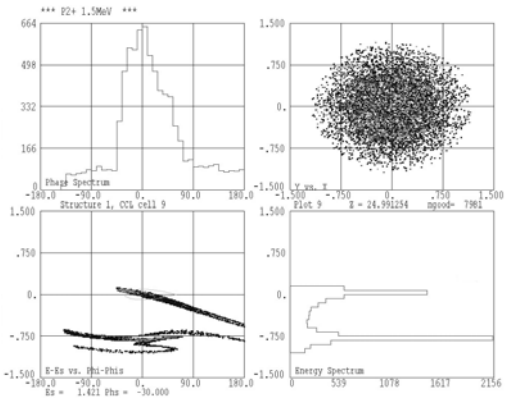

Fig. 1. The profile of the last cell.

Table-1 Main parameters of APF-IH linac

Charge to mass ratio(q/A)	He(1/4),P2+(2/31)
Frequency (MHz)	60
Input energy (kev/u)	20
Output energy (keV/u)	49
Cell numbers	9
Cavity length (cm)	43.2
Cavity radius (cm)	50.5
RF power (kW)	4.56
Drift tube radius (mm)	22
Drift tube radius (mm)	9
Synchronous phase	-90,-30,30,30,-30,-30deg.

After the PMLOC simulation of the iterating phase patterns of the drift tubes, the phases, the transverse acceptance of particles were determined. Furthermore, the double bunchers in the 1st and 2nd cell were selected in order to raise transmission. The determination of the optimum phases, listed in table 1, was based on the simulation results that showed which phases could obtain the largest acceptance of transverse and longitudinal directions.

3. Cavity electromagnetic simulation

For cavity electromagnetic simulations, the relationship between the mesh, frequency, and power, was firstly investigated using Microwave Studio. The simulation results indicate that the necessary power for accelerating ions up to 48.4keV/u from 20keV/u is 4.56kW. The decrease in frequency should be due to the increase in capacitance associated with the increase in DT diameter. The increased capacitance reduces the decrease of voltage (power). Ultimately, the optimum frequency was obtained with an ERT length of 20 mm and a DT diameter of 44 mm.

After the completion of all simulations and design processes, the final CAD data was sent to a manufacturer where the linac parts were fabricated and assembled. For the assembly of the parts, a nonconventional method was employed. Screws were used to join and align the acceleration drift tubes, the stems and the ridges. In this work, the main acceleration structure was fabricated using a 5-axis NC (numerical control) machine to cut the shapes of the drift tubes, the stems, the ridges, and the cooling roots without alignment. The well machined structure will have a highly effective cooling system and Q value. The linac model and the fabrication method are illustrated in Fig.2.

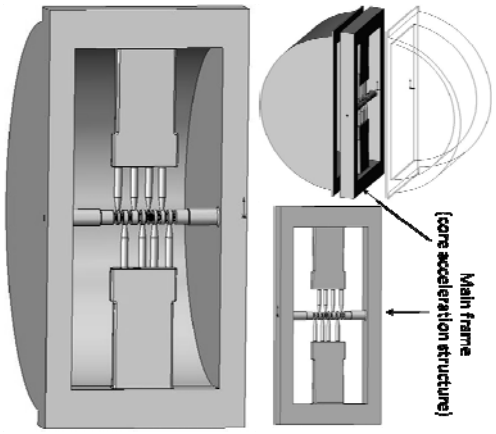

Fig. 2. A 3-D illustration of the cavity, fabricated using the 5-axis NC high accuracy machining method.

4. Cavity high frequency characteristic experiment and fabrication of acceleration system

The cavity optimal resonant frequency was measured to be 59.97MHz, which is 99.95% of the design limit. The Q value was measured to be 10,000, which is 91% of the value obtained from the simulations. The electric field distribution in the cavity was measured using the perturbation ball method. Both the measured result and the simulation result, individually highlighted in the left plots of Fig.3, are similar. The comparison of the normalized value from measurements and simulations are shown in the right plot of Fig.3, showing that the electric field of each gap is well reproduced in the simulations.

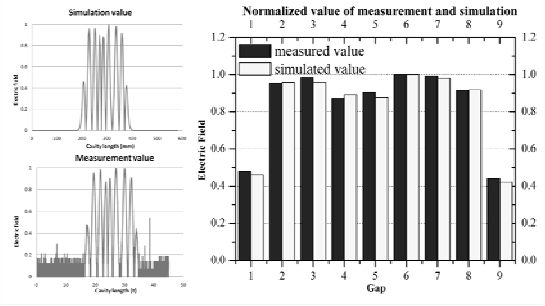

Fig. 3. Comparison of measurement value and simulation value

Using this newly-fabricated linac, the acceleration system was setup as shown in Fig.4. On the injection side this system includes: 1. a permanent-magnetic PIG ion source, which can extract charged particles at 10kV; 2. an accelerating tube which can accelerate particles to a desired energy; 3. an Einzel lens (EL) which is adopted to focus particles. On the exit side, the system includes a quadruple electrostatic lens, an analyzing magnet of 3.3kG, and a 10 mm slit. The total length of this compact system is approximately 3.3m. In order to measure the amount of current, four faraday cups (FC) were attached – two FC's at the entrance and exit of the accelerating tube, and two FC's at the output side of the linac and the analyzing magnet. The final beam spectrum is obtained from the accelerated He^+ ion beam current measured at FC-4.

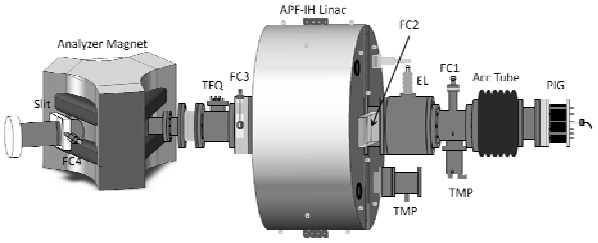

Fig. 4. He^+ accelerating test system.

5. Experiment and discussion

5.1 CW He^+ acceleration experiment

The He^+ output beam spectrums for the supplied powers of 330W and 450W are shown in Fig.5 and Fig.6, respectively. The accelerated beam peak of 48.4keV/u shows that the current is 95nA when the supplied power reaches 330W and rises to 205nA with EL. When the power increases to 450W, the higher beam peak stands at 56.5keV/u and the current is 230nA. At 450W with EL, the 56.5keV/u peak also expands and results in a current of 410nA.

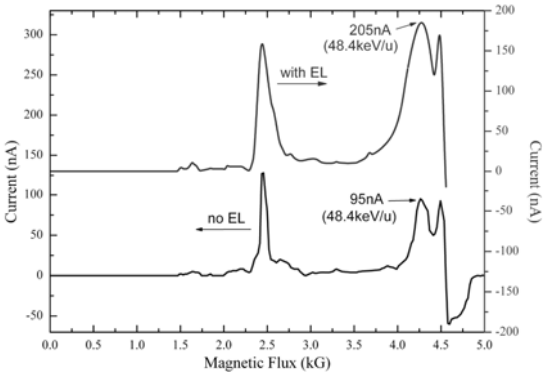

Fig. 5. Beam spectrum of 330W RF power.

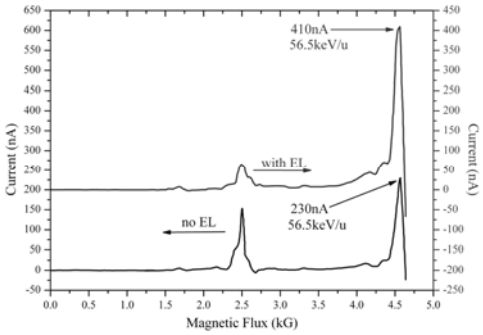

Fig. 6. Beam spectrum of 450W RF power

The results of the He^+ acceleration experiment shows that a 330W RF power is necessary to accelerate the incident He^+ beam up to 48.4keV/u from 20keV/u. The result from the Microwave Studio simulation was 304 W (calculated for a simulated power of 4.56kW for P^{2+}) which means that the electric conductivity of this linac cavity surface is about 92% (304W / 330W) of pure copper and agrees with the Q value ratio from the simulation (91%). Compared with conventional designs of the electric conductivity, only 80% ~ 85%, it is reasonable to state that the increased power efficiency is due to the greater accuracy in the fabrication process of the apparatus.

5.2 Discussion on energy variability

Based on the experimental results, it was considered that the APF-IH linac design of 9 cells could be used to accelerate multi-particles like $^{11}B^+$ and $^{31}P^{2+}$. The output energy spectrum peak is directly related to the change of the feeding power. Fig.7 shows the simulation results of the energy variability (solid lines) agree with the experimental results (indicated with triangle symbols).

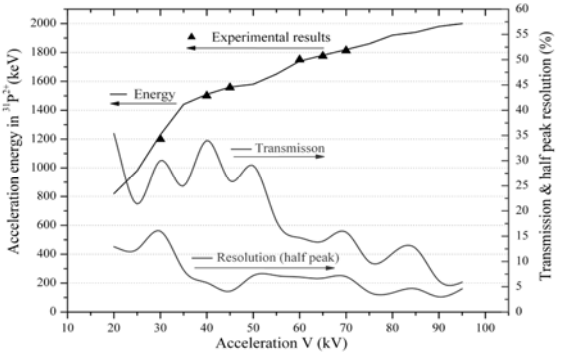

Fig. 7. Relations of simulation of energy and transmission & resolution. The acceleration energy was evaluated in phosphorus.

6. Summary

An APF-IH linac of a power-efficient structure was successfully designed and fabricated to accelerate He^+ ions up to 193.5keV (1.5MeV in $^{31}P^{2+}$). In this work the design process was completely based on numerical design and simulations; orbit calculation software and a 3-D electromagnetic solver was used to design and evaluate the cavity. Based on various cavity designs and the simulation results, the optimum cavity design was fabricated using a 5-axis NC machine to machine the core acceleration structure without alignment. The high frequency characteristic experiment of the cavity showed that measured values including frequency, power, and the Q value, agree with the desired design limits.

According to the CW He^+ acceleration experiment, the experimental power needed to accelerate particles agrees well with the simulation results. The available energy variability was also investigated, and showed that accelerated energy peak could be altered by changing the feeding power for He^+ acceleration. The energy variability of P^{2+} acceleration will be investigated in future work.

References

[1] T. Hattori, K. Sasa, M. Okamura, T. Ito, et al, *Fusion Eng. and Des*. **32-33** (1996) 359-363
[2] K. Yamamoto, T.Hattori, et al, *Nuclear Instruments and Methods in Physics Research B* **188** (2002) 229–232
[3] http://www.solidworks.com/
[4] http://www.cst.com/
[5] http://laacg1.lanl.gov/laacg/services/download_PMI.phtml

A.1 DNS and LES of Turbulent Flows in Concentric/Eccentric Annular Channels in Analogy to Subchannels of Sodium-cooled Fast Reactor Fuel Subassemblies

Hisashi NINOKATA and Elia MERZARI

DNS computations have been performed for non-isothermal flows in concentric and eccentric annular channels [1]. The data collected has been used to evaluate different SGS model in order to develop an effective LES methodology on the boundary fitted coordinates [2]. The algorithm used to solve the Navier-Stokes equations coupled with the energy equation is described in [2, 3, 4]. Several other models have been tested, among which the dynamic mixed model, the self-similarity model and another variant of the dynamic model [5]. The dynamic model and its variant performed fairly well from the point of view of *a priori* and *a posteriori* tests. They may be considered the ideal choice for the simulation of the flow in annular channels and rod-bundles [3].

The results of the LES simulations have been validated for available DNS and experimental data [2, 3] in concentric and eccentric annuli. Important aspects of the flow field such as transition from laminar to turbulent flow accompanied by a formation of the street of counter-rotating vortices in the region near the narrow gap have been confirmed and reproduced through the present methodology [5]. In particular, the effect of transverse curvature on the inner wall, as well as the effect of eccentricity on the wall shear stress, has been successfully simulated.

Contemporarily, in the narrow gap the local profile of the streamwise velocity evolves from a purely laminar solution to a solution characterized by the presence of turbulence production near the walls. Shear stress in the narrow gap region evolves from an almost laminar condition for a Reynolds number equal to 3,200 to an increasingly turbulent flow solution [5].

For non-isothermal flows of Pr = 0.71 and Ra = 2,160,000, in a concentric annulus channel with D_{in}/D_{out} = 0.6, the mesh sizes are chosen to be of the order of the Kolmogorov length scale. A total of 32 million meshes are employed in its DNS to calculate velocity and temperature distributions inside the annulus. Figure 1 shows comparisons of time-averaged and normalized temperature distributions at different angles to demonstrate excellent agreement of the DNS with experiment. LES results have been compared and show, in general, good agreement with DNS, where in the SGS modeling of the energy equation, filtering introduces a source term which could be approximated by the additional variables to be proportional to the temperature gradient with the turbulent viscosity given by the SGS model and turbulent Prandtl number. Total number of meshes in the LES is about one million (1/30 of the DNS case). Figure 2 shows snapshots of temperature contours in the case wheere the narrow gap is on the upper side. It is shown the plume hits the upper wall resulting in high value of variance near the outer wall and stronger temperature fluctuations are generated even near the bottom of the outer wall.

We have performed LES of the flow in two-subchannels connected by a narrow gap for an infinite triangular lattice rod bundles, typical of fuel subassembly of sodium-cooled LMFBRs, with periodic boundary conditions in the cross section and in the streamwise direction. Figure 3 (a) streamlines and (b) contour plot for the cross flow velocity are a result of LES for a low Reynolds number turbulent flow (Re=5,500) in a tight lattice rod bundle with P/D=1.05. The rectangles in (b) represent the regions where coherent structures can be clearly identified. The values are normalized by the 0.1 times the bulk velocity in the axial direction. The vector plot of the horizontal flow components shows a vortex positioned near the gap driving the cross flow between the two subchannels, thus mimicking the same phenomenon described previously for eccentric channels and other related geometries ([1]). The cross velocity has a sinusoidal behavior (Fig. 4) that is consistent with the principal mode of turbulence. This oscillatory behavior is called global flow pulsation and has been successfully reproduced by LES.

References

[1] H. Ninokata, E. Merzari and A. Khakim, “Analysis of low Reynolds number turbulent flow phenomena in nuclear fuel pin subassemblies of tight lattice configuration”, *Nucl Eng& Des* **239** pp. 855-866 (2009).

[2] E. Merzari and H. Ninokata, “Development of an LES methodology for complex geometries”, *J. Nucl Eng Tech*, Vol. **41**, No. 7, pp. 893-907 September (2009).

[3] E. Merzari and H. Ninokata, “A-Priori Test of the Flow in an Annular Channel With Differential Heating at the Walls,” *Proc. ASME 2009 Fluids Engineering Division Summer Meeting FEDSM2009* [FEDSM2009-78467], Vail, Colorado USA, August 2-6 (2009).

[4] E. Merzari, A. Khakim, H. Ninokata, “Large Eddy Simulation of the Flow in Tight-Lattice Rod Bundles at Low Reynolds Number,” *Proc. ASME 2009 Fluids Engineering Division Summer Meeting FEDSM2009* [FEDSM2009-78471], Vail, Colorado USA, August 2-6 (2009).

[5] E. Merzari and H. Ninokata, “Anisotropy and Coherent Structures for the flow in Annular Channels”, *Flow, Turbulence and* Combustion, DOI: 10.1007/s10494-008-9170-2 (2009)

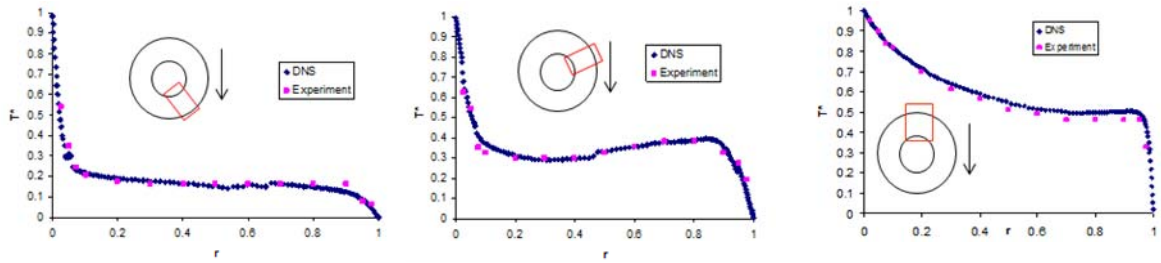

Figure 1. Radial temperature distributions at different angle positions in the concentric annulus: comparisons of DNS and experiment

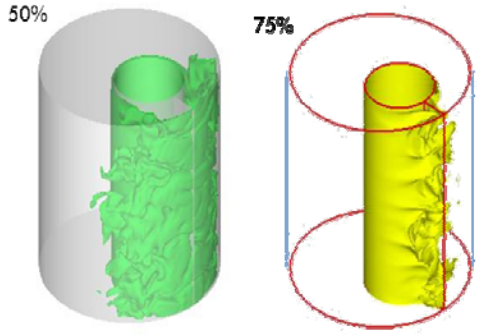

Figure 2. Normalized temperature contours in an eccentric channel: T*=0.5 (left) and T*=0.75 (right) with $T^*=(T-T_{out})/(T_{out}-T_{in})$.

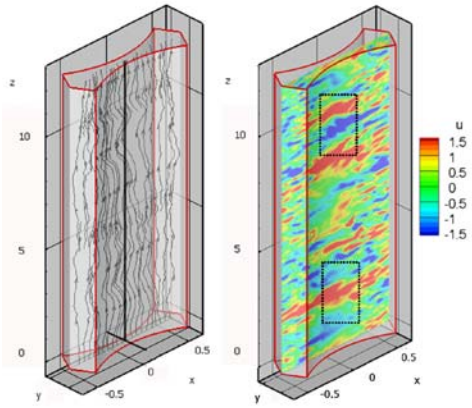

Figure 3. (a) Streamlines (b) Contour plot for the instantaneous cross flow velocity in an infinite triangular lattice rod bundle P/D=1.05, Re=5,500.

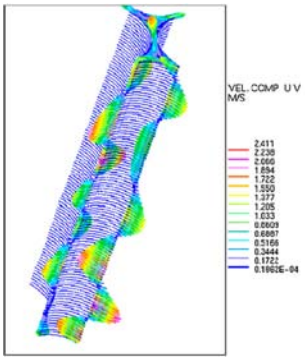

Figure 4. Flow oscillation between subchannels and cross flow velocity components.

A.2 CFD Analysis of Thermally Stratified Flow in Horizontal Pipe with Upward Bend

Marco PELLEGRINI and Hisashi NINOKATA

During protected loss of flow transients in loop-type fast breeder reactors, temperature distribution of the coolant and the particular geometrical arrangement in the upper plenum, may create an uneven temperature distribution at the hot leg inlet. This possibility, in case of very low flow rates, can cause thermal stratification in the horizontal portion of the pipes.

Analysis of the thermal stratification is important for estimating stresses on the pipes and also for the introduction of additional pressure losses which can influence the course of the transient.

Numerical analyses of such phenomena must be validated through experimental results, in order to show the benefits and the limitations introduced by the numerical study. In this contest the purpose of the present work is the validation of computational fluid dynamics tools for the evaluation of thermal stratification behavior in horizontal pipe through an experimental benchmark [1] [2] [3].

In Fig. 1 the facility, consisting of a "U bend", is shown. Water enters the inlet section with velocity V_{in} = 0.0178 m/s, and temperature T_0 = 300 K. At time t_0 the fluid at the inlet is heated during Δt = 53 s for a linear temperature increase of ΔT = 6.83°C.

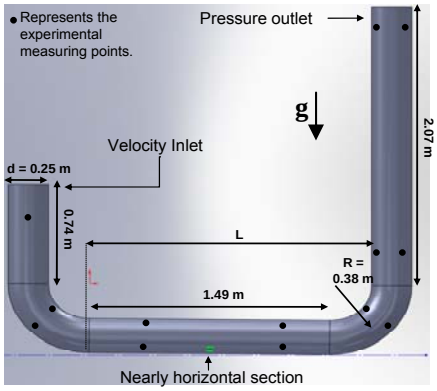

Fig. 1. Experimental facility.

After the fluid is heated the hot water reaches the first bend and, due to the buoyancy force, it stratifies on the upper region of the horizontal portion of the pipe. The hotter portion of the stratified fluid, moving with higher velocity, reaches the second bend where the simultaneous contribution of buoyancy and centrifugal forces creates a region characterized by large vortexes which introduce mixing and pressure drops.

The behavior of the transient (stable stratification and mixing in the elbow) is governed by important non dimensional parameters, i.e., Froude number F, Reynolds number Re, Peclet number Pe, the non dimensional time $\tilde{t}_0$ and the grade of pipe bending R/d, which are shown in Table 1.

Table 1 Non dimensional numbers characterizing the transient.

F	Re	Pe	$\tilde{t}_0$	R/d
0.22	5000	30,000	7.5	1.52

Spatial discretization of the domain to be simulated is done using symmetric condition on the flow direction; convective terms are discretized using second order upwind scheme. The temporal discretization is done employing a time-step δt = 0.25 s and using a fully implicit scheme. Pressure, momentum and energy equations are solved using the SIMPLE [4] algorithm.

Three calculations cases, shown hereafter in the present study, refer to k-ε model for the turbulence modelization using two different approaches for the wall treatment, namely Two-Layer (TL) (Wolfshtein assumptions [5]) and low-Reynolds (LR) approaches. In particular: CASE-A employs k-ε anisotropic and LR model; CASE-B utilizes k-ε anisotropic and TL model; CASE-C uses k-ε Realizable and TL model. To compute the calculation the commercial code Star CCM+ 5.02.009 was employed.

Fig. 2 shows the temperature contours at $t = 4 \cdot \Delta t$ on the symmetry plane which illustrates the persistence of the stratification in the nearly horizontal portion of the pipe and mixing appearing in the downward bend pipe region.

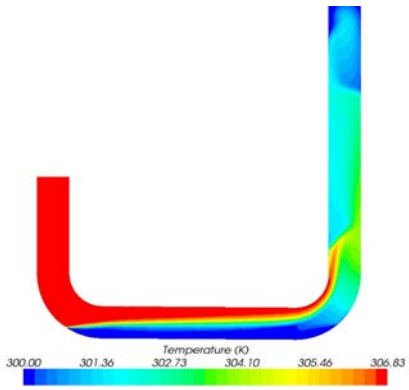

Fig. 2. Instantaneous temperature contours on the symmetry plane at t= 212 s for the Realizable Two Layer model (CASE-C).

The experiment provides temperature data for the measuring points (located 1 cm from the wall) whose position are qualitatively identified by the black dots in Fig. 1. The benchmark between the three calculations and the experimental data was carried and shown in Fig. 3.

In Fig. 3 the temperature differences for the three cases at $t = 4 \cdot \Delta t$ are shown. All the cases are able to evaluate the persistence of the stratification in the horizontal region (S/d 7-10). On the other hand poor predictions are obtained in the bend regions and in particular in the second bend (*S/d* 12-14). In this region the experimental results are provided for a 45° inclination plane and on a horizontal plane at the exit of the bend (Fig. 1). The experiment shows that on the diagonal plane, the temperature starts to shift from the lowest and highest temperature during the transient (i.e. 300K and 306.83K). This behavior is shown to be reasonably predicted by all the three simulations.

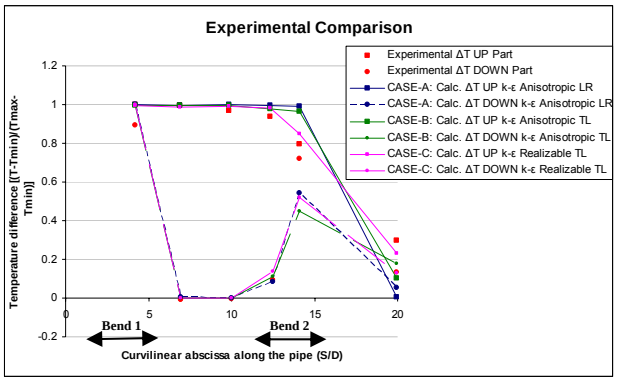

Fig. 3. Experimental and computational comparison of the temperature difference at t= 212 s.

At the bend exit instead the experiment shows that intermediate and similar temperatures on the measuring points are obtained. For the inner region of the pipe this means that the hot flow does not proceed along the vertical wall, as shown in Fig. 2 for CASE-C. Results for CASE-A and B instead demonstrate an opposite behavior. Finally all the three cases have poor predictions of the temperature increase evaluated in the outer part of the pipe. This can be imputed to lack of accuracy in the prediction of fluid recirculation in this region which underestimates the effective mixing.

In conclusion, a preliminary analysis of thermal stratification in bent pipes shows that the modeling efforts must concentrate on the evaluation of the region downward the stratification. The right validation of this region is indeed delicate and of primary importance for the pressure drop evaluation and modelization.

As a final remark, it is important to notice that the experimental results are provided very close to the pipe walls and therefore, due to low flow conditions, inside or near the boundary layer. As a consequence the proper and accurate modelization of this region has a deep impact on the success of the benchmarking.

Acknowledgement

The work was carried under the project "Statistical Approach in Fast Reactor Safety Evaluation" supported by JNES.

References

1. P.L. VIOLLET, "Observation and numerical modelling of density currents resulting from thermal transients in a non rectilinear pipe", *Journal of Hydraulic Research*, Vol. **25**, 1987, No. 2.
2. P.L. VIOLLET, "The modeling of turbulent recirculating flows for the purpose of reactor thermal-hydraulic analysis", *Nuclear Engineering and Design*, **99**, (1987), 365-377.
3. P.L VIOLLET, J.P. BENQUE, J. GOUSSEBAILE, "Two-dimensional numerical modeling of nonisothermal flows for unsteady thermal-hydraulic analysis", *Nuclear Science and Engineering*, **84**, (1987) 350-372.
4. S.V. PATANKAR, "Numerical heat transfer and fluid flow", McGraw Hill Book Company, 1980.
5. M. WOLFSHTEIN. "The velocity and temperature distribution in one-dimensional flow with turbulence augmentation and pressure gradient", *International Journal of Heat Mass Transfer,* Vol. **12**, pp. 310-318, (1969).

A.3 New Approach to Evaluate Lattice Expansion of Light Water Reactor Fuel Elements on Criticality Safety of Transport Packages under Impact Accidents

Masanori ARITOMI and Mitsufumi ASAMI

In order to safely transport packages containing light water reactor fuel assemblies, it is essential to maintain the fuel assemblies in a subcritical state in accidents during transport. To evaluate nuclear criticality safety, an estimator is required to determine an absolutely safe level based not only on hypothetical accidents but also on practical accident levels which, to some extent, are based on actual accidents[1]. The purpose of the present study is to suggest the arrangement of the deformation range of the fuel assembly after an actual accident, and to obtain the maximum value of the neutron effective multiplication factor based on the criticality safety assessment for the transport cask.

In the present study, two kinds of criticality calculations for the package were considered: large scale pin pitch shift and small scale pin pitch shift(see Fig.1). For the large scale pin pitch shift, a parameter which determines the location of each fuel pin which constitutes the fuel assembly was introduced so that the criticality calculation for the fuel assembly with non-uniform lattice pitch can be performed parametrically. The result of the criticality calculation using the parameter of large scale pin pitch shift made it clear that the neutron reactivity is sensitive to the fuel pin pitch because each fuel pin pitch is related to a ratio of the fissile to the moderator, and that the relationship of the ratio to the neutron reactivity depends on the type of fuel assembly (i.e. PWR or BWR, see Fig.2).

For the small scale pin pitch shift, the study focused on the small displacement of each fuel pin. The small displacement of each fuel pin pitch can be described probabilistically using the stochastic geometry routine[2] in MCNP code. Using the scheme in combination with the scheme for the large scale pin pitch shift, the maximum value of the neutron effective multiplication factor of the package after an accident can be obtained. However, the effects of the small scale pin pitch shift were small compared with the effects of the large scale pin pitch shift (see Fig.3).

This scheme is useful to determine the maximum neutron effective multiplication factor for the criticality safety evaluation.

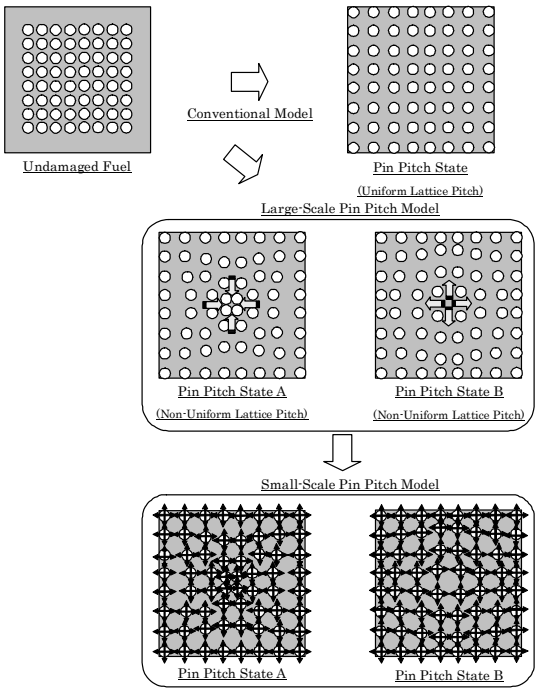

Fig.1 Schematic views of large scale and small scale pin pitch models

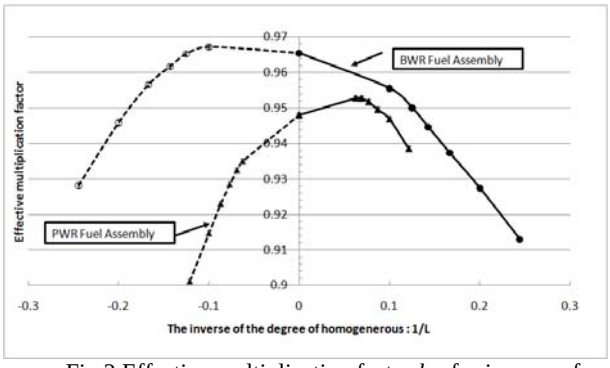

Fig.2 Effective multiplication factor k_{eff} for inverse of homogeneity degree $1/L$

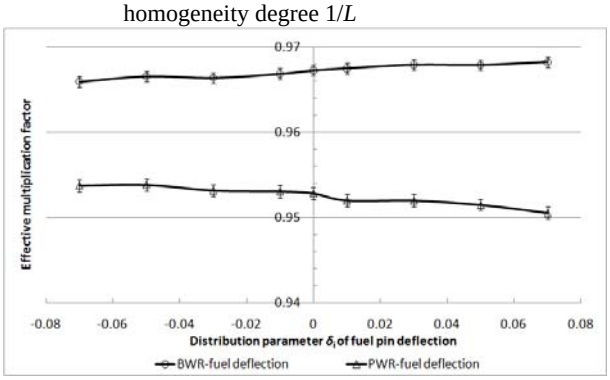

Fig.3 Effective multiplication factor k_{eff} for fuel distribution parameter δ_i of fuel pin's small displacement

Reference

[1] M. Asami and M Aritomi, "Investigation of subcriticality in LWR fuel transport accidents," *Proceedings of Radioactive Materials Transport*: Into the Renaissance, 13-14 May 2009(CD-ROM)

A.4 Evaluation of Supercritical CO_2 Centrifugal Compressor Experimental Data by CFD Analysis

Masanori ARITOMI amd Kazuhisa TAKAGI

A supercritical CO_2 gas turbine of 20MPa is suitable to couple with the Na-cooled fast reactor since Na - CO_2 reaction is mild at the outlet temperature of 800K, the cycle thermal efficiency is relatively high and the size of CO_2 gas turbine is very compact. Fig.1 shows Cycle design using supercritical CO_2. In this gas turbine cycle, a compressor operates near the critical point. The property of CO_2 and then the behavior of compressible flow near the critical point changes very sharply. So far, such a behavior is not examined sufficiently. Then, it is important to clarify compressible flow near the critical point. In this paper, the experimental data of the centrifugal supercritical CO_2 compressor have been evaluated by CFD analyses using a computer code "CFX". In the analyses, real gas properties of CO_2 were achieved by simulating density. The test compressor consists of three kinds of impeller. Fig.2 show these impeller figures. First, impeller A has 16 blades and the overall diameter is 110mm. Second, impeller B has 16 blades and the overall diameter is 76mm. Third, impeller C has 12 blades and the overall diameter is 56mm. Each impeller has each diffuser. Fig.3 shows experimental data with impeller A. This experiment had been gained over critical point. So, CFD analysis was conducted for each impeller and each diffuser. The results were compared and evaluated for the three different impeller and diffuser sets. Main output of calculation is a value of the total pressure at diffuser outlet, which agreed very well with that of the experiment. Total and static pressure distributions, relative velocity distributions and temperature distributions surrounding impeller and diffuser were obtained. Adiabatic efficiency was also evaluated. Fig.4 show slip factor (sigma) at range of supercritical. Slip factor is impotant to measure relative velocity given by impeller. General slip factor of stanitz-sigma also is shown. Comparired with these factors, It was confirmed that stanitz-sigama is higher than sigma. It needs exact evaluation in different operation range from now.

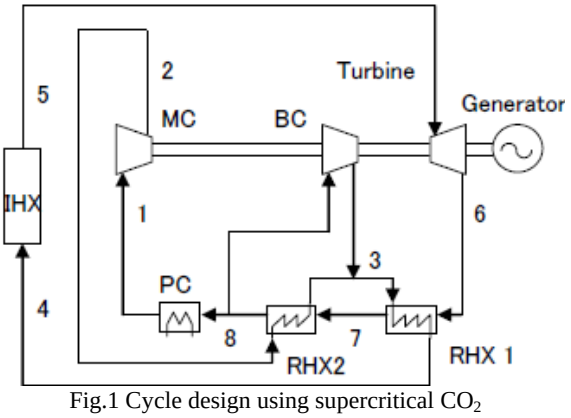

Fig.1 Cycle design using supercritical CO_2

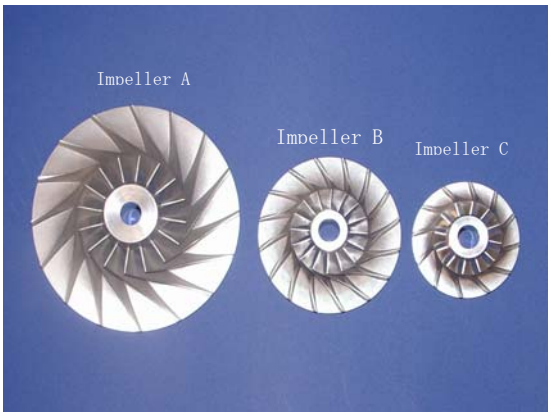

Fig.2 Each impeller

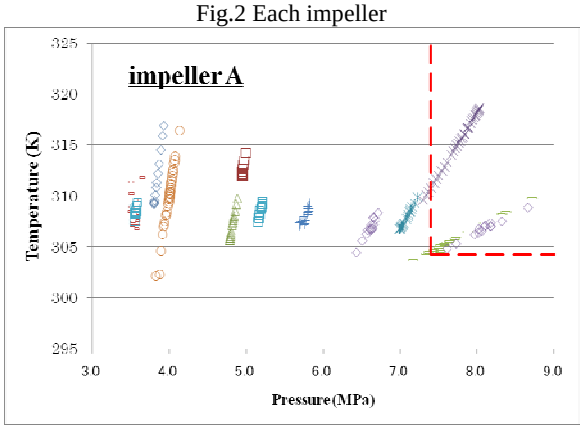

Fig.3 Experimental data with impeller A

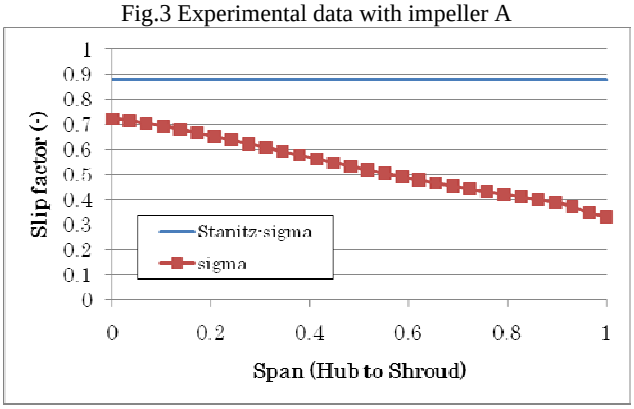

Fig.4 Comparison of slip factor at range of supercritical

Reference

[1] Takao ISHIZUKA, Yasushi MUTO, Masanori ARIOTMI, Nobuyuki TSUZUKI and Hiroshige KIKURA, Fundamental research on the cooling characteristic of PCCS with dropwise condensation, *17th International Conference on Nuclear Engineering (ICONE17)*, Brussels, Belgium, Vol. **1,** pp.813-822, 2009

A.5 Experimental Study for Estimating Bubble Volume and Shape by using Image Analysis in Stagnant

Masanori ARITOMI, Noriyuki WATANABE and Noriaki INABA

Two-phase flow is encountered in many applications: nuclear reactors, thermal plants, chemical plants, and some heat exchangers. In these designs and operations, the understanding of thermal-hydraulic characteristics in two-phase flow is important. Especially, because it is difficult to predict the void fraction in the subcooled boiling flow since boiling and condensation arise in the same time with nonthermal equilibrium. In the interfacial area transport equation of two fluid model, the parameter of interfacial behaviors is important because exchanging of mass and energy come through the interfacial. Gunther, Thorncroft, Bibeau, Prodanovic expressed the bubble behaviors by measuring bubble diameter, bubble waiting time and bubble growth rate by using high-speed cameras. The void fraction, interfacial area concentration and interfacial heat transfer, which are necessary to achieve the constitutive equations of two-fluid model, are calculated by bubble volume and interfacial area. Therefore, measuring of the bubble volume and interfacial with high accuracy is important. Interfacial heat transfer, which is necessary parameter to indicate energy balance in two-fluid model, shows that retaining energy of vapor molecule contributes to interfacial. Considering bubble condensation that vapor molecules in the bubble are cooled, interfacial heat transfer is calculated by vapor volume and interfacial area. Heat quantity is calculated by time-variable quantities of bubble volume ($\Delta V / \Delta T$) and multiplied by vapor density and latent heat. Therefore, considering that bubble shape changes temporally, it is necessary to explain that the variation of bubble volume is occurred by vapor condensation or the variation of calculated bubble volume by bubble shape change. However, calculating bubble volume is mostly by using shape approximation by simply through despite the bubble shape intricately varies. To estimate the bubble shape, image analysis is used. Image analysis for the shape estimations is used to observe from bubble behaviors in the stagnant water to bubble nucleation in the boiling conditions.

Despite there is a lot of studies focused on bubble shapes, the studies of accuracy bubble volume by shape approximation process is still a few. The purpose of this study is to calculate bubble volume by using shape approximation process and to compare with known real bubble volume. The results of this experiment show the average calculated bubble volume and its variance by image analysis. Finally, a new calculation method of bubble volume is suggested with considering the shape of the bubbly by image analysis.

By using image analysis, It is pronounced that variations of bubble shape affect the calculated bubble volume. The calculated bubble volume depends on the traditional method of long axis rotation and short axis rotation with ellipse approximation. In case of using long axis rotation, calculated bubble volume tends to be underestimated with low variance. In case of using short axis rotation, calculated bubble volume tends to be overestimated with high variance. In addition, it is considered that bubble shape affects the calculated bubble volume. To solve this problem, the bubble depth, which is unknown in one-dimension, is approximated to the average between long axis length and short axis length. As the result, the average of calculated bubble volume nearly equal to real bubble volume. Using stereo visualization for accuracy improvement of the calculated bubble volume, the bubble volume is calculated by measuring bubble depth. As the result, the calculated bubble volume is slightly overestimated with low variance in large real volume conditions. As predicted that the bubble shape of overestimated volume is dimpled ellipsoidal-cap like skirted, which the center of bubble is depressed.

In this study, original method for obtaining the calculated bubble volume is proposed by considering the influence of bubble shape. In case of using the correlation between short axis length and long axis length with approximating bubble shape to low aspect ratio, the average of calculated bubble volume nearly equals to the real bubble volume with low variance. This result shows that the method has same accuracy as the method of calculating bubble volume by stereo visualization.

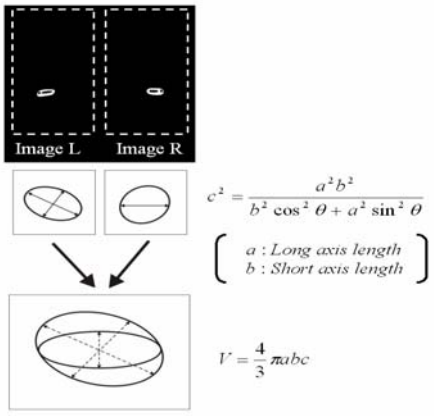

Fig.1 The method of calculate bubble volume by stereo images

Reference

[1] Masanori Aritomi, Fundamental Study of Thermal-Hydraulic Instabiity on Reduced-Moderation Natural Circulation BWR, *Annual Cooperative Research Report with Japan Atomic Power Co.*, March 2010.

A.6 Multi-wave Sensors for Two-Phase Flow Observations in Vertical Rectangular Channel

Masanori ARITOMI, Hiroshige KIKURA, and M Kunta Biddinika

Gas-liquid two-phase flow is an important phenomena appearing in in many industrial applications such as chemical plants and power generation plant. The phenomena exists also in natural life living since it is the most common flows of fluids in nature. A number of experimental studies have been carried out to understand the fundamental mechanism of two-phase flow.

This presented work is rather a fundamental study than an engineering work with directly applied background. Nevertheless, a strong engineering demands fundamental studies in order to improve available basic knowledge and its application for technological design.

Two-phase bubbly flow condition in rectangular channel has been studied by Richter (2001) using wire-mesh tomography. Various test results have been presented in 3-dimension on the sensitivity of flow parameter and gas injection configuration. In this experimental study, some similar flow condition has been studied by using ultrasonic velocity profile technique which measures velocity distributions along a measuring line.

The velocity profile is measured by ultrasonic multi-wave sensors which have separately 8 MHz and 2 MHz basic frequency. The technique also requires tracer particles as ultrasonic wave reflectors. The measurements were carried out to the upward flow in a vertical rectangular channel made from Plexiglas. The channel dimension is 100 mm x 20 mm x 1700 mm and the flow is at ambient pressure and temperature.

The two-phase flow observation was carried out by measuring velocity profiles of four (4) two-phase flow conditions. Those were obtained by varying liquid velocity and maintaining constant gas velocity.

The velocity profiles are obtained by averaging 50.000 instantaneous velocity profiles. The vertical axis is the velocity and the horizontal axiz is the distance from the wall. However, since it is difficult to measure the velocity in the long distance from the surface of the transducer, only the distance up to the center of the channel is observed. In order to show the variation of water velocity, the red profiles of single-phase liquid flow are presented in addition to the blue ones of two-phase bubbly flow.

In the low liquid velocity, two-phase flow construct core-peak flow since the bubbles tend to move upward in the center of the channel rather than in the vicinity of the wall. This can be observed from the flow of 100 mm/s liquid flow and 2.5 mm/s of gas flow. Meanwhile, in the high liquid velocity, the flow tends to construct wall-peak flow since the bubbles tend to move upward in the vicinity of the wall rather than in the center of the channel. This phenomena can be observed from the flow of 150 mm/s and 200 mm/s liquid flow by constant 2.5 mm/s of gas flow.

The similar condition was also observed by using wire-mesh tomography (WMT) (Richter, 2001). The WMT has a capability of cross-sectional measurement over the channel.

In order to obtain more observation of the flow condition, it is required to measure the velocity profiles not only along wide-side of the channel, as it is presented here, but also the narrow-side of the channel. So that the flow condition in the vicinity of the narrow-side wall can be observed.

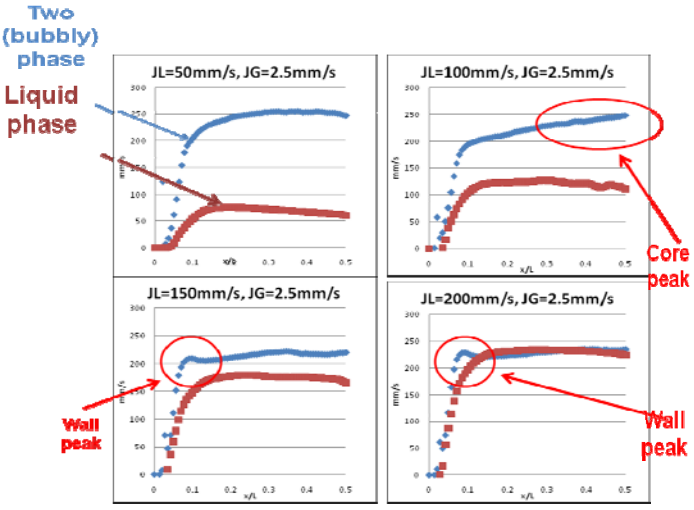

Figure 1. Velocity profiles of four flow conditions

As the results, by controlling the liquid velocity while the gas velocity is constant, the flow condition can be controlled from core-peak condition to wall-peak condition. This observation can be done by using one multi-wave transducer and this result has a good agreement with the previous study using wire-mesh tomography.

Reference

[1] M. K Biddinika, D Ito, H. Takahashi, H. Kikura, M. Aritomi, Multi-wave Sensors for Two-Phase Flow Observations in Vertical Rectangular Channel, *3rd international workshop on process tomography(IWPT-3)*, Tokyo, Japan, No.98(April 17-19, 2009).

A.7 Experimental Study on Self-triggering of Vapor Explosion with Droplet of Lead-Bismuth Eutectic in Water

Minoru TAKAHASHI and Rongyuan SA

1. Introduction

Lead alloy-cooled fast reactor (LFR) offers enhanced inherent safety and reliability due to a number of advantageous physical characteristics: good neutronic performance of the high atomic number, chemical inertness with air and water, high boiling temperature, and low vapor pressure at operating temperatures. It is another economical advantage that steam generators (SG) can be inserted in primary coolant flow in a reactor vessel. However, if SG tubes break, a rapid discharge of water and steam/water mixture into the low-pressure primary coolant circuit (high-temperature lead alloy) forms a dispersed flow, which is called the coolant-coolant thermo-hydrodynamic interactions (CCI). The CCI has the potential of vapor explosion.

In order to solve the thermal-hydraulic safety issue for development of the LFR, it is necessary to use small-scale experiments to investigate the basic influencing factors on violent boiling and/or vapor explosion in LBE droplets-water experiment and to obtain basic experimental data, for example, vapor explosion criteria, peak pressure, debris shape and expanded vapor size.

2. Experimental Apparatus and Procedure

An experiment was conducted to investigate characteristics of thermal-hydraulic interaction between lead-bismuth eutectic (LBE) and water when a LBE droplet dropped into a water pool (Fig. 1). A pure LBE in a ceramic crucible was heated by a high frequency induction heater. The temperature of the droplet was measured by a ceramic-covered K type thermocouple. When the droplet dropped into the water from the crucible, the behavior of the droplets and vapor were recorded by a high-speed camera. Local transient pressure signal was measured by a pressure transducer during the fragmentation. The shapes and sizes of the fragments were determined after collecting the fragments.

3. Results

The violent boiling occurred when the droplet temperature was higher than 350°C (Fig. 2). The violent boiling occurred when the interface temperature was higher than homogeneous nucleation temperature and water temperature was at the room temperature. However, the process was mild, and the peak pressure was limited in low value of 1.5-2.0KPa. With the increase of droplet temperature, the debris of the molten droplet changes from the integral frozen block to discrete flakes, needle type of solid particle and powder. In high temperature range of T_{drop}>350°C, the expansion velocities are faster and the final expanded vapor sizes are larger.

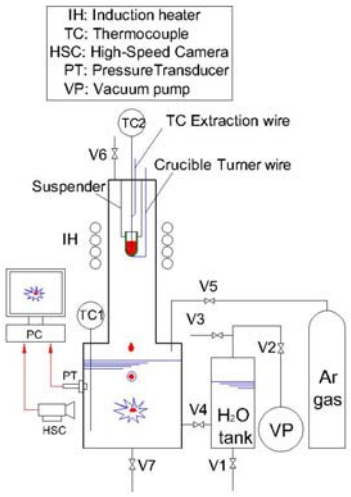

Fig. 1 Experimental apparatus

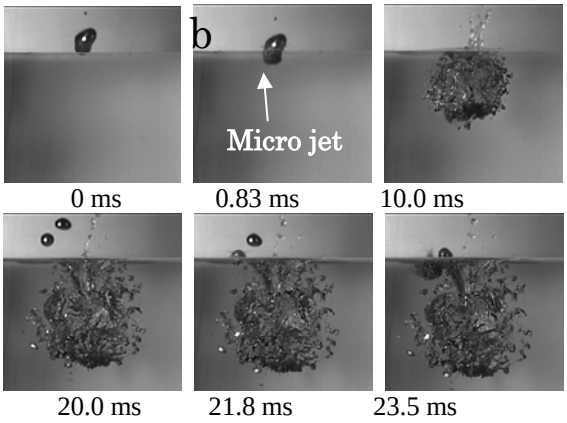

Fig. 2 Behavior of violent boiling for droplet at 400°C and water at 20.5°C

4. Conclusions

Vapor explosion did not occur and violent boiling occurred in the present LBE droplets-water experiment. Fragmentation occurred for droplets at high temperature.

Reference

R. Sa, M. Takahashi, "Experimental Study on Self-triggering of Vapor Explosion with Droplet of Lead-Bismuth Eutectic in Water," *The 13th Int. Topical Meet. on Nucl. Reactor Ther. Hydr. (NURETH-13*), Kanazawa., Japan, Sep. 27-Oct. 2, 2009, N13P1220.

A.8 Effect of Argon Gas Injection on Acoustics Noise and Onset of Sodium Cavitation in Venturi

Minoru TAKAHASHI and Teddy ARDIANSYAH

1. Introduction

Cavitation must be avoided in primary coolant circuits of sodium-cooled fast reactors, or the influence must be minimized in hydrodynamic design of the sodium-cooled fast reactors. Non-condensable gas content in the fluid has an influence on cavitation inception. This gas could act as nucleation sites for the growth of cavitation bubbles and change the onset cavitation condition in case of water cavitation. However, the influence of the non-condensable gas on liquid sodium cavitation has not been investigated in detail. The present experiment is conducted to investigate the effects of argon gas injection on the noise characteristics and onset conditions of sodium cavitation.

2. Experimental Apparatus and Procedure

Liquid sodium cavitation experiment was conducted using a sodium loop facility. This sodium loop facility can be operated at the temperature up to 500°C and at the maximum flow rate of 20 L/min. Argon gas was used as cover gas in an expansion tank. The test section is made of SS-316 equipped with gas injector to inject argon gas into the flowing liquid sodium. The venturi with the inner diameter of 6.5 mm was used to create cavitation bubbles (Fig. 1). The acoustics noise signals generated from cavitation bubbles were measured by using an accelerometer. The downstream pressure of the test section was measured by using a pressure transducer.

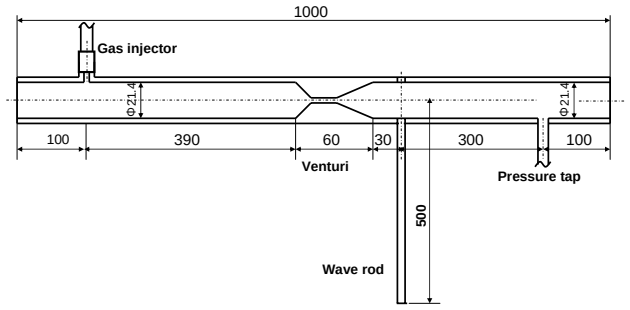

Fig. 1 Venturi for test section

The cavitation coefficient K is defined by

$$K = (P_0 - P_V) \Big/ \left[\rho \left(V_1^2 - V_0^2 \right) / 2 \right] \qquad (1)$$

where ρ is the liquid sodium density, V_1 the velocity at venturi region, V_0 the velocity at downstream region, P_0 the static pressure in the downstream, and P_V the sodium saturation pressure.

The experiment was conducted at liquid sodium stagnant pressure of 0.06-0.18 MPa, liquid sodium temperature of 300°-400°C and argon gas injection flow rate of 0-5 cc/min.

3. Results

Fig. 2 shows the noise intensity against the cavitation coefficient. The cavitation inception condition is around $K \approx 1$ without appreciable influence of argon gas injection. Also, the noise intensity cavitation was not influenced by gas injection at 300° and 400°C. However, the noise intensity peak decreased at 400°C, because of the damp of noise by the gas bubbles. During cavitation conditions, choking-like phenomena were observed in which the superficial velocities of liquid sodium remained relatively constant.

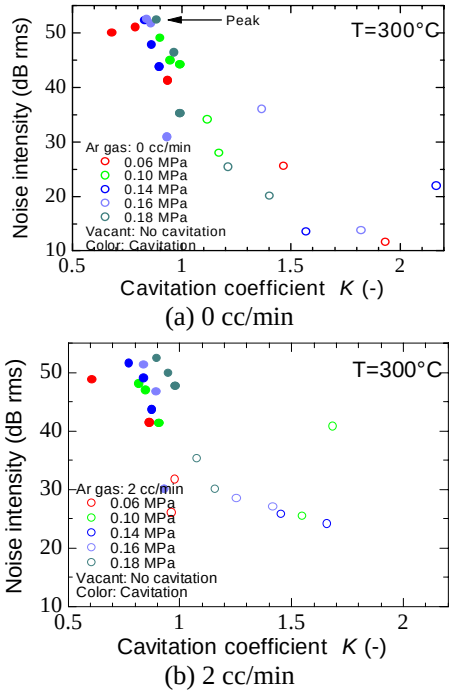

Fig. 2 Noise intensity as a function of cavitation coefficient at 300°C (Vacant symbol: no cavitation, Colored symbol: occurrence of cavitation)

4. Conclusions

Injecting argon gas into the flowing liquid sodium did not alter its noise intensity significantly in developed cavitation conditions both at 300° and 400°C. There was a reduction in the noise intensity peak at 400°C which might be caused by the damp of noise by gas bubbles.

Reference

T. Ardiansyah, M. Takahashi, M. Nakagawa, K. Miura, M. Asaba, "Effect of Argon Gas Injection on Acoustics Noise and Onset of Sodium Cavitation in Venturi," *The 13th Int. Topical Meet. on Nucl.r Reactor Ther. Hydr. (NURETH-13)*, N13P1217, Kanazawa, Japan, Sep. 27-Oct. 2, 2009.

A.9 Active Carbon Recycling Energy System Using Nuclear Power

Yukitaka KATO

INTRODUCTION

Energy supply security is important matter for industrial and economical developments of a society. Steep change and instability of the market prices of primary energy sources is causing economic confusion in any ages. This paper discuss for establishment of energy supply security from the stand point of carbon recycle use. Carbon is the most important energy media for manufacturing industry and social life of human being. Carbon supply security is an essential condition for a sustainable society. In Japan, the supply of fossil fuels of primary energy almost depends on import. Enthalpy of import fuel is 82% (18.9×10^{18} J) of all of using primary energy in Japan (METI, 2007). 17% of fossil fuel is converted in plastics products, and the rest of fossil fuels is consumed for just heat sources. The Kyoto protocol came into effect in 2005. Japan has undertaken obligation to follow the protocol, and is required drastic reduction of carbon dioxide (CO_2) emission. However, CO_2 reduction connects with restriction of usage of carbon resources and causes depression of activity of manufacturing and service industries. Co-establishment of carbon supply security and reduction of CO_2 emission is an important subject for a development of a modern society.

A new energy system in which carbon is reused cyclically was discussed. A carbon recycle system has already existed in nature as a natural carbon neutral system. In this paper, a concept of an Active Carbon Recycling Energy System, ACRES, was proposed against the natural system. CO_2 is regenerated artificially in hydrocarbons consuming a nuclear power with no-CO_2 emission, and re-used cyclically in ACRES. ACRES recycles carbon, and transform energy without CO_2 emission. Because ACRES was expected to solve above carbon problems, the feasibility of ACRES was discussed thermodynamically.

PROPOSAL OF ACRES

Conventional water energy systems and ACRES

ACRES is compared with conventional recycle energy systems in this section. Conventional recycle energy systems based on water is depicted in Fig. 1. Fig. 1(a) shows conventional steam engine in which water/vapor phase change is use for energy conversion. Primary energy is used for evaporation of water, and a phase change from steam to water provides energy output. Fig. 1(b) indicates hydrogen system in which water is decomposed into hydrogen (H_2) and oxygen by energy input, and oxidation of H_2 provides energy output. H_2 energy system is superior to vapor system at long-term energy storage with small loss and higher energy density. However, H_2 needs quite large work for compression up to 700 bars in storage, high-cost security to explosion prevention and system complexity for energy conversion for energy output like fuel cells. Those requirements are still subject for market development of H_2 energy system.

A concept of the proposed ACRES is shown in Fig. 2. Carbon dioxide (CO_2) with/without water is the ground state of carbon. CO_2 is converted into hydrocarbons and alcohols by energy input using some catalytic technologies (Kusama, 1996). Produced hydrocarbon is useful for co-production process. The hydrocarbon provides thermal and electricity energies during oxidation into CO_2. The hydrocarbons are capable to be used as raw material for industrial materials. The hydrocarbon is ease to be stored and transferred under lower compression pressure with small explosion risk in comparison with H_2. The hydrocarbons have quite high affinity with common manufacturing industries. If the carbon recycle system can be established thermally and kinetically, it is expected that the system is diffused easily into conventional industries. Natural carbon recycle energy system has already been existed by plant lives in nature, and an ideal recycle system. However, potential amount of bio-mass is not enough for a modern society. Especially it is less than 10 % of all demand of energy in Japan. The natural recycle system is not enough for energy demand in Japan (Kameyama and Kato, 2005). Then, an artificial active carbon recycle system was proposed as ACRES in this study. Feasibility of ACRES was discussed from enthalpy balances in this paper.

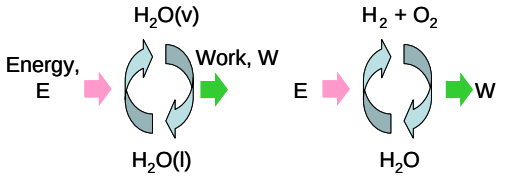

Fig. 1 Conventional recycle energy systems using water

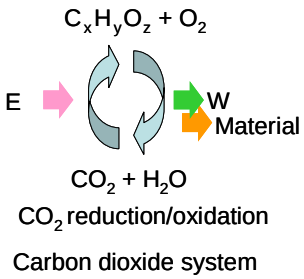

Fig. 2 Concept of ACRES

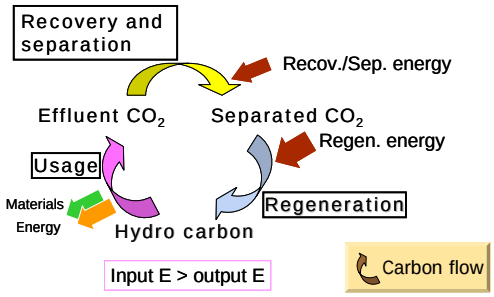

Fig. 3 The three elemental processes in ACRES.

Structure of ACRES

The structure of ACRES shown in Fig. 3 consists of three elemental processes of hydrocarbon usage, CO_2 recovery and separation, and hydrocarbon regeneration. In the usage process, the hydrocarbon can be used for both heat source and material. CO_2 generated from hydrocarbon consumption is recovered by physical and chemical sorptions. Sorbed CO_2 in a sorption material is separated thermally from material by a heat input. This process produces high-concentrated CO_2. Recovered CO_2 is regenerated into hydrocarbon in the regeneration process. The regeneration process is endothermic and need energy input. In ACRES, total energy input at recovery and separation (E_S), and regeneration (E_R) should be larger than the energy output at the usage process (E_U).

$$E_S+E_R > E_U \quad (1)$$

ACRES is energy consumption process, then, a discussion of the energy balance of the system is required for the feasibility evaluation of the system.

ENTHALPY EVALUATION OF ACRES

Practical hydrocarbons are examined those availability in ACRES by an enthalpy balance evaluation.

Availability of ACRES with methane

Methane as a basic hydrocarbon was discussed firstly. Structure of an ACRES in which methane was recycled was shown in Fig. 4. In usage process of methane, methane combustion (Eq. 2) produces heat, methane steam reforming (Eq. 3) produces hydrogen, and polymerization of methane (Eq. 4) produces polymeric materials.

$$CH_4+2O_2 \rightarrow CO_2+4H_2O \quad (2)$$

$$CH_4+H_2O \rightarrow 4H_2+CO_2 \quad (3)$$

$$xCH_4 \rightarrow (-CH_2-)_x + x/2H_2 \quad (4)$$

CO_2 is recoverable by physical adsorptions of active carbons or zeolites, or a chemical sorption by carbonation of calcium oxide (CaO) at the CO_2 recovery and separation process. CaO is absorbable chemically CO_2 at temperatures of 500 - 800°C (Eq. 5). CaO can remove CO_2 from hydrocarbon reaction system at the reaction temperature for CO_2 production with small sensible heat loss, and also enhance reaction rate and yield of the CO_2 production reaction (Kato, 2003).

$$CaO + CO_2 \rightarrow CaCO_3 \quad (5)$$

In a process of methane regeneration form CO_2, a two-step reaction of hydrogen production by water electrolysis and methanation of CO_2 with the hydrogen (Eqs. (6) and (7)) is available.

$$4H_2O \rightarrow 4H_2+2O_2 \quad (6)$$

$$CO_2+4H_2 \rightarrow CH_4+2H_2O \quad (7)$$

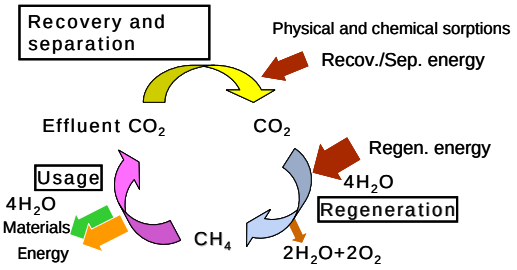

Fig. 4 Structure of ACRES with methane

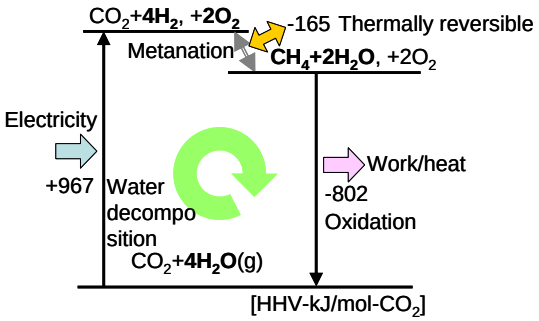

Fig. 5 Enthalpy balance of ACRES with methane

Enthalpy balance of ACRES for methane is shown in Fig. 5. Required enthalpies per one molecule of methane for the processes of usage and regeneration are depicted in high-heat value (HHV). The recovery and separation process needs relatively smaller enthalpy than one of other processes, and is capable to be driven by waste heat at relatively lower-temperature (less than 100°C). Because enthalpy evaluation for the recovery and separation process had uncertainties, the process was not accounted in this system evaluation. Regeneration process was assumed that hydrogen was used for hydrocarbon regeneration by the two-step reaction in Eqs. (6) and (7). Production of H_2 of 4 mol needs an enthalpy of 967 kJ/mol-CH_4. Methanation of CO_2 with H_2 is an exothermic reaction of 165 kJ/mol-

CH_4. Regenerated methane has a reaction enthalpy of 802 kJ/mol-CH_4. A circulation rate (η) which is a formation enthalpy ratio between regenerated hydrocarbon and required hydrogen is defined as following.

$$\eta = \frac{\text{Formation enthalpy of regenerated hydrocrabon}}{\text{Formation enthalpy of hydrogen of required amount for hydrocarbon regeneration}} \quad (8)$$

η of methane ACRES was 83%. It means that enthalpy loss generates in methanation process. However, when the same amount of enthalpy is stored in methane or H_2, methane storage pressure is reduced to one third for H_2 storage. Compression work can be reduced also to 1/3 for methane storage in comparison with H_2 storage. For comparison of energy efficiency between ACRES and H_2 system, a comprehensive discussion is needed. A chemical reaction equilibrium for CO_2/methane system is shown in Fig. 6. It was assumed in the evaluation that the reaction proceeded at an equivalent ratio under a pressure of 100 kPa. CO_2/methane system is reversible around 500°C. Exothermic heat of methanation is recoverable by another endothermic reactions like a steam reforming. Enthalpy loss of methanation can be minimized by coupling with other endothermic reaction processes.

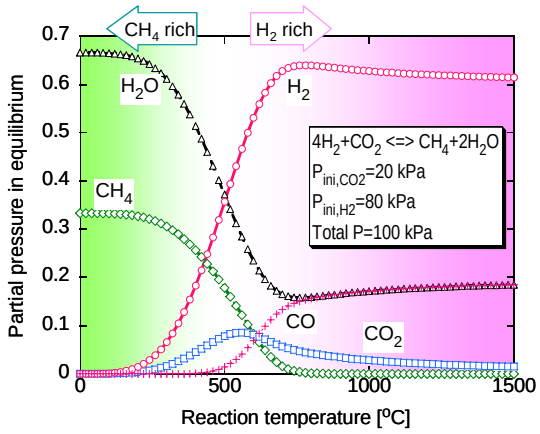

Fig. 6 Chemical reaction equilibrium for CO_2/methane system

ηs of some hydrocarbons were calculated.

CO (104%) > methanol (93%) > ethanol (88%) > methane (83%) (9)

A higher η means that enthalpy loss for regeneration of the hydrocarbon becomes smaller. Methanol and ethanol are generally in liquid phase, ease for transportation and storage, and applicable to vehicle. Carbon monoxide (CO) has the highest η in the hydrocarbons.

VALUE OF ACRES

Value of ACRES is that the system uses carbon cyclically, and does not emit CO_2 into atmosphere. Non-carbon primary energy sources are essential for ACRES. ACRES with CO was the most effective recycle system in this study. CO regeneration needs heat at a temperature above 700°C. High-temperature gas reactor (HTGR) was the most suitable energy source for ACRES because of high-temperature output up to 950°C with non-carbon emission and enough amount of fuel for a country demand (Fujikawa, 2004). Thermo-chemical reduction of CO_2 is ideal process for reduction method like water reduction. Electrolysis of CO_2 with an electric output from a power plant of a HTGR is also one of candidate. High-temperature electrolysis of CO_2 using both heat and electricity outputs from HTGR is expected to have higher efficiency than atmospheric electrolysis like water high-temperature electrolysis.

CONCLUSIONS

For an establishment of a practical ACRES, selections of recycling hydrocarbon media and primary energy source for the system drive were important. Methane was the most ease material for regeneration and cyclic use. Methanol or ethanol with ACRES was suitable for vehicle use. CO was the most suitable for a recycle media in ACRES, because CO had higher energy density and affinity than H_2 to chemical processes in conventional manufacturing industries. HTGR was a candidate of primary energy source of ACRES. ACRES with CO driven by heat output from HTGR was the most applicable combination. ACRES was expected to have higher efficiency than H_2 energy system and be a candidate of energy systems for establishment of carbon supply security in a modern society.

References

- Fujikawa, S. et al., Achievement of Reactor-Outlet Coolant Temperature of 950°C in HTTR, *J. Nucl. Sci. Technol.*, **41**(2004), 1245.
- Kameyama, H. and Y. Kato ed., *HONEBUTO Energy Road Map (Honebuto no Energy Road Map)*, Kagaku-Kogyo-Sha, Tokyo, Japan (2005)
- Kato, et. al., Study on a Regenerative Fuel Reformer for a Zero-Emission Vehicle System, *J. Chem. Eng. Japan*, **36** (2003) pp. 860.
- Kusama, H. et al., CO_2 hydrogenation to ethanol over promoted Rh/SiO_2 catalysts, *Catalysis Today*, **28** (1996) 261.
- Minister of Economy, Trade and Industry (METI), Figure No. 201-1-3: Energy balance of Japan in 2004, *The White Paper for Energy in 2006 FY*, METI, Tokyo, Japan (2006)

A.10 Dehydration and Hydration Behavior of Mg-Al Mixed Hydroxide for Chemical Heat Storage

Junichi RYU and Yukitaka KATO

Introduction

The heat storage technologies of waste heat from industrial processes and co-generation systems will contribute to "Energy Saving". Especially, chemical heat storage technology is very interesting in view of their heat storage capacity. In recent years, the technologies of chemical heat pump and chemical heat storage are widely studied for the reduction of energy consumption and CO_2 emission. Chemical heat pump system with the reaction between magnesium oxide (MgO) and water vapor has been reported by our group. [1]

$$MgO + H_2O \rightleftarrows Mg(OH)_2 \quad \Delta H = -81.2 \text{ kJ mol}^{-1}$$

In this system, dehydration of magnesium hydroxide as heat storage operation will proceed at 250°C thermodynamically; however, thermal energy above 350°C is required practically. Recently, new type material for chemical heat storage – metal salt added magnesium hydroxide, and magnesium containing mixed hydroxide – were proposed by our group. These materials can store thermal energy around 280 °C. In this work, dehydration and hydration behavior of Mg-Al mixed hydroxides were studied and it were evaluated as chemical heat storage material. [2,3]

Experimental

Mg-Al mixed hydroxides were prepared by co-precipitation method. The reaction between sample and water vapour was tested by thermogravimetric method. The molar fraction of hydroxide in the sample and reaction conversion were calculated from the weight change of sample.

Results

The thermal decomposition curves of Mg-Al mixed hydroxides are shown in Figure 1. Decomposition, that is, dehydration of $Mg(OH)_2$ started from about 150°C, while those of the Mg-Al mixed hydroxides shifted to a lower temperature as the Al content increased.

Figure 2 shows the hydration behaviour of $Mg_{0.75}Al_{0.25}(OH)_{2.25}$ under the reaction temperature of 110°C and vapor pressure of 57.8 kPa, after dehydration at 250°C for 30 min. The values of hydration conversion was 39.8%.

The heat-storage capacities of $Mg_{0.75}Al_{0.25}(OH)_{2.25}$ was estimated as 594 kJ kg^{-1} and this value is 6 times higher than authentic $Mg(OH)_2$ under same reaction condition.

The reaction mechanism and the stability of these materials for cyclic operations of hydration/dehydration under practical conditions should be studied further.

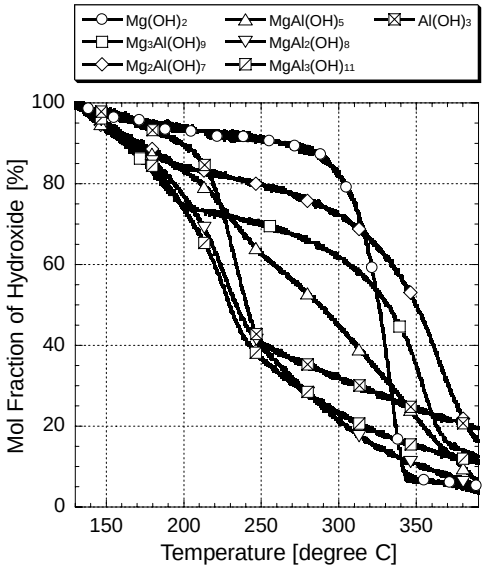

Figure 1 Thermal decomposition curves of Mg-Al mixed hydroxides.

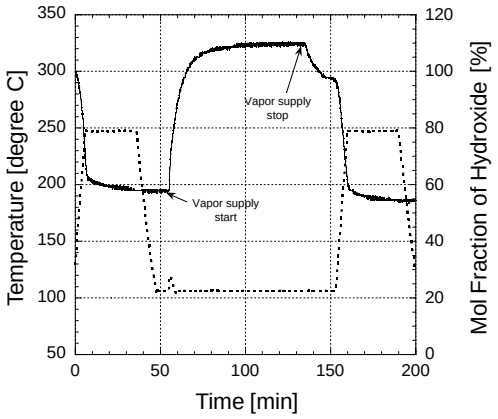

Figure 2 Dehydration and hydration behavior of $Mg_{0.75}Al_{0.25}(OH)_{2.25}$.

References

[1] Y. Kato et al., *Appl. Therm. Eng.*, **16**, 852 (1996).
[2] J. Ryu et al., *J. Chem. Eng. Jpn.*, **40**, 1281 (2007).
[3] J. Ryu et al., *Chem. Lett.*, **37**, 1140 (2008).

A.11 Calculation of Heavy-Ion Stopping Power in Warm Dense Uranium Targets Using Temperature-Dependent Dielectric Response Functions

Yoshiyuki OGURI and Jun HASEGAWA

1. Introduction

For detailed design of ion-driven warm dense matter (WDM) experiments[1], the stopping power of heavy projectiles in targets with a given temperature and a given density must be numerically examined with an acceptable accuracy under a reasonable modeling of the beam-target interactions.

We have shown that the dependence of projectile stopping on the target temperature and density is not negligible in hydrodynamic behavior of low-Z (aluminum) targets[2]. In this analysis we applied a robust but simple binary encounter model[3] for the energy deposition from the projectile to the electrons in the target. To evaluate the electron phase-space distribution in each target atoms in any temperature and density, we used a finite-temperature Thomas-Fermi (TF) model[4]. However, binary encounter models can take into account only the close collisions, and excitations of collective electron motions are ignored. Additionally, the accuracy of TF calculations is sometimes not enough for light atoms.

In this paper, to overcome the problems above, we introduce a numerical method based on dielectric response functions for calculation of the heavy-ion stopping in warm dense targets, instead of the simple binary encounter model. Also we examine targets of a high-Z element, for which the TF model is more realistic. As a high-Z element, we apply uranium (U, Z = 92), since the equation of state of such a heavy element at high pressures could be important, e.g., for transient hydrodynamic behaviors in severe nuclear accidents. Effects on the homogeneity of energy deposition profile in sub-range targets during irradiation by pulsed heavy-ion beams are discussed.

2. Numerical method

In this work, each atom in the target with arbitrary temperature and density was described as an inhomogeneous electron gas. The radial electron density $n_e(r)$ and mean velocity distribution $v_e(r)$ in a target atom were calculated with a finite-temperature TF model[4].

The projectile stopping power was calculated based on the Brandt-Kitagawa (BK) theory[5] as in the following. To obtain the total electronic stopping cross section S_e, we integrated differential cross sections corresponding to the energy deposition to each electron shell in the target atom. In a similar manner to the method by Ziegler[6], we have

$$S_e = \frac{z_p^2 e^4}{4\pi\varepsilon_0^2 m v_p^2}\int_0^{R_{WS}} n_e(r)L(r)\cdot 4\pi r^2 dr, \qquad (1)$$

where z_p and v_p denote the atomic number and the velocity of the projectile, respectively. ε_0 and m are, respectively, the dielectric constant of vacuum and the electron mass. The parameter R_{WS} denotes the Wigner-Seitz radius determined by the target atomic density N_{atom}. The function $L(r)$ is the r-dependent stopping number corresponding to the energy transfer to the electron shell at a radius r. Using the BK effective charge theory[5], we have

$$L(r) = \frac{i}{\pi\omega_p(r)^2}\int_0^\infty \frac{dk}{k}\left|\frac{\rho^*(k)}{z_p}\right|^2 \int_{-kv}^{kv} \omega\, d\omega\left(\varepsilon(k,\omega)^{-1}-1\right), \qquad (2)$$

where $\rho^*(k)$ is the Fourier transform of the total charge density distribution around the nucleus approximated by

$$\rho(r) = z_p\delta(r) - \frac{N}{4\pi\Lambda^3}\left(\frac{\Lambda}{r}\right)e^{-r/\Lambda}, \qquad (3)$$

with a screening length Λ. The local electron density in the target is described in terms of the local plasma frequency

$$\omega_p(r) = \sqrt{\frac{e^2 n_e(r)}{\varepsilon_0 m}}. \qquad (4)$$

In Eq. (2), $\varepsilon(k, \omega)$ is the longitudinal dielectric constant which depends on the wave-number k and the angular frequency ω:

$$\varepsilon(k,\omega) \equiv \varepsilon_{Re}(k,\omega) + i\varepsilon_{Im}(k,\omega), \qquad (5)$$

where ε_{Re} and ε_{Im} denote, respectively, the real and the imaginary part of the dielectric constant.

For applications to hydrodynamic calculations, we have to calculate the response of various electron gases ranging from quantum degenerate plasmas to classical hot plasmas. For this purpose we applied an expression for the dielectric function of plasmas of all degeneracies incorporating both thermal and quantum effects. The real part is given by[7]

$$\varepsilon_{Re}(k,\omega) = 1 + \frac{\chi_0^2}{4z^3}\left(g(u+z) - g(u-z)\right), \qquad (6)$$

where the function $g(x)$ is defined by

$$g(x) \equiv \int_0^\infty \frac{y\,dy}{e^{Dy^2-\eta}+1}\ln\left|\frac{x+y}{x-y}\right| = -g(-x), \qquad (7)$$

with

$$\chi_0^2 \equiv \frac{1}{\pi k_F a_0}, \qquad (8)$$

and Bohr radius a_0. In the formulae above, we have

introduced usual reduced variables

$$u \equiv \frac{\omega}{k v_F}, \quad z \equiv \frac{k}{2k_F}, \tag{9}$$

with the Fermi wave number k_F. For the imaginary part, we have[7]

$$\varepsilon_{Im}(k,\omega) = \frac{\pi\chi_0^2}{8z^3}\left(\frac{1}{D}\right)\ln\left\{\frac{1+e^{\eta-D(u-z)^2}}{1+e^{\eta-D(u+z)^2}}\right\}, \tag{10}$$

where parameters η and D denote, respectively, the chemical potential μ and the Fermi energy E_F normalized to the temperature $k_B T$:

$$\eta \equiv \frac{\mu}{k_B T}, \quad D \equiv \frac{E_F}{k_B T}. \tag{11}$$

The projectile charge state q can be evaluated using a scaling formula[6]

$$q = z_p\left\{1 - e^{-0.95(y_{rel}-0.07)}\right\}, \tag{12}$$

with

$$y_{rel} \equiv \frac{v_{rel}}{v_0 z_p^{2/3}}. \tag{13}$$

In the above formula, $v_0 = 2.19\times10^8$ cm/s is the Bohr velocity. In order to include the enhancement of projectile ionization in a high temperature environment[8], we used the relative velocity v_{rel} between the projectile and the target valence electrons instead of the projectile velocity, according to the BK theory. If isotropic motion of the valence electrons is assumed, we have

$$v_{rel} = \frac{\left(v_p + v_{ve}\right)^3 - \left|v_p - v_{ve}\right|^3}{6 v_p v_{ve}}, \tag{14}$$

where v_{ve} is the averaged valence electron velocity. In order to obtain v_{ve}, the electrons in the target atom were partitioned into the core and the valence component using the method by Cappelluti[9]. The core-valence boundary $r = r_c$ can be determined by an r-dependent energy variable

$$W(r) \equiv \int_0^r 4\pi r'^2 w(r') dr', \tag{15}$$

which has the outermost minimum at $r = r_c$. In the formula above, $w(r)$ is the total energy density given by

$$w(r) = w_{kin}(r) + w_{ei}(r) + w_{ee}(r), \tag{16}$$

with

$$w_{kin}(r) \equiv \frac{m v_e(r)^2}{2} n_e(r), \tag{17}$$

$$w_{ei}(r) \equiv -\frac{Ze^2}{4\pi\varepsilon_0 r} n_e(r), \tag{18}$$

$$w_{ee}(r) \equiv \frac{1}{2}\left(\frac{e^2}{4\pi\varepsilon_0}\right) n_e(r) \int_{r'}^{R_{WS}} \frac{n_e(r')}{|r-r'|} \cdot 4\pi r'^2 dr'. \tag{19}$$

Using the boundary $r = r_c$, the averaged velocity of valence electrons was evaluated by

$$v_{ve}(r) = \frac{\int_{r_c}^{R_{WS}} v_e(r) n_e(r) dr}{\int_{r_c}^{R_{WS}} n_e(r) dr}. \tag{20}$$

Using the projectile charge state q given by Eq. (12), the screening radius Λ is calculated as

$$\Lambda = \frac{0.48\left(N/z_p\right)^{2/3}}{z_p^{1/3}\left\{1-\left(N/z_p\right)/7\right\}}, \tag{21}$$

where N is the number of electrons bound in the projectile ion and is given by $N \equiv z_p - q$. Thus the form factor $\rho^*(k)$ in Eq. (3) was calculated by

$$\rho^*(k) = z_p\left\{\frac{q + (k\Lambda)^2}{1 + (k\Lambda)^2}\right\}. \tag{22}$$

Finally, the total stopping cross section S was obtained by summing up S_e and the nuclear stopping cross section[10].

3. Results and discussion

Based on the method above, we calculated stopping cross sections of U targets with different conditions as a function of the projectile energy from 10 keV/u to 10 MeV/u. Sodium (Na, $z_p = 11$) was applied as the projectile species.

Figure 1(a) shows the temperature dependence of the stopping cross section plotted as a function of the projectile energy. The target density ρ is fixed at the sold density ρ_{solid}. Note that this curve is equivalent to a "Bragg peak", if the abscissa is converted to the penetration depth into the target. We see that the change of the stopping power due to the temperature rise is so small that no serious degradation is expected for the heating homogeneity. For comparison, evaluated values on a well-established database[11] are plotted in this figure. These are well-reproduced by the calculation especially for the cold target, except for low projectile energies.

Figure 1(b) illustrates the result of calculation, where the target density has been reduced to 20% of the solid density. One sees that compared with Fig. 1(a), the peak height more remarkably increases when the target is heated to $kT = 100$ eV. Nevertheless, at projectile energies far away from the peak, the temperature effect is relatively small.

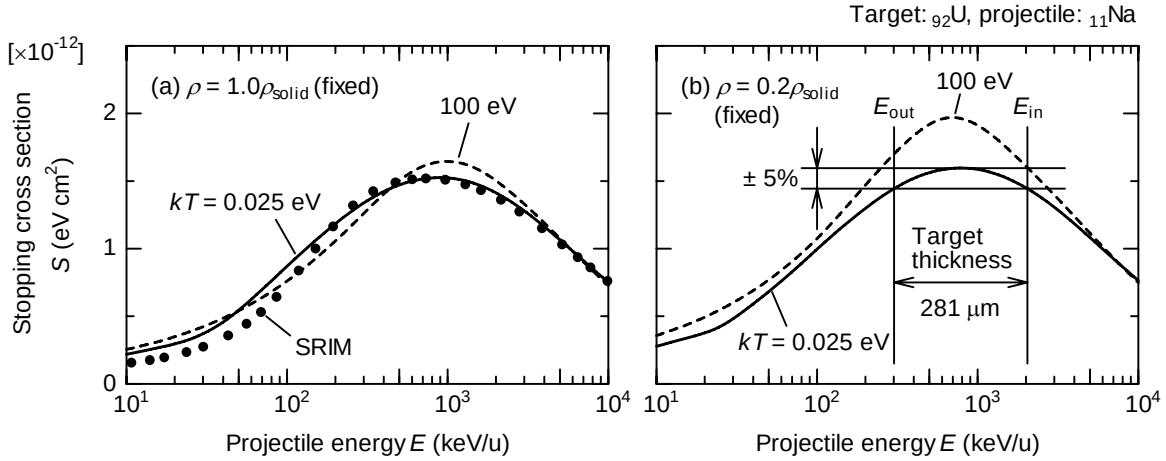

Fig. 1: Temperature-dependence of the stopping cross section of $_{92}$U targets with (a) $\rho = 1.0\rho_{solid}$ and (b) $\rho = 0.2\rho_{solid}$ (foam) for $_{11}$Na projectiles as a function of the projectile energy. The SRIM[11] data are plotted for comparison in the figure (a).

For experiments with the $\rho = 0.2\rho_{solid}$ foam target, by using the solid curve in Fig. 1(b), we can determine a possible combination of the target thickness and the projectile energy to achieve an energy deposition profile with a given homogeneity. If the limit of the acceptable inhomogeneity is ±5% for the room-temperature target, we see from the figure that the incident energy E_{in} and the exit energy E_{out} should be 2.04 MeV/u and 302 keV/u, respectively. This corresponds to an energy loss of 85% of the incident projectile energy. By integrating $1/(N_{atom}S) = (-dE/dx)^{-1}$ from E_{in} to E_{out}, the target thickness is calculated to be 281 μm for the $\rho = 0.2\rho_{solid}$ target.

On the other hand, if a target with the same thickness is heated up to kT = 100 eV, the projectile energy behind this target decreases down to

$$E_{out} = E_{in} - \int_0^{281\,\mu m} \left(-\frac{dE}{dx}\right)_{kT=100\ eV} dx = 66\ \text{keV/u}. \quad (23)$$

In this case, from Fig. 1(b), we see that the inhomogeneity of the energy deposition increases up to ±38%. This is due to the increases of the stopping power with the temperature at any depth in the target.

4. Conclusions

The dielectric response functions of plasmas with all degeneracies were successfully applied to the calculation of heavy-ion stopping in the beam-heated U target. We found that the stopping power increases with the temperature, especially at low target densities. This result is similar to that previously obtained based on the binary encounter model for low-Z target, although the observed temperature effect was relatively small.

In order to minimize the inhomogeneity of the energy deposition profile in ion-driven WDM experiments, careful attention should be paid for the combination of the projectile energy and the target thickness, not only for low-Z but also for high-Z targets.

References

[1] L. R. Grisham, *Phys. Plasmas*, **11**, pp. 5727–5729 (2004).
[2] Y. Oguri and J. Hasegawa, *Bull. Res. Lab. Nucl. Reactor.*, **32**, pp.23–25 (2008).
[3] E. Kührt and R. Wedell, *Phys. Lett.*, **86** A, pp. 54–56 (1981).
[4] D. Salzmann, *Atomic Physics in Hot Plasmas* (Oxford University Press, New York, 1998), ISBN 0-19-510930-9.
[5] W. Brandt and M. Kitagawa, *Phys. Rev.* B. **25**, pp. 5631–5637 (1982).
[6] J. F. Zielgler, J. P. Biersack and U. Littmark, *The Stopping and Range of Ions in Solids, Volume 1 of the Stopping and Ranges of Ions in Matter* (Pergamon Press, 1985), ISBN 0-08-021603-X.
[7] N. R. Arista and W. Brandt, *Phys. Rev.* A **29**, pp. 1471–1480 (1984).
[8] K. Shibata, K. Tsubuku, T. Nishimoto, J. Hasegawa, M. Ogawa, Y. Oguri and A. Sakumi, *J. Appl. Phys.* **91**, pp. 4833–4839 (2002).
[9] E. Cappelluti and L. D. Site, *Physica* A **303**, pp. 481–492 (2002).
[10] W. D. Wilson, L. G. Haggmark and J. P. Biersack, *Phys. Rev.* B **15**, pp. 2458–2468 (1977).
[11] J. F. Ziegler and J. P. Biersack, *Computer Code SRIM2006*, United States Naval Academy, Annapolis, MD, http://www.srim.org (2006).

A.12 Performance Evaluation of a μ-PIXE System with Glass Capillary Beam Focusing

Jun HASEGAWA and Yoshiyuki OGURI

A compact μ-PIXE system using a tapered glass capillary for beam focusing has been developed. The purpose of this study is to evaluate the performance of this novel μ-PIXE system and reveal limiting factors with the help of numerical simulations. Figure 1 shows an experimental setup for μ-PIXE analysis. A capillary optics and its control devices are installed in a large vacuum chamber, which is evacuated by a turbo molecular pump to less than 10^{-3} Pa. At the center of the chamber, a borosilicate glass capillary is mounted on a stainless-steel support rod. The fabrication of the capillary is described elsewhere[1]. The typical inlet and outlet diameter of the capillary are 0.8 mm and 10-20 μm, respectively. A 2-MeV proton beam from a Tandem accelerator is injected into the capillary inlet and a micro beam is extracted from the capillary outlet. Two remote-controlled actuators adjust the tilt angle of the support rod in horizontal and vertical planes to align the capillary on the beam axis. To confirm the alignment of the capillary optics, beam spot patterns are photographed by imaging plates every time the capillary is replaced. A target for μ-PIXE analysis is located about 1 mm downstream from the capillary outlet. Two motorized stages move the target folder in horizontal and vertical directions with a minimum step of 1 μm to scan the target two-dimensionally. A Si-PIN detector and a silicon charged-particle detector are installed at ±135º to measure X-rays and backscattered protons, respectively. A Mylar film of 100 μm thick is located in front of the X-ray detector to stop backscattered protons. During the measurement the capillary glass wall emits fluorescence due to proton bombardment, causing the background noise on the silicon charged-particle detector. To attenuate the fluorescence, a carbon foil of 100 μg/cm^2 is also put in front of the detector. The signals from these two detectors are processed by amplifiers and recorded by PC-controlled multichannel analyzers.

To check the performance of the μ-PIXE system, a copper thin plate was mounted on an aluminum target holder and scanned with a 2-MeV proton micro beam extracted from a ø10-μm capillary. The variation of X-ray yield y is expressed as a function of the beam center position x as follows:

$$y(x) = r^2\{\cos^{-1}(x/r) - 0.5\sin[2\cos^{-1}(x/r)]\}. \qquad (1)$$

Here, r is the beam radius. By fitting the measured Cu-K X-ray intensity profile with this formula, we evaluated the effective beam spot size on the target. For the demonstration of two-dimensional element mapping, cupper fine mesh (ø8-μm wire, 1000 mesh/inch) was used in the present study. A 2-MeV proton micro beam from the ø10-μm capillary scanned the mesh fixed on a sheet of graphite. The two-dimensional distribution of copper was reconstructed from Cu-K X-ray intensities normalized by backscattered proton counts.

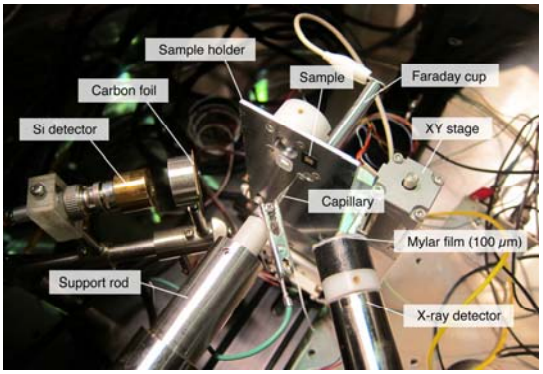

Fig. 1. An experimental setup for μ-PIXE analysis using a tapered glass capillary.

A silicon charged-particle detector mounted on the target holder measured the energy spectra of protons focused by the capillary. A 50-μm thick tantalum plate with a pinhole of 100 μm diameter and a 0.8-μm thick aluminum foil were located immediately in front of the detector to increase the spatial resolution and to prevent localized proton dose on the detector, respectively. To examine the energy spectra of protons scattered in the capillary separately, the detector assembly was set 15 cm downstream from the capillary outlet, resulting in an angular resolution of 0.67 mrad.

We investigated the trajectories of protons in the tapered glass capillaries by a Monte-Carlo code, which was originally developed for this purpose. The code takes into account only elastic collisions between protons and nuclei in the capillary wall, so the classical Rutherford formula is used to calculate the scattering cross sections. On the other hand, the energy loss of protons is evaluated from the electronic stopping power given in SRIM2008. We performed Monte-Carlo calculations by using the shape data of the capillary wall actually used in experiments. The number of incident particles was typically 10^6.

Figure 2 shows a beam spot pattern recorded on an imaging plate when we used a capillary with an outlet diameter of 20 μm. Since this image was taken far from the capillary outlet (65 cm downstream), the pattern expresses the divergence angle distribution of protons extracted from the capillary outlet. The figure shows that the micro beam obviously consists of two different components. The central intense spot (called “core” in this paper) is attributed to protons passing through the capillary

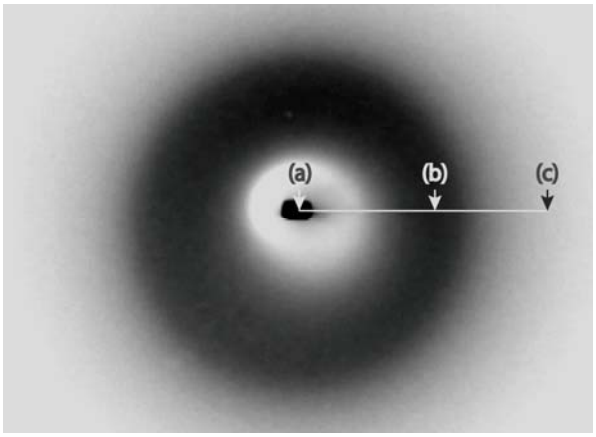

Fig. 2. The angular distribution of protons extracted from a ø20 μm capillary.

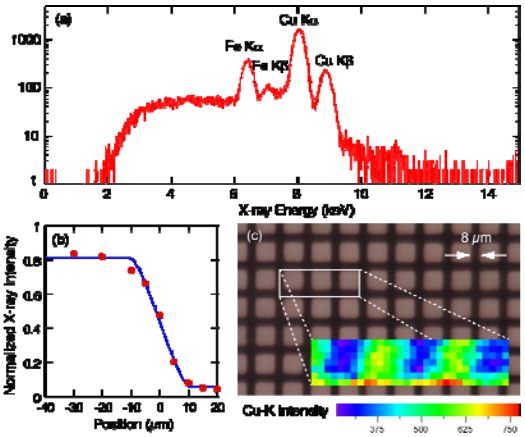

Fig. 3. (a) A typical X-ray spectrum measured for a copper plate target. (b) A Cu-K X-ray intensity profile measured at the edge of the copper plate (circular dot) and a fitted curve based on Eq. (1) (solid line). (c) A magnified photograph of copper fine mesh and a copper distribution reconstructed from the Cu-K X-ray intensities.

without collision; the surrounding doughnut-shape pattern (called "halo") is due to protons scattered by the capillary inner wall. Note that the signal at the core was saturated because the beam intensity of the core was much higher than that of the halo. The divergence angle of the core was around 1 mrad in this case, but it can change depending on the incident beam optics. On the other hand, the averaged divergence angle of the halo component was 7-8 mrad. The inner edge, i.e. the minimum divergence angle, of the halo is determined by the taper angle of the capillary inner wall near the outlet. Since the halo contributes X-ray production in the target as well as the core, it affects the spatial resolution of μ-PIXE measurement, which will be discussed based on results from Monte-Carlo simulations later.

A typical X-ray spectrum obtained in the copper plate measurement is shown in Fig. 3a. Except for large Cu-K lines, one can see relatively large Fe-K lines, which probably come from the chamber wall (stainless steel) bombarded by backscattered protons. In Fig. 3b, the integrated count of Cu-K lines are plotted as a function of the beam center position (circular dot). These X-ray counts were normalized by the total RBS count measured by the silicon detector. A curve fitted to the data by Eq. (1) is also shown in the figure (solid line). The effective beam diameter evaluated from the fitted curve was 20.6 μm, which is roughly twice larger than the capillary outlet diameter (10 μm). This result indicates that the halo component with larger divergence angle may degrade the spatial resolution of the measurement. A magnified photograph of the cupper fine mesh and a two-dimensional distribution of copper reconstructed from observed Cu-K X-ray intensities are shown in Fig. 3c. In the element mapping, the beam current from the capillary was around 0.1 nA and the measurement time was 30 s for each position. By using a step size (2 μm) smaller than the beam spot size, thin copper wires (~8 μm) were well resolved in the reconstructed image even though the effective beam spot size (~20 μm) is much larger than the wire width.

The energy spectra of protons observed at different divergence angles are shown in Fig. 4. The measurement points are indicated in Fig. 2 with arrows. The energy spectrum of the core component (Fig. 4a) was very sharp even though it had a small low-energy tail, which was probably attributed to scattering at the detector pinhole edge. On the other hand, in the energy spectra taken for the halo component (Fig. 4b and 4c), the peak position of the spectrum shifted towards the lower energy side with increasing divergence angle. Moreover, the spectra were much broader than that of the core, indicating that almost all halo particles lost their energy because of elastic and inelastic collisions with atoms in the capillary wall. However, thanks to relatively small energy losses (< 10% of the initial energy) in most cases, the halo particles can still contribute the X-ray yield in μ-PIXE measurement.

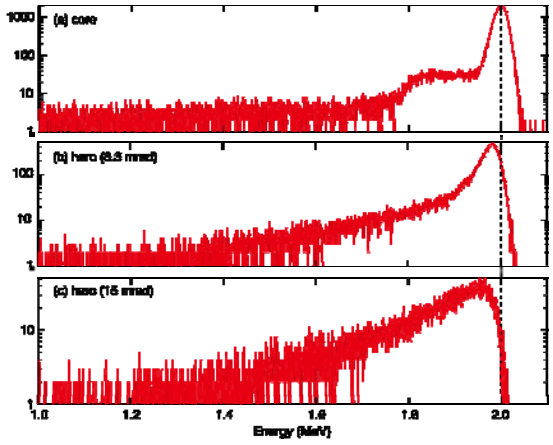

Fig. 4. Proton energy spectra of core and halo components in a micro beam produced by a ø20-μm tapered capillary. The divergence angles corresponding to the measurement points are indicated in Fig. 2 with arrows.

Figure 5a shows proton trajectories in a ø20-μm capillary obtained by a Monte-Carlo simulation. Note that

this figure includes trajectories only for the protons passing through the capillary. Obviously, only a small part of the capillary near the tip (≤0.5 mm from the tip) could contribute the beam focusing, meaning that almost all particles hitting at the rest part of the capillary were lost in the capillary wall. One of the possible explanations for this result is that since the capillary wall has a convex shape, particles scattered towards the capillary outlet need to run relatively long path in the capillary wall to escape from it, leading to serious energy losses and deflections due to succeeding collisions. The calculated energy spectrum of the halo particles is shown in Fig. 5b. The spectrum has a low-energy tail similar to those in the spectra shown in Fig. 4. A two-dimensional distribution of particles at the detector plane (65 cm downstream) is also shown in Fig. 5c. The beam spot pattern recorded on the imaging plate was well reproduced by the Monte-Carlo simulation. Under this condition, the calculated beam-focusing factor was 1.66.

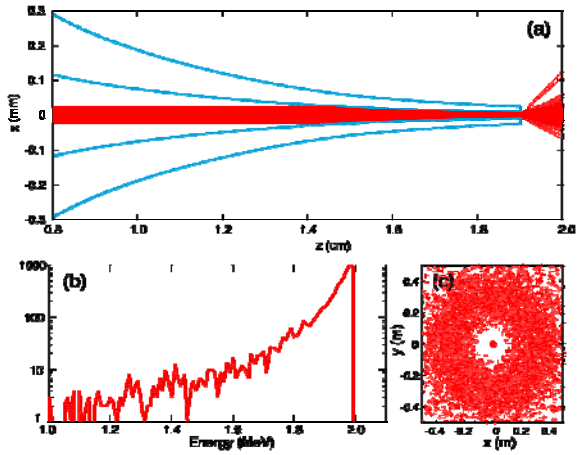

Fig. 5. (a) Proton trajectories in a tapered capillary (ø20 μm) calculated by a Monte-Carlo simulation. (b) The energy spectrum and the spatial distribution of protons on a detector plane are also shown.

The particle distributions at various distances from the capillary outlet are shown in Fig. 6. The beam size just behind the capillary outlet (Fig. 6a) is well defined by the outlet size (10 μm), but the particle distribution begins to spread with increasing distance (Fig. 6b and 6c). At 7 mm from the outlet, the core component and the halo component are almost separated, so the enhancement of beam intensity is no longer available at this point. Figure 6d shows the beam intensity distributions as a function of beam radius. Since the total number of detected particles is not so large (~4000), the statistical fluctuations are included in the profiles. At the capillary outlet (0 mm), the profile is almost uniform except for the sharp peak at the beam edge, which is due probably to halo particles scattered with small takeoff angles. At a distance of 1 mm, the intensity decreases slightly and a halo wing appears. This wing degrades the spatial resolution of the μ-PIXE measurement to some extent, which does not contradict the effective beam spot size determined by the edge-scanning experiment. The uniformity of the central part of the beam is good even at 7 mm because the central part is almost occupied by core particles, which are assumed to have a uniform distribution at the inlet of the capillary.

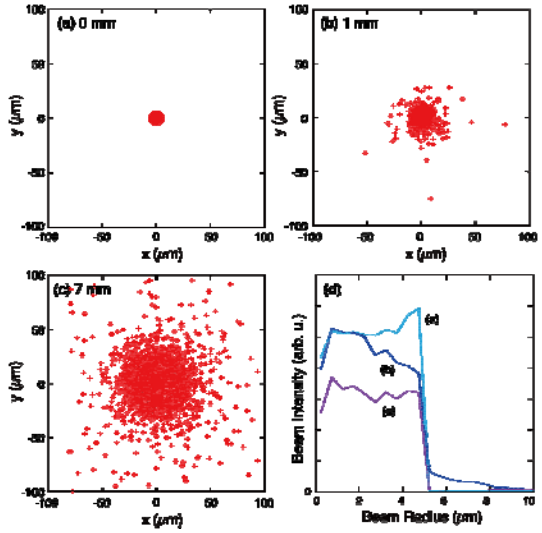

Fig. 6. Particle distributions and beam intensity profiles calculated at various distances from the capillary outlet: (a) 0 mm, (b) 1 mm, (c) 7 mm, (d) beam intensities.

The transmission of the proton beam through the 10-μm capillary was only 0.4% from the Monte-Carlo simulation, which means that 99.6% of the incident 2-MeV protons are stopped in the capillary wall and deposit heat on it. To obtain a micro beam current of 1 nA, we need to input 250 nA into the capillary. In this case, the deposited beam power on the capillary reaches 0.5 W, probably leading to the deformation of the capillary glass if there is no cooling. The use of a metallic cylinder to cover the whole part of the capillary may be effective to improve the heat conductance from capillary glass to surrounding metallic parts. Of course, active cooling using coolant can be a strong option to solve this problem.

On the other hand, the beam-focusing factor for the ø10-μm capillary was around 1.7. Although there is a tendency that the beam-focusing factor increases with decreasing capillary outlet diameter, a drastic increase in the beam-focusing factor cannot be expected as long as we use the capillary having the wall shape similar to those used in this study. The use of concave inner wall shapes may have the potential to improve the beam-focusing factor and the transmission of the capillary.

References

[1] J. Hasegawa, S. Shiba, H. Fukuda, and Y. Oguri, Nuclear *Instruments and Methods in Physics Research Section B: Beam Interactions with Materials and Atoms* **266,** 2125-2129 (2008).

A.13 Development of Electron Cyclotron Emission Imaging System on LHD

Shunji TSUJI-IIO

A combined system of Microwave Imaging Reflectometry (MIR) and the Electron Cyclotron Emission Imaging (ECEI) has been developed for Large Helical Device (LHD) at NIFS. Microwave imaging diagnostics has potential to observe fluctuations of electron density and electron temperature profiles in magnetically confined high temperature plasmas. When the plasma density and temperature are sufficiently high, the electron cyclotron emission (ECE) is approximated to be black body radiation in magnetically confined plasmas. The electron temperature profile can be determined by measuring intensity of each frequency of ECE, since the ECE frequency corresponds to the radial position. By using a 1-D receiving antenna array, 2-D ECE profiles (radial and poloidal directions) can be obtained. The electron temperature is considered to be equal on the same magnetic flux surface so that ECE imaging (ECEI) can be one of the most powerful diagnostics to investigate MHD instabilities.

Developed ECEI system is equipped with the same imaging optics of MIR. Consequently this system enable us to observe both density and temperature fluctuations simultaneously. As an example, in LHD plasma with n_{e0} = 3×10^{19} m^{-3} and B_{ax} = 2.75 T (R_{ax} = 3.6 m), the second harmonic ECE of 96.5 - 104.5 GHz corresponds to the observation range of 4.44 m to 4.55 m in the major radius.

Our MIR/ECEI system consists of the following three devices; 1) imaging optics, 2) horn-antenna mixer array (HMA) and 3) multi-frequency detector. The optical system has three optics, illumination optics for MIR, focusing optics and local oscillator (LO) optics. The MIR and ECE signals from plasma are focused on HMA with the focusing optics. The focusing optics is shared between MIR and ECEI to measure the same plasma region. Since LO frequencies for ECEI and MIR are different, they are received with different horn antennas and are mixed with an acrylic beam splitter (BS). In this system, a 2-D HMA and 1-D HMA are adopted for MIR and ECEI, respectively. Since an end-fire type antenna element is adopted in HMA, 2-D HMA can be easily composed by stacking 1-D HMAs.

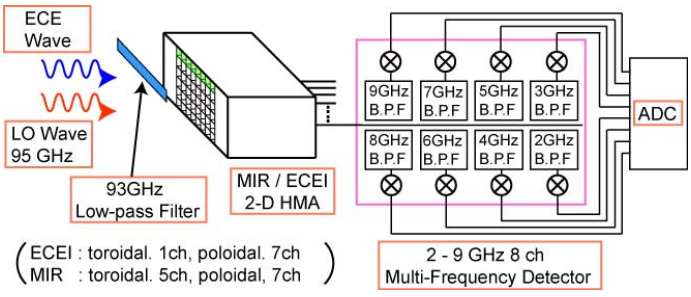

Fig.1 Block diagram of ECEI antenna and IF system

While HMA was designed to use in the frequency range of V-band (50 - 75 GHz), it has a good response in required frequency range, 75 – 110 GHz (W-band). The frequency spectrum of ECE is detected with a multi-frequency detector composed on a high frequency PCB using the microstrip line technology. It is a more compact and low-cost solution than using coaxial band-pass filters. It consists of 3 sections as follows; IF amplifiers (DC - 12 GHz, 30 dB), the 8-ch band-pass filter (BPF) bank and power detectors. IF amplifier uses the same MMIC amplifier adopted in HMA. The 8-ch BPF bank is made by edge coupled filters, which are resonator lines coupled with the main transmission line. The length of the resonator line is about a quarter wavelength of the central frequency of each BPF. The central frequencies are set at 1 GHz step up to 9 GHz from 2 GHz. The designed bandwidth of each BPF is 500 MHz. The power detector is a zero bias Schottky diode showing positive peak detection. Each circuit is matched with own frequency. The sensitivity is about 1 V/mW at 2 GHz while the sensitivity decreases with frequency.

An example of the ECE signal in a preliminaly ECEI experiment, which uses the 1-D HMA is shown in Fig.2. In this case, additional amplifiers (50 dB, 2 - 18 GHz) are inserted between the HMA and the multi-frequency detector. The waveform of the ECE signal at 101 GHz which corresponds to R = 4.5 m is similar to that of the electron temperature measured by Thomson scattering at R = 4.483 m, when ECH is absent. This result indicates that the V-band HMA can be applied to the W-band (75 – 110 GHz) ECEI receiver.

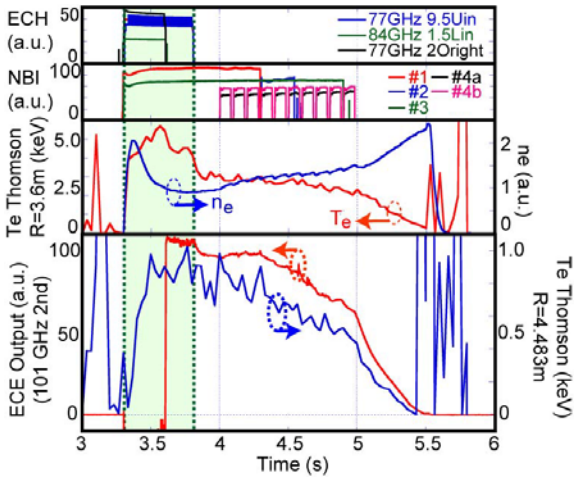

Fig.2 Example trace of ECE signal with discharge waveforms.

A.14 Virial Theorem for Helical Coils with Cable in Conduit Configuration

Hiroaki TSUTSUI, Takayuki HABUCHI, Sunji TSUJI-IIO and Ryuichi SHIMADA

1. Introduction

Recently, we had developed a tokamak with virial-limit coils (VLCs) which are multi-pole helical hybrid coils combining toroidal field (TF) coils and a center solenoid (CS) coil based on the virial theorem. The theorem shows that strength of magnetic field is restricted by working stress in the coils and their supporting structure. Applying the theorem to a toroidal coil with a shell structure, we obtained the optimal configuration of the coil. Although the virial theorem includes only an averaged stress, the optimal condition of the toroidal coil is experimentally proved because the shell configuration is uniform in structure.

Realistic coil systems, however, does not have a uniform structure. In such a configuration, large stresses caused by bending and torsion exist, while they are not evaluated in the virial theorem because their average is zero.

In this work, we extend the virial theorem to a helical coil, and show the optimal condition in stress with bending and torsion.

2. Helical Coil

First of all, we consider a helical coil with a toroidal configuration of a major radius R and a minor radius a as shown in Fig. 1. In the case that the aspect ratio $A = R/a$ is large enough, the magnetic energy U_{M} of the toroidal coil is given by

$$U_{\mathrm{M}} = U_{\mathrm{TF}} + U_{\mathrm{PF}}, \tag{1}$$

$$U_{\mathrm{TF}} = \frac{\mu_0 a^2}{4R} I_\theta^2, \tag{2}$$

$$U_{\mathrm{PF}} = \frac{\mu_0 R}{2}\left(\log\frac{8R}{a} - 2\right) I_\phi^2, \tag{3}$$

where U_{TF} and U_{PF} are the energy of the toroidal and poloidal fields, I_ϕ and I_θ are the toroidal and poloidal currents, respectively. Next we introduce the length of a helical coil L and its pitch angle α,

$$L = 2\pi a\sqrt{N^2 + A^2}, \tag{4}$$

$$\tan\alpha = \frac{2\pi R}{2\pi N a} = \frac{A}{N}, \tag{5}$$

as is shown in Fig. 1, where

$$N = \frac{I_\theta}{I_\phi}, \tag{6}$$

is the ratio of the toroidal current and the poloidal current, which means a pitch number of the coil. Using these two parameters L and α as independent variables in the magnetic energy U_{M}, the net electromagnetic force F_{L} in the longitudinal direction and the net moment of electromagnetic force M_α are obtained from the partial differentiations of magnetic energy U_{M} with respect to L and α,

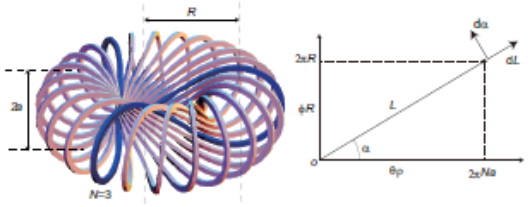

Figure 1: Helical coils of a pitch number N = 3 and their coil trajectory on the torus of a minor radius a and a major radius R. A pitch angle α and a length L of the coil are mutually related with the coil sizes a and R.

$$F_L = \left.\frac{\partial U_{\mathrm{M}}(L,\alpha)}{\partial L}\right|_{I=\mathrm{const.}} = \frac{U_{\mathrm{M}}}{L}, \tag{7}$$

$$M_\alpha = \left.\frac{\partial U_{\mathrm{M}}(L,\alpha)}{\partial \alpha}\right|_{I=\mathrm{const.}} = \frac{\mu_0 I_\phi^2}{2} aN\left\{\log 8A - 2 - \frac{N^2}{2A^2} + \frac{A^2}{N^2}\right\}. \tag{8}$$

The moment M_α, therefore, changes the pitch angle α and the aspect ratio A, and contributes to bending and torsional stresses, while the force F_{L} homologously deforms the coil and contributes to a membrane stress which is a averaged normal stress in a cross section of the conductor. Since the virial theorem includes only avareged stress, the virial theorem is exactly satisfied as follows:

$$\langle\tilde{\sigma}_L\rangle = \frac{V_\Omega}{U_{\mathrm{M}}}\sigma_L = 1, \tag{9}$$

Where σ_L is an axial normal stress in the conductor,

$$\sigma_L = \frac{F_L}{\pi d^2}, \tag{10}$$

and V_Ω is the volume of the conductor defined by

$$V_\Omega = \pi d^2 L. \tag{11}$$

Because the virial theorem includs σ_L only, the volume integrals of the other components of stress tensor vanish.

In the case that the aspect ratio $A = R/a$ is large enough, the toroidal coil is regarded as a cylindrical coil of radius a

and length $2\pi R$ with a periodic condition. Since the moment M_α results from the change of the pitch angle, it directly makes a bending stress and changes the pitch angle. According to the Frenet frame, the trajectory has three unit vectors whose directions are tangential, principal normal and binormal. In the helical configuration, only the principal normal direction, which is the minor radius direction, dose not depend on the pitch angle, and it is kept its direction against the change of α. Then the moment M_α has the minor radius direction, and derives a bending stress around the minor radius direction.

Although the direction of the electromagnetic moment M_α is the minor radius direction, it is entirely possible that the moment of the reaction to M_α has the other direction. Next, we consider a cross section of the conductor θ = const. The finite radius changes the minor radius from a to $a \pm d$ and its trajectory is modified as shown in Fig. 2 while the center in the conductor remains on the original trajectory depicted in Fig. 1. Although three trajectories on Fig. 2 have different pitch angles, their increment d_α has a same value because the conductor radius d is kept for distortions as follows:

$$\mathrm{d}(a \pm d) = \mathrm{d}a = L \sin\alpha \mathrm{d}\alpha = 2\pi R \mathrm{d}\alpha.$$

Since the length of conductor is conserved in the distortion, the next relations hold,

$$\begin{aligned} \mathrm{d}R &= L\mathrm{d}\alpha\cos\alpha = 2\pi N a \mathrm{d}\alpha, \\ \mathrm{d}R_{\pm d} &= L_{\pm d}\mathrm{d}\alpha\cos\alpha_{\pm d} = 2\pi N(a \pm d)\mathrm{d}\alpha \\ &= (1 \pm \frac{d}{a})\mathrm{d}R. \end{aligned} \tag{12}$$

Therefore, the difference of dR caused by dα is

$$\mathrm{d}R_{\pm d} - \mathrm{d}R = \pm\frac{d}{a}\mathrm{d}R,$$

and a torsion angle dβ is related with dα as follows:

$$\mathrm{d}\beta = \frac{\mathrm{d}R_{+d} - \mathrm{d}R}{d} = 2\pi N \mathrm{d}\alpha. \tag{13}$$

Since $2\pi N$ is much greater than unity, the electromagnetic moment M_α is mainly supported by the torsional moment,

$$\begin{aligned} M_\theta &= \left.\frac{\partial U_{\mathrm{M}}(L,\alpha)}{\partial(2\pi N\alpha)}\right|_{I=\mathrm{const.}} = \frac{1}{2\pi N}M_\alpha \\ &= \frac{\mu_0 I_\phi^2}{4\pi}a\left\{\log 8A - 2 - \frac{N^2}{2A^2} + \frac{A^2}{N^2}\right\}, \end{aligned} \tag{14}$$

where the direction of the moment M_θ is the poloidal direction.

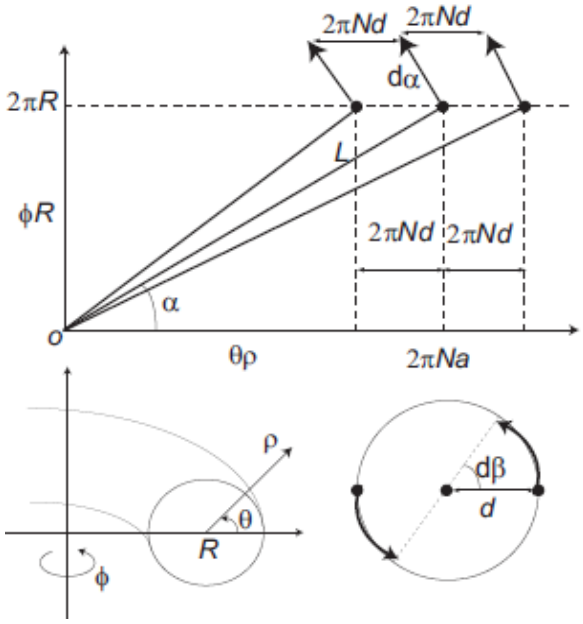

Figure 2: The relation of the pitch angle increment dα and an angle of torsion dβ. The angle of torsion is caused by the difference of trajectory length.

3. Spring Model

The effect of the moment M_α is also interprited by a spring model. Consider a cylindrical spring made of a helical conductor of radius d and length L where the electromagnetic forces F_L and F_R are loaded to the spring as shown in Fig. 3, where F_R is defined by

$$\begin{aligned} F_R &= \left.\frac{\partial U_{\mathrm{M}}(L,\alpha)}{\partial R}\right|_{I=\mathrm{const.}} \\ &= \frac{\mu_0 I_\phi^2}{2}\left\{\log 8A - 2 - \frac{N^2}{2A^2} + \frac{A^2}{N^2}\right\}. \end{aligned} \tag{15}$$

Since the force F_R can be regarded as a spring load W defined by

$$W = \frac{\partial U_{\mathrm{M}}}{\partial(2\pi R)} = \frac{F_R}{2\pi}, \tag{16}$$

a moment vector $\boldsymbol{M}$,

$$\boldsymbol{M} = a\boldsymbol{e}_\rho \times W\boldsymbol{e}_\phi = M_\theta \boldsymbol{e}_\theta, \tag{17}$$

acts on the spring, and agrees with Eq. 14, where torsional and bending moments are

$$M_{\mathrm{T}} = aW\cos\alpha = M_\theta\cos\alpha, \tag{18}$$

$$M_{\mathrm{B}} = aW\sin\alpha = M_\theta\sin\alpha, \tag{19}$$

respectively. Since the section modulus of a circular cross section of radius d is

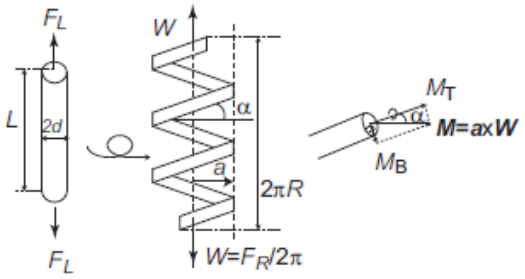

Figure 3: A spring model. A cylindrical spring with radius a and length $2\pi R$ is made of a conductor with length L and diameter $2d$. A uniform tension F_L, and torsional and bending moments M_T, M_B act on a cross section of the conductor.

$$Z = \frac{\pi d^3}{4}, \tag{20}$$

the maximum torsional and bending stresses τ_T, σ_B are determined as follows:

$$\begin{aligned} \tilde{\tau}_T &= \frac{V_\Omega}{U_M}\frac{1}{2Z}M_T \\ &= 2\frac{a}{d}\left(1+\frac{\frac{A^2}{N^2}-\frac{N^2}{A^2}}{\log 8A-2+\frac{N^2}{2A^2}}\right)\frac{N}{A}, \end{aligned} \tag{21}$$

$$\begin{aligned} \tilde{\sigma}_B &= \frac{V_\Omega}{U_M}\frac{1}{Z}M_B \\ &= 4\frac{a}{d}\left(1+\frac{\frac{A^2}{N^2}-\frac{N^2}{A^2}}{\log 8A-2+\frac{N^2}{2A^2}}\right). \end{aligned} \tag{22}$$

The maximum principal stress is also determined as follows:

$$\begin{aligned} \tilde{\sigma}_{\max} &= \frac{\tilde{\sigma}_B}{2}+\sqrt{\tilde{\sigma}_B^2+4\tilde{\tau}_T^2} = \frac{\tilde{\sigma}_B}{2}\left(1+\frac{L}{2\pi R}\right) \\ &= 2\frac{a}{d}\left(1+\frac{\frac{A^2}{N^2}-\frac{N^2}{A^2}}{\log 8A-2+\frac{N^2}{2A^2}}\right)\left(1+\sqrt{1+\frac{N^2}{A^2}}\right) \end{aligned} \tag{23}$$

Because a coil index $c = a/d$ is much greater than unity, the torsional and bending stresses are dominant, and the helical coil without torsional and bending stresses of $F_R = 0$, whose solution is depicted in Fig. 4, its maximum stress is drastically reduced. The pitch number of the coil is located between FBC and VLC. Figure 5 shows the distribution of σ_{max} normalized by the coil index c against A and N. Its value enormously increases with distance of optimal-condition line which is a red line in Fig. 4 and a blue line in Fig.5.

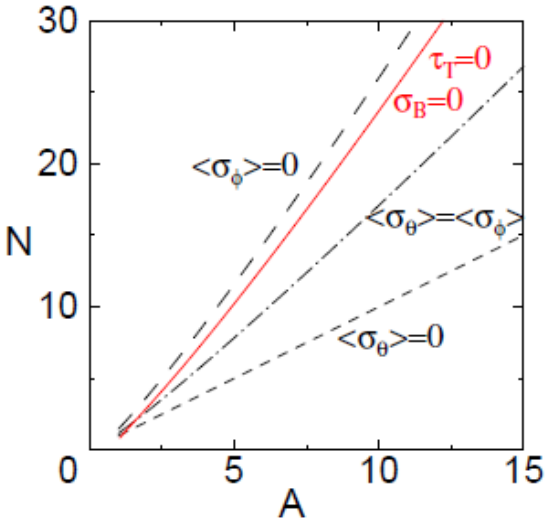

Figure 4: Relations between aspect ratio A and pitch number N. Solid, dash-doted, dashed and doted lines are in the case of $\sigma_B = \tau_T = 0$, $\langle \sigma_\theta \rangle = \langle \sigma_\theta \rangle$, $\langle \sigma_\theta \rangle = 0$ and $\langle \sigma_\theta \rangle = 0$, respectively.

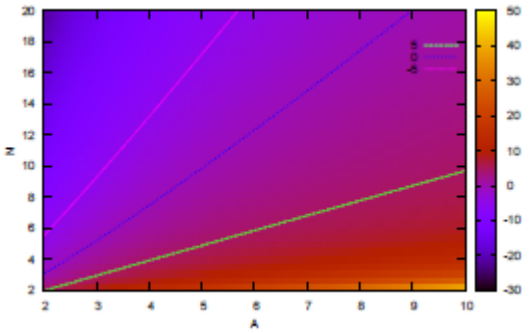

Figure 5: A contour of σ_{max}/c as a function of the aspect ratio A and the pitch number N, where c is a coil index a/d.

4 Conclusions

We evaluated the stress distribution in a helical coil, and obtained the virial theorem in this configuration. In our previous works based on a shell configuration, averaged stresses, which appear in the virial theorem, are important because of its uniform structure. Since a helical coil, however, has a spring configuration, bending and torsion are important and their values are much larger than those of averaged (membrane) stresses. In this work, we obtained the moment M_α of electromagnetic force and the bending and torsional moment M_θ of the reaction of the electromagnetic moment as a function of the aspect ratio A and the pitch number N. Using this formula, we showed the optimal pitch number satisfying $M_\theta = 0$.

A.15 Diagnostics of Oxygen-Rare Gas Mixed Plasmas Excited by Microwave Discharge

Hiroshi AKATSUKA, Atsushi NEZU and Haruaki MATSUURA

Oxygen plasmas are widely applied in microelectronic processes, such as oxide layer formation, amorphous silicon film preparation for photovoltaic application, etc. It is already found that the characteristics of materials prepared by the oxygen plasmas are improved with increasing ratio of admixture of rare gases like Ar or Kr. This is attributed to the variation in the plasma parameters of oxygen plasmas diluted by rare gases. We are experimentally examining variation in the plasma parameters of oxygen plasma diluted with rare gases [1, 2]. In the present study, we originally measured the dissociation degree of oxygen molecule in the rare-gas diluted oxygen plasmas as functions of molar admixture ratio of rare gas, which is determined by actinometry method, one of the OES methods [3, 4]. We also measured the electron temperature and density by a Langmuir double probe, and the gas temperature by OES measurement as a rotation temperature of OH radicals.

Figure 1 shows a schematic diagram of experimental setup. The microwave is generated by a magnetron, adjusted by a three-stub tuner and guided to a discharge tube through waveguides. The frequency of the microwave is 2.45 GHz and the power applied is 300 W. The inner diameter of the quartz tube is 26 mm. The quartz discharge tube is set in a microwave cavity connected to the waveguide, which is terminated by an adjustable short-circuited plunger. The discharge gas is a gas mixture of oxygen with one of rare gases of helium, neon, or argon. We examined the dependence of the dissociation degree of oxygen molecule on the rare gas mixture ratio.

Figure 2 shows the results of dissociation degree measured at 300 mm downstream from the intersection of the discharge tube and the waveguide. Generally, the dissociation degree increases with increasing the rare gas admixture. However, the amount of increase is at most 5 – 7 % with the rare-gas admixture ratio less than 30 %. Under the foregoing experimental conditions, the heavier the mixed rare-gas molecule is, the more the dissociation degree becomes. On the other hand, when the rare-gas admixture ratio exceeds 50 %, the helium admixture raises the dissociation degree markedly. This tendency is found for any other positions of the discharge tube. It is also found that the dissociation degree becomes lower as the plasma flows to the downstream direction in general. However, when the helium admixture ratio is more than 80 %, the dissociation degree was found to be constant, or rather, increase a little. It is considered that this is due to the collisions of oxygen molecule with metastable states of helium atoms [5]. Further study is necessary to elucidate the reason for the enhancement of the dissociation.

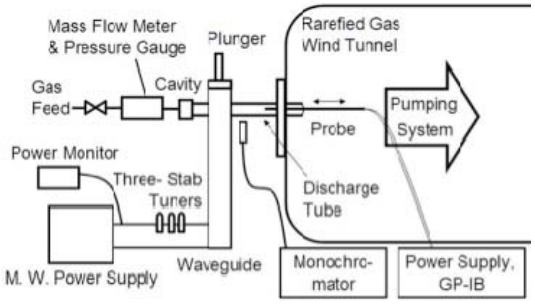

Fig.1: Experimental setup.

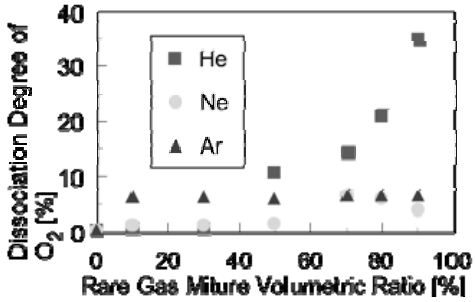

Fig. 2. Dependence of dissociation degree of O_2 on the rare gas mixture volumetric ratio at z = 300 mm by actinometry measurement.

References

[1] K. Naoi, T. Sakamoto, H. Matsuura and H. Akatsuka, *J. Adv. Oxid. Technol.*, **8**, [1], 25-32 (2005).
[2] T. Sakamoto, K. Naoi, H. Matsuura and H. Akatsuka, *Jpn. J. Appl. Phys.*, **45**, [1A], 243-246 (2006).
[3] T. Sakamoto, H. Matsuura and H. Akatsuka, *J. Adv. Oxid. Technol.*, **10**, [2], 247-252 (2007).
[4] S. Kakizaka, T. Sakamoto, H. Matsuura and H. Akatsuka, *J. Adv. Oxid. Technol*, **10**, [2], 253-259, (2007).
[5] W. Takai, A. Nezu, H. Matsuura and H. Akatsuka, *The 2010 Annual Meeting Record IEE Japan*, Vol. **1**, p. 220 (2010) [in Japanese].

A.16 Measurement of Nitrogen Dissociation Degree of Nitrogen Plasma by Actinometry Method with Subtraction of First Positive Band Spectrum

Hiroshi AKATSUKA, Atsushi NEZU and Haruaki MATSUURA

Nitrogen plasma is widely used for industries, and one of the most essential parameters is often the dissociation degree of nitrogen molecules. Many methods have been proposed to examine it, for example, VUVLAS [1] or actinometry in VUV wavelength [2], which, indeed, requires VUV spectrometric equipment. Conventional actinometry method is also frequently adopted, where the following reactions are applied [3]:

$$N + e^- \rightarrow N^*(3p\ ^4S^o) + e^-,\ E = 13.80\ \text{eV}, \quad (1)$$
$$Ar + e^- \rightarrow Ar^*(4p) + e^-,\ E = 13.12\ \text{eV}, \quad (2)$$
$$N^*(3p\ ^4S^o) \rightarrow N^*(3s\ ^4P_{5/2}) + h\nu,\ 746.83\ \text{nm}, \quad (3)$$
$$Ar^*(4p) \rightarrow Ar^*(4s) + h\nu,\ 811.5\ \text{nm}. \quad (4)$$

However, when we apply the above scheme to the nitrogen plasma with low dissociation degree, the band spectrum of the first positive system (1PS) seriously overlaps the lines of nitrogen atoms. If we can calculate the 1PS band spectrum like 2PS [4], we can determine the dissociation degree of nitrogen molecule in the nitrogen plasma, which is precisely the objective of the present study.

The experimental apparatus is described in Ref. 5. We considered collisional quenching of the excited levels in Eqs. (1) – (4), since the discharge pressure is about 1 Torr in the present experiment. We first obtain the first positive band spectrum of the vibrational quantum numbers $\Delta v = v' - v'' = 2$ in the wavelength region of 730 – 760 nm, and determine the vibrational and rotational temperatures T_v and T_r [5]. After we subtract the 1PS spectrum as a background, we obtain the nitrogen line at 746.83 nm [3]. In addition to the spectroscopic examination, probe measurement is performed to estimate electron temperature and density.

Figure 1 shows an example of measured dissociation degree plotted against the rare-gas mixture ratio for the microwave discharge nitrogen plasma diluted by one of the rare gases.

When helium is mixed into the nitrogen plasma, we found a small increase in the nitrogen dissociation degree. This can be attributed to an increase in the electron temperature by the helium admixture, which is confirmed by the probe measurement. On the other hand, when the argon or krypton was mixed, we found lowering of electron temperature and resultant reduction in the nitrogen dissociation degree. For the foregoing three rare gases, the variation in their dissociation degree is reasonable. However, Fig. 1 shows that the neon admixture strongly enhances the nitrogen dissociation degree. This tendency was found at rather downstream position like 140 mm downer from the intersection of the waveguide. One of the possible mechanisms is that the energy-transfer collision between the metastable neon (16.62 or 16.72 eV) with nitrogen molecule [6]. Further discussion and experimental verification by other methods are necessary to understand the dissociation phenomena of nitrogen molecules by neon admixture.

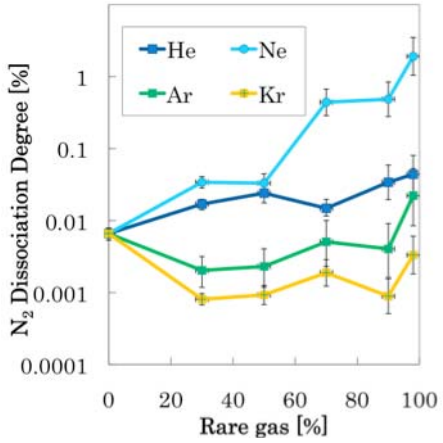

Fig. 1 Dependence of the nitrogen dissociation degree of rare gas-diluted nitrogen microwave discharge plasma on the molar ratio of rare gas. The total pressure is set at 1 Torr, and measured at z = 60 mm.

References

[1] S. Takahashi, S. Takashima, K. Yamakawa, S. Den, H. Kano, K. Takeda and M. Hori: *J. Appl. Phys*. **106** (2009) 053306.
[2] T. Nakano, S. Kumara and S. Samukawa: *J. Appl. Phys*. **92** (2002) 2990.
[3] Y. Ichikawa, T. Sakamoto, H. Matsuura and H. Akatsuka: Jpn. *J. Appl. Phys*. **49** (2010) in print.
[4] S. Nunomura, M. Kondo and H. Akatsuka: *Plasma Sources Sci. Technol.* **15** (2006) 783.
[5] T. Sakamoto, H. Matsuura, and H. Akatsuka: *J. Appl. Phys.* **101** (2007) 023307.
[6] K. Kuwano, A. Nezu, H. Matsuura and H. Akatsuka: *Meeting Abst. Phys. Soc. Jpn*. **65** [1] (2010) 224.

A.17 Optical Emission Characteristics of Atmospheric-Pressure Non-Equilibrium N_2-Ar Plasmas and Application to Process Monitoring of Surface Modification

Hiroshi AKATSUKA

With an aim to understand the mechanism of surface processing by atmospheric-pressure non-equilibrium discharge plasma jets, we measured the vibrational and rotational temperatures in the plasmas by means of optical emission spectroscopy (OES) measurement method. We used torch-shaped atmospheric-pressure non-equilibrium discharge plasma power supply consisting of a microwave power source [1] and high-frequency (5.0 – 10 kHz) DC pulse power supply [2]. Upon comparing vibrational and rotational temperatures determined from the OES measurement method using two types of atmospheric-pressure non-equilibrium discharge plasma jets, results indicate that the microwave discharge plasma jet has considerably low vibrational and rotational temperatures. Figure 1 shows a relationship between input power and vibrational and rotational temperatures of the plasma jets measured by optical emission spectroscopy. As the partial flow rate of N_2 component increases in the discharge gas, the temperatures were found to increase monotonically for both discharge apparatus [3].

We also carried out plasma surface processing of PET film to measure the changes in water contact angle before and after the processing. Figure 2 shows the variation in the water contact angle of PET film. We found monotonic decrease in the contact angle of the processed PET film as the plasma rotational temperature increased [1]. Similar tendency was also found for the microwave discharge plasma [4]. This fact indicates that the rotation temperature can be a good measure to monitor the processing with atmospheric non-equilibrium plasmas in the practical situations [5]. We are proposing that the OES measurement should be the most practical diagnosing tool of industrial plasma processing [6].

We thank Prof. Toshifumi Yuji of University of Miyazaki for his continuous study. We also thank late Professor Emeritus Ryouhei Itatani of Kyoto University for giving us opportunity to carry out these studies.

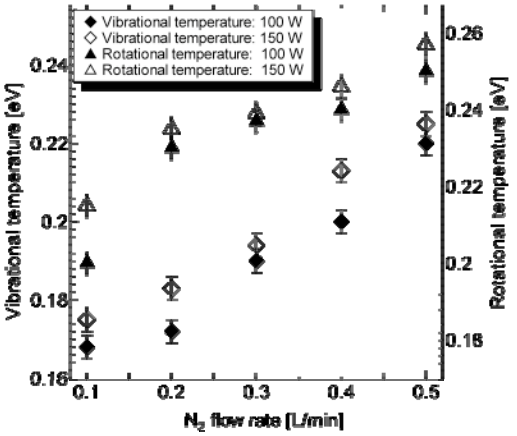

Fig. 1. Relationship between input power and vibrational and rotational temperatures at atmospheric-pressure non-equilibrium Ar and N_2 gas (microwave and high-frequency DC pulse) discharge plasma jets measured by optical emission spectroscopy.

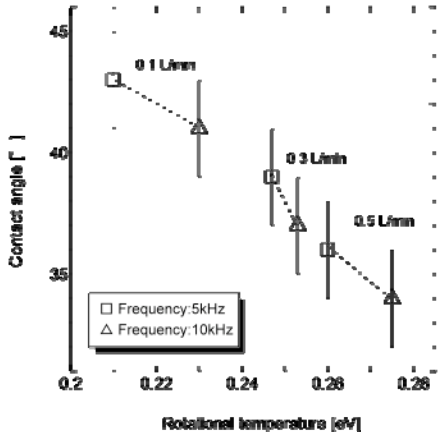

Fig. 2. Water contact angle of PET film plotted against the rotational temperature of the atmospheric pressure argon and nitrogen.

References

[1] T. Yuji, K. Fujioka, S. Fujii and H. Akatsuka: *IEEJ Trans*. **2** (2007) 473.
[2] T. Yuji, Y. Suzaki, T. Yamawaki, H. Sakaue and H. Akatsuka: *Jpn. J. Appl. Phys*. **46** (2007) 795.
[3] T. Yuji, S. Fujii, N. Mungkung and H. Akatsuka: *IEEE Trans. Plasma Sci.* **37** (2009) 839.
[4] T. Yuji, T. Urayama, S. Fujii, Y. Iijima, Y. Suzaki and H. Akatsuka: *IEEJ Trans. FM* **128** (2008) 449 [in Japanese].
[5] T. Yuji, T. Urayama, S. Fujii, N. Mungkung and H. Akatsuka: *Surf. Coat. Technol*. **202** (2008) 5289.
[6] T. Yuji, H. Akatsuka, N. Mungkung, B. W. Park and Y. M. Sung: *Vacuum* **83** (2009) 124.

B.1 Transmutation of Iodine-129 in Accelerator Driven System

Ismailov KAIRAT, Kenji NISHIHARA[1] and Masaki SAITO

INTRODUCTION

Nuclear energy production entails generation and accumulation of Plutonium, Minor Actinides (MA) and Long Lived Fission Products (LLFP) which present crucial challenges concerning safety, non-proliferation, environmental protection, ect., for sustainable nuclear energy development.

Among LLFP Iodine-129 is one of the major contributors to the biosphere release dose rates because of its high geochemical mobility.

The inherent advantage of ADS regarding neutron excess generation is well recognized and serves as a solid base to promote it for reduction of long-term dose by transmutation of LLFP into stable or short-lived isotopes.
The objective of present study is the determination of optimal design for long-lived fission fragments transmutation in subcritical system.

METHODOLOGY

As reference case ADS of JAEA type for simultaneous MA and Iodine transmutation [1] was considered. Iodine transmutation in the Axial and Radial blankets was considered. The LLFP assembly in blankets consisted of homogenized mixture of Iodide (NaI, CuI), moderator $ZrH_{1.7}$, cladding material and coolant. It was shown that ADS with such type of LLFP loading was able to transmute 250 kg/y of MA and 56 kg/y of Iodine (46 kg of isotope I-129 and 10 kg of I-127) that supports ten 100MWe class PWRs.

In present study the transmutation of Iodine loaded in pin with detailed structure was analyzed in order to verify that ADS with such design was able to transmute MA and Iodine with support factor of 10. Three types of Iodine pin design were considered:

a) Heterogeneous separated $ZrH_{1.7}$ and NaI (Sodium Iodide with smear density of 90%) pins combination;
b) Homogeneous mixture of $ZrH_{1.7}$ and NaI;
c) Annular NaI enclosing $ZrH_{1.7}$ moderator.

Criticality coefficient value was kept at 0.97. Liquid PbBi was used as spallation target and coolant for core region and inside Iodine assemblies.

The computer code MCNPX (v27a) [2,3] was utilized for calculations with combination of JENDL-3.3 and JENDL-HE libraries.

The nuclear processes for elements with absent information in above mentioned databases were simulated by Bertini model of Intra Nuclear Cascade. Evaporation and fission processes of the excited residual nucleus were simulated by Dresner model.

RESULTS

The transmutation rates of I-129 in dependence on pin diameter of each design type for Radial and Axial blankets individually were determined. So, diameter of pin and NaI to $ZrH_{1.7}$ ratio were the parameters in this survey. The obtained optimum parameters for each blanket were used in calculations of the I-129 transmutation rates for system with Radial and Axial blankets. The mass of transmuted Iodine was less than 46kg/y though initially loaded mass was significantly increased (up to 2 tonnes).

In this respect the “In core/Radial” loading concept was considered. Different layouts were investigated and for each case the important parameters including average NaI pin temperature, initial proton beam current, fuel composition and power peaking factor were studied. Among all layouts the one that satisfied to most of conditions was chosen. Introduced "In core/Radial" concept allows to transmute more Iodine with decreased initial loading. Since even with such concept it was not possible to reach the transmutation of 46kg/y it was decided to add to system the Axial blankets above and under the core with height equal to 20cm.

It was demonstrated that introduced final ADS design with the “In core/Radial/Axial” Iodine loading concept was able to transmute simultaneously 250kg of MA and 46kg of I-129 annually that supports 10 PWRs with significantly decreased initial loading mass of I-129 of 1 tonne in comparison to Radial/Axial blankets concept (2 tonnes).

REFERENCES

1. K. NISHIHARA, H. TAKANO, K. MINATO and H. OIGAWA, *Proc. GLOBAL 2001*, Paris, France, 9–13 September 2001, CD-ROM
2. D.B.PELOWITZ *et al*, “MCNPX, User's Manual, Version 2.5.0”, LA-CP-05-0369 (2005).
3. D.B.PELOWITZ *et al*, “MCNPX, 2.7.A Extensions”, LA-UR-08-07182 (2009).

B.2 Systematic Measurement of keV-Neutron Capture Cross Sections and Capture Gamma-Ray Spectra of Stable Se Isotopes

Masayuki IGASHIRA, So KAMADA, Tatsuya KATABUCHI, and Motoharu MIZUMOTO

1. Intoroduction

Nuclear waste includes long-lived fission products (LLFPs). Currently, the deep geological disposal of nuclear waste is the national policy in Japan. However, it needs the long-term management that prevents the public from suffering radiological hazard due to LLFPs. Thus, the nuclear transmutation of LLFPs into stable or shorter-lived nuclides is an attractive alternative to decrease the hazard.

The neutron capture cross sections of LLFPs are important physical quantities for the research and development of nuclear transmutation systems, because the performance of system using neutron capture reaction depends on these quantities directly.

The nuclide ^{79}Se is one of the most important LLFPs. However, there is no experimental data for its neutron capture cross section, because of difficult sample availability.

On the other hand, keV-neutron capture cross sections and capture γ-ray spectra of stable Se isotopes contain important information useful for the calculation of capture cross sections of ^{79}Se. We have been performing the systematic measurement and calculation of keV-neutron capture cross sections and capture gamma-ray spectra of stable Se isotopes. In this report, we present the experimental results for the capture cross sections and capture gamma-ray spectra of ^{78}Se at an incident neutron energy around 550keV.

2. Experiments

The detail of experimental procedure has been given in Ref. [1]. Only brief description is given here.

The capture cross section and capture gamma-ray spectrum of ^{78}Se were measured in an incident neutron energy around 550 keV, using the 3 MV Pelletron accelerator of the Research Laboratory for Nuclear Reactors at the Tokyo Institute of Technology. An experimental arrangement is shown in Fig.1.

Pulsed neutrons were produced by the ^{7}Li(p,n)^{7}Be reaction with a pulsed proton beam (1.5 ns width, 4 MHz repetition rate) from the accelerator. The incident neutron spectrum on a capture sample was measured by a Time of Flight (TOF) technique with a ^{6}Li-glass scintillation detector (102-mm diam.× 6.4-mm thick).

The ^{78}Se sample was highly isotopically enriched metal (99.4% enrichment), and its net weight was about 2 g. A gold sample was used as a standard sample of capture cross section. The distance between the neutron source and the sample was 20 cm.

Capture gamma rays emitted from the sample were detected with a large anti-Compton NaI(Tl) spectrometer by means of a TOF method. The main NaI(Tl) detector of the spectrometer had a diameter of 15.2 cm and a length of 30.5 cm, and was centered in an annular NaI(Tl) detector (33.0 cm OD ×35.6 cm length) for Compton suppression. The detectors were shielded with a combination of various materials: borated paraffin, borated polyethylene, Cd, ^{6}LiH and potassium free lead [2]. Capture gamma rays were observed at an angle of 125° with respect to the proton beam direction. The pulse height (PH) and TOF of signals from the spectrometer were sequentially recorded in a list-mode data format and then, were analyzed of line.

The runs with the ^{78}Se and ^{197}Au samples and without the sample (blank) were repeated cyclically, thereby for changes in experimental conditions such as the incident neutron spectrum averaging out.

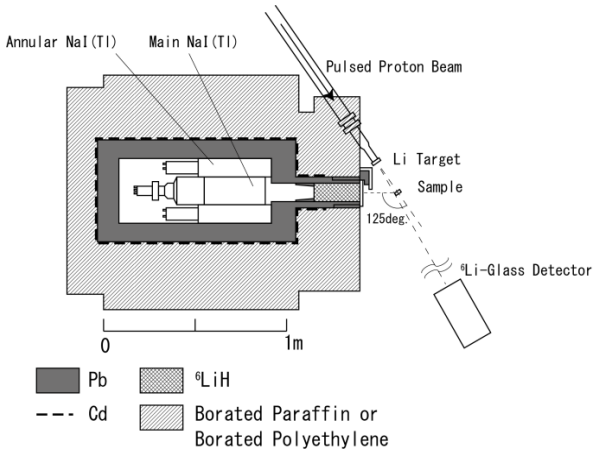

Fig.1 Experimental setup for capture cross section measurements of ^{78}Se.

3. Data Processing

The incident neutron energy spectrum on the sample was derived from the TOF spectra measured with the ^{6}Li-glass detector for the blank run.

In order to obtain the capture yields of the ^{78}Se and ^{197}Au samples, a PH weighting technique [3] was applied to the net capture gamma-ray PH spectra.

The number of incident neutrons in the ^{197}Au run was determined by the capture yield of ^{197}Au and the averaged capture cross section of ^{197}Au, which was obtained from the evaluated data of ENDF/B-VII [4] and the neutron energy spectrum. The number of incident neutrons in the ^{78}Se run was derived from that in the Au run and the neutron monitor counts of the ^{6}Li-glass detector.

The averaged neutron capture cross section of ^{78}Se was derived from the number of incident neutrons and the capture yield of the ^{78}Se sample.

Corrections for the neutron self-shielding and multiple-scattering in the sample were made by a Monte-Carlo method [5], taking account of impurities in the sample. Moreover, other corrections were made for the gamma-ray scattering and absorption in the sample, for the effect of chemical and isotopic impurities in the sample on the capture yields.

The capture gamma-ray spectra were derived by unfolding the net capture gamma-ray PH spectra with a computer code, FERDOR [6], and the response matrix of the gamma-ray spectrometer.

4. Results and Discussion

The derived capture cross sections of ^{78}Se are shown in Figs. 2. Our measurements in the different energy range 15–100 keV are also shown. Any other previous measurements in this energy range have not been performed. The evaluated data of JENDL-3.3[7] and ENDF/B-VI.8 [8] were shown for comparison.

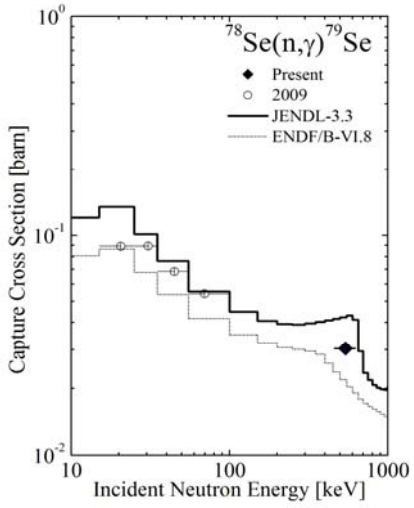

Fig. 2 Neutron capture cross section of ^{78}Se.

In the evaluation of JENDL-3.3, the capture cross sections of ^{78}Se was calculated from a statistical model with a spherical optical potential, and the γ-ray strength function was determined from the average radiation width (0.23 eV) and the average spacing (1390 eV) of s-wave neutron resonances. The evaluations of JENDL-3.3 are larger than the present value by about 40% at around 550keV. On the other hand, ENDF/B-VI.8 underestimated the capture cross section by 30%.

The measured capture γ-ray spectrum of ^{78}Se is shown in Figs. 3. Known descrete levels of the residual nucleus ^{79}Se are shown as bars in the same energy scale as emitted γ-rays. The primary transitions from the capture state to low-lying states were observed. Cascade transitions among low-lyng states were observed around 0.8 MeV.

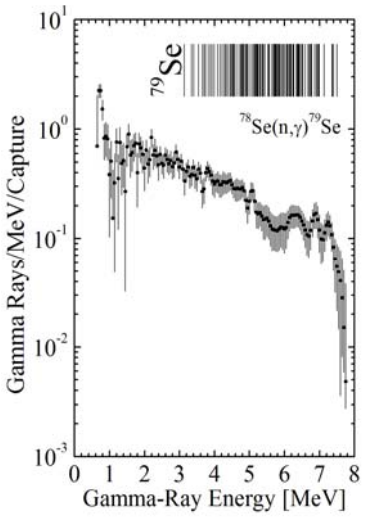

Fig. 3 Neutron capture gamma ray spectrum of ^{78}Se.

5. Conclusions

We have measured the neutron capture cross section and capture gamma-ray spectrum of ^{78}Se at around 550 keV to provide nuclear data relevant to the study on the transmutation of LLFPs and to obtain important physical quantities such as gamma-ray strength function and nuclear level density, which are useful for the theoretical calculation of capture cross sections of ^{79}Se, one of the most important LLFPs.

References

[1] S. Mizuno *et al*., *J.Nucl. Sci. Technol*., **36**, 493 (1999).
[2] M. Igashira, H. Kitazawa and N. Yamamuro, *Nucl. Instrum. Methods*, **A245**, 432 (1986).
[3] R.L. Macklin and J.H. Gibbons, *Phys. Rev.*, **159**, 1007 (1967).
[4] ENDF/B-VII.0 data file for ^{197}Au (MAT=7925), evaluated by P. G. Young (2006).
[5] K. Senoo *et al*., *Nucl. Instrum. Methods*, **A339**, 556 (1994).
[6] H. Kendrick and S.M. Sperling, *Gulf Radiation Technology*, **GA-9882** (1970).
[7] K. Shibata, T. Kawano, T. Nakagawa *et al*., *J. Nucl. Sci. Technol*., **39**, 1129 (2002).
[8] V. McLane, Members of Cross Section Evaluation Working Group, "ENDF-201 ENDF/B-VI Summary Documentation Supplement I ENDF/HE-VI Summary Documentation," BNL-NCS-17541, Brookhaven National Laboratory (BNL) (1996).

B.3 Extraction of U(VI), Pd(II), and Re(VII) from Nitric Acid Solutions using Pyrrolidone Derivatives as Extractants

Yuya TAKAHASHI, Masanobu NOGAMI, Hiroyasu HOTOKEZAKA, and Yasuhisa IKEDA

Amide compounds have been studied as alternative extractant to TBP for separating An(VI) and/or An(IV). Especially, amide compounds have high extractability for U(VI) [1]. It has been reported that pyrrolidone derivatives (NRPs) are used as highly selective precipitant to U(VI) [2] and that polyvinylpyrrolidone resin has high selectivity toward U(VI) . In our previous study, we found out that NRPs such as *N*-cyclohexyl-2-pyrrolidone (NCP), *N*-octyl-2-pyrrolidone (NOP), and *N*- dodecyl-2-pyrrolidone (NDP) are useful extractants for separating U(VI) from HNO_3 solutions containing simulated fission products. Using these NRPs, extractabilities of U(VI) increase with increasing [HNO_3] from approximately 7% ([U(VI)] = 10 mM, [HNO_3] = 0.1 M, [NRPs] = 1.0 M) to 90% ([U(VI)] = 10 mM, [HNO_3] = 3.0 M, [NRPs] = 1.0 M). Furthermore, these NRPs were found to have selectivity to U(VI). However, it was confirmed that Re(VII) used as a simulant for Tc(VII) and Pd(II) are also extracted with U(VI) species [3].

In order to examine extraction properties of Pd(II) and Re(VII) species in more detail, hence, we have studied extraction behavior of Pd(II) and Re(VII) from HNO_3 aqueous solutions to CH_2Cl_2 solution containing NCP. As a result, the distribution ratios (*D*) of Re(VII) and Pd(II) were found to have a maximum at 1.0 M HNO_3 and 3.0 M HNO_3, respectively. The extraction behavior of Re(VII) is similar to the phenomenon that the *D* values of Tc(VII) decrease with increasing [HNO_3]. This phenomenon has been reported to be due to competition with the extraction of HNO_3. Furthermore, plots of log*D* for Re(VII) and Pd(II) against log[NCP] were found to give straight lines with slopes of 2.2 and 2.3, respectively. This suggests that Re(VII) and Pd(II) are extracted as $HReO_4(NCP)_2$ and $Pd(NO_3)_2(NCP)_2$, respectively.

References

[1] C-H. Shen, B-R. Bao, G-D. Wang, J. Qian, Y-Z. Bao, and Z-B. Cao, *J. Radioanal. Nucl. Chem.*, **162**, 207 (1992).

[2] a)T. R. Varga, M. Sato, *et al*., *Inorg. Chem. Commun.*, **3**, 637 (2000).
b)Y. Ikeda, E. Wada, *et al*., *J.Alloy. Compd.*, **374**, 420 (2004).

[3] Y. Takahashi, H. Hotokezaka, K. Noda, Y. Ikeda, *Proccedings of Seventh International conference on nuclear and Radiochamistry*, Budapest, Hungary 24-29 August 2008 [CD-ROM].

B.4 Crystal Structure of *Trans*-Tetrakis(4-methylpyridine)Dioxorhenium(V) Hexafluorophosphate

Takeshi KAWASAKI, Ali CANLIER, Shubhamoy CHOWDHURY, Yasuhisa IKEDA

Rhenium(V) complexes as radiopharmaceuticals for therapy and diagnosis continue to attract attention, because rhenium isotopes have suitable radionuclear properties for the applications, *i.e.*, ^{186}Re: E_{max} = 1.1 MeV for β-emission and E_{max} = 0.137 MeV for γ-emission with $t_{1/2}$ = 90.6 h, ^{188}Re: E_{max} = 2.1 MeV for β-emission and E_{max} = 0.155 MeV for γ-emission with $t_{1/2}$ = 17 h [1,2]. On the other hand, *trans*-dioxiorhenium(V) (ReO_2^+) complexes have been known to exhibit interesting properties as redox- and photo-active catalysts [3-5]. To our knowledge, the title compound of $[ReO(4\text{-Mepy})_4]PF_6$ (4-Mepy = 4-methylpyridine) (**I**), was already synthesized by Brewer & Gray[6], but crystallographic characterization of **I** have not been reported. In this work, we report a single crystal structure of **I**.

The complex **I** crystallized in the centrosymmetric space group *C*2/*C*. The crystal structure is constructed by the packing of the $[ReO_2(4\text{-Mepy})_4]^+$ cation and the octahedral PF_6^- anion as shown in Fig. 1. Re(1) is located on an inversion center and P(1) lies on a C_2 axis parallel to the *b* axis. Re(1) exhibits a ReN_4O_2 octahedral coordination geometry with the two O atoms in the apical positions and the four N atoms of the four 4-Mepy ligands in the equatorial plane. The N(1)-Re(1)-N(2) angle and all N-Re(1)-O angles are almost 90 ˚. The bond lengths of Re(1)=O(1), Re(1)-N(1), and Re(1)-N(2) are 1.769(2), 2.147(2) and 2.146(2), respectively. These values are similar to those found for other *trans*-dioxorhenium(V) complexes [7-15].

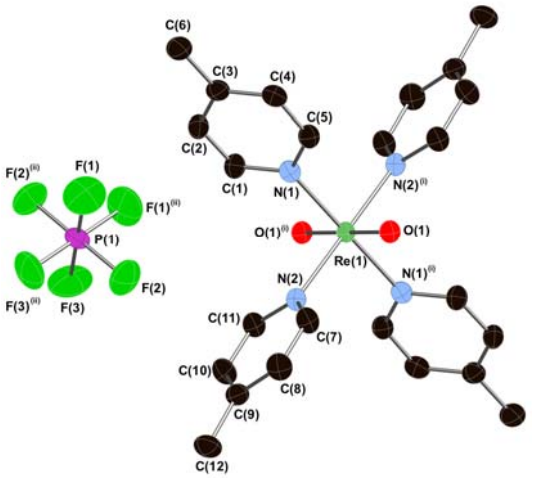

Fig. 1 View of $[ReO_2(4\text{-Mepy})_4]^+$ cation and PF_6^- anion with 50 % thermal ellipsoids. Hydrogen atoms are omitted clarity.

References

[1] J.R. Dilworth and S.J. Parrott, *Chem. Soc. Rev.*, **27**, 43 (1998).
[2] W.A. Volkert and T.J. Hoffman, *Chem. Rev.*, **99**, 2269 (1999).
[3] J.K. Grey, I.S. Butler, and C. Reber, *Can. J. Chem.*, **82**, 1083-1091 (2004).
[4] D.W. Pipes and T.J. Meyer, *J. Am. Chem. Soc.*, **107**, 7202 (1985).
[5] H.H. Thorp, J.V. Houten, and H.B. Gray, *Inorg. Chem.*, **28**, 889 (1989).
[6] J.C. Brewer, and H.B. Gray, *Inorg. Chem.*, **28**, 3334 (1989).
[7] S. Bélanger, and A.L. Beauchamp, *Inorg. Chem.*, **35**, 7836 (1996).
[8] A. Canlier, T. Kawasaki, S. Chowdhury, and Y. Ikeda, *Inorg. Chim. Acta*, **363**, 1 (2010).
[9] J.S. Gancheff, C. Kremer, O.N. Ventura, S. Domínguez, C. Bazzicalupi, A. Bianchi, L. Suescun, and A.W. Mombrú, *New J. Chem.* **30**, 1650 (2006).
Higashi, T., (1995). *ABSCOR*. Rigaku Corporation, Tokyo, Japan.
[10] A. Kochel, *Acta Cryst*., E**62**, m1740 (2006).
[11] C. Kremer, E. Kremer, S. Domínguez, E. Chinea, A. Mederos, and A. Castiñeiras, *Polyhedron*, **15**, 4341 (1996).
[12] B. Machura, R. Kruszynski, R. Penczek, J. Mrozi´nski and J. Kusz, *Polyhedron*, **27**, 797 (2008).
[13] R.L. Luck and R.S. O'Neill, *Polyhedron*, **20**, 773 (2001).
[14] K.R. Reddy, Â. Domingos, A. Paulo, and I. Santos, *Inorg. Chem*., **38**, 4278 (1999).
[15] M. Siczek, M.S. Krawczyk, and T. Lis, *Acta Cryst*., E**65**, m1057 (2009).

B.5 Zinc Isotope Fractionation using Anion Exchange Chromatography with Hydrochloric acid Solution

Tatsuya SUZUKI and Masao NOMURA

The zinc injection into the coolant of nuclear reactors has been carried out for the dose reduction. It is preferable to use ^{64}Zn -depleted zinc for this purpose to avoid the activation of ^{64}Zn in the reactor. We have proposed the isotope separation process by use of chromatographic method based on the isotope fractionation effect in the anion exchange reaction. By the way, the zinc isotope fractionation has been studied in the geochemical and environmental fields [1,2]. The isolation of zinc from the biological or geochemical sample is necessary as the pretreatment process for the isotope ratio measurement in order to eliminate the interference. The anion exchange is most popular technique for the zinc isolation. The evaluation of the isotope fractionation in the anion exchange is necessary, since the isotope fractionation in nature is generally low. The zinc isotope fractionation in the anion exchange in 12 *M* (*M* = mol dm^{-3}) hydrochloric acid solution was reported [3]. This fractionation coefficient of ^{68}Zn/^{66}Zn was reported to be 2×10^{-5}, i.e. the isotope fractionation coefficient of one mass, $\varepsilon/\Delta M = (r/r_0 - 1)/(m_h - m_l)$, is 1×10^{-5}, where r, r_0, m_h and m_l are the fractionated isotope ratio, the ordinal isotope ratio, and the mass of heavier isotope, and the mass of lower isotope, respectively. This value is only one datum of zinc isotope fractionation in the anion exchange. It is too little data in order to develop the zinc isotope separation. In the present work, the zinc isotope fractionation in anion exchange chromatography in hydrochloric acid solution is investigated in detail. The chemical structures of zinc existed in solution and adsorbed on resin are also discussed for the understanding the isotope fractionation. The isotope fractionation

The high-porous benzimidazole type anion exchange resin was used for the investigation of the zinc isotope fractionation in the anion exchange reaction. Our used benzimidazole type anion exchange resin has two functional groups. These two functional groups are shown in Fig.1. 4-(1-methylbenzidazole-2-yl)phenyl is tertiary amine. 4-(1,3-dimethylbenzidazole-2-yl)phenyl is obtained by the quaternization of 4-(1-methylbenzidazole-2-yl) phenyl. The quaternization ratio of our used resin was 58.8%. This resin is embedded in the high porous silica beads. The diameter of silica beads is 40 ~ 60 μm.

The total capacity of this resin is 0.8 meq/g-dry. The adsorption experiments were performed by batch technique in order to evaluate the distribution coefficients of zinc. The concentrations of hydrochloric acid were 0.01 ~ 4 *M*. Seven columns connected in series were used for the isotope fractionation chromatography. The diameter of each columns and the length were 8mm and 1m, respectively. The above mentioned benzimidazole type anion exchange resin was packed into these columns. These columns have water jacket for the temperature control. The experimental temperature was kept at 298 K. The breakthrough experiments using 0.1 *M* of zinc dissolved in 0.5, 1, 2, and 4 *M* hydrochloric acid solutions were performed. The zinc chemical structures in water, 2 *M* hydrochloric acid solution and anion exchange resin were analyzed by extended X-ray absorption fine structure (EXAFS) spectroscopy. The concentrations of zinc ion in solutions were 0.1 *M*. The ratio of the anion exchange resin was 0.1 g / 30 cm^3. In the case of EXAFS analysis of resin, wet resin taken out of 2 *M* hydrochloric acid solution was used.

The typical result of isotope fractionation is shown in Fig. 2. This isotope fractionation is obtained by using 1 *M* hydrochloric acid solution. This figure says that the heavier isotopes are disproportionately located in solution phase. The zinc concentration profile, "breakthrough curve", is also shown in Fig. 2. The isotope fractionation coefficient, $\varepsilon/\Delta M$, is calculated by using the zinc isotope fractionation curve of ^{66}Zn/^{64}Zn and the zinc concentration profile. The isotope fractionation coefficients in various concentrations of hydrochloric acid solutions are shown in Fig. 3. The isotope fractionation coefficient reported in ref. [3] is also indicated in Fig. 3. The isotope fractionation coefficient decreases with increase in the concentration of hydrochloric

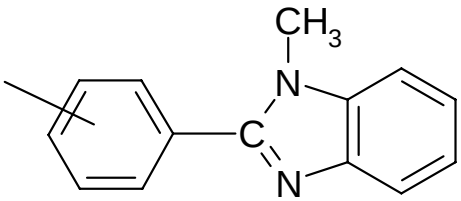

a) 4-(1-methylbenzidazole-2-yl)phenyl

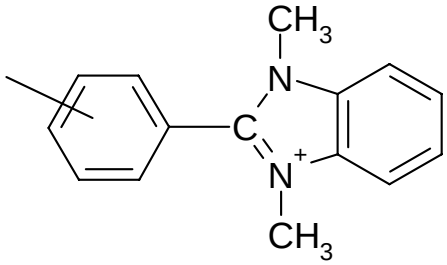

b) 4-(1,3-dimethylbenzidazole-2-yl)phen

Fig. 1 Functional groups of benzimidazole type anion exchange resin

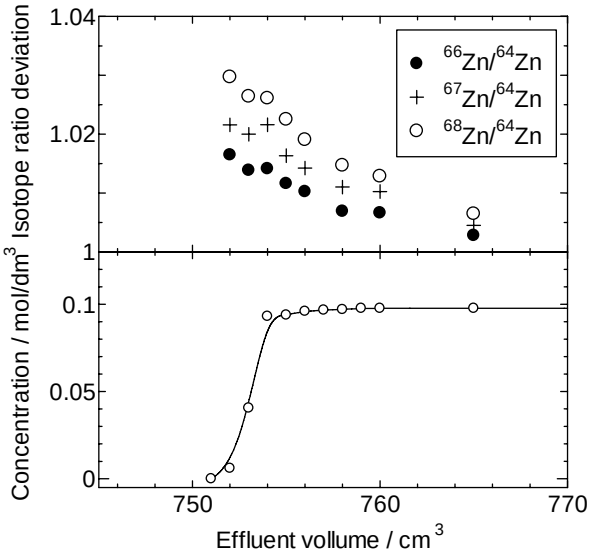

Fig.2 Zinc breakthrough curve and isotope fractionation in anion exchange chromatography using 1*M* hydrochloric acid solution

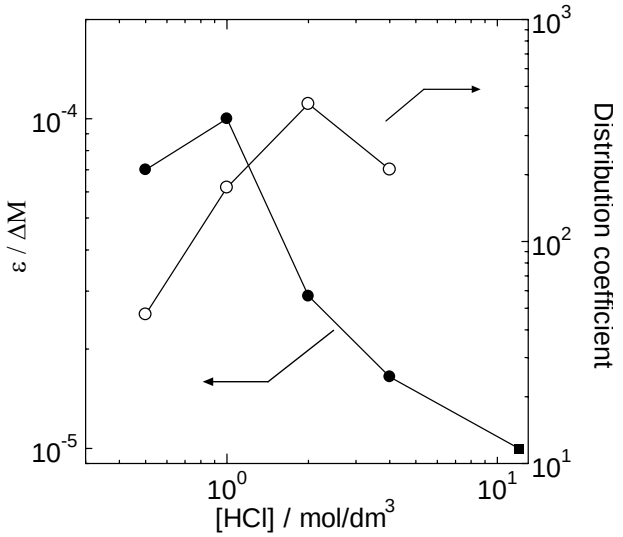

Fig. 3 Distribution coefficient of zinc ion and zinc isotope fractionation coefficient. ●: Present study, ■: literature datum in ref.[3].

acid solution over 1 *M*, and it can be confirmed that the obtained values in the present study and the literature value have a reasonable locational relation in this graph. The distribution coefficients of zinc ions on anion exchange resin are also indicated in this figure. It was found that the distribution coefficients have maximum under the condition of 2 *M* hydrochloric acid solution, while the maximum of isotope fractionation coefficients is 1 *M*. The kinds of chloro complexes in each concentration hydrochloric acid solution are calculated by using the stability constants for understanding these phenomena. The calculated fraction of zinc chloro complexes is shown in Fig. 4. The species which adsorb on the anion exchange resin were the anionic complexes, while the species which exist in solution were

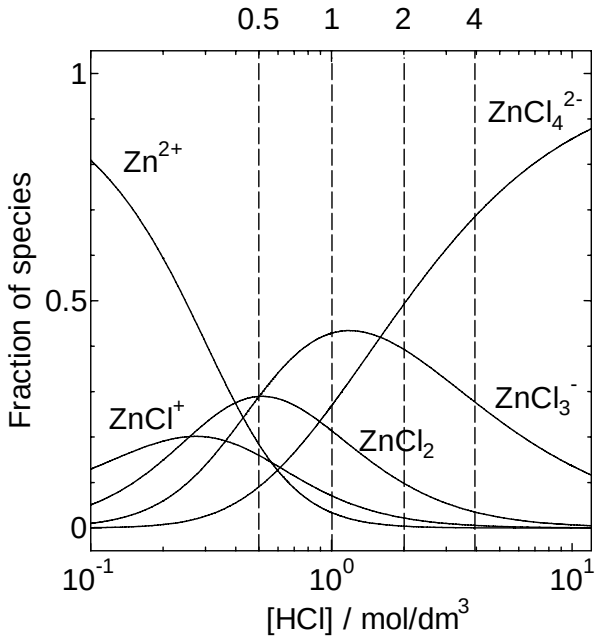

Fig. 4 Fraction of zinc chloro complexes in hydrochloric acid solution.hydrochloric acid solution. The used stability constants were β_1=1.6, β_2=6.3, β_3=12.6, and β_4=7.9.

the cationic complexes and the neutral complex. According to Fig. 4, the total amount of the cationic and neutral complexes decreases with increase in the hydrochloric acid solution, while the total amount of the anionic complexes increases. The average number of chlorine ions coordinated with zinc ion is over 2 in more than the hydrochloric acid concentration of 0.5 *M*. The increase of distribution coefficients of zinc ion with increase in the chlorine ion was explained by increase of the anionic zinc chloro complexes. The decrease in the case of 4 *M* hydrochloric acid solution is explained by the competition reaction in the adsorption of chlorine ion on the anion exchange resin. The isotope fractionations don't occurred without the isotope exchange reaction between the different chemical forms. In the case of zinc anion exchange, it is important that the isotope exchange reaction between the unadsorbed complexes and the anionic complexes. That is, the isotopes exchange reaction between $ZnCl_2$ and $ZnCl_3^-$ is thought to be most important. The reaction between $ZnCl_3^-$ and $ZnCl_4^{2-}$ also could be considerable, because the divalent complex is more strongly adsorbed on the anion exchange resin than the univalent complex. The abundance of $ZnCl_2$ has the maximum peak in 0.5 *M* hydrochloric acid solution, and decreases with increase in the hydrochloric acid concentration over 0.5 *M*. The highest abundance of $ZnCl_3^-$ is 1.2 *M* hydrochloric acid solution. The highest isotope fractionation coefficient may be existed in between 0.5 and 1.1 M hydrochloric acid solution. The chemical structures of zinc existed in the solutions and adsorbed on resin were investigated by EXAFS analysis, and this result is shown in Table 1. R and N in Table 1 are the obtained values calculated from EXAFS spectra. The coordination number

Table 1 EXAFS analysis of zinc chemical structure.

		R/Å	*N*	*N'*
Water	O	2.07	4.3	4
2*M* HCl	O	2.08	1.2	1.5
	Cl	2.26	2.0	2.5
Resin / 2*M* HCl	Cl	2.27	3.2	4

R: distance between Zn and coordinated O or Cl, N: number of coordinated O or Cl,
N': normalized number of coordinated O or Cl, considering that zinc complexes has the tetrahedral structure..

of the bivalent zinc ion is 4, so the obtained N in Table 1 is overestimated or underestimated. The coordination numbers were normalized to 4. The number of coordinated chlorine ions in 2 *M* hydrochloric acid solution was 2.5, and this number was less than the average number calculated using stability constants. However, it is confirmed that the zinc complex ions is totally negative in 2 *M* hydrochloric acid solution. No coordinated water molecules with zinc ion adsorbed on anion exchange resin was observed. This result means that the adsorbed zinc is $ZnCl_4^{2-}$. Since the wet resin taken out of the solution is used for the EXAFS analysis, this result might not show the chemical structure of zinc adsorbed on resin in solution. Although the dominant species exits in the resin phase is $ZnCl_4^{2-}$, it would not be denied that $ZnCl_3^-$ presents in the anion resin phase. To summarize the above, the zinc isotope fractionation in the anion exchange is attributed to the reaction of $[Zn(H_2O)_2Cl_2]^0 \leftrightarrows [Zn(H_2O)Cl_3]^- \leftrightarrows [ZnCl_4]^{2-}$. The zinc complexes have the tetrahedral structure, and the distance from zinc ion is different by the water molecules or the chlorine ions coordinated with zinc ion. The distance of water molecule and zinc ion is shorter than one of chlorine ion and zinc ion (see Table 1), and this means that the bonding force of the water molecule with zinc ion is stronger than the chlorine ion. Because the heavier isotope is generally enriched into the side with stronger chemical bond, the heavier zinc isotope is disproportionately located in the complexes with more water molecules. The zinc complexes with more water molecules more present in solution phase, so the heavier isotope is disproportionately located in solution phase.

In conclusion, the zinc isotope fractionation in the anion exchange in the hydrochloric acid solution was investigated. It was confirmed that the heavier zinc isotopes is disproportionately located in solution phase and the isotope fractionation coefficients depend on the concentration of hydrochloric acid. The maximum isotope fractionation coefficient was appeared in the case of 1*M* hydrochloric acid solution. The hydrochloric acid concentration obtaining the maximum isotope fractionation coefficient was different from the condition obtaining the maximum distribution coefficient. The isotope fractionation is explained by the isotope exchange reaction between the zinc chloro complexes. The disproportional distribution of the heavier zinc isotopes in solution phase was explained by the zinc complex structures.

References

[1] C. N. Maréchal, P. Télouk and F. Albarède, *Chemical Geology*, **156**, 251-273 (1999).
[2] S. Pichat, C. Douchet and F. Albarède, *Earth Planet. Sci. Lett.*, **210**, 167-178 (2003).
[3] C. Maréchal and F. Albarède, *Geochim. Cosmochim. Acta*, **66**, 1499-1509 (2002).

B.6 Nanofluidic-Based Separation System of Radionuclide Ions by Controlling Electrostatic Forces

Takehiko TSUKAHARA

In order to establish partitioning methods for high level liquid wastes, various separation techniques of actinide and lanthanide ions have been investigated. Their techniques are divided broadly into two categories, that is, one is solvent extraction process such as TRUEX, TALSPEAK, DIDPA processes *etc*., and the other is chromatographic process using resins impregnated with specific extractants. However, since both processes are passive techniques that depend on single nanometer-scale liquid/liquid and liquid/solid interfaces, it would be difficult to improve innovatively the separation selectivity of metal ions. Therefore, the separation technique should be switched from passive to active to control the behavior of radionuclide in molecular level.

From this point of view, we have recently focused on nanofluidic spaces (10 – 100 nm scale spaces) and investigated properties of liquids confined in the nanofluidic spaces. As a result, we found that the water molecules in them have unique behavior such as higher viscosity, slower motion, and faster proton mobility that cannot be observed in bulk phase, and proposed that such phenomena are due to the effect of surface charges on properties of water [1 - 3]. Based on the results, when the aqueous solution containing metal ions flows in the nanofluidic space, the differences of electrostatic forces between each hydrated metal ion and surface charges are expected to affect the behavior of metal ions. Herein, we demonstrate a novel nanofluidic-based separation, in which the metal ions can be separated according to differences in free energy for ion hydration in the nanofluidic spaces.

The nanofluidic spaces were fabricated on a fused-silica substrate by means of electron beam lithography and plasma etching. After the straight-shaped nanospaces were connected to U-shaped microspaces, the 10 mM nitric acid solution containing Cesium (Cs^{I}), Strontium (Sr^{II}), Cerium (Ce^{III}), Europium (Eu^{III}), and Uranium (U^{VI}) ions (sample A; Cs : Sr : Ce : Eu : U = 1.0 : 1.0 : 1.0 : 1.0 : 1.0) filled in the vial was introduced in the nanospaces using pressure controller (see Figure 1). The solution (sample B) through nanospaces was recovered, and the concentrations of metal ions in sample B were measured by Induced-Coupled-Plasma (ICP), followed by comparison with those in sample A.

Figure 2 shows the bar-graphs of relative concentration ratio for samples A and B in the size of 300 to 3000 nm. It is found that the relative ratio (RR) of Ce^{III} and U^{VI} ions increases with decreasing space size, while the RR value of Eu^{III} decreases in the space sizes less than 1000 nm. In the case of Cs^{I} and Sr^{II} ions, the RR values were constant without depending on the space size. These results indicated that Ce^{III} and U^{VI} ions could flow quite faster than Eu^{III} ion in nanofluidic spaces.

Although the investigation of the detailed mechanism that same trivalent ions such as Ce^{III} and Eu^{III} can be separated by flowing in nanofluidic spaces is still in progress, this nanofluidic technique will provide clear advantages for the mutual separation of trivalent ions such as lanthanide.

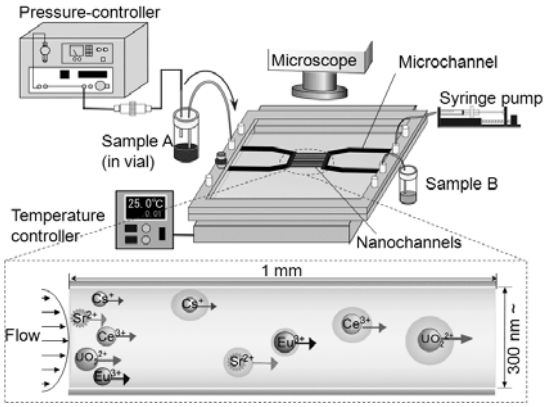

Figure 1. Schematic Illustration of nanofluidic control system.

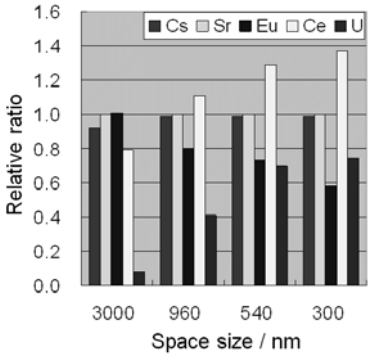

Figure 2. Space size-dependence of relative concentration ratios (Sr is normalized as 1.0).

References

[1] T. Tsukahara, et al., *Angew. Chem. Int. Ed*., **46,** 1180 (2007),
[2] T. Tsukahara, et al., *J. Phys. Chem.* B, **113**, 10808 (2009).
[3] T. Tsukahara, et al., *Chem. Soc. Rev.*, **39**, 1000 (2010).

B.7 One-dimensional peanut-shaped C_{60} polymers with positive and negative Gaussian curvatures: Toward the open for a new science of quantum electronic systems in Riemannian geometric space

Jun ONOE, Takahiro ITO, Yasunori TODA, Hiroyuki SHIMA,
Hideo YOSHIOKA and Shin-ichi KIMURA

1. Introduction

Since the first report on C_{60} photo-polymerization [1], there have been many reports on C_{60} polymers obtained by various kinds of methods, as shown in Table 1 [2]. We have hitherto produced them from photo and electron-beam (EB) irradiation of pristine C_{60} films, and investigated their structural and electric properties. As shown in Fig. 1, photo-polymerization provides two-dimensional (2D) semiconducting dumbbell-shaped C_{60} polymers (left) with a resistivity of 10^3 Ωcm [3-9], whereas EB-polymerization does metallic peanut-shaped C_{60} polymers with that of 1-10 Ωcm [10-18]. These resistivity values were obtained using four-probe measurements at room temperature under atmospheric conditions, which are both much smaller than that (10^8–10^{14} Ωcm) of solid C_{60} [19, 20].

Table 1. Summary of fullerene polymers formed by various kinds of methods.

Method	Reactant	Cross-linkage	Structrure
Photo-irradiation	C_{60} film	dumbbell single-bond	1D 2D hexagonal 1D
High-Temperature and High-pressure	Solid C_{60}	dumbbell	1D orthorhombic 2D tetragonal 2D hexagonal 3D tetragonal/ hexagonal
Charge transfer	AC_{60}* Na_2RbC_{60} Na_4C_{60}	dumbbell single-bond single-bond	1D orthorhombic 1D orthorhombic 2D tetragonal
Solid catalysis	C_{60} powder KCN	dumbbell	dimer/trimer
Electron-beam	Solid C_{60} C_{60} film	dumbbell peanut-shaped dissociation	dimer 1D 3D amorphous

*A denotes alkali metals.

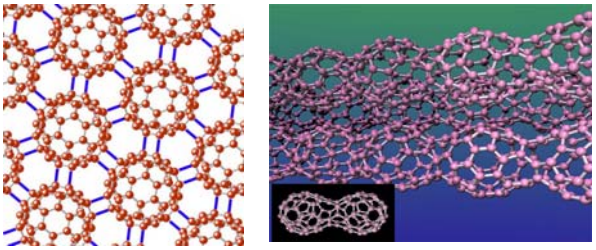

Fig. 1. Schematic illustration of 2D hexagonal dumbbell-shaped C_{60} polymers (left) and quasi-1D peanut-shaped C_{60} polymers (right) [taken from Refs. 9 and 14].

As shown in Fig. 1 (left), the 2D C_{60} polymer has a [2+2] four-membered cross-linkage between adjacent C_{60} molecules by dissociation of C=C double bonds of each C_{60}. In this case, the whole system is not regarded as a π-electron conjugated system, thus exhibiting semiconducting. On the other hand, as sown in Fig. 1 (right), the peanut-shaped polymer has a coalesced structure via the general Stone-Wales rearrangement [21, 22] between adjacent C_{60} molecules. The EB-polymer can be regarded as a π-electron conjugated system, thus exhibiting metallic. In addition, when we focus on the geometric aspect for the EB-polymer, this peanut-shaped structure has both positive and negative Gaussian curvatures [23], which is different from well-known π-electron conjugated carbon allotropes (see Table 2).

Table 2. Classification of π-electron conjugated carbon allotropes by using Gaussian curvature.

π-electron system	Gaussian curvature	N-membered ring
graphite	0	6
fullerenes	＋	5、6
nanotubes	0（body）、＋（cap）	5、6
Mackay crystal* (hypothetical)	—	6 , 8
peanut-shaped polymers	＋、—	5 – 8

*see Fig. 9 (taken from Ref. 41)

In the present review, we will introduce our recent works on the optical and electronic properties of the peanut-shaped C_{60} polymer with positive and negative Gaussian curvatures obtained using femtosecond time-resolved spectroscopy [24] and high-resolution photoelectron spectroscopy [25, 26], respectively. In particular, we will discuss the effects of Gaussian curvatures on the electronic states of the polymer on the basis of Schrödinger equation on Riemannian surface [27, 28]. Finally, we will describe the perspective of the peanut-shaped C_{60} polymer from a viewpoint of topological science.

2. Optical properties

To investigate optical properties of the peanut-shaped C_{60} polymer, we examined the dynamics of photo-excited carriers in the polymer, using two-color pump-probe femtosecond spectroscopy (a temporal resolution of 200 fs) in which a coaxial configuration between the pump (1.07 eV) and probe (1.55 eV) laser beams provides a high

signal to noise ratio (*S/N*) [24, 29]. C_{60} films (200 nm thick) were formed on a CsI substrate in the UHV chamber by sublimation of the C_{60} powder at 673 K. The peanut-shaped C_{60} polymer sample was prepared by 3 kV EB-irradiation, and its formation was confirmed using *in situ* infrared spectroscopy [30]. We also prepared a pristine sample without EB irradiation as a reference. The films thus formed were mounted on the cold finger of an optical cryostat, and the lifetime of photo-excited carriers in the films was recorded as a function of the substrate temperature (20–300 K). The details of the measurement system and conditions were described in Ref. 24.

Typical transient $\Delta T(t)$, the difference in transmission from that of an equilibrium condition as a function of the delay time between the pump and probe pulses, for the peanut-shaped C_{60} polymer and pristine C_{60} films are shown in Figs. 2 (a) and 2 (b), respectively.

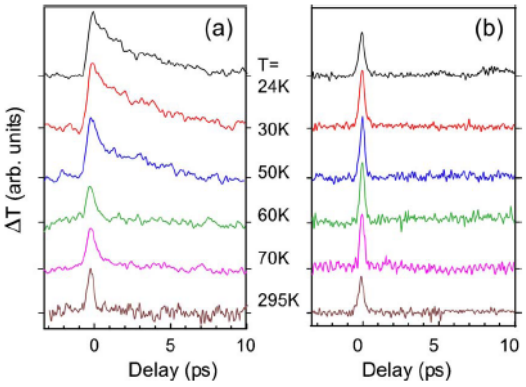

Fig. 2. Typical transmission change DT(t) vs decay time for (a) peanut-shaped C_{60} polymer film and (b) pristine C_{60} film over a wide temperature range of 20–300 K [taken from Ref. 24].

In the high temperature range exceeding 60 K, $\Delta T(t)$ is identical for both samples and show an instantaneous response (hereafter we call this the "fast compnent"). This common feature remains largely unchanged over the whole temperature range. On the other hand, in the low temperature range below 60 K, $\Delta T(t)$ for the polymer sample shows an additional relaxation component with a slow decay (hereafter we call this the "slow component"), which becomes dominant in the low temperature range. It is noted that the fast component is still present even at the lowest temperature examined in the present work, though its outline is largely obscured by the slow component, as shown in Fig. 2 (a). As a result of considering the temperature-dependent fast component [24], since the excitation energy of the incident pulses (pump: 1.07 eV, probe:1.55 eV) is well below the optically allowed interband transitions of C_{60} molecules [17], the present observed instantaneous response can be attributed to two-photon absorption (TPA). In addition, the transmission change is found to be linearly dependent on the pump laser power, thus indicating that the signal consists of a TPA process involving one pump photon and one probe photon. This assignment agrees well with the transient profile, which is largely consistent with the correlation between the incident pulses.

We next consider the *T*-dependent slow component appearing at a lower temperature for the peanut-shaped polymer sample. Using the two-component exponential decay function,

$$\Delta T(t) = A_f \exp(-t/\tau_f) + A_s(T)\exp[-t/\tau_s(T)],$$

where A and τ denote the amplitudes and relaxation times as a function of temperature, respectively, and the notations *f* and *s* refer to the fast and slow components, respectively, we can obtain a good fit with the data of Fig. 2 (a) for the polymer sample. Because the fast component could be regarded as *T*-independent, A_f and τ_f were fixed at constant values throughout the fitting procedure. The results of $\tau_s(T)$ and $A_s(T)$ obtained using the formula are shown in Figs. 3 (a) and 3 (b), respectively.

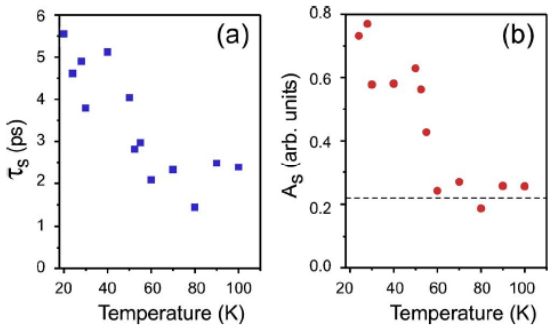

Fig. 3. Temperature dependence of (a) decay time τ_s and (b) amplitude A_s for the slow component obtained from an exponential fitting to $\Delta T(t)$. The dashed line indicates the background level [taken from Ref. 24].

A signal with a decay time of a few picoseconds starts to appear below 60 K and becomes dominant with further lowering the temperature. A *T*-dependent transient signal with a similar decay time has been observed for various quasi-1D compounds [29, 31], in which the appearance of relaxation bottleneck reflects an energy gap associated with the Peierls transition. Thus, the slow component appearance indicates an energy gap formation below 60 K for the peanut-shaped C_{60} polymer as well as quasi-1D compounds such as $K_{0.3}MO_3$. Consequently, the results of Figs. 2 and 3 suggest that the peanut-shaped C_{60} polymer is a 1D or quasi-1D metallic carbon.

Figures 4 (a) and 4 (b) show a schematic diagram of the transition processes accounting for the fast and slow transient components, respectively. For an excitation energy smaller than the interband energy gap, only the TPA process contributes to the $\Delta T(t)$, resulting in an instantaneous response during the correlation between the incident two pulses. The TPA transition is also applicable to the pristine sample. On the other hand, in the presence of a narrow energy gap, even when the gap includes large fluctuations, the photoexcited carriers from higher excited states to the gap states and vice versa

contribute to the ΔT(t). The T-dependent ΔT(t) reflects the T-dependence of the energy gap and order parameter fluctuations.

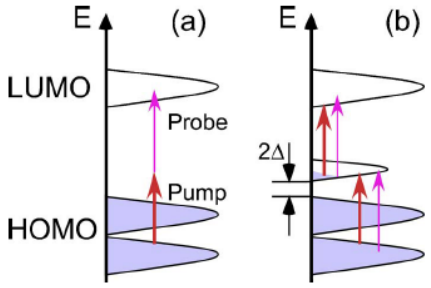

Fig. 4. (a) Schematic diagram of a TPA process consisting of one pump photon and one probe photon. (b) Interband carriers relaxation processes in the presence of an energy gap at a lower temperature [taken from Ref. 24].

In typical quasi-1D compounds exhibiting the Peierls transition, the decay time diverges near the transition temperature at which efficient phonon transitions (both emissions and re-absorptions) greatly make the relaxation time longer at the beginning of the gap formation. However, as shown in Fig. 3 (a), there is no clear divergence at around 60 K, and instead the decay time and amplitude increase monotonically with decreasing temperature down to 20 K. We consider the different behavior of the decay time is presumably due to a topological effect driven from the positive and negative Gaussian curvatures at present, but it is further necessary to study the present subject.

3. Electronic properties

To clarify the origins of the metallic I-V characteristics of the peanut-shaped C_{60} polymer, we examined its valence electronic structure around the Fermi level (E_F), using *in situ* high-resolution ultraviolet photoelectron spectroscopy (UPS). Prior to deposition, a 100 mg of C_{60} powder (99.98 % pure) introduced into a Knudsen cell (K–cell) was heated at 473 K for a few hours to remove residual organic solvents from the powder in a preparation chamber (base pressure: 1×10^{-7} Pa). Thereafter, a C_{60} film (20–30 nm thick) was formed on a copper (Cu) substrate by sublimation of the pretreated C_{60} powder in the K–cell at 673 K for 3 min in the preparation chamber. Subsequently, the pristine C_{60} film was transferred to an analysis chamber (base pressure: 1×10^{-8} Pa) and measured *in situ* by UPS with an energy resolution of 10-20 meV and with the monochromatic He Iα (21.218 eV) or He IIα (40.806 eV) emission line. Although we used He Iα in Ref. 25, we used He IIα emission line in order to examine the π-electron behaviour near the E_F for the outermost layers of the EB-irradiated film in Ref. 26. After the measurements, the film was returned to the preparation chamber and irradiated with 3 kV-EB for 0.5, 1.5, 2.5, 5.0, and 12 h. We confirmed by *in situ* infrared spectroscopy that 12 h of EB–irradiation was sufficient to allow the C_{60} molecules to completely coalesce, thus forming a peanut–shaped C_{60} polymer all over the film. Every after each EB-irradiation time, the film was transferred to the analysis chamber for *in situ* UPS measurements. The zero value in binding energy for the present measurements was determined from the E_F (= 0 eV) of a Au film, which was deposited on the same Cu substrate as for the pristine and EB-irradiated C_{60} films, by fitting its UPS spectrum with a Fermi distribution function at the measurement temperature (350 K). In the present substrate temperature, the E_F of a semiconductor is located in the middle between the valence and conduction bands by thermal broadening, and is almost the same position as that of a metal with thermal broadening at the temperature.

Figure 5 shows the UPS spectra of the EB-irradiated C_{60} film for several irradiation times (350 K), along with the pristine C_{60} film measured at 300 K: 0 h (red), 0.5 h (orange), 1.5 h (green), 2.5 h (sky blue), and 5.0 h (blue). For the pristine C_{60} film (red line), some intensive narrow bands such as HOMO and HOMO–1 were observed, because of the weak interaction between adjacent C_{60} molecules. On the other hand, as EB-irradiation time increases, each band becomes broadened in response to the disappearance of molecular character caused by EB–induced polymerization between adjacent C_{60} molecules, and the valence electronic states spread monotonically toward the E_F with increasing the EB-irradiation time. After 5 h of EB-irradiation, the electronic states reach to the E_F, as illustrated by the blue line.

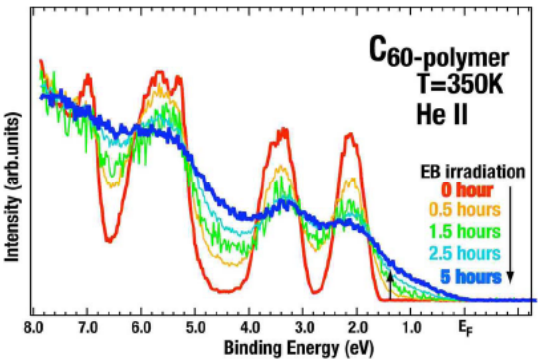

Fig. 5. EB-time evolution of valence photoelectron spectra of a C_{60} film in a wide binding energy region. All spectra were obtained at 350 K except that of pristine C_{60} film at 300 K (taken from Ref. 26).

To understand this behavior near the E_F in details, we next measured the EB-irradiation time–dependence of UPS spectra of the film in the binding energy of 3 eV below the E_F. Figure 6 shows the evolution of UPS spectra of the C_{60} film in the binding energy region as a function of EB–irradiation time, where insets shows the symmetrised spectra in the vicinity of the E_F: 0 h (red), 0.5 h (orange), 2.5 h (sky blue), and 5.0 h (blue) in order to remove the effect of thermal broadening from those spectra. Because the S/N ratio of the spectrum of 1.5 h–irradiated C_{60} film (the green line shown in Fig. 6) was

poor in comparison with that of the others, it was omitted in this figure. As shown in Fig. 6, the electronic states in the binding energy range of 0–2 eV is gradually increased in response to the broadening of the HOMO band located at around 2.4 eV, as the EB-irradiation time increases. This indicates that EB-irradiation time reduced the energy gap, which is related to the electron-transport properties, of a C_{60} film continuously. This finding implies that the electronic properties of a C_{60} film can be controlled from an insulator to a metal via a semiconductor continuously only within a EB-irradiated area, which is interesting when the EB-irradiated C_{60} polymer is applied to the fabrication of electronic devices.

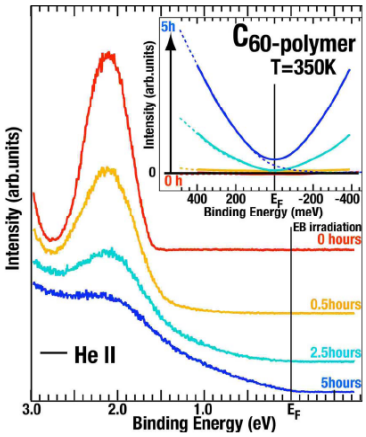

Fig. 6. EB-time evolution of valence photoelectron spectra of a C_{60} film in the binding energy of 3 eV below the Fermi level. Inset shows the symmetrized spectra in the vicinity of the Fermi level in order to remove the effect of thermal broadening from the spectra (taken from Ref. 26).

Why does the electronic properties of the C_{60} film change continuously from insulating to metallic via semiconducting as EB irradiation time increases? One of the reasons is attributed to the change in polymerization degree upon EB irradiation. We performed the first-principle calculations of the energy gap for the dimer (C_{60}-C_{60}), trimer (C_{60}-C_{60}-C_{60}), and one-dimensional system (-C_{60}-) with a give cross-linked structure between adjacent C_{60} molecules [18], and obtained them to be 0.333, 0.107, and 0.021 eV, respectively, along with that of 1.668 eV for C_{60} which is in an excellent agreement with experimental results of 1.6–1.8 eV [32]. Otherwise, the other reason is attributed to that the general Stone-Wales rearrangement between adjacent C_{60} molecules proceeds as EB irradiation time increases.

We next discuss the UPS results obtained after 12-h EB irradiation. Figure 7 shows UPS spectra of pristine C_{60} (blue line) and peanut–shaped C_{60} polymer (red line) films obtained at a substrate temperature of 300 K and 350 K, respectively, where the inset shows the UPS spectrum of the peanut–shaped C_{60} polymer near the E_F. For the peanut–shaped C_{60} polymer, each band is broadened in response to the disappearance of molecular character caused by EB–induced polymerization between adjacent C_{60} molecules, and the valence electronic states spread toward the E_F. In order to clarify the behavior of the electronic structure of the peanut−shaped C_{60} polymer in the vicinity of the E_F, we measured more precise UPS spectra of the pristine C_{60} and peanut–shaped polymer films in the binding energy of 3.0 eV below the E_F, as shown in the inset of Fig. 7. It was found that the photoelectron spectrum of the peanut–shaped polymer is much greater than that of the pristine C_{60} film near the E_F and clearly comes across the E_F edge. These findings suggest that the peanut–shaped C_{60} polymer has a metallic electronic structure. However, the results shown in the inset of Fig. 7 were measured at 350 K, thus the effect of a thermal broadening on the spectra should be taken into account. This implies that the peanut-shaped polymer is possible to be not only metal or semimetal but also narrow-gap semiconductor.

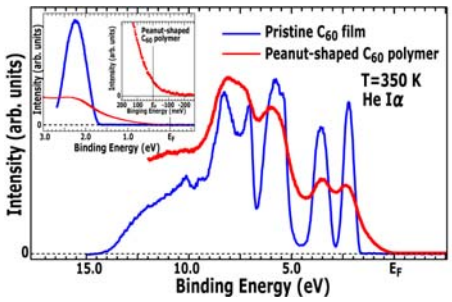

Fig. 7. *In situ* high-resolution UPS spectra of pristine C_{60} film (blue line) and peanut–shaped C_{60} polymer (red line) obtained at 300 K and 350 K, respectively. Inset shows the UPS spectrum of the peanut–shaped C_{60} polymer near the E_F (taken from Ref. 25).

Then we next examined the temperature dependence of the UPS spectra in the vicinity of the E_F for the peanut-shaped C_{60} polymer, because the thermal broadening effect reduces with decreasing temperature. For example, Figure 8 shows the plot of the Fermi distribution function near the E_F in the range of 50 – 350 K (350 K: red, 200 K: orange, 150 K: green, 100 K: sky blue, and 50 K: blue). At 350 K, there is a large thermal broadening in the distribution function in a similar manner to the spectrum shown in the inset of Fig. 7. As temperature is going down from 350 K to 50 K, thermal broadening becomes smaller and the Fermi step at the E_F appears clearly at 50 K, as shown in Fig. 8.

We examined the *T*-dependence of UPS spectra near the E_F for the peanut-shaped C_{60} polymer. Figure 9 shows the UPS spectra measured at 50 K (blue, top), 100 K (sky blue, second top), 150 K (green, middle), 200 K (orange, second bottom), and 350 K (red, bottom). It is found that the spectrum comes across the E_F even at 50 K, thus indicating that the peanut-shaped polymer is metal. Interestingly, the spectral function does not show a Fermi step clearly even at 50 K unlike the prediction shown in Fig. 8. Two or three dimensional metal such as $TaSe_2$ and Rhodium always exhibit a Fermi step, but quasi-1D metal such as $K_{0.3}MO_3$ and $(TaSe_4)I$ does not show such the step [33]. Accordingly, the results of Fig. 9 suggest

that the peanut-shaped C_{60} polymer is a 1D or quasi-1D metal, which is consistent with the results of its photo-excited carriers dynamics described in the previous section.

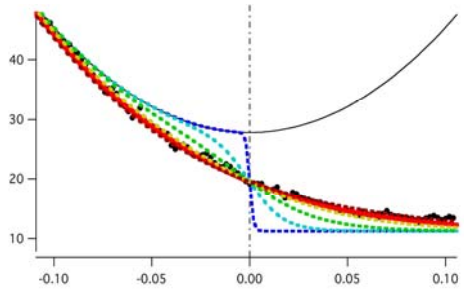

Fig. 8. Plot of the Fermi distribution function as a function of temperature (red: 350 K, orange: 200 K, green: 150 K, sky blue: 100 K, and blue: 50 K). The horizontal axis denotes the energy level (eV) in the vicinity of the Fermi level (= 0 eV), where the negative and positive areas mean the occupied and unoccupied levels, respectively. The vertical axis denotes the density of states (arbitrary unit).

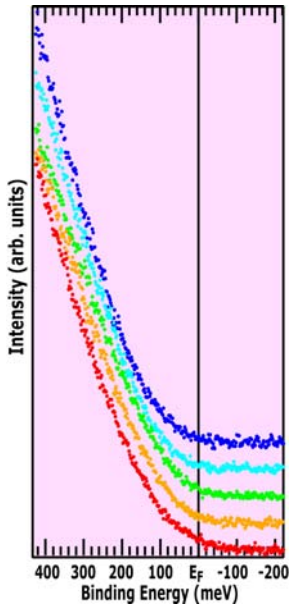

Fig. 9. Temperature dependence of UPS spectra in the vicinity of the E_F: 350 K (red), 200 K (orange), 150 K (green), 100 K (skyblue), and 50 K (blue).

If the peanut-shaped polymer is 1D metal, its electrons should exhibit a Tomonaga-Luttinger liquids (TLL) behavior in which the density of states (DOS) shows a power-law dependence of the binding energy and of temperature (the value of exponent α is less than unity) [36]. For example, for metallic single-wall carbon nanotubes (SWCNT), a TLL behavior was observed (α = 0.5) [35], which is the direct evidence of 1D metal. In a similar manner to SWCNT, we examined the T-dependence of UPS spectra near the E_F in the range of 30–350 K, using a monochromatic He IIα emission line. We also observed a TLL behavior for both binding energy and temperature and obtained α to be 0.6 [28], thus demonstrating that the peanut-shaped C_{60} polymer is 1D metal as well as SWCNTs. Here we have a next question: what is the difference in the correlation exponent (α) value between SWCNT and the peanut-shaped polymer? And what is the difference physically meaningful?

4. Riemannian geometrical effects on TLL correlation exponent

To explain the difference in the TLL correlation exponent value between them, we have focused our attention on the difference in their topology based on Gaussian curvature, as shown in Table 2. At the first step, we regarded the electron motion on the 1D peanut-shaped C_{60} polymer as free electrons moving on a quantum hollow cylinder with periodic radius modulation (see Fig. 10) resulting in 1D curved surface with positive and negative Gaussian curvatures aligned alternatively and periodically. On such the curved surface, Schrödinger equation dealing with electron motion cannot be written in Euclidean space but in Riemannian space [27]. As a consequence, the single-particle DOS, $n(\omega)$, near the E_F should exhibit a power-law singularity as follows,

$$n(\omega) \propto |\hbar\omega - E_F|^{\alpha}, \quad \alpha = \frac{K + K^{-1}}{2} - 1.$$

Where K (>0) is a parameter to express the strength of electron-electron interactions, and can be written as

$$K = \lim_{q \to 0} \sqrt{\frac{2\pi\hbar v_F + g_4(q) - g_2(q)}{2\pi\hbar v_F + g_4(q) + g_2(q)}}.$$

Where, v_F denotes the Fermi velocity, and $g_4(q) = V(q, m)$ and $g_2(q) = V(q, m) - V(2k_F, m)$ show q-dependent coupling constants. $V(q, m)$ is the Fourier transform of the screened interaction. The details of the present results and discussion were described in Ref. 27.

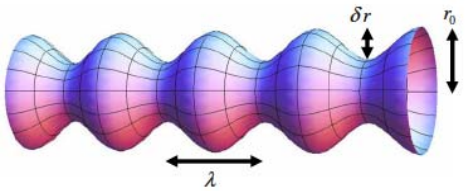

Fig. 10. Schematic illustration of a quantum hollow cylinder with a periodic radius modulation (taken from Ref. 27).

Figure 11 shows the δr dependence of both K and α for different k_F values. The insets in Fig. 11 show the k_F dependence of K and α at $\delta r/a$ =2.0. Figure 11 demonstrates that the K decreases and the α increases significantly with increasing the δr for the ratio $\delta r/a$ exceeding 2.5. Such the δr-driven shift in the K and the α

is attributed to the effects of Gaussian curvatures on the nature of TLL states. Consequently, it is interesting to note that the difference in TLL correlation exponent α value between SWCNT and 1D peanut-shaped polymer can be explained in terms of the Riemannian geometrical effects.

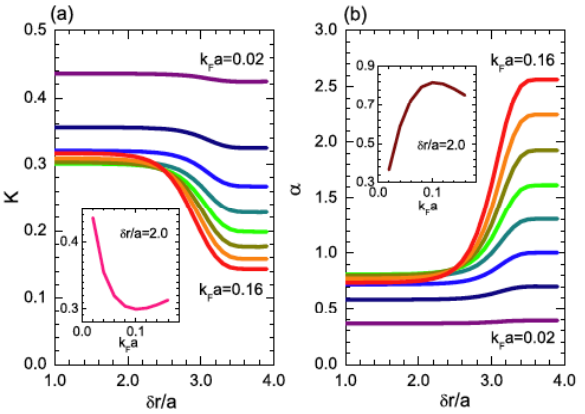

Fig. 11. Plot of the δr dependence of the K and α. Insets show non-monotonic behaviors of the K and α as a function of the k_F at $\delta r/a$=2.0 (taken from Ref. 27).

5. Summary & Perspective

We have reviewed our recent works on the optical and electronic properties of the peanut-shaped C_{60} polymer formed by EB irradiation of C_{60} films. This polymer was found to be a 1D metal and can be regarded as a new allotrope of π-electron conjugated carbon materials when they are classified using Gaussian curvature. Indeed, the 1D metallic polymer exhibits a different behavior of optical and electronic properties from well-known 1D metal materials: no divergence in the decay time upon an energy gap formation associated with the Peierls transition, and the TLL exponent value larger than that of 1D metal SWCNT with zero Gaussian curvature. In particular, the difference in the TLL correlation exponent is caused by the Gaussian curvature that drives effective potentials acting on electrons motion on the Riemannian surface.

There have been some reports on carbon materials with a negative Gaussian curvature experimentally [36-38]. However, they were just observed using transmission electron microscope and not shown to have any electronic properties until now. To our best knowledge, the 1D metallic peanut-shaped C_{60} polymer is the first existed material with well-known physical properties that are affected significantly by Gaussian curvature in the Schrödinger equation on Riemannian surface. Curvature effects on electronic, electric, and magnetic properties have been hitherto predicted theoretically [39-45], for example so-called Mackay crystal shown in Fig. 12 [39]. We believe that the 1D metallic peanut-shaped C_{60} polymer is a good material to verify the theoretical predictions and open a new materials science in Riemannian space world.

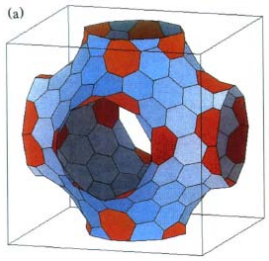

Fig. 12. Schematic illustration of the unit cell of Mackay crystal consisting of 6- and 8-membered rings colored by blue and red, respectively [taken from Ref. 39].

Acknowledgments

One of the authors (J.O.) is greatly thankful to PRESTO/CREST-JST, Murata Foundation, Sumitomo Foundation, and SCAT-Telecom for supporting the present works financially.

References

1) A.M. Rao, P. Zhou, K-A. Wang, G.T. Hager, J.M. Holden, Y. Wang, W.-T. Lee, X-X. Bi, P.C. Eklund, D.S. Cornett, M.A. Duncan, and I.J. Amster: *Science* **259**, 955 (1993).
2) J. Onoe, T. Nakayama, A. Nakao, Y. Hashi, K. Esfarjani, K. Ohno, Y. Kawazoe, M. Aono, and K. Takeuchi: *Clusters and Nanomaterials* (Springer Series in Cluster Physics), Springer-Verlag, p.135 (2002), and references therein.
3) J. Onoe and K. Takeuchi: *Phys. Rev. B* **54**, 6167 (1996).
4) J. Onoe, A. Nakao, and K. Takeuchi: *Phys. Rev. B* **55**, 10051 (1997).
5) J. Onoe and K. Takeuchi: *Phys. Rev. Lett.* **79**, 2987 (1997).
6) K. Esfarjani, Y. Hashi, J. Onoe, K. Takeuchi, and Y. Kawazoe: *Phys. Rev. B* **57**, 229 (1998).
7) T. Nakayama, J. Onoe, K. Nakatsuji, J. Nakamura, K. Takeuchi, and M. Aono: *Surf. Rev. Lett.* **6**, 1073 (1999).
8) J. Onoe, T. Nakayama, A. Nakao, Y. Hashi, K. Esfarjani, Y. Kawazoe, M. Aono, and K. Takeuchi: *Mol. Cryst. Liq. Cryst.* **340**, 689 (2000).
9) J. Onoe, T. Nakayama, M. Aono, and T. Hara: *J. Appl. Phys.* **96**, 443 (2004).
10) T. Hara, J. Onoe, H. Tanaka, Y. Li and K. Takeuchi: *Jpn. J. Appl. Phys.* **39**, 1872 (2000).
11) T. Hara, J. Onoe, and K. Takeuchi: *J. Appl. Phys.* **92**, 7302 (2002).
12) J. Onoe, T. Nakayama, M. Aono, and T. Hara: *Appl. Phys. Lett.* **82**, 595 (2003).
13) T. Hara and J. Onoe: *Eur. Phys. J. D* **24**, 389 (2003).
14) J. Onoe, T. Nakayama, M. Aono, and T. Hara: *J. Phys. Chem. Solids* **65**, 343 (2004).
15) J. Onoe, A. Nakao, and A. Hida: *Appl. Phys. Lett.* **85**, 2741 (2004).
16) T.A. Beu, J. Onoe, and A. Hida: *Phys. Rev. B* **72**, 155416 (2005).
17) S. Ueda, K. Ohno, Y. Noguchi, S. Ishii, and J. Onoe: *J. Phys. Chem. B* **110**, 22374 (2006).
18) T.A. Beu and J. Onoe: *Phys. Rev. B* **74**, 195426 (2006).
19) C. Wen, J. Li, K. Kitazawa, T. Aida, I. Honma, H. Komiyama, and K. Yamada: *Appl. Phys. Lett.* **61**, 2162 (1992).
20) J. Mort, R. Ziolo, M. Machonkin, D.R. Huffman, and M.I. Ferguson: *Chem. Phys. Lett.* **186**, 284 (1991).

21) A.J. Stone and D.J. Wales: *Chem. Phys. Lett.* **128**, 501 (1986).
22) H. Ueno, S. Osawa, E. Osawa, and K. Takeuchi: *Fullerene Sci. Technol.* **6**, 319 (1998).
23) The definition of "Gaussian curvature" is described in the review article (by H. Shima *et al.*) in this special issue.
24) Y. Toda, S. Ryuzaki, and J. Onoe: *Appl. Phys. Lett.* **92**, 094102 (2008).
25) J. Onoe, T. Itoh, S. Kimura, K. Ohno, Y. Noguchi, and S. Ueda: *Phys. Rev. B* **75**, 233410 (2007).
26) J. Onoe, T. Ito, and S. Kimura: *J. Appl. Phys.* **104**, 103706 (2008).
27) H. Shima, H. Yoshioka, and J. Onoe: *Phys. Rev. B* **79**, 201401(R) (2009).
28) T. Ito, J. Onoe, H. Shima, H. Yoshioka, and S. Kimura: to be submitted.
29) J. Onoe and K. Takeuchi: *J. Phys. Chem*. **99**, 16786 (1995).
30) K. Shimatake, Y. Toda, and S. Tanda: *Phys. Rev. B* **75**, 115120 (2007).
31) J. Demsar, K. Biljakovic, and D. Mihailovic: *Phys. Rev. Lett.* **83**, 800 (1999).
32) R.K. Kremer: *Appl. Phys. A* **56**, 211 (1993).
33) B. Dardel, D. Malterre, M. Grioni, P. Weibel, Y. Baer, and F. Levy: *Phys. Rev. Lett.* **67**, 3144 (1991).
34) J. Voit: *Rep. Prog. Phys.* **57**, 977 (1994).
35) H. Ishii, H. Kataura, H. Shiozawa, H. Yoshioka, H. Otsubo, Y. Takayama, T. Miyahara, S. Suzuki, Y. Achiba, M. Nakatake, T. Narimura, M. Higashiguchi, K. Shimada, H. Namatame and M. Taniguchi: *Nature* **426**, 540 (2003).
36) D.E. Luzzi and B.W. Smith: *Carbon* **38**, 1751 (2000).
37) M. Terrones, F. Banhart, N. Grobert, J.-C. Charlier, H. Terrones, and P.M. Ajayan: *Phys. Rev. Lett.* **89**, 075505 (2002).
38) A.G. Nasibulin, P. V. Pikhitsa, H. Jiang, D. P. Brown, A.V. Krasheninnikov, A.S. Anisimov, P. Queipo, A. Moisala, D. Gonzalez, G. Lientschnig, A. Hassanien, S.D. Shandakov, G. Lolli, D.E. Resasco, M. Choi, D. Tománek, and E.I. Kauppinen: *Nature Nanotech.* **2**, 156 (2007).
39) A.L. Mackay and H. Terrones: *Nature* **352**, 762 (1991).
40) S.J. Townsend, T.J. Lenosky, D.A. Muller, C.S. Nichols, and V. Elser: *Phys. Rev. Lett.* **69**, 921 (1992).
41) N. Park, M. Yoon, S. Berber, J. Ihm, E. Osawa, and D. Tomanek: *Phys. Rev. Lett.* **91**, 237204 (2003).
42) H. Terrones and M. Terrones: *New J. Phys.* **5**, 1261 (2003).
43) H. Taira and H. Shima: *J. Phys. Conf. Ser*. **61**, 1142 (2007).
44) S. Ono and H. Shima: *Phys. Rev. B* **79**, 235407 (2009).
45) S. K. Baek, H. Shima, and B. J. Kim: *Phys. Rev. E* **79**, 060106(R) (2009).

B.8 XAFS Analysis of Molten Inorganic Metal Fluorides Containing Thorium Fluoride

Haruaki MATSUURA, Atsushi NEZU and Hiroshi AKATSUKA

To develop the recycle process for the molten salt reactor, an electrochemical method has been considered to be one of the options of separation techniques of actinides (An) and lanthanides (Ln). The lithium fluoride-calcium fluoride (LiF-CaF_2) eutectic melt can be used as the solvent for the electrodeposition of Nd and Th, while LiF-NaF and LiF-KF eutectic melts cannot be used for the same purpose theoretically. To clarify the correlation between structures of molten An (Ln)F_n and their physico-chemical properties would lead to find better electrolysis conditions to improve the efficiency of the pyrochemical reprocessing. However, structural information of the ternary $x$$ThF_4$-$a$LiF-$b$$CaF_2$ mixtures has not been reported yet by any techniques. In this study, molten 0.25ThF_4-0.75LiF, 0.25ThF_4-58LiF-0.17CaF_2 and 0.25ThF_4-0.45LiF-0.30CaF_2 are specially focused for the structural investigation.

XAFS measurements in transmission modes have been performed at BL27B/PF/KEK. The Th L_{III}-edge XAFS spectra have been collected with fixed time scan method by the X-ray from a double Si (111) crystals monochromator. ThF_4 was synthesized by ThO_2 under fluorine gas (40 ml/min) at 650 ^oC for 4 h at Tohoku University. Mixtures made by ThF_4, LiF (Soekawa Co. 4N) and CaF_2 (Soekawa Co. 4N) were melted once in a glassy carbon crucible at 1073 K in a quartz tube filled with an argon atmosphere in high purity. Then, they were mixed with boron nitride powder (BN, Showa Denko Co. ltd), and pressed into pellets in 7 mm diameter and 1 mm thickness. The mixing weight ratio of ThF_4 to BN was ca. 1: 2.5. To prevent chemical reaction of sample and contamination of ThF_4 to outside by heating during XAFS measurements, these pellets were installed in a double barrier cell. The 1st barrier is made with pyrolitic boron nitride [1] and the 2nd barrier is made with boron nitride (HIP). The electric furnace [2] was filled with He gas at ca. 30 kPa.

In the solid state of 0.25ThF_4-0.75LiF, the coordination number of thorium (N_i) and inter ionic distance between thorium and fluorine first neighbour (r_i) were 9 and 2.35Å, respectively. These structural parameters correspond to the structure of Li_3ThF_7 reported in the literature. N_i's and r_i's in all solid states were nearly constant among the mixtures investigated. Radial structure functions of molten 0.25ThF_4–aLiF–$b$$CaF_2$ are shown in Fig. 1. In the molten states, N_i's decreased from 9 to ca. 7.5 and r_i's also decreased from 2.35 to ca. 2.30Å, thus the similar local structure around thorium was preserved. On the other hand, in the case of 0.20TbF_3-aLiF-$b$$CaF_2$ mixtures, N_i and r_i tend to be varied with depending on concentration of CaF_2. It is conjectured that this fact relates to the amount of F^- supplied by solvent melts. In the molten TbF_3-aLiF-$b$$CaF_2$, structural variation appears at b>0.32 and N_i is slightly larger than 6 (Tb^{3+}:F^-=1:8.6). While in the case of 0.25ThF_4-0.45LiF-0.30CaF_2, the ratio of Th^{4+}: F^- is 1:8.2. Compared to the TbF_3 mixtures, larger amount of F^- is required for the modification of the local structure in the ThF_4 mixtures. Therefore the local structure of Th^{4+} would not be varied considerably by the addition of CaF_2.

EXAFS experiments have been carried out with the approval of the Photon Factory Program Advisory Committee (Proposal Nos. 2008G065, 2009G193, 2009G544). HM is grateful to le STUDIUM for the financial support of his staying in France. These studies were jointly performed with Drs. C. Bessada, and D. Zanghi (CEMHTI, CNRS) as the course of an agreement for cooperation between CEMHTI and Tokyo Tech.

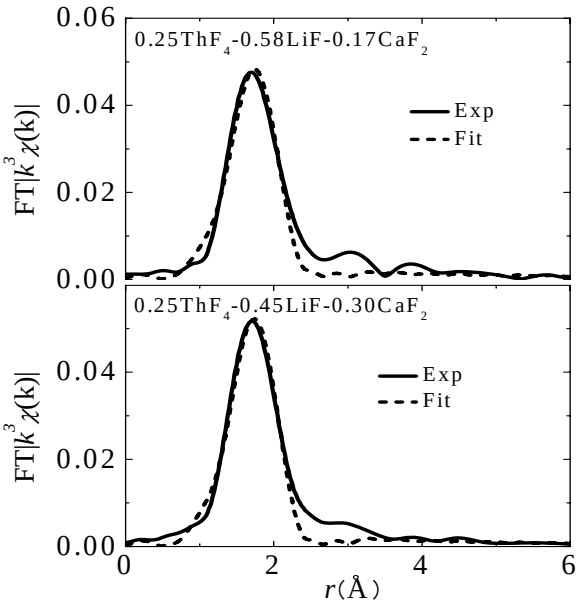

Fig. 1 radial structure functions of experiment and curve fitting of the 0.25ThF_4–aLiF–$b$$CaF_2$ mixtures at molten states

References

[1] A. –L. Rollet et al, *NIM B*, **226**, 447 (2004)

[2] H. Matsuura et al, *J Fluor. Chem.*, **130**, 53 (2009)

B.9 Local Structural Analysis on Terbium Fluoride Mixtures at High Temperature

Haruaki MATSUURA, Atsushi NEZU and Hiroshi AKATSUKA

Solid rare earth metal fluorides (LnF_x) are known to be useful materials in industrial applications (e.g. solid electrolytes and optical lens). Moreover, the development of pyrochemical reprocessing of spent nuclear fuels in molten fluorides or the molten salt nuclear reactor in nuclear engineering requires a better knowledge of their structural and physico-chemical properties at high temperature. In a recent study, it has been reported that the LiF-CaF_2 eutectic melt can be used as solvent for the electrodeposition of Nd and Th, while LiF-NaF and LiF-KF eutectic melts cannot be used for the same purpose theoretically. However, the structure of LnF_x and actinide fluorides (AnF_x) in LiF-CaF_2 eutectic melt has not been clarified yet. In this study, 0.20TbF_3-0.80LiF, 0.20TbF_3-0.62LiF-0.18CaF_2, 0.20TbF_3-0.48LiF-0.32CaF_2, 0.50TbF_3-0.50LiF, and 0.50TbF_3-0.38LiF-0.12CaF_2 mixtures are specially focused for the structural investigation.

XAFS measurements in transmission mode were performed at BL27B beamline in Photon Factory / KEK. Tb L_{III}-edge (7.519 keV) XAFS spectra were collected with a fixed time scan method by using Si (111) double crystals monochromator. Mixtures of TbF_3, LiF and CaF_2 in various compositions were melted once in a glassy carbon crucible at 1123 K in a glove box filled with an argon atmosphere in high purity. Then, they were mixed with boron nitride powder (BN), and pressed into pellets in 7-10 mm diameter and 1 mm thickness. It has been found that if the source of oxidation (e.g. moisture) as impurity exists in an electric furnace, TbF_3 reacts with BN to be $TbBO_3$ at ca. 1073 K. Therefore, to prevent chemical reaction during heating process in XAFS measurements, these pellets were installed in a cell made with pyrolytic boron nitride [1] and the electric furnace [2] was filled with He gas. EXAFS data were analysed by using the WinXAS ver.3.1 and 3rd and 4th cumulants were introduced for the curve fitting analyses of EXAFS data at molten phase due to their large anharmonic effect.

The experimental data on molten 0.20TbF_3-*a*LiF-*b*CaF_2, mixtures are shown in Fig. 1. In molten 0.20TbF_3-0.62LiF-0.18CaF_2 mixture, coordination number of terbium (N_i) and inter ionic distance between terbium and fluorine first neighbour (r_i) were quite similar to those in 0.20TbF_3-0.80LiF mixture, thus the similar octahedral configuration was formed. On the other hand, in ternary 0.20TbF_3-0.48LiF-0.32CaF_2 mixtures, N_i decreased from 8 to 6.8 and r_i did not change on melting. In addition, the Debye-Waller factor was relatively larger than those of the rest of the mixtures investigated. Therefore, the local structure around Tb^{3+} tends to be varied with depending on concentration of CaF_2. It is conjectured that the difference among structural variation in molten phase relates to the amount of F^- supplied by solvent melts. In 0.20TbF_3-0.48LiF-0.32CaF_2 mixture, the largest amount of F^- is supplied by the solvent melts among all mixtures investigated, i.e. Tb^{3+}: F^-=1.8.6. Thus N_i would indicate slightly larger than 6. In ternary 0.50TbF_3-*a*LiF-*b*CaF_2 mixtures, the effect of CaF_2 would appear more strongly than that in the ThF_4 mixtures. Since only 4 times amount of F^- can exist around a Tb^{3+} in 0.50TbF_3-0.50LiF mixture, the octahedral configurations should be connected by the edge and corner sharing. Some part of networking structure would be broken by addition of even small amount of CaF_2 (*b*CaF_2=0.12), and local structure around Tb^{3+} would be distorted from octahedral configuration.

EXAFS experiments have been carried out with the approval of the Photon Factory Program Advisory Committee (Proposal Nos. 2008G065, 2009G193, 2009G544). This research has been done in a collaboration study between JAEA (Dr. Y. Okamoto) and Tokyo Tech.

References

[1] A. –L. Rollet et al, *NIM B*, **226**, 447 (2004)
[2] H. Matsuura et al, *J Fluor. Chem.*, **130**, 53 (2009)

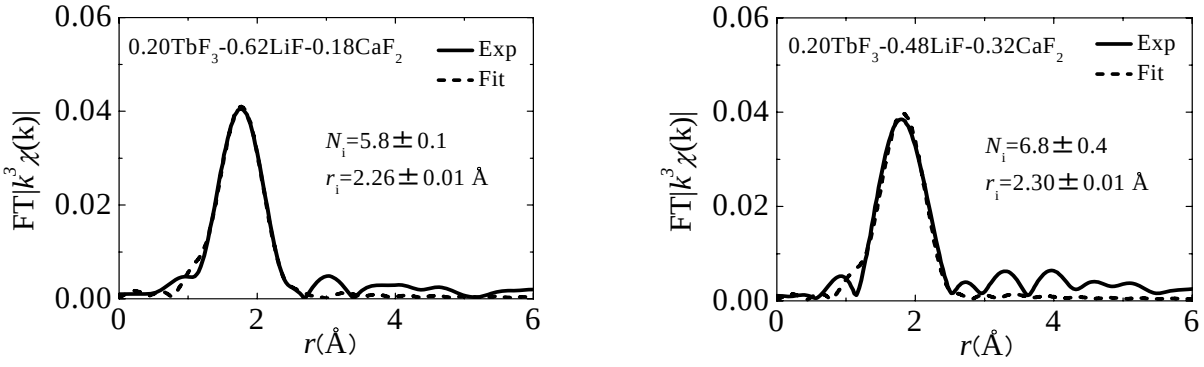

Fig. 1 radial structure functions of experiment and curve fitting of the 0.20TbF_3–*a*LiF–*b*CaF_2 mixtures at molten states

B.10 Corrosion Resistance of Fe-Al Alloy-Coated Steel under Bending Stress in High Temperature Lead-Bismuth Eutectic

Minoru TAKAHASHI and Eriko YAMAKI

1. Introduction

For the development of the lead alloy-cooled reactor, one of the main issues is to develop corrosion resistant materials for candidate cladding and structural materials in high temperature liquid lead alloy. Fe-Al alloy coating layer is effective for protection of steels from lead-bismuth eutectic (LBE) corrosion because a thin, dense and stable protective layer of Al oxide effective for corrosion resistance is formed on the surface of Fe-Al alloy by oxidation with oxygen in LBE. However, it is concerned that these protective layers may be damaged under various stress conditions.

The purposes of the present study are to investigate the behavior of the coating layers on the surface of the base metals under the loading condition and to evaluate the effect of the coating layers on corrosion resistance in LBE.

2. Experimental Apparatus and Procedure

The shape and sizes of specimens with the thickness of 0.5 mm are shown in Fig. 1. The specimens were coated with Fe-Al alloy deposited by unbalanced magnetron sputtering (UBMS) method. Corrosion resistance and integrity of the Fe-Al coating layers were investigated under bending stress in high temperature LBE as shown in Fig. 2. Steels of Recloy10 and HCM12A without coating and Fe-Al alloy-coated steel of HCM12A were exposed to LBE pool with low oxygen concentration (up to 5.2×10^{-8} wt%) at 550 and 650°C under 45kg-loading for 240 and 500 h.

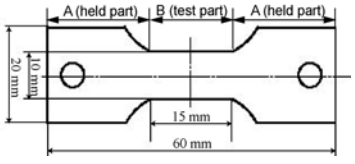

Fig. 1 Specimen for corrosion test under loading test

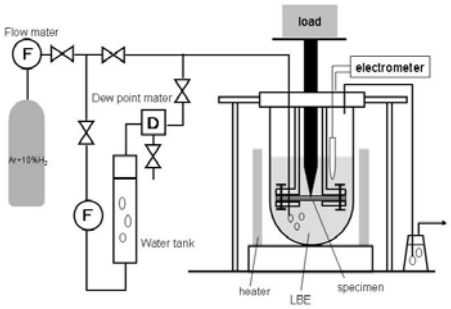

Fig. 2 Experimental set-up for bending and corrosion test

3. Results

The steels without coating did not show large dissolution of constituent elements into LBE or penetration of LBE. However, the surface conditions of these steels changed under loading in LBE for 500 h. Fe-Al alloy-coated HCM12A showed neither LBE corrosion nor the change of surface condition after exposure to LBE at 550ºC for 500 h under loading although adhesion of the coating layer was not good.

After exposure to LBE at 650°C for 240 h, Fe-Al alloy-coated HCM12A showed penetration of LBE into the base metal and dissolution of base metal to LBE around cracks of the coating layer (Fig.3 (a)). LBE entered the cracks across the coating layer and contacted directly with the base metal. The dissolutions of the base metal as well as that of the pre-coating layer was observed.

The coating layers detached from the base metal near the top surface of the specimen under compression stress (Fig. 3 (b)). LBE was observed in the gap between the base metal and the coating layer by EDX. Penetration of LBE into the base metal and dissolution of the base metal at this top surface were more significant than those at the bottom surface mentioned above.

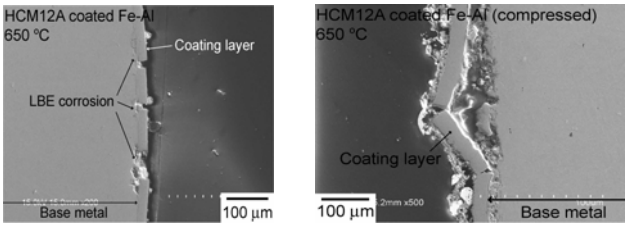

(a) (b)

Fig. 3 Cross sections of HCM12A specimen with Fe-Al alloy coating after corrosion test at 650 °C under loading for 240 h, (a) Near bottom surface under tensile stress; (b) Near bottom surface under compression stress

4. Conclusions

LBE corrosion was not observed appreciably in the base metal and coating layer after the tests at 550°C for 550 h. The coating layers could be barrier for corrosion resistance from LBE at 550 °C, although the coating scales are cracked by the load. At 650 °C, because the base metal was contacted directly with LBE through cracks across the coating layer, penetration of LBE to base metal and dissolution of base metal into LBE occurred. Fe-Al coating layer was not corroded by LBE.

Reference

E. Yamaki, M. Takahashi, "Corrosion Resistance of Fe-Al Alloy-Coated Steel under Bending Stress in High Temperature Lead-Bismuth Eutectic," *Proceedings of ICAPP '09*, Tokyo, Japan, May 10-14, 2009, Paper 9021.

B.11 Physical Property Change of CVD-Diamond, Silicon and Silicon Carbide due to Neutron Irradiation at High Temperature

Toyohiko YANO, Yoshirou YAMAMOTO and Katsumi YOSHIDA

Diamond films on single crystal silicon and polycrystalline silicon carbide substrates were neutron-irradiated in JMTR up to a fluence of $8.1x10^{24}$ n/m^2 (E>0.1MeV) at 725^{o}C. Lattice parameter expanded 0.39, 0.20~0.27, 0.001%, in diamond, silicon carbide and silicon, respectively. Raman peaks of diamond at 1335 cm^{-1} was weakened and shifted 8 cm^{-1} after the irradiation, but after annealing up to 1500^{o}C relatively large peak at 1329 cm^{-1} and the peaks corresponding to disordered graphite were observed. Lattice parameter of diamond slightly decreased from the irradiation temperature and up to 1300^{o}C, but was not recovered completely after annealing at 1400^{o}C. sp^2 clusters may be induced during irradiation and grow by annealing. The change in lattice parameter of silicon was negligible but broad scattering around 25^o (2θ/CuKα) was observed, indicating the presence of amorphous region. Mobility of monovacancy at room temperature, different from those of diamond and silicon carbide, should be a cause of different irradiation response of silicon [1].

1. Introduction

In present experimental fusion facilities, radio-frequency heating of the plasma is a necessary support heating system. In that system, ceramic windows with very low tanδ and very high heat-transfer properties are necessary. Diamond seems to be the best material for that window and was actually applied to the JT-60 fusion experimental device due to its very high thermal conductivity in the order of >1000 W/m·K and low tanδ in the order of $<1.3x10^{-4}$ at 170 GHz before neutron irradiation. It is well known that physical properties such as length, thermal conductivity, tanδ are greatly influenced by fast-neutron irradiation. A small number of reports on physical property change of diamond have been published.

In the previous report [2], the property changes of the CVD-diamond, single-crystal silicon and polycrystalline silicon carbide irradiated up to a fluence of $5.3x10^{24}$ n/m^2 (neutron energy: E_n>0.1MeV) at 380^{o}C in the Japan Materials Testing Reactor (JMTR) were clarified as follows. (1) Neutron irradiation induces graphite-like sp^2 clusters besides point defects in CVD diamond, which cannot recover after annealing up to 1500^{o}C. Due to the formation of sp^2 clusters, swelling of diamond is greater than that of silicon carbide. Lattice swelling was partially recovered by thermal annealing provided the annealing temperature is above the irradiation temperature. The recovering of the swelling increases with annealing temperature though it was not completed even at 1300^{o}C that was the highest experimented one. (2) Silicon carbide shows a response to neutron irradiation similar to diamond, but does not transform into other crystalline or non-crystalline forms. Therefore, most point-like defects were distributed throughout the crystal and then they should annihilate after high temperature annealing up to 1400^{o}C by recombination. (3) Silicon was partly amorphized, and showed very slight expansion due to the irradiation.

In this study, physical property changes of CVD-diamond, single-crystal silicon and polycrystalline silicon carbide those were concurrently neutron-irradiated in the same reactor at higher temperature of 725^{o}C are observed, and changes in physical properties were compared in the case of the lower temperature irradiation.

2. Experimental Procedures

Diamond films on single-crystal silicon or silicon carbide substrates were prepared by the CVD method. The thickness of the coating was about 10 μm. This diamond coating was polycrystalline and no special orientation. The substrates used were semiconductor-grade single-crystal silicon with the (111) plane parallel to the surface, and high thermal conductivity sintered polycrystalline SiC (mainly 6H). The size of both substrates was 10 mm in diameter and 1 mm in thickness. These specimens were neutron-irradiated in JMTR up to a fluence of $8.1x10^{24}$ n/m^2 (neutron energy: E_n>0.1 MeV) at 725^{o}C. After irradiation, changes in X-ray diffraction pattern, Raman spectrum and microstructure were observed.

3. Results and Discussion

3.1. CVD-diamond

The lattice parameter expanded by 0.39% after neutron irradiation at 725^{o}C, which was almost half of the case irradiated at 380^{o}C (0.76%). The full-width at half-maximum of the (113) diffraction peak slightly increased to 0.29^o (2θ/CuKα) from 0.21^o before irradiation, and mostly same as the case of the specimen irradiated at 380^{o}C (0.32^o). The change in lattice parameter of diamond due to isochronal annealing is shown in Fig. 1. The lattice parameter change of the lower temperature irradiated specimen [2] and of an unirradiated specimen were also plotted. The lattice parameter of the present irradiated specimen was almost constant up to 800^{o}C and slightly decreased over that temperature up to 1200^{o}C. On the contrary, that of the specimen irradiated at lower temperature (380^{o}C) did not change up to around 400^{o}C, which corresponded to the irradiation temperature, and

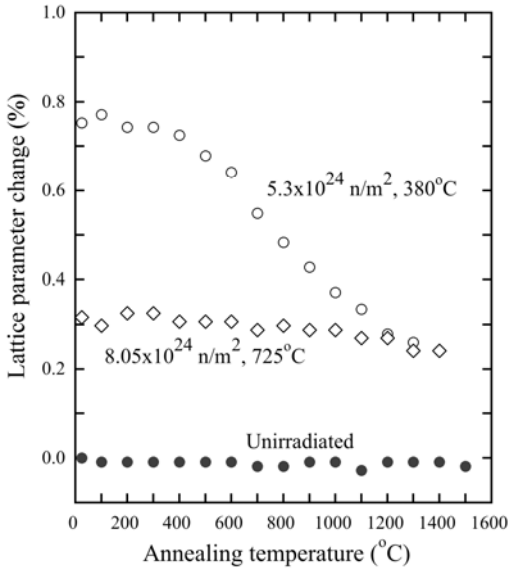

Fig. 1. Change in lattice parameter of diamond due to isochronal annealing for 1 h.

above that temperature the lattice parameter started to contract and decreased continuously up to around 1200°C.

It is interesting that the value of the present specimen after annealing at 1300°C and that of the lower temperature irradiated specimen were the same. At 1400°C, both specimens did not recover to the state of pre-irradiation, and still showed about 0.20% swelling.

Fig. 2 illustrates Raman spectra of the unirradiated specimen, as-irradiated specimen at 785°C and annealed specimen at 1500°C. The unirradiated specimen showed a single strong peak at 1335 cm^{-1}, which is a typical peak from diamond (sp^3), and a broad peak around 1520 cm^{-1}. After neutron irradiation, a relatively sharp and symmetric peak was observed at peak position of 1327 cm^{-1}, which is slightly shifted to lower wave number. Also broad peak at 1500 cm^{-1} was observed. After annealing at 1500°C, a relatively sharp peak was observed at 1329 cm^{-1}, very close to the original position of the diamond peak. New peaks at 1390, 1410 and 1580 cm^{-1} were observed. These peaks did not develop in the as-irradiated specimen. These peaks were also observed for the specimen irradiated at 380°C and annealed at 1500°C.

After neutron irradiation, the diamond Raman peak near 1327 cm^{-1} shifted 8 cm^{-1} to lower wave numbers. Compare with the lower temperature irradiation case [2], the amount of shift and deformation of peak shape was small, indicating less damage. No clear peaks at around 1580~1620 cm^{-1} corresponding graphite sp^2 was observed, thus degree of broken sp^3 bonding is less significant at higher temperature irradiation.

Due to the isochronal annealing, the lattice parameter slightly shrank from irradiation temperature with increasing annealing temperature, but did not recover until the pre-irradiation state after annealing at 1400°C. The value after the annealing at 1400°C of the present specimen and that of the lower temperature irradiated specimen was the same. The Raman spectrum of the present specimen after 1500°C annealing indicates an increase in intensity of the diamond peak at almost the same shift (1329 cm^{-1}) as before irradiation. New peaks at 1390, 1410 and 1580 cm^{-1} were developed which were not observed before annealing. Both peaks at 1390 and 1580 cm^{-1} can be assigned to those of disordered graphite (sp^2 bonding), but the peak at 1410 cm^{-1} cannot be assigned. Therefore, sp^2 components should exist after annealing at 1500°C, which correspond to the incomplete recovery of the lattice parameter.

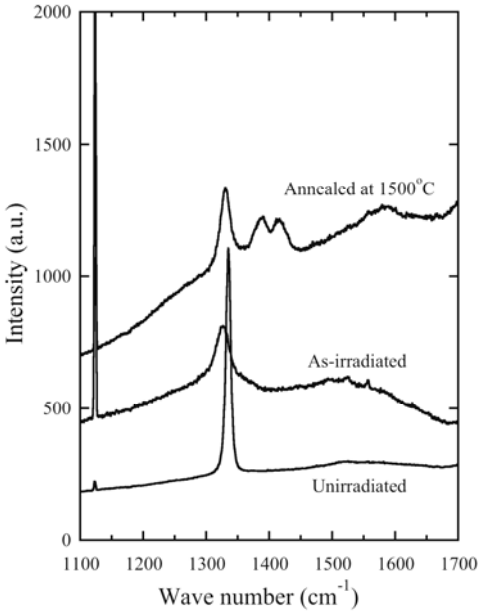

Fig. 2. Raman spectra of diamond in the range from 1100 to 1700 cm^{-1}. Unirradiated, as-irradiated to $8.05x10^{24}$ n/m^2 at 725°C and post-irradiation-annealed specimen at 1500°C for 1 h. The peak at 1125 cm^{-1} was Hg from room light.

2. Silicon

Only very little expansions of 0.001% were observed for the present higher irradiation temperature specimen. The full-width at half-maximum of the (531) peak has not changed (about 0.12°). Another significant change in the XRD peaks was that of a broad peak at 17-27° with a maximum at 23°, as shown in Fig. 3. This peak was not observed before neutron irradiation. This broad peak was slightly sharp in the case of higher temperature irradiated specimen. After annealing at 1000°C, the intensity of this broad peak was weakened but it did not disappear completely. These features were common for higher and lower temperature irradiation.

Raman spectra of the unirradiated and irradiated silicon are shown in Fig. 4. At 521 cm^{-1}, a strong peak was observed commonly in the unirradiated and irradiated

specimens, that is attributed for crystalline Si. After neutron

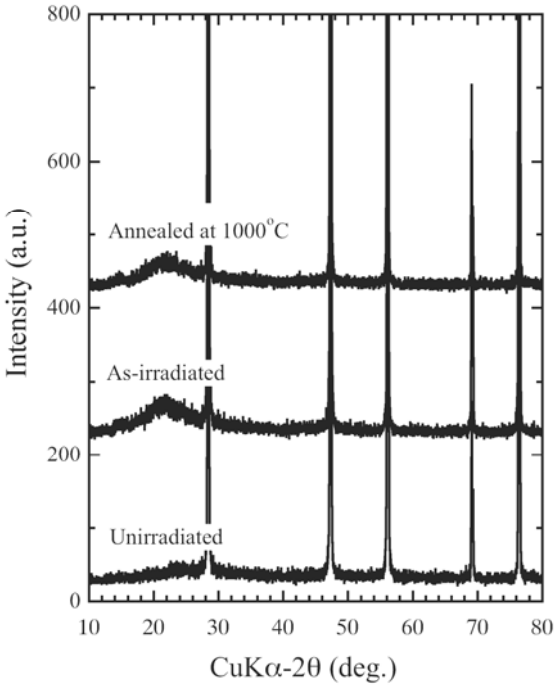

Fig. 3. X-ray diffraction patterns of silicon, unirradiated and as-irradiated to $8.05x10^{24}$ n/m^2 at 725°C and post-irradiation-annealed at 1000°C for 1 h.

irradiation, a new broad peak at around 480 cm^{-1}, attributed for amorphous silicon, was observed both for higher and lower temperature specimens.

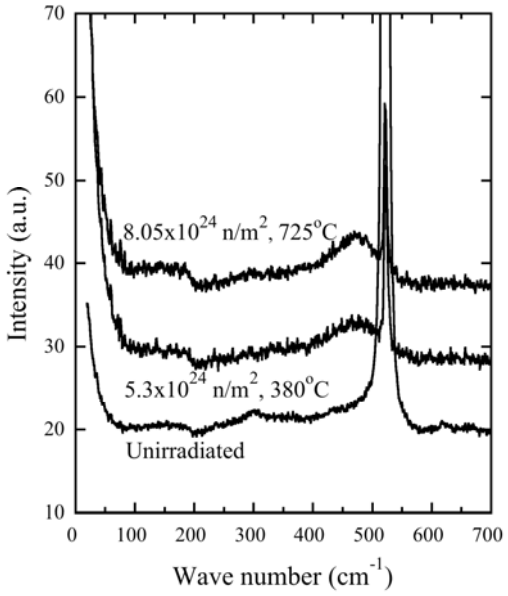

Fig. 4. Raman spectra of silicon in the range from 50 to 700 cm^{-1}. Unirradiated, irradiated to $8.05x10^{24}$ n/m^2 at 725°C and irradiated to $5.3x10^{24}$ n/m^2 at 380°C.

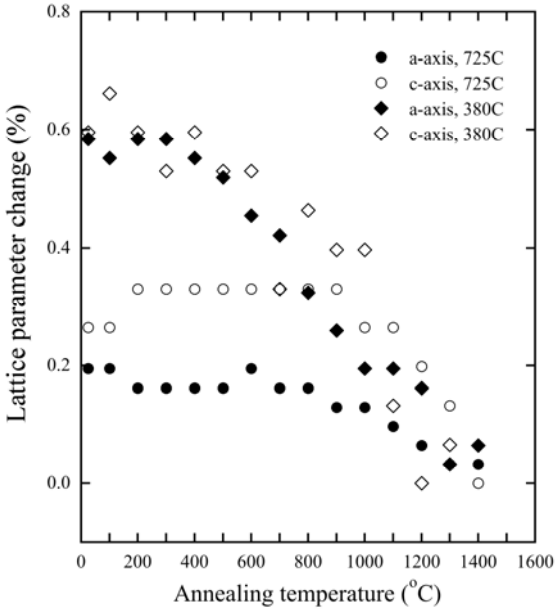

Fig. 5 Change in lattice parameter of silicon carbide irradiated to $8.05x10^{24}$ n/m^2 at 725°C and irradiated to $5.3x10^{24}$ n/m^2 at 380°C due to isochronal annealing for 1h.

3.3. Silicon carbide

The lattice parameter of silicon carbide after 785°C irradiation expanded by 0.20% along the a-axis and 0.27% along the c-axis, which was smaller in the case of 380°C irradiation, 0.58% along the a-axis and 0.60% along the c-axis. The change of the present specimen was not isotropic. Full-width at half-maximum of the (219) peak increased to 0.31° (2θ/CuKα) by the irradiation, compared to unirradiated and irradiated specimen at the lower temperature, 0.18 and 0.20°, respectively. Only black-dots like contrasts were observed by lower magnification electron microscopy, but at high-resolution observation the modification of crystalline lattice were observed. The a- and c-axis lattice parameters of the present SiC started to decrease from about 1000°C, and continuously contracted by isochronal annealing up to about 1400°C. After annealing at 1400°C, these values were fully recovered to the pre-irradiation values, and anisotropy was diminished, as shown in Fig. 5.

3.4. Comparison of three materials

Diamond, silicon and silicon carbide belong to a very similar crystal structure based on the diamond structure. Their atomic bonding nature has predominantly covalent character. Silicon and SiC are semiconductors, whereas diamond is basically an insulator. The melting point of Si (1414°C) is much lower than that of silicon carbide (2830°C) and diamond (>3000°C). The reported displacement energies of diamond (80 eV) and SiC (45-90 eV) are higher than that of silicon (11-22 eV).

The lattice parameter expanded to relatively large values of 0.39 and 0.20~0.27% in diamond and silicon carbide, respectively, compared with a very small value of 0.001% in silicon. Pravdyuk et al.[3] remarked that swelling of diamond exceeded that of SiC after the same neutron fluence of the order of 10^{24}n/m^2 at 100-200^{o}C. The present result on swelling also indicated the same feature whereas the irradiation temperature was higher than in the early study. One of the reasons of the very small lattice expansion in silicon can be attributed to the estimation that the relative volume change per interstitial ($\Delta\Omega i$=+0.55) in silicon is only slightly in excess of that of a vacancy ($\Delta\Omega v$=-0.50) [4]. From Raman spectroscopy and X-ray diffraction, an amorphization of the crystal was clearly observed only in silicon as broad peaks at 17-27^o by XRD and by Raman peaks at 480 cm^{-1}. In silicon, an amorphous phase is formed as a result of neutron irradiation over a fluence of 10^{25}n/m^2 besides vacancy clusters. This result was supported by the molecular dynamic simulation by Rubia et al. [5] induced by 3-5 keV displacement cascades in silicon carbide and silicon, where amorphization took place only in silicon, otherwise the disordered region retains the basic crystal structure in SiC. As a reason of a larger expansion of diamond than that of silicon carbide, we can attribute a diamond graphite transition induced in diamond. The atomic volume of graphite (0.0088 nm^3) is much greater than that of diamond (0.0057 nm^3), therefore homogeneous nucleation of small sp^2 clusters may induce lattice expansion. A further basic difference during irradiation is the vacancy mobility. The mobility of interstitials is high in all three materials, in spite of the high mobility of monovacancies and divacancies less than room temperature or a few hundreds degree C only in silicon, respectively. Large differences in radiation response in silicon from those in diamond and silicon carbide are basically corresponding to the differences in mobility or stability of defects and thus the remaining defects in the crystals despite of similar geometric structures.

4. Conclusions

CVD-diamond on single-crystal silicon or poly-crystalline silicon carbide substrates were neutron-irradiated up to a fluence of 8.1x10^{24} n/m^2 (E_n>0.1MeV) at 785^{o}C. Changes in XRD patterns, Raman spectra and microstructure were observed after irradiation and post-irradiation annealing, and compared with the results on the specimens irradiated to 5.3x10^{24}n/m^2 at 380^{o}C.

(1) Neutron irradiation induced no clear graphite-like sp^2 clusters besides point defects in CVD diamond at 785^{o}C. sp^2 clusters probably nucleated during irradiation, and grow and could not recover after annealing up to 1500^{o}C. Due to the nucleation of these clusters, swelling of diamond may be greater than that of silicon carbide. Lattice swelling decreased from around the irradiation temperature, but recovery was not completed due to the presence of sp^2 clusters.

(2) Silicon was partly amorphized independent of irradiation temperature. The very small expansion was explained by the small difference in relative volume change per interstitial and that of a vacancy despite of the small displacement energy. Furthermore, the mobility of monovacancies at room temperature, different from that of diamond and silicon carbide, should be a cause of irradiation response.

(3) Silicon carbide did not transform into other crystalline or noncrystalline form. Therefore, most point-like defects were distributed throughout the crystal and then they annihilate during annealing up to 1400^{o}C by pair recombination.

References

[1] T. Yano, T. Sawabe, K. Yoshida and Y. Yamamoto, *J. Nucl. Mater.*, **368-388** (2009) 1018.
[2] T. Yano, Y. Yamamoto and T. Iseki, *J. Nucl. Mater.*, **307-311** (2002) 1102.
[3] N. F. Pravdyuk, V. A. Nikoraenko, V. I. Karpuchin and V. N. Kuznetsov, "Property of Reactor Materials and Effects of Radiation Damages", Ed. D. J. Litter, *Butterworth* (1962). p. 57.
[4] W. Mayer and H. Peisl, *J. Nucl. Mater.* **108&109** (1982) 627.
[5] T. Diaz de la Rubia, M. -J. Caturla and M. Tobin, *Mat. Res. Soc. Proc.* **373** (1995) 555.

B.12 Immobilization of Strontium and Cesium into α-SiAlON Ceramics Assisted with Co-Doping of Yttrium

Katsumi YOSHIDA and Toyohiko YANO

Introduction

Nuclear power plants generate spent nuclear fuels, and the disposal of radioactive waste becomes a critical issue. The amount of spent nuclear fuel has increased continuously and it is necessary to reduce the radiotoxicity derived from high-level nuclear waste. The study on the transmutation of long-lived fission products (LLFP) into short-lived or stable nuclides in nuclear reactors or accelerators has been performed for the reduction of radiotoxicity.[1)] In order to transmute the LLFP in nuclear reactors or accelerators, an inert matrix is needed for the immobilization of radioactive nuclides. Si_3N_4 ceramics are considered to be a candidate for an inert matrix of LLFP since they show excellent properties as an inert matrix.[2),3)] SiAlON is a solid solution based on Si_3N_4, i.e., Al^{3+} and O^{2-} are substituted for Si^{4+} and N^{3-} in Si_3N_4 structure, respectively. Alpha-SiAlON can be denoted by the general formula of $M_xSi_{12-(m+n)}Al_{m+n}O_nN_{16-n}$, where M is metal cations incorporated into large interstices of the α-SiAlON network, and x contents of the metal cations.[4)-8)] Strontium (^{90}Sr) and cesium (^{135}Cs, ^{137}Cs) are high-level nuclear wastes in spent fuel waste which have a half-life of 29.1, $2.30x10^6$ and 30.0 years, respectively.[1)] The half-life of ^{90}Sr is not so long (29.1 years), but heat generation due to rapid decay is large. In this study, we tried to fabricate α-SiAlON ceramics containing stable isotopes instead of LLFP such as radioactive $^{135,137}Cs$ and ^{90}Sr by hot-pressing, i.e., immobilize simulant element into α-SiAlON structure, and the applicability of α-SiAlON ceramics as the inert matrix for transmutation of radioactive $^{135,137}Cs$ and ^{90}Sr was investigated.

Experimental Procedures

Starting Materials and Sintering

Alpha-Si_3N_4, AlN, and α-Al_2O_3 were used as the starting materials. Stable nuclides, ^{88}Sr and ^{133}Cs were selected as the simulant nuclides for radioactive nuclides, ^{90}Sr and $^{135, 137}Cs$, respectively, and the starting materials were mixed with each metal carbonate ($SrCO_3$, Cs_2CO_3) and Y_2O_3. The composition of the powder was adjusted to be 0.7 as x-value of α-SiAlON containing Y and M (Sr or Cs), and 7:3 and 9:1 as the atomic ratio of Y and M (Sr or Cs), respectively. The starting powder was mixed for 24 h by wet ball-milling. After ball milling, the slurry was dried, and then crushed and sieved. The mixed powder was put into a graphite mold, and then hot-pressed at 1800°C for 1 h in nitrogen flow under a uniaxial mechanical pressure of 32 MPa.

Characterization

Bulk density of specimens was measured by Archimedes' method. Hot-pressed specimens were crushed into powder, and their crystalline phase identification and lattice parameter measurement were performed using X-ray diffractometer. The bending strength of hot-pressed specimens was measured by three-point bending test at room temperature. Elemental analysis of hot-pressed specimens was performed by energy dispersive X-ray spectrometer equipped on a transmission electron microscope (TEM) in order to investigate the distribution of elements in the sintered body.

Results and Discussion

Crystalline Phase and Lattice Parameter

When Y_2O_3 was added with $SrCO_3$ or Cs_2CO_3 to the starting powder, single α-SiAlON phase was formed in sintered bodies after hot-pressing. The *a*-axis and *c*-axis parameters of α-SiAlON fabricated from the starting mixtures containing both Y_2O_3 and $SrCO_3$ were very similar with the values of Y-doped α-SiAlON ($Y_{0.6}(Si_{9.3}Al_{2.7})(O_{0.9}N_{15.1})$) reported in ref. 9. In the case of α-SiAlON fabricated from the starting mixtures containing both Y_2O_3 and Cs_2CO_3, its *a*-axis and *c*-axis parameters were very similar values of $Y_{0.4}(Si_{10.2}Al_{1.8})(O_{0.6}N_{15.4})$ reported in the literature. From these results, Y_2O_3 addition to the starting materials would assist the formation of α-SiAlON phase.

Distribution of Sr and Cs in α-SiAlON phase

Distribution of Sr and Cs in α-SiAlON grain was evaluated by EDS equipped on TEM. In the case of the sintered bodies fabricated from the starting mixtures containing both Y_2O_3 and $SrCO_3$, Y and Sr were detected in the grain in addition to Si and Al. This result agreed closely with the starting composition. It is suggested that Y and Sr dissolved into interstitial site in α-SiAlON structure. On the contrary, Y, Si and Al were detected in the sintered body fabricated from the starting mixtures containing both Y_2O_3 and Cs_2CO_3, but Cs was not detected. From this result, it indicated that only Y dissolved into interstitial site in α-SiAlON structure in the specimen. The ionic radii of Y^{3+}, Sr^{2+} and Cs^+ ions for a six-folded coordinate have been reported to be 0.090, 0.118 and 0.167 nm, respectively[10)]. Some researchers have mentioned that an upper limit of the metal cation radius incorporated into α-SiAlON phase would be around 0.100 nm.[7),8)] It was reported that *a*- and *c*-axes parameter of α-SiAlON increased with increasing the amount of Y for incorporation into α-SiAlON lattice.[11)] From these data, it was suggested that Y^{3+} incorporated into

α-SiAlON phase served to expand the interstices of α-SiAlON, and then Sr^{2+} with a little larger ionic radius than 0.100 nm was incorporated into α-SiAlON phase. In the case of Cs^{+}, its ionic radius is much larger than 0.100 nm, and Cs^{+} could not be incorporated into the interstices in spite of expansion of interstices by the incorporation of Y^{3+}.

Bulk Density and Bending Strength

Their bulk densities of α-SiAlON obtained in this study were 3.31-3.32 g/cm^3. These values were slightly higher than the calculated bulk density of Y-doped α-SiAlON. In consideration of the application of ceramics as an inert matrix, densification is very important. Generally, dense ceramics show higher thermal and mechanical properties than those of porous ceramics. High thermal and mechanical properties provide mechanical stability for ceramics during neutron irradiation since neutron irradiation induces the swelling, i.e., expansion, and heat evolution. The α-SiAlON ceramics incorporated with Y and Sr or Y and Cs showed the bending strength of 930 and 910 MPa, respectively. It was reported that α-SiAlON ceramics incorporated with Y (composition; $Y_{0.41}(Si_{10.2}Al_{1.8})(O_{0.6}N_{15.4})$) were fabricated by hot-pressing at 1750°C and their bending strength was around 600 MPa.[6] The α-SiAlON ceramics fabricated in this study showed a higher bending strength than the hot-pressed α-SiAlON incorporated with Y in ref.6. From these results, it was found that the immobilization of Sr in α-SiAlON phase was successfully achieved with co-doping of Y, and α-SiAlON ceramics will be an inert matrix for transmutation of radioactive Sr. The amount of Y and Sr which can be immobilized into 1 kg of α-SiAlON in maximum was calculated to be around 30 g and 70 g based on the present compositions, respectively.

Summary

Immobilization of LLFP such as radioactive Sr and Cs into α-SiAlON ceramics was evaluated using stable isotope instead of radioactive isotopes, and the applicability of α-SiAlON ceramics as the inert matrix for transmutation of radioactive ^{135,137}Cs and ^{90}Sr was investigated. When Y_2O_3 was added with $SrCO_3$ or Cs_2CO_3 to the starting materials in optimum compositions, α-SiAlON single phase was obtained after hot-pressing at 1800°C. From the EDS analysis, it was suggested that Y assisted the expansion of interstices of α-SiAlON and the incorporation of Sr^{2+} with the slightly larger ionic radius than 0.100 nm into α-SiAlON lattice. In the case of Cs addition with Y, Cs was not incorporated into interstices due to much larger ionic radius of Cs^{+} than 0.100 nm. Bulk density of hot-pressed α-SiAlON ceramics was higher values and densification proceeded well. Form these results, it was found that the immobilization of Sr in α-SiAlON was successfully achieved with co-doping of Y, and α-SiAlON ceramics will be an inert matrix for transmutation of long-lived radioactive Sr.

Acknowledgement

This study was partly supported by the Japan Atomic Energy Agency Cooperative Research (A) on the Nuclear Fuel Cycle Program.

References

[1] I. Kimura, *Science of Machine*, **51**, 1109-1117 (1999) [in Japanese].
[2] M. Akiyoshi, T. Yano and M.L. Jenkins, *Philos. Mag. A*, **81**, 683-697 (2001).
[3] T. Yano, M. Akiyoshi, K. Ichikawa, Y. Tachi and T. Iseki, *J. Nucl. Mater*., **289**, 102-109 (2001).
[4] S. Hampshire, H.K. Park, D.P. Thompson and K. H. Jack, *Nature*, **274**, 880-882 (1978).
[5] G. Grand, J. Demit, J. Ruste and J.P. Torre, *J. Mater. Sci*., **14**, 1749-1751 (1979).
[6] M. Mitomo, H. Tanaka, K. Muramatsu, N. Ii and Y. Fujii, *J. Mater. Sci*., **15**, 2661-2662 (1980).
[7] D. Stutz, P. Greil and G. Petzow, *J. Mater. Sci. Lett*., **5**, 335-336 (1986).
[8] C.J. Hwang, D.W. Susnitzky and D.R. Beaman, *J. Am. Ceram. Soc*., **78**, 588-592 (1995).
[9] *NIRIM Research Report*, **32**, 19-33(1982) [in Japanese].
[10] R.D. Shannon, *Acta Crystallogr*., **A32**, 751-767 (1976).
[11] K. Ishizawa, N. Ayuzawa, A. Shiranita, M. Takai, N. Uchida and M. Mitomo, *J. Ceram. Soc. Japan*, **94**, 183-185 (1986) [in Japanese].

C.1 Study on Numerical Simulation of Nuclear Pumped Laser by Coupled Pulse Reactor

Toru OBARA and Hiroki TAKEZAWA

A coupled pulse reactor consisting of fast pulse cores made of a uranium alloy and a subcritical thermal laser module comprising laser cell tubes and moderator is one of the most promising designs for nuclear pumped laser (NPL) experiments. The typical design of the pulse reactor is the combination of the BARS-6 and Stand B used in IPPE, Russia[1]. In the pulse reactor, NPL experiments are performed by making the fast pulse core prompt supercritical. Neutrons from the pulse cores cause fissions in the uranium coating the inside surface of the laser cell tubes in the module. Fragments from the fission excite the laser gas medium in the tube. Highly enriched uranium is used in the Russian reactor for the fast burst cores and the inner coating of the laser cell tubes to the pump laser.

The purpose of this study was to do numerical simulation of Nuclear Pumped Laser by Coupled Pulse Reactor to know the detail characteristics of the laser. This paper describes the possibility of performing NPL experiments using the pulse reactor concept with low-enriched uranium by performing kinetic analysis of the prompt supercritical condition.

It is necessary to know the power density caused by the fissions in laser cell tubes during the transient condition to discuss the possibility of laser pumping. The neutronic characteristics of the fast pulse cores and thermal laser module are different, and the coupling of the two regions is loose. So a space-dependent kinetic analysis for loosed coupled systems should be performed. A space-dependent kinetic analysis method for loose coupled system to analyze the prompt supercritical condition has been developed by the authors [2][3]. The code was used in the kinetic analysis. Figure 1 shows the calculation geometry. Regions 4 and 5 represent fast pulse cores made of uranium metal. The enrichment is 100% for highly enriched uranium and 20% for low-enriched uranium. Region 2 represents the subcritical laser cell tubes with diameters of about 5 cm. Uranium metal is coated on the inside surface of the cells. The enrichment for highly enriched uranium and low-enriched uranium was the same as that of fast pulse cores. Polyethylene was placed between the tubes as a moderator. The temperature rise of the laser module during the pulse operation was negligible with respect to reactivity feedback to the overall systems, so the temperature rise and thermal expansion of the pulse cores were included in the reactivity feedback calculation during the transient condition. The purpose of the analysis was to determine the power density in the cell tubes during the pulse operation, so only prompt neutrons were considered for the calculations.

The calculation results show that it is possible to provide enough energy to the laser gas medium in the cell tubes not only in the reactor with highly enriched uranium but also in the reactor with low-enriched uranium. It is also possible to provide enough energy to both the laser cell tubes in the inner region and the cell tubes in the outer region, far from the pulse cores. We found some delay of the peak of the power in the cell tubes in the outer region, which was caused by neutron thermalization and diffusion in the thermal laser module.

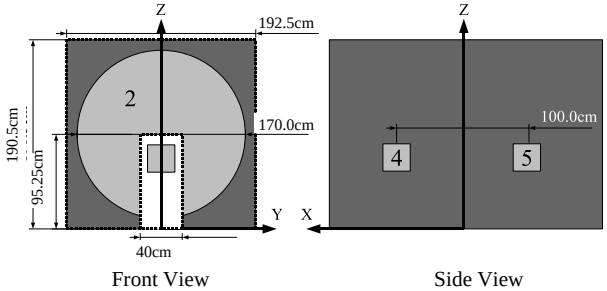

Fig. 1. Geometry of the pulse reactor.

REFERENCES

1. P. P. D'yachenko et al., "STAND B Reactor-Laser System", *Atomic Energy*, **88(5)**, 352 (2002).
2. Hiroki Takezawa and Toru Obara, "Calculation of the Integral Kinetic Model Transient Parameters by the Monte Carlo Method for Space-Dependent Kinetic Analysis," *Nuclear Science and Engineering*, **164,** 80 (2010).
3. Hiroki Takezawa and Toru Obara, "New Approach to Space-Dependent Kinetic Analysis Based on the Integral Kinetic Model with the Monte Carlo Method," submitted to Nuclear Science and Engineering.
4. V. N. Kononov et al., "Nuclear Pumped Lasing Experiments on Fast Burst Rearctor Bars-6," *Proc. of ICENES'96*, Obninsk, Russia, 336 (1996).

C.2 Study on Neutron Transmutation Doping for Silicon Semiconductor using PWR Fuel Core

Toru OBARA and Byambajav MUNKHBAT

Nowadays, the use of electric vehicles such as hybrid cars and electric trains is increasing rapidly. Each such vehicle requires a considerable number of large-diameter power semiconductor devices, suggesting an ever-growing demand for such devices in the near future. Thus, the mass production of large-diameter semiconductors is becoming an important issue for many manufacturers.

There are many methods to produce large-diameter semiconductors and the most promising method to produce highly uniform doped semiconductor material is neutron transmutation doping (NTD). The NTD method is based on a nuclear reaction in which a thermal neutron is captured by the naturally occurring stable isotope ^{30}Si to form the unstable isotope ^{31}Si; this unstable isotope decays by the emission of a 1.471 MeV β^- with a half life of 2.62 hours to the stable isotope ^{31}P [1].

The purpose of this study is to design a small nuclear reactor using conventional PWR fuel core, which can be possible to supply the fuel by conventional PWR fuel fabrication factory, dedicated to the production of highly uniform doped large-diameter semiconductor material.

In this work, a design concept for a small nuclear reactor for NTD of large-diameter (30 cm) semiconductors using conventional PWR fuel is proposed. The optimum core size was determined in the previous work [2]. However the optimum core design was rather atypical such as 8×8 fuel pins are in a fuel assembly and the core contains 36 (6×6) such assemblies. In keeping with this optimum size as possible, the fuel assembly is changed into conventional 17×17 PWR fuel assembly in the current work.

The core size is 64.26 cm × 64.26 cm × 100 cm and core contains only 9 (3×3) PWR fuel assemblies. Enrichment of the fuel is 4 wt%. Coolant and moderator is light water. 40 cm thick graphite reflector is placed around core. Burnable poison Gd_2O_3 is used to suppress excess reactivity. The reactor power is 15 MWth and the operating pressure is 1 atm. Four Si ingots that are each 30 cm in diameter can be irradiated in the reflector region at same time. It is assumed that the Si ingot is pure natural Si crystal and the height is 100 cm, the same as the core height.

Criticality and burn-up analyses are performed. The results show that the reference core has a large excess reactivity at the beginning of the core life time. Burnable poison Gd_2O_3 is used in order to suppress the excess reactivity. There are many options for using burnable poison effectively; several suitable combinations that would not result in decreasing core life time were determined.

Soluble boron is eliminated to make the reactor design simpler. Proposed reactor design is based on the research reactor concept and its power density is low, thus it is feasible to suppress excess reactivity by movement of control rods.

The approximate semiconductor production rate of the reactor is estimated. The production rate was determined as ratio between the mass of doped Si ingot produced and the time required for such production. Since the desired resistivity of the doped Si ingot depends on the number of ^{31}P nuclei introduced by NTD, the required time depends on several factors such as fuel cycle and how uniformly the Si ingot is doped; subsequent irradiation is often needed in order to achieve uniform doping. But these factors are not considered in the present estimation; the thermal neutron flux in the reflector region is only used.

The proposed reactor can be critical for over 600 days but large excess reactivity was expected. This large excess reactivity can be suppressed using a combination of different fuel assemblies which have different numbers of fuel rods with burnable poison and different concentrations of burnable poison. From the steady-state single-channel analysis, it is confirmed that the coolant bulk temperature is always less than 50°C and the cladding surface temperature is also less than 70°C. Thus, it is possible to remove heat from the core at 1 atm pressure. The approximate production rate of the reactor was estimated. At a target resistivity of 50 Ωcm, the reactor production rate was around 80 kg/hour. It could be a good production rate for large-diameter NTD.

A simple and small size nuclear reactor for large-diameter NTD can be designed using conventional PWR fuel elements. The estimated production rate could be good production rate for large-diameter NTD.

REFERENCES

1. M. TANENBAUM, A.D. MILLS, "Preparation of Uniform Resistivity n-Type Silicon by Nuclear Transmutation," *Journal of the Electrochemical Society*, Volume **108**, Issue 2, pp. 171-176 (1961).
2. TORU OBARA, LIEM PENG HONG, NAOYUKI TAKAKI, "Basic Concept of Water Moderated Small Reactor for Neutron Transmutation Doping," *Trans. Am. Nucl. Soc.* **99**, 745 (2008).

C.3 Study on Peu-à-Peu Fuel Loading Scheme in Small PBR

Toru OBARA and Dwi IRWANTO

In a pebble bed reactor, the unloading machinery is a complex system that can lead to some challenging problems if something unexpected happens to the device. If this device could be removed, the reactor would likely become more practical both in terms of design and operation, while at the same time reducing the cost needed to construct and operate the reactor. For this kind of system, a suitable fuel-loading scheme is the Peu à Peu (little by little) fueling scheme. [1]

In the Peu à Peu modus, the fuel is little by little loaded into the core so that the fuel in the core continuously increases. At the bottom of the core, there is no unloading device; as such, the fuels are never discharged and remain at the bottom of the core during reactor operation. This means that the burnup cycle and reactivity is controlled by the addition of fuel. This simplification allows the fuel-loading process to be conducted in a very simple way, but it has some disadvantages in terms of low burnup and high power peaking. [2]

Some studies have been performed previously, but they have used a diffusion-based method for neutronic analysis, whereas the transport method is more accurate. The large empty cavity region in the core, which is bigger than that of conventional PBRs during most of the reactor operation period, makes accurate calculations difficult in the diffusion-based method.

The purpose of study is to perform the exact and detail calculations needed to analyze the Peu à Peu fuel-loading scheme and to optimize the core design, fuel composition, and fuel-loading scheme to improve its burnup characteristics.

The Monte Carlo method was used to perform calculations with high accuracy at the top region of the core near the large cavity. In the real application of the Peu à Peu concept, the fuel elements are inserted continuously into the core, while in this study, for calculation purposes, the fuel elements were inserted in a stepwise procedure. The reactor core was subdivided into several axial fueling zones. At the startup, the lower layers of the core were filled with fuel elements, leading to the first criticality. At certain time intervals, one fuel layer after the other was added, depending on the requirements of criticality and compensation for the burnup; a burnup calculation was performed for each fuel-loading step. The calculation procedures for the Peu à Peu modus using the Monte Carlo method require numerous steps.

Before the calculation of the whole core, an analysis for infinite geometry was performed. By analyzing the power generated per mass consumed for each combination of the uranium enrichment value and the packing fraction from the parametric survey, we found that the maximum burnup value could be expected if the inserted fuel element was 12 wt% U-235 enrichment with a 7% volume packing fraction of coated fuel particle in a pebble ball.

Using these values, a whole-core calculation for 20 MWth reactor was performed. The reactor had a radius of 125 cm and a height of 500 cm. At the startup, the core height was 85 cm and at the end of the operation, the height was 480 cm with the remaining 20 cm being an empty cavity. The fuel feed rates are varies with time depending on the requirements of criticality. This reactor design with the Peu à Peu fuel-loading scheme could maintain its criticality up to 12 years. The average burnup value of this design was 9.37×10^4 MWD/T-U, which is comparable to that of the conventional PBRs design.

During reactor operation, burnup values at the top of the core were smaller compared to those at the bottom of the core. The same characteristic was also found at the end of the reactor operation, when the burnup value was 3.27×10^5 MWD/T-U at the bottom layer and 1.72×10^4 MWD/T-U at the top layer, with a wide range of difference between the bottom and the top of the reactor core.

In order to optimize the burnup characteristic, several analyses were performed. By keeping the power density at a constant value, we performed a calculation by increasing the radius of the reactor up to 200%, which would result in four times the volume of the initial reactor size. As the radius and power increased, the average burnup of the reactor did not change remarkably. In fact, the average burnup values changed as little as 1% or less. So, to increase the burnup value of this design, increasing the radius of the reactor would not be an effective option.

Further analysis is necessary to increase burn up for effective utilization of fuel using the method developed in this study. This new design and method is important due to its advantages of involving a small reactor, a very simple fuel-loading scheme, and the high efficiency of a gas-cooled reactor.

REFERENCES

1. E.TEUCHERT, et al, “Simplification of the Pebble Bed High-temperature Reactor”, *Proc. of SR/TIT*, Tokyo, Japan (1991).
2. P.H.LIEM, “Design Procedures for Small Pebble-Bed High Temperature Reactors”, *Annals of Nuclear Energy*, **23**, No. 3, p. 207 (1996).

C.4 Ultra Long Life Space Reactor loaded with Am and Cm

Masanori NAKAMURA, Hiroshi SAGARA and Masaki SAITO

INTRODUCTION

In the future the activities of human in space will need much electric power for long time. However, it's difficult to satisfy these demands by solar energy and battery such as fuel cell because the low solar power density and very severe mass restriction by the ability of rocket performance. Space nuclear reactor is a very attractive answer to solve above problem. Furthermore, long-life is an essential element. Space reactor is very attractive in its utilization for the human activities in the space. And human activity in the Moon and Mars requires large electric power for the long time in the future. Many concepts have been suggested to satisfy these contradicted conditions. Highly enriched uranium fuel concept is suggested mainly. However, U enriched over 20% is defined as a significant quantity in military utilization by IAEA[1].Because minor actinide (MA) of spent fuel in LWR has large neutron capture cross section, loading MA can enables long life core both thermal and fast reactor[2] Though neutron spectrum of this study is fast, it has used not sodium but lithium[3]. It enables high efficiency of electricity conversion because of high boiling point and specific heat. Because gravity and air utilization in space is negligible or small, removal heat of convection and conductivity is not effective. Am nitride is used because Am is very stable to nitride chemically. Main isotope of Am is ^{241}Am and ^{243}Am in spent LWR fuel. Transmutation procedure of ^{238}Pu from ^{241}Am sustains long-life core in fast spectrum.

METHODOLOGY

Computer codes, SLAROM[4], JOINT and CITATION[5] and cross section library, JFS-3-J-3.2R, which is based on Japanese Evaluated Nuclear Data Library JENDL3.2, are used in the present calculation. The SLAROM input consists only of the PREP block to obtain 70-group effective cross sections of each material region by homogeneous cell calculation. JOINT is used to convert 70-group effective cross section data sets from the SLAROM output to the CITATION input. The nuclear characteristics are investigated using a calculation of two-dimensional RZ diffusion theory with depletion chain by CITATION. In this calculation, each zone has uniform nuclide number densities with 176 zones and the same set of microscopic cross sections.

RESULUTS AND DISCUSSION

As shown in Fig.1, it is showed that reactivity grows large during 80 years, decreases after the peak, and has life-time of 250 years in case A. Case B replaced a part of outer core Am with Cm. Because Cm has high ν value, it has large effect to increase reactivity initially and core life time increase to 280 year. Case C which replaced Cm of case E with Pu achieves life time of 300 year and ratio of peak and initial reactivity is kept under 1% simultaneously. However, taking into account of dpa(displacement per atom) cross section of cladding SS316 core life-time has been restricted by 200 years.

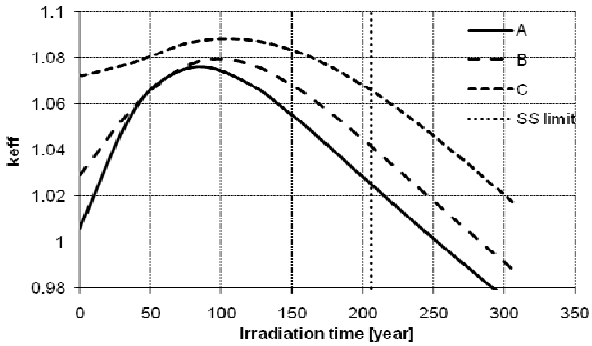

Fig.1 Burn-up reactivity change during irradiation in Am based fuel core

REFERENCES

1. International Atomic Energy Agency , IAEA
2. M. Saito, "Multi-Component Self-Consistent Nuclear Energy System for Sustainable Growth," *Progress in Nuclear Energy*, Vol. **40**, No.3-4, 2002Safeguards Glossary 2001 Edition (2001)
3. M.Kambe *et al*.,Innovative Fast Breeder Reactor Concept 'RAPID' for Improvement of Rector Performance and Proliferation Resistance *Nucl. Eng. and Design* (1996)
4. M.Nakagawa *et al*, SLAROM: A Code for Cell Homogenizations Calculation of Fast Reactor, JAERI 1294, Japan Atomic Energy Research Institute,(1984)
5. T.B.Fowler *et a*l,Nuclear Reactor Core Analysis Code: CITATION, *Oak Ridge National Laboratory report*, ORNL-TM-2496, Rev2,USA(1971)

C.5 Long-life FBR with Inner Blanket by Doping MA

Erina HAMASE, Masaki SAITO and Hiroshi SAGARA

INTRODUCTION

Minor Actinides (MAs) discharged from the nuclear reactor spent fuel entails a significantly long term radiological burden in geological repository. As a simultaneous challenge to minimize such a burden and enhance the proliferation resistance, the concept of Protected Plutonium Production (P^3) was proposed[1,2]. In this proposal, MAs such as ^{237}Np and ^{241}Am are considered to work as a fertile material since ^{238}Pu produced by transmutation of these MAs plays a role as a fissile material in fast neutron spectrum. Therefore, it is considered that MAs have a potential to contribute to both the reduction of burnup reactivity change and the higher burnup. In the present paper, the potential of MAs in heterogeneous fast breeder reactor is surveyed for the longer life time core.

METHODOLOGY

For reactivity and burnup calculation, *SLAROM*[3], *JOINT* and *CITATION*[4] were used with the cross section library, JFS-3-J-3.2R[5]. 70-group effective cross sections were made by homogeneous square cell calculation in the *SLAROM*, and *JOINT* converts 70-group effective cross section data format to the *CITATION* input. Reactivity and burnup calculation were performed with *CITATION* based on the diffusion theory with nuclide transmutation chain.

As a reference (REF) case, a large scale Fast Breeder Reactor (FBR)[6] was utilized with Mixed Oxide (MOX) fuel containing 27.8/30.4wt% Pu in the active (inner/outer) core and depleted uranium in the inner and outer blanket as shown in **Fig. 1**. In CASE A, 100% of MA was doped in the inner blanket with 144.8 [cm] radius (ΔR). From the CASE B to F, 10, 20, 30, 40 and 50% of MA, respectively, was doped into the active core in addition to 100% of MA doping to the inner blanket.

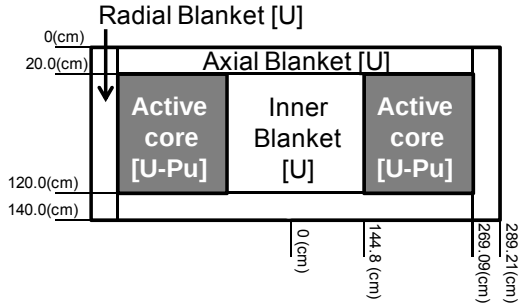

Fig. 1 Geometry of reference FBR core with inner blanket

RESULT

Figure 2 shows an illustrative scope of irradiation time-dependent eigen value (k_{eff}) for REF, CASE A to F. It is found that doping MAs into only the inner blanket contributes to the long-life core compared with REF. It is explained that ^{238}Pu transmuted from MA in the inner blanket plays a role as a fissile material. Furthermore, in case of doping MA not only the inner blanket but also the active core (CASE B to F), the maximum available Effective Full Power Days (EFPDs) is significantly extended compared with CASE A. In CASE F, at 5,100EFPDs, burnup reactivity change becomes positive because the incineration region is shifted gradually from the active core to the inner blanket as shown in **Fig. 3**. It is found that long-life core can be achieved by MA doping to both of the inner blanket and the active core because of ^{238}Pu transmuted from MA working as the fissile material and shifting the region of incineration geometrically from the active core to the inner blanket.

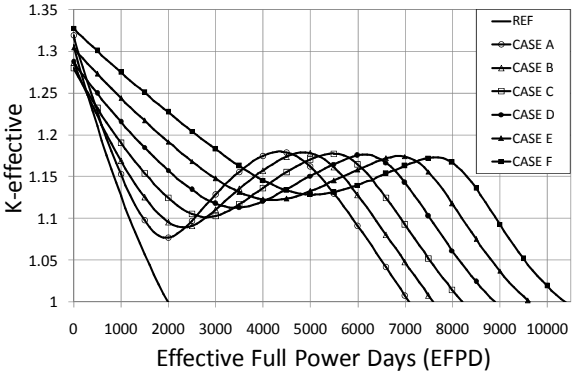

Fig. 2 Effect of MA doping to inner blanket and active core on reactivity

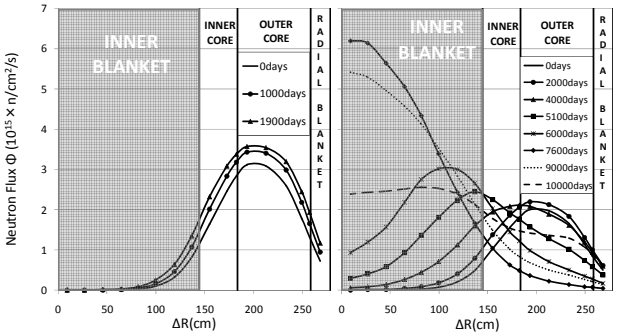

Fig. 3 Neutron flux distribution during irradiation in REF (left) and CASE F (right)

REFERENCES

1. M. Saito, *Prog. Nucl. Energy*, **40**[3-4], 365-374 (2002).
2. M.Saito, *Int. J. Nucl. Sci. Tec.* **1**[23], 127-138 (2005).
3. M. Nakagawa *et al* , JAERI 1294, JAEA, (1984).
4. T. B. Fowler *et al*., ORNL-TM-2496, Rev2 (1971).
5. G. Chiba *et al*., *J. Nucl. Sci. Technol.*, **1**[4], 335-340 (2002).

6. M. Naganuma, *et al*., JNC TN9400 2005-051 (2005)

C.6 Development of Methodology for Plutonium Categorization (III) - Effect of Radiation -

Yoshiki KIMURA, Masaki SAITO and Hiroshi SAGARA

INTRODUCTION

To evaluate the proliferation resistance of Pu, a function "*Attractiveness (ATTR)*" was proposed as a ratio of potential of fission yield to characterization of technical difficulty converting to nuclear explosive devices (NEDs) [1, 2, 3]. In the present paper, *ATTR* was improved by the introduction of the effect of radiation dose in the technical difficulty.

METHODOLOGY DEVELOPMENT

In previous studies, the potential of fission yield was described by Rossi-alpha, the ratio of super-criticality to prompt neutron lifetime. The high decay heat makes Pu handling and NED manufacturing technically more difficult, and the high spontaneous fission neutron emission rate reduces the explosive yield and enhances the probability of pre-detonation. Therefore, the characterization of technical difficulty converting to NEDs was assumed as functions of specific decay heat (DH [W/kg]) and spontaneous fission neutron rate (SN [n/g/s]) of Pu metal [1, 2, 3].

In addition to DH and SN, the high radiation is also considered as a barrier against the diversion of nuclear materials. In the present paper, radiation dose rate (RD) of Pu metal unshielded at the distance of 1 meter is also introduced as the technical difficulty, following the IAEA categorization based on the physical protection of nuclear materials [4]. New evaluation function of *ATTR* is proposed as,

$$ATTR = \frac{\frac{\alpha_\infty}{\alpha_\infty^{239}}}{\frac{DH}{DH^{238}} + \frac{SN}{SN^{238}} + \frac{RD}{RD^{238}}} \qquad (1)$$

In Eq. (1), the Rossi-alpha and all technical difficulty factors are normalized by their maximum values in Pu isotopes. The Rossi-alpha, which was described as potential of fission yield, was normalized by that of pure ^{239}Pu (α_∞^{239}). The technical difficulty factors were normalized by those of ^{238}Pu (DH^{238}, SN^{238} and RD^{238}). The radiation dose rate were estimated quantitatively with the methodology used in Ref.[5]. The source photon spectrum were obtained from ORIGEN decay and photon library [6], and the shielding by Pu itself and surrounding air were estimated using MCNP4C(02) code [7] with library of MCPLIB02 (photon) [8] and FSXLIB-J33(neutron) [9].

EVALUATION OF PLUTONIUM DENATURING

The left side in Fig. 1 shows the *ATTR* of Pu normalized by that of pure ^{239}Pu as a function of the doping rate of each Pu isotope to pure ^{239}Pu. It also shows the example of Pu categorization proposed by Pellaud [10] and defined by IAEA [11]:

(a) *Weapon grade* (less than 7% of ^{240}Pu) [10],
(b) *Usable* (more than 7% and less than 30% of ^{240}Pu) [10],
(c) *Practically Unusable* (more than 30% of ^{240}Pu) [10], and
(d) *Exempt* from safeguards (more than 80% of ^{238}Pu) [11].

The right side in Fig. 1 shows the results calculated by us based on another evaluation function, Figure of Merit (FOM_2) and its categorizations [12].

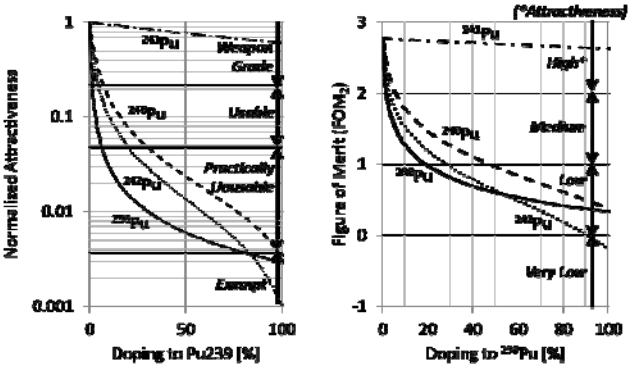

Fig.1 *Attractiveness* (left) and Figure of Merit (right) for Pu denaturing

Attractiveness of Pu decreases dramatically by even-mass-number Pu isotopes doping, because technical difficulty is enhanced with doping of them. The results calculated by using *ATTR* function have a similar tendency to the results calculated by using FOM_2 function.

REFERENCES

1. M. Saito *et. al.*, *ANS TRANSACTIONS*, Vol. 96 (2007)
2. M. Saito *et al.*, *ANS TRANSACTIONS*, Vol. 98 (2008)
3. M. Saito, *Proc. Global09*, Paris, Sep. 6-11, (2009)
4. IAEA, INFCIRC/225/Rev.4 (1999)
5. V. Artisyuk *et al.*, *J. Nucl. Sci. Technol.*, **45**[10], 1009-1015 (2008)
6. "ORIGEN 2.2," CCC-371, RSICC (2002)
7. "MCNP4C," CCC0700, RSICC (2000)
8. "MCNPDATA," DLC-200, RSICC (2000)
9. JAERI-DATA/CODE 2003-011, JAERI (2003)
10. B. Pellaud, *J.Nucl.Mat.Management*,**31**,30 (2002)
11. AEA, INFCIRC/153 (1972)
12. C. Bathke *et al.*, *Proc. Global09*, Paris, Sep. 6-11, (2009)

C.7 Development of Two-Beam type IH-RFQ Linac

Noriyosu HAYASHIZAKI and Toshiyuki HATTORI

High intense heavy ion beam acceleration in the low energy region is one of the most difficult conditions to achieve, because the space charge effect is extremely strong. In order to generate a high intensity beam using linacs, we have to suppress the space charge effect and avoid beam loss as much as possible. Multibeam acceleration scheme solves the problem by dividing a single high intensity beam into several beams and several linacs are used to accelerate the beams in parallel. After the acceleration stage the beams are merged using a funneling system. In this scheme a single cavity is used to accelerate only one beam. Therefore, if one cavity could be used to accelerate several beams, a significant gain would be made in installation space and operational cost saving.

In this study we have investigated a multibeam type radio frequency quadrupole (RFQ) linac to accelerate several beams using a single cavity. The RFQ electrodes are placed in an IH type cavity which has a high shunt impedance for low energy beam acceleration [1]; This structure is known as a IH-RFQ linac. GSI in Germany proposed a multibeam type IH-RFQ linac with several beam channels in a single cavity [2].

We manufactured a two-beam type IH-RFQ linac as a prototype of the multibeam type IH-RFQ linac [3]. The schematic drawing and the main parameters of the two-beam type IH-RFQ linac are shown in Fig. 1 and Table 1, respectively. An ion source injects a C^{2+} beam of 5 keV/u and 60 mA/channel into the linac. The linac produces an output beam of 60 keV/u and 44 mA/channel. Therefore, a single RFQ cavity is used to accelerate a C^{2+} beam of approximately 88 mA.

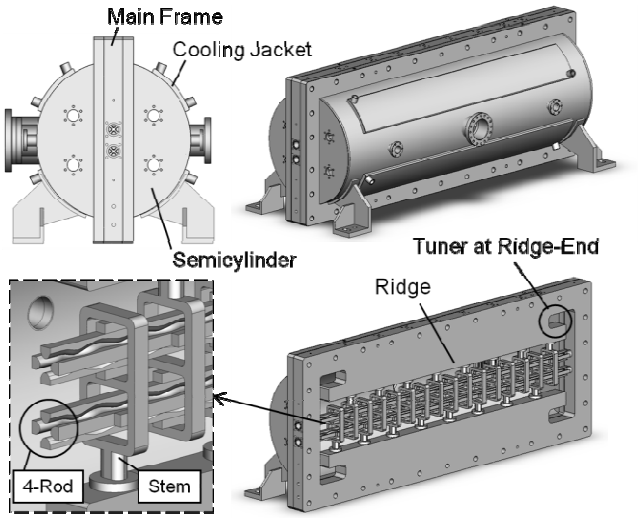

Fig. 1. Schematic drawing of the 2-beam type IH-RFQ linac.

Table 1. Main parameters of the two-beam type IH-RFQ linac.

Acceleration particle	C^{2+}
Input energy	5 keV/u
Output energy	60 keV/u
Q_0	5900 (measured value)
Operating frequency	47 MHz (measured value)
Wall loss	32 kW (estimated by measured Q_0)
Beam loading	34 kW
Cavity diameter	492 mm
Rod length	1481.2 mm
Average aperture radius	7.6 mm
Normalized acceptance	1.21 π mm mrad (RMS)
Input beam current	60 mA/channel
Input emittance	0.1 π mm mrad (RMS, normalized)
Output beam current	44 mA/channel
Output emittance	0.24 π mm mrad (RMS, normalized)

We also developed a two-beam laser ion source with DPIS (Direct Plasma Injection Scheme) as an injection system for the two-beam IH-RFQ linac. The target is a carbon plate (purity 99.5%) and a manipulator is used to move the target up and down. A voltage of 30 kV is produced on the ion source while the linac is running. The maximum energy per shot of the Nd:YAG laser is 700 mJ (350 mJ/channel). The current and valence of carbon ions in the laser ablation plasma were analyzed using the time-of-flight (TOF) method.

The lifetime of the carbon target was estimated for the beam acceleration test of the two-beam type IH-RFQ linac. In this study the output beam from the linac was not used for any applications, so we decided to allow the variation of the peak current to be within 10 %. As a result, during the beam acceleration test the manipulator was used to change the target position after the 500th shot.

Using this linac system we were able to accelerate carbon ions from 5 keV/u to 60 keV/u and generate an output beam current of about 108 mA (2×54 mA/channel). A coherency between the two beams, derived from the imbalance of the beam loading, was observed in the acceleration test with carbon ions.

References

[1] T. Hattori, et al., *Fusion Engineering and Design*, **32-33** 359 (1996).
[2] U. Ratzinger, et al., *Nuclear Instruments and Method in Physics Research A*, **415** 281 (1998).
[3] Takuya Ishibashi, Noriyosu Hayashizaki, Toshiyuki Hattori, *Nuclear Instruments and Methods in Physics Research A*, **606** 116 (2009).

C.8 New Public Commons and Network of Nuclear Site Regions

Tetsuo SAWADA

The further activation of locals is one of the main issues of "New Public Commons [1]." And it is the most important key to promote the new siting and replacement of nuclear power stations. More than forty years have past since the earliest stage of invitation of nuclear power stations to regional areas in Japan. For this period, the efforts for the development of regional industries and the improvement of regional life obtained a level of results. However, now a new turn is required in the regional development, as the perception of wealthy has been gradually changed.

The primary objective of this study is to make a network among regional areas where nuclear power stations and related facilities are located. It should further the understanding for nuclear energy, stimulate the "emergence" through the cooperative works among regional areas. As a result, such efforts will enhance the Social Responsibility of conducts related to the nuclear energy. i.e., Nuclear SR (NSR) [2].

1. Introduction

In November 2008, the 13th International Maximarathon [3] was held between Kyoto city and Takahama town in Wakasa bay area. Through this meeting, it has been envisioned and shared that regional nuclear towns have common characteristic issues concerning the development of the local life. The issues are: (1) they have avoided depopulation but it seems superficial, (2) the developments of regional areas are still closely subsidized by the government, (3) the understanding of nuclear energy by local peoples is not well improved, (4) there may be a twisted situation in the region, (5) they have little cooperation with other nuclear power siting regions, (6) the implication of nuclear energy is misunderstood by the people of consumer area such as large cities.

For the first step, we have established an opportunity where we can cooperatively create platform that will assist the regional developments which meet the wish and desire of local peoples. Various partners can change information, know-how, knowledge and experience which will stimulate new activity for the creation leading to emergence. Here the emergence is the way of complex systems and patterns arise out of a multiplicity of relatively simple interactions. Through the emergence, a situation of creation of new values may occur among individuals who do not have actual relationships until then.

2. Practice

The major components of the 13th Maximarathon were as follows: (1) a long-distance relay race from Kyoto to Wakasa Takahama town (about 100 km), (2) the runners' relay of a message baton that prays for the peaceful use of nuclear energy, (3) social gatherings at several regions such as Kyoto, Takahama and other towns where the relay passed, (4) visiting of local schools and goodwill exchange with pupils and students.

The results of this event were: (1) we had opportunity for effective exploration of mutual understanding of local people, workers and scientists related to nuclear business, and people of consumer city; (2) within a sports event, various people with little opportunity to meet in daily life got a chance to encourage fellowship; (3) the pupils and students had a chance to share the message for future as well as to release message to the world.

3. A new platform: Tour de Atom

According to the above-mentioned successful fruits, we have received a lot of expectation to promote a new platform for the interchange opportunity leading to emergence. As a result, we have originated "Tour de Atom." This platform will make a harmonization among regions, other various partners beyond generations. Then it can make networks in a region, among the regions, between regional area and city through Japan. These networks should be shared with the concerned people in the world.

The 1st Tour de Atom was held at Wakasa Bay area in 2009 which started Takahama town and reached to Tsuruga city, with engaging rural towns in between them. In Wakasa Bay area, we have 15 nuclear power stations including Monju fast reactor. In the 1st Tour de Atom , about 60 runners relayed a message of "萬物生光輝", that is a calligraphy by former Prime Minister Yasuhiro Nakasone (see Figure 1), for the peaceful use of nuclear energy as well as a video message that was planned and made by students of Takahama junior high school. Then Tour de Atom 1.5 was held between Tsuruga and Fukui city in June 2010, when Conference of Energy Ministers of APEC was being held. Succeedingly, the 2nd Tour de Atom [4] was held from Fukui city to Shika town in Ishikawa prefecture in October 2010.

In Shika town, Hokuriku electric power company has two nuclear power stations. In 2011, these messages will be relayed to the next nuclear siting town: Kashiwazaki-Kariwa in Niigata prefecture.

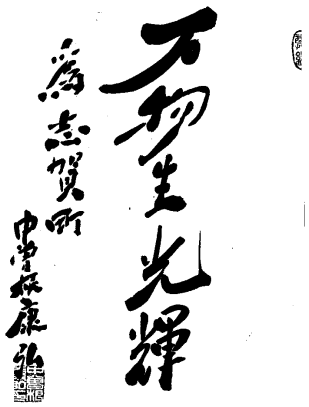

Figure 1 Calligraphy by former PM Nakasone: "All things shine brilliantly.

4. Summary

It is required to cope with any situation surrounding nuclear power and related activities. According to the concept of New Public Commons, a new approach is needed for the improvement of the relationship between nuclear energy and society. The history of nuclear power deployment and the experience in the efforts of co-existence and mutual prosperity in Japan will be a good practice to the countries which are going to introduce nuclear power. The platform of Tour de Atom is a kind of practical field of nuclear knowledge management that will stimulate emergence through the networks to be formed on the platform. This can connect partners who have been isolated until then and raise the potential capability of regional areas. It will then improve the quality of living both in the energy producing and supplying areas and the energy consuming areas. In this sense, the Tour-de-Atom platform is a tool to practice the Nuclear Social Responsibility (NSR).

Reference:

[1] Declaration of “New Public Commons”. June 4, 2010. http://www5.cao.go.jp/entaku/en/pdf/declaration-english.pdf

[2] T. Sawada, et al, Nuclear corporate social responsibility: an approach toward a roadmap for gaining social confidence, *Int. J of NGEE*, vol. **1**, Nos. 3 (2007)

[3] The 13th Maximarathon in Japan from the JAIF TV. http://www.youtube.com/watch?v=h9PrOSFI4yo((c) Japan Atomic Industry Forum)

[4] The 2nd Tour de Atom; http://www.jaif.or.jp/ja/jaiftv/index.html ((c) Japan Atomic Industry Forum)

Ⅲ. Co-operative Researches

Ⅲ.1 Co-operative Researches within Tokyo Institute of Technology

Under the generic proposition: "The Release and Utilization of Energies existing in Atoms, Molecules and Nuclei" which has been hoisted since the reorganization of RLNR, we advertise for collaborations with any department and laboratory within Tokyo Institute of Technology in order to develop researches for the improvement of energy utilization with safety, mass transmutation by nuclear reactions with high efficiency, and construction of energy system concept with high societal acceptability. The RLNR will promote these collaborations by offering the organizations, facilities, equipments and space as the research base for research project teams and research groups crossing over within Tokyo Tech. We are going to adopt unique and innovative themes which make maximum use of the activities of this research laboratory.

Co-operative Researches

- CO_2 electrolysis cell for carbon recycling energy system
  Fusion joint research, Multidisciplinary Education and Research Center for Energy Science, Tokyo Institute of Technology Global COE Program

- Feasibility study for carbon recycling energy system
  Fusion joint research, Multidisciplinary Education and Research Center for Energy Science, Tokyo Institute of Technology Global COE Program

Ⅲ.2 Co-operative Researches with Outside of Tokyo Institute of Technology

- Development of High-accuracy Flow Measurement System using Advanced Measurement Technique
  Tokyo Electric Power Co.

- Fundamental Study of Thermo-Hydraulic Instability on Reduced-Moderation Natural Circulation BWR Concept (Clarification of Condensation Phenomena under Non-Condensable Gas)
  Japan Atomic Power Co.

- Study on Technical Standards for Safety Transportation of Decommissioned Wastes of Nuclear Power Plant
  Nuclear Fuel Transport Co., Ltd.

- Study on Isotopic Separation with Microchips
  ING Corporation.

- Fundamental Study on Advanced Turbid Water Treatment
  NPO. Saiseisya

- Two-Phase Flow Dynamics for Future Light Water Reactor Development
  Korea Atomic Energy Research Institute, Korea

- Experimental and Analytical Studies on Multi-Dimensional Two-Phase Flow
  PSF Zittau, Germany

- Advanced Fluid Dynamics and Developed of Measurement Technique
  Chulalongkorn University, Thailand

- Thermal Hydraulics for Advanced Water Cooling Reactors
  Bhabha Atomic Research Center, India

- Future Light Water Reactor Development
  Chulalongkorn University, Thailand

- Study of Na-cooled fast reactor supercritical CO_2 turbine system
  Ministry of Education, Culture, Sports, Science and Technology

- Development of an atmospheric scanning positron microscope
  National Institute of Advanced Industrial Science and Technology

- Advanced study on heavy ion linac
  National Institute of Radiological Sciences

- Study of C^{6+} ion hybrid single IH cavity linac with Direct Plasma Injection Scheme for cancer therapy
  Grant-in-Aid for Scientific Research

- Research and Development of High Performance Ceramics
  Chiba Institute of Technology, Tokai University

- Establishment of Fabrication Process of Silicon-Containing Ceramics for Ineat Matrix of TRU Elements
  Japan Atomic Energy Agency

- Study on Novel Process of SiC/SiC Composite by Electrophoretic Deposition Method
  Japan Aerospace Exploration Agency (JAXA)

- Study on the Improvement of Irradiation Resistance of Ceramics by Their Orientation Control
  National Institute for Materials Science (NIMS)

- Research and Surveys on the Future Fast Reactor System (V)
  Mitsubishi Heavy Industry Co. LTD

- Studies on Separation of Uranium Species Using Polyvinylpolypyrrolidone
  Japan Atomic Energy Agency and Tokai University

- A Study of Extraction Behavior of ReO_4^- by Using Monoamide Compounds
  Japan Atomic Energy Agency

- A Study on Partitioning of Lanthanoid and Actinoid Species
  Japan Atomic Energy Agency

- A Study on Separation of Uranyl Species Using Alginic Acid
  Prof. R.M. Hassan, Assiut University, Egypt

- A Study on Electron Transfer Reaction between Uranyl(V) and Uranyl(VI) Carbonate Complexes
  Professor I. Grenthe, Royal Institute of Technology, Sweden

- A Study on Electrochemical Reactions of Uranyl Species in Choline Based Ionic Liquids
  Professor A.P. Abbott, University of Leicester, U.K.

- Studies on Structures of Uranyl Complexes in Ionic Liquids
  Dr. C. Hennig, Forschungszentrum Rossendorf, Germany

- Studies on Electrochemical Reactions of Uranyl(VI) Species in Ionic Liquids
  Japan Atomic Energy Agency

- Neutron Capture Cross Section Measurement
  n_TOF Collaboration

- Development of a new gamma-ray detector for keV-neutron capture experiment
  Osaka University, Japan Atomic Energy Agency

- Study on keV-Neutron Capture Cross Sections of Fe isotopes
  Dong-A University, Kyungpook National University

- Study on Nuclear Data by using a High Intensity Pulsed Neutron Source for Advanced Nuclear System

- Development of Cleaning Technology on Semiconductor Equipment Process for Atmospheric-Pressure Non-Equilibrium DC Pulse Plasma Jet
  University of Miyazaki, Oita University, Oita Device Technology Co., Ltd., JASCO Engineering Co.

- Optical Emission Characteristics of Atmospheric-Pressure Nonequilibrium Microwave Discharge and High-Frequency DC Pulse Discharge Plasma Jets
  University of Miyazaki, ADTEC Plasma Technology Co. Ltd., King Mongkut's University of Technology Thonburi.

- Space Charge Measurements of Surface Cleaning Sample Using Atmospheric-Pressure Non-equilibrium Discharge Plasma Jet
  University of Miyazaki, ADTEC Plasma Technology Co. Ltd., FiveLab Co.,Ltd.

- Spectroscopic Diagnostics of Pulse Discharge Argon Plasmas of Atmospheric Pressure
  Kyushu University.

- High-Energy Density Physics Research Using Induction Synchrotrons
  High Energy Accelerator Research Organization (KEK)

- Development of Liquid Lithium Target for Neutron Production in Neutron Irradiation System for Neutron Capture Therapy based on by Accelerators
  Kyoto University.

- Development of Low-Load Wood Drying System using Heat Pump, Practical Technical Project to Promote the Development of New Agriculture Policy
  Ministry of Agriculture, Forestry and Fisheries

- Chemical heat pump for waste heat recovery from iron making process
  Environmentally Friendly Steel Process Technology,
  NEDO commissioned project

- Material Development of Chemical Heat Storage for Effective Use of Industrial Waste Heat
  Industrial Technology Research Grant Program from New Energy and Industrial Technology Development Organization (NEDO) of Japan

- *In situ* high-resolution photoelectron spectroscopic study of 1D peanut-shaped C_{60} polymers
  UVSOR Facility, Institute for Molecular Science

- DFT study of low-dimensional peanut-shaped C_{60} polymers
  Yokohama National University

- Photodynamic properties of nanomaterials
  Department of Applied Physics, Hokkaido University

- Fabrication of AZO transparent electrodes for Organic Photovoltaic cells
  Department of Electronic Engineering and Applied Physics, Osaka City University

- Riemannian geometrical effects on Tomonaga-Luttinger Liquids exponent of 1D metal peanut-shaped C_{60} polymer
  Department of Applied Physics, Hokkaido University, Department of Physics, Nara Women's University

- A Study on Surface and Interface of Organic Photovoltaic Cells
  J-Power Co. Ltd

- Study on the Initial Processes in the Recognition and Repair of DNA Double-Strand Breaks
  Strategic Promotion Program for Basic Nuclear Research by the Ministry of Education, Culture, Sports, Science and Technology of Japan

- Survey on the Trend in Scientific Research on Zoology and Related Field
  Survey on the Trend in Scientific Research, Japan Society for the Promotion of Sciences, Japan

- Analyses of the Repair of DNA Double-Strand Breaks Generated by Low Dose/Low Dose Rate Radiation
  Central Research Institute of Electric Power Industries

- Study on Electron density fluctuations by Microwave Imaging Reflectometry
  National Institute for Fusion Science

- Separation and recovery of molybdenum in spent fuel by ion exchange technique
  Japan Atomic Energy Agency

- Basic study on immobilization treatment of phosphate-including low-level radioactive liquid waste
  Japan Atomic Energy Agency

- Study on ion exchange behavior of actinides, VII group elements and fission products
  Japan Atomic Energy Agency

- NuSAC Co. Ltd.

- High temperature NMR spectroscopy in molten salts: Application to molten fluoride mixtures for future nuclear reactors
  Conditions Extrêmes et Matériaux: Haute Température et Irradiation, and le STUDIUM (Agency for research and hosting foreign research associates)

- Characterization of structure and physico-chemical properties of molten rare-earth metal halides
  Japan Atomic Energy Agency

- Innovative characterization of materials under severe condition
  Conditions Extrêmes et Matériaux : Haute Température et Irradiation,
  Centre National de la Recherche Scientifique

- NMR and EXAFS approach on the structure of molten fluorides at high temperature for molten salt reactor
  Conditions Extrêmes et Matériaux : Haute Température et Irradiation, Université de Paris VI
  Université P. Sabatier (molten salt reactor project)

- Investigation of Biophysical Chemistry in Extended-Nano regions using Nuclear Magnetic Resonance Method
  Mizuho Foundation for the Promotion of Sciences, Engineering research aid projects

- Hydrothermal Synthesis Process of Metal Oxidized Nanomaterials using Supercritical Water
  Preceding Basic Engineering Research Program, Japan Atomic Energy Agency

- Core Research for Evolutional Science and Technology (CREST)
  Development of Ion Transport Method in Extended-Nano Space for Photo Fuel Cell

Ⅲ.3 Themes Supported by Grants-in-Aid for Scientific Research of the Ministry of Education, Culture, Sports, Science and Technology

- Material Development of Porous Ceramics for Diesel Particulate Filter Based on In-Situ Crystal Growth and Orientation : Grant-in-Aid for Young Scientists (B)

- Study on Fast-Neutron Capture Cross Sections of Long-Lived Nuclear-Waste Selenium 79

- Development of new quantum electronic science in Riemannian geometric space

- Strategic Promotion Program for Basic Nuclear Research

- Angiocinematography Using Particle-Induced Dual-Wavelength Pulsed-X-rays for Minimization of Dosages of Contrast-Medium and Radiation

- Development of a Variable-Energy, Variable-Intensity, On/Off Switchable Gamma-Ray Needle-Source for Brachytherapy.

- Development of a Microbeam Cell-Irradiation System Using Flexible Glass Tubes

- Development of a Tiny X-ray Source for In-situ Irradiation Using Laser-Induced Shock Waves and Piezo Elements

- High-Efficient High-Temperature Process by Hybrid Method using Chemical Heat Storage

- Development of Hydrogen Separation Membrane Composited with Metal Membrane–Porus Metal Membrane Using Anti-Build-Up Method

- New Strategy for the Prediction and Control of Radiosensitivity Based on the Life Cycle and Homeostasis of DNA Double-Strand Breaks Enzymes

- Basis of Biological Effects of Hyperthermia – Ku as a Model Protein”

- Development of Nanofluidic-Based Separation System of Radioactive Nuclide Ions by Controlling Electrostatic Forces and Surface Charges

- NMR Studies on Water and Radionuclides Confined in Bentonite Clay under High-Temperature and -Pressure Conditions”.

- NMR Studies on Molecular Structures and Dynamics of Liquid-Phase Cluster Molecules in Soft Material Interfaces

Ⅳ. List of Publications

H. Ninokata, E. Merzari and A. Khakim: Analysis of low Reynolds number turbulent flow phenomena in nuclear fuel pin subassemblies of tight lattice configuration; *Nuclear Engineering and Design,* **239** pp. 855-866 (2009).

Sheng Wang**,** Hisashi Ninokata**,** Elia Merzari**,** Kangbin Lei**,** Xilian Luo**,** Luyi Lu**,** Kiwamu Kase: Numerical study of a single blade row in turbomolecular pump; *VACUUM***,** Vol. **83,** No. 8, pp.1106-1117, May (2009).

E. Merzari, E. Baglietto and H. Ninokata: Large Eddy Simulation of the Flow in a T-junction; *Proc. ICAPP 2009*, Tokyo, Japan, May (2009).

E. Merzari, I.C. Bang and H. Ninokata: Numerical Simulation of the Flow in a Natural Circulation Loop with Nanofluids and Differential Heating; *Proc. ICAPP 2009*, Tokyo, Japan, May (2009).

A. Khakim, E. Merzari and H. Ninokata: Feasibility study of the application of exotic pin for tight-lattice fuel assembly; *Proc. ANS annual meeting 2009*, Atlanta, USA, June (2009).

E. Merzari and H. Ninokata: URANS Simulation of Parallel Jets Mixing in a Rectangular Confinement; *Proc. ANS annual meeting 2009*, Atlanta, USA, June (2009).

H. Futagami and H. Ninokata: Analysis for Rarefied Gas Flow in a Rotating Cylinder; *Proc. ASME 2009 Fluids Engineering Division Summer Meeting FEDSM2009* [FEDSM2009-78356], Vail, Colorado USA, August 2-6 (2009).

Sheng Wang Kangbin Lei Xilian Luo Kiwamu Kase, Elia Merzari, Hisashi Ninokata: Cylindrical Couette Flow of a Rarefied Gas From Macro- to Micro-Scales; *Proc. ASME 2009 Fluids Engineering Division Summer Meeting FEDSM2009* [FEDSM2009-78359], Vail, Colorado USA, August 2-6 (2009).

Elia Merzari and Hisashi Ninokata: A-Priori Test of the Flow in an Annular Channel With Differential Heating at the Walls; *Proc. ASME 2009 Fluids Engineering Division Summer Meeting FEDSM2009* [FEDSM2009-78467], Vail, Colorado USA, August 2-6 (2009).

Elia Merzari Azizul Khakim Hisashi Ninokata: Large Eddy Simulation of the Flow in Tight-Lattice Rod Bundles at Low Reynolds Number; *Proc. ASME 2009 Fluids Engineering Division Summer Meeting FEDSM2009* [FEDSM2009-78471], Vail, Colorado USA, August 2-6 (2009).

Sheng Wang, Kangbin Lei, Xilian Luo, Kiwamu Kase, Elia Merzari, Hisashi Ninokata: Simulation of Eccentric-Shaft Journal Microbearing by DSMC; *Proc. ASME 2009 Fluids Engineering Division Summer Meeting FEDSM2009* [FEDSM2009-78572], Vail, Colorado USA, August 2-6 (2009).

E. Merzari and H. Ninokata: Development of an LES methodology for complex geometries; *Journal of Nuclear Engineering and Technology* Vol. **41**, No. 7, pp. 893-907 September (2009).

R. Li, A. Yamaguchi, E. Merzari, H. Ninokata, F. Watanabe and M. Mori: Computational Fluid Dynamics Study on Flow Modeling of Liquid Droplet Impingement Erosion in BWR; *Proc. 13th Topical Meeting on Nuclear Reactor Thermal Hydraulics (NURETH-13)*, N13P1355, Kanazawa, Japan, September 27-October 2 (2009).

H. Horie, H. Matsumiya, K. Miyagi, Y. Nishi, T. Grenci, M. H. Fontana, F. J. Moody, H. Ninokata, G. E. Wilson, A. Yamaguchi: Phenomena Identification and Ranking Tables (PIRTs) for 4S Loss of Offsite Power, Failure of a Cavity Can, and Sodium Leakage from Intermediate Piping Scenarios; *Proc. 13th Topical Meeting on Nuclear Reactor Thermal Hydraulics (NURETH-13)*, N13P1093, Kanazawa, Japan, September 27-October 2 (2009).

E. Merzari and H. Ninokata: Proper Orthogonal Decomposition of the Flow in a Rod-Bundle; *Proc. 13th Topical Meeting on Nuclear Reactor Thermal Hydraulics (NURETH-13)*, N13P1372, Kanazawa, Japan, September 27-October 2 (2009).

Elia Merzari, Hisashi Ninokata: Emanuela Colombo, Fabio Inzoli, URANS Simulation of Confined Parallel Jets Mixing; *Proc. 13th Topical Meeting on Nuclear Reactor Thermal Hydraulics (NURETH-13)*, N13P1373, Kanazawa, Japan, September 27-October 2 (2009).

Tomoko Ishizu., Hiroshi Endo and Hisashi NINOKATA: On Void Reactivity Limitation for the Core Loaded with Mixed Nitride Fuels; *Journal of Nuclear Science and Technology*, Vol. **46**, No. 10, p. 981–994 (2009).

E. Merzari, A. Khakim, H. Ninokata and E. Baglietto: Unsteady Reynolds-averaged Navier-Stokes: toward accurate prediction of turbulent mixing phenomena; *International Journal of Process Systems Engineering*, Vol. **1**, No. 1 pp. 100-123 (2009).

E. Merzari, H. Ninokata, A. Mamhood, M. Rohde: Proper Orthogonal Decomposition of the Flow in Geometry Containing a Narrow Gap; *Journal of Theoretical and Computational Fluid Dynamics* (Received April 8, 2008; accepted June 9, 2009): DOI 10.1007/s00162-009-0152-3

(2009).

E. Merzari, A. Khakim, H. Ninokata and E. Baglietto: Toward an Accurate Approach for the Prediction of the Flow in a T-junction: URANS; *Journal of Nuclear Engineering and Technology,* Vol. **41**, No. 9, pp. 1191-1204 (2009).

Rui Li, Elia Merzari and Hisashi Ninokata: Numerical Study on Liquid Droplet Impingement Erosion in BWRs; *Proc. ANS Winter Meeting 2009*, Washington DC, USA, November (2009).

Riccardo Mereu, Emanuela Colombo, Fabio Inzoli, Elia Merzari and Hisashi Ninokata: Large Eddy Simulation of Confined Parallel Jets; *Proc. ANS Winter Meeting 2009*, Washington DC, USA, November (2009).

Jyunko Takanashi, Shigeki Horibuchi, and Masanori Aritomi: Study on Water System for Cutting Asphalt Road (1st Report, Development of Water Treatment System for Cutting Asphalt Road); *Transactions of the Japan Society of Mechanical Engineers*, *Part B*, Vol. **75**, No. 760, pp. 2504-2510 (2009).

Masanori Aritomi: Development of asbestos harmless treatment system on pulling down sites , *Journal of Resources and Environment* , Vol. **45**, No. 8, pp. 86-90 (2009).

M. Kawakubo, M. Aritomi, H. Kikura and T. Komeno: An Experimental Study on the Cooling Characteristics of Passive Containment Cooling Systems; *Journal of Nuclear Science and Technology,* Vol. **46** No. 4, pp. 339-345(2009).

Daisuke Ito, Hiroshige Kikura, and Masanori Aritomi: Application of wire-mesh tomography to two-phase flow measurement in narrow channel; *Transactions of the Japan Society of Mechanical Engineers, Part B*, Vol. **76**, No. 763, pp. 481-482(2010).

Nobuyoshi Tsuzuki, Yasuyoshi Kato, Yasushi Muto, Takao Ishizuka, Motoaki Utamura, and Masanori Aritomi: Nusselt number correlation of microchannel heat exchanger with S-shaped fins; *Transactions of the Atomic Energy Society of Japan*, Vol. **9**, No. 1, pp. 13-20(2010).

Hidekazu Asano and Masanori Aritomi: Long-term integrity of waste package final closure for HLW geological disposal, (vi) consistency of the structural integrity evaluation model for the weld joint; *Journal of Nuclear Science and Technology*, Vol. **47**, No. 1, pp. 70-83(2010).

Hiroshige Kikura, Hideki Murakawa, and Masanori Aritomi: Velocity profile measurements in bubbly flow using multi-wave ultrasound technique; *Chemical Engineering Communications*, Vol. **197**, No. 2, pp. 114-133 (2010).

M. Kawakubo, M. Matsuzaki, H. Kikura, and M. Aritomi: Study on Dropwise Condensation Heat Transfer in Presence of Non-condensable Gas; *Japanese Journal of Multiphase Flow*, Vol. **24**, No. 1, pp. 63-69(2010).

Yusuke Shimizu, Daisuke Ito, Hiroshige Kikura, Masanori Aritomi, Masahiro Takei: Flow Measurement in Open Channel using Ultrasonic Array Sensor; *3rd international workshop on process tomography(IWPT-3)*, Tokyo, Japan, Paper No.45(April 17-19, 2009).

Yasuaki Shimohara, Daisuke Ito, Hiroshige Kikura, Masanori Aritomi, Masahiro Takei: Micro Bubbly Flow Measurement using Narrow Wire-Mesh Sensor; *3rd international workshop on tomography(IWPT-3)*, Tokyo, Japan, Paper No.37(April 17-19, 2009).

M. K Biddinika, D Ito, H. Takahashi, H. Kikura, M. Aritomi: Multi-wave Sensors for Two-Phase Flow Observations in Vertical Rectangular Channel; 3rd international workshop on process tomography(IWPT-3), Tokyo, Japan, No.98(April 17-19, 2009).

Takao Ishizuka, Yasushi Muto, Masanori Aritomi, Nobuyoshi Tsuzuki, Hiroshige Kikura: Design and Analysis of the Axial bypass Compressor blade of the Supercritical CO2 Gas Turbine; *17th International Conference on Nuclear Engineering(ICONE-17)*, Brussels, Belgium, ICONE17-75136(July 12-16, 2009).

Takagi Kazuhisa, Yasushi Muto, Takao Ishizuka, Masanori Aritomi, Hiroshige Kikura: Research on Flow Characteristics of a Supercritical CO2 Axial Compressor Blades by CFD Analysis; *17th International Conference on Nuclear Engineering(ICONE-17)*, Brussels, Belgium, ICONE17-75626(July 12-16,2009).

Tomohiro Furukawa, Yoshiyuki Inagaki, and Masanori Aritomi: Corrosion behavior of FBR structural materials in high temperature supercritical CO2; *17th International Conference on Nuclear Engineering, Proceedings (ICONE-17)*, Vol. **1**, pp. 307-312(2009).

Hideharu Takahashi, Hideki Kawai, Sao Yasui, Hiroshige Kikura, and Masanori Aritomi: Flow field measurement in a concentric rotating cylinders type photosynthetic bio-reactor using UVP; *The 15th Kanto Branch Meeting of the Japanese Society of Mechanical Engineers*, Ibaraki, Japan, pp. 129-130, (2009-3).

Hiroshige Kikura, Daisuke Ito, and Masanori Aritomi:

Gas-liquid two-phase flow measurement in narrow channel using micro wire-mesh sensor; *The 14th National Symposium on Power and Energy Systems (SPES 2009) of the Japan Society of Mechanical Engineers*, Tsukuba, Japan, D110(2009-6-29), in Japanese.

Hiroshige Kikura, Masahiro Kawakubo, Noriaki Inaba, Masanori Aritomi, and Msayuki Arai: Visualization of droplet diameter on drop-wise condensation; *The 37th Symposium on Visualization of the Visualization Society of Japan*, Shinjyuku, Japan, B206(2009-7-22), in Japanese.

Hideharu Takahashi, Hiroshige Kikura, Hideki Kawai, and Masanori Aritomi: Ultrasonic Measurement in Algal Cultivation using Taylor Couette Vortex Flow; *Proc. JSMF Annual Meeting 2009*, Kumamoto, Japan, B123 (2009-8-7).

Masamichi Nakagawa , Tooru Kobayashi, Minoru Takahashi, and Masanori Aritomi: Fundamental Stability on A Sheet Jet of Liquid Lithium for the Target and Coolant of BNCT using Accelerators; *Proc. JSME Annual Meeting*, Iwate, Japan, S0504-2-5 (2009-9.14).

Masamichi Nakagawa, Tooru Kobayashi, Minoru Takahashi, and Masanori Aritomi: Flow Schemes of Liquid Lithium for the Target and Coolant of BNCT using Accelerators; *JSMF Annual Meeting 2009,* B332 (2009-8-9), in Japanese.

Masanori Aritomi, Jyunko Takanashi, and Shigeki Hosobuchi: Development of Water Treatment System for Cutting Asphalt Road (I); *Proc. Mechanical Engineering Congress 2009 (MECJ-2009)*, Vol.**5**, pp.69-70(2009-9.16).

Jyunko Takanashi, Shigeki Hosobuchi, and Masanori Aritomi: Development of Water Treatment System for Cutting Asphalt Road (II); *Proc. Mechanical Engineering Congress 2009 (MECJ-2009)*, Morioka, Japan, Vol.**5**, pp.71-72 (2009-9.16).

P.T. Krishna Kumar, Hiroshi Sekimoto: Reduction of systematic uncertainty in the transmission measurement of iron using entropy based mutual information; *Radiation Measurements*, **44**[2], 168-172 (2009).

S. Okui, H. Sekimoto: Research and Development of the Software for Visualizing Nuclear Reactor and Neutronics; *Proc. of 2009 International Congress on Advances in Nuclear Power Plants (ICAPP '09)*, Tokyo, Japan, May 10-14, 2009.

S. Permana, A. Waris, N. Takaki, H. Sekimoto: All Heavy Metals Closed-Cycle Analysis on Water-Cooled Reactors of Uranium and Thorium Fuel Cycle Systems; *Proc. of 2009 International Congress on Advances in Nuclear Power Plants (ICAPP '09)*, Tokyo, Japan, May 10-14, 2009.

S. Permana, N. Takaki H. Sekimoto: Breeding and Plutonium Characterization Analysis on Actinides Closed Water-Cooled Thorium Reactor; *Proc. of 2009 International Congress on Advances in Nuclear Power Plants (ICAPP '09),* Tokyo, Japan, May 10-14, 2009.

Ismail, Peng Hong Liem, Sidik Permana, Naoyuki Takaki, Hiroshi Sekimoto: Symbiotic systems consisting of large-FBR and small water-cooled thorium reactors (WTR); *Ann. Nucl. Energy*, **36**[8], 1076-1085 (2009).

P.T. Krishna Kumar, Hiroshi Sekimoto: Simulation of optical model parameters with reduced model deficiency 3 by D-optimal criterion; *Ann. Nucl. Energy*, **36**[8], 1208-1210 (2009).

Hiroshi Sekimoto: Five Requirements for Nuclear Energy and CANDLE Reactors; *Materials for Heavy Liquid Metal Coolant and Related Technologies* (HeLiMeRT 2009), Jeju, Korea, May 18-19, 2009.

Hiroshi Sekimoto: CANDLE Reactor: An option for simple, safe, high nuclear proliferation resistant, small waste and efficient fuel use reactor; *NATO Advanced Research Workshop "Nuclear Power and Energy Security"*, Yerevan, Armenia, 26-29 May 2009.

H. Sekimoto, A. Nagata: Core Height Shortening of CANDLE Reactor by Employing MOTTO Cycle; *Trans. American Nuclear Society*, **101** (CD) (2009).

H. Sekimoto, A. Nagata: Optimization of Power Profile of CANDLE Reactor by Using MOTTO Cycle; *ICENES2009:14th International Conference on Emerging Nuclear Energy Systems,* Ericeira, Portugal, 29th June – 3th July, 2009.

Hiroshi Sekimoto: CANDLE Reactor: An option for simple, safe, high nuclear proliferation resistant, small waste and efficient fuel use reactor; *Nuclear Power and Energy Security* (ed. S. Apikyan and D. J. Diamond), pp. 197- 204, Springer (2009).

Hiroshi Sekimoto: Five Requirements for Nuclear Energy and CANDLE Fast Reactor; *CP1244, 2nd International Conference on Advances in Nuclear Science and Engineering – ICANSE2009*, Bandung, Indonesia, 3-4 November 2009, AIP, pp. 3-11 (2010).

Zaki Su'ud, Hiroshi Sekimoto: Local blockage analysis of lead-cooled next-generation nuclear power reactors; *Int. J. Nuclear Energy Science and Technology*, **5**[2], 162-170 (2010).

L. Cinotti, C. F. Smith, H. Sekimoto: Lead-Cooled Fast Reactor (LFR): Overview and Perspectives; *Proc. of GIF*

Symposium, Paris, France, September 9-10, pp. 173-180, 2009.

C. F. Smith, L. Cinotti, H. Sekimoto: Lead-Cooled Fast Reactor (LFR): Ongoing R&D and Key Issues; *Proc. of GIF Symposium*, Paris, France, September 9-10, pp. 181-190, 2009.

Shinya Ishida, Hiroshi Sekimoto: Applicability of Dynamic Programming to the Accelerator Driven System (ADS) Fuel Cycle Shuffling Scheme for Minor Actinide (MA) Transmutation; *Ann. Nucl. Energy*, **37**[3], 406-411 (2010).

Hiroshi Sekimoto: Study on Innovative Nuclear Reactor CANDLE; *Science Portal China*, April 10, 2009.

Hiroshi Sekimoto: Study on Innovative Nuclear Reactor CANDLE; *Science Front of China and Japan*, 2010, JST China Research Center, pp. 89-92(2010).

Hiroshi Sekimoto: Study on CANDLE Burnup (XXII); Research Review and Future Plan; *Annual Meeting of Atomic Energy Society of Japan*, H25 (2010).

Hiroshi Taguchi, Sinsuke Nakayama, Tsuyoshi Okawa, Hiroshi Sekimoto: Study on CANDLE Burnup (XXIII); Power Flattening by Inserting Thorium in the Central Core; *Annual Meeting of Atomic Energy Society of Japan*, H26 (2010).

Sinsuke Nakayama, Hiroshi Taguchi, Tsuyoshi Okawa, Hiroshi Sekimoto: Study on CANDLE Burnup (XXIV); Power Flattening for Several Cores; *Annual Meeting of Atomic Energy Society of Japan*, H27 (2010).

Tsuyoshi Okawa, Hiroshi Sekimoto, Sinsuke Nakayama, Hiroshi Taguchi: Study on CANDLE Burnup (XXV); CANDLE Core Using Pb-208 Coolant; *Annual Meeting of Atomic Energy Society of Japan*, H28 (2010).

Shinya Ishida, Hiroshi Sekimoto: Study on ADS Fuel Shuffling Using Dynamic Programming; *Annual Meeting of Atomic Energy Society of Japan*, H29 (2010).

Noriyosu Hayashizaki, Takuya Ishibashi, Taku Itoa and Toshiyuki Hattori: Multi-beam RFQ linac structure for heavy ion fusion; *Nuclear Instruments and Methods in Physics Research Section A*, **606** (2009)107-110.

Takuya Ishibashi, Noriyosu Hayashizaki and Toshiyuki Hattori: Design of two-beam-type IH-RFQ linac; *Nuclear Instruments and Methods in Physics Research Section A*, **606** (2009)116-119.

Lu Liang, Toshiyuki Hattori, Noriyosu Hayashizaki, Takuya Ishibashi, Jun Tamura: 3D electromagnetic simulation of C^{6+} hybrid single cavity linac for cancer therapy; *Proceedings of Particle Accelerator Society Meeting 2009*, 794-796.

Toshiyuki Hattori, Taku Ito, Lu Liang, Noriyosu Hayashizaki, Takuya Ishibashi, Jun Tamura, Tatsuya Inoue, Hironobu Iwanami, Kazuhito Oka, Yoshiki Shimaya: Design of Hybrid Single IH Cavity Linac for BNCT; *Proceedings of Particle Accelerator Society Meeting 2009*, 797-799.

Takuya Ishibashi1, Noriyosu Hayashizaki, Toshiyuki Hattori: Measurement of electric field distribution in 2-beam type IH-RFQ linac; *Proceedings of Particle Accelerator Society Meeting 2009*, 1035-1037.

Noriyosu Hayashizaki, Nagayasu Oshima, Ryunosuke Kuroda, Ryoichi Suzuki: Development of an RF cavity for an atmospheric scanning positron microscope; *Proceedings of Particle Accelerator Society Meeting 2009*, 1111-1113.

T. Yano, J. Yamane and K. Yoshida: Low Temperature Sintering of Si_3N_4 Ceramics and Its Applicability as an Ineart Matrix of the Transuranium Elements for Transmutation of Minor Actinides; *Key Engineering Mater.*, Vol.**403**, pp.23-26 (2009).

T. Yano, T. Sawabe, K. Yoshida, and Y. Yamamoto: High-Temperature Neutron-Irradiation Effects on CVD-Diamond, Silicon and Silicon Carbide; *J. Nucl. Mater*., Vol.**386-388** (2009) 1018-1022.

T. Sawabe, M. Akiyoshi, K. Ichikawa, Katsumi Yoshida and Toyohiko Yano: Microstructure of Heavily Neutron-Irradiated SiC after Annealing up to 1500^{o}C; *J. Nucl. Mater*., Vol. **386-388** (2009) 333-337.

S. Yamazaki, K. Yoshida and T. Yano: Recovery of Neutron-Induced Damage of Si Analyzed by Thermal Expansion Measurement; *J. Nucl. Mater.*, Vol.**386-388** (2009) 328-332.

K. Yoshida, K. Matsukawa and T. Yano: Microstructure and Mechanical Properties of Silicon Carbide Fiber-Reinforced Silicon Carbide Composite Fabricated by Electrophoretic Deposition and Hot-Pressing; *J. Nucl. Mater.*, Vol.**386-388** (2009) 643-646.

K. Yoshida, K. Matsukawa, M. Imai and T. Yano: Formation of Carbon Coating on SiC Fiber for Two Dimensional SiC_f/SiC Composites by Electrophoretic Deposition; *Mater. Sci. Engineer. B*, Vol.**161**, pp.188-192 (2009).

W. Khongwong, M. Imai, K. Yoshida and T. Yano: Synthesis of β-SiC/SiO_2 Core-Shell Nanowires by Simple Thermal Evaporation; *J. Ceram. Soc. Jpn*., Vol.**117**[2], pp.194-197 (2009).

W. Khongwong, M. Imai, K. Yoshida and T. Yano: Influence of Raw Powder Size, Reaction Temperature, and Soaking Time on Synthesis of β-SiC/SiO_2 Core-Shell Nanowires via Thermal Evaporation; *J. Ceram. Soc. Jpn*., **117**[4], pp.439-444 (2009).

Y. Kameshima, A. Nakajima, K. Okada and T. Yano: Preparation of Pt Particles Dispersing Nanocomposites by Thermal Treatment of Tetrachloroplatinate/Layered Double Hydroxide (LDH); *J. Ceram. Soc. Japan*, **117**[11], 1229-1232 (2009).

N. Matsumoto, K. Yoshida, K. Hashimoto and Y. Toda: Preparation of β-Tricalcium Phosphate by Chelete Reaction of Calcium Ion with Phosphonic Acid; *Trans. Mater. Res. Soc. Japan*, **34**[1], 81-84 (2009).

N. Matsumoto, K. Yoshida, K. Hashimoto and Y. Toda: Synthesis and Characterization of Hydroxyapatite Using Polymerized Complex Method by Chelation of Calcium Ions with Organic Phosphonic Acid; *J. Ceram. Soc. Japan,* **117**[3], 249-254 (2009).

K. Yoshida, Y. Fukuhara, K. Hashimoto, Y. Toda, M. Imai and T. Yano: Sinterability and Mechanical Properties of β-Tricalcium Phosphates Doped with Both Na and Mg Ions; *J. Soc. Inorg. Mater., Japan (Muki-Materiaru)*, **16**[340], 165-170 (2009).

H. Hyuga, M. I. Jones, K. Yoshida, N. Kondo, K. Hirao, H. Kita: The Influence of a Solid Lubricant Dispersion on Tribological Behavior of Si_3N_4 Based Composites under Water Lubrication; *J. Ceram. Process. Res*., **10**[3], 367-372 (2009).

H. Hyuga, K. Yoshida, N. Kondo, H. Kita, A. Sugai, H. Okano and J. Tsuchida: Fabrication of Pressureless Sintered Dense Beta-SiAlON via a Reaction-Bonding Route with ZrO_2 Addition; *Ceram. Int.*, **35**[5], 1927-1932 (2009).

W. Khongwong, M. Imai, K. Yoshida and T. Yano: Effect of Reaction Condition on Synthesis of SiC Nanowires by Simple Thermal Evaporation; *Proceeding of the 3rd International Conference on Processing Materials for Properties (PMP III)*, Center for Research and Development in Higher Education, Hokkaido University, Japan, pp. 863-868 (2009).

T. Yano and K. Yoshida: Neutron Irradiation Effects on Various Silica Materials for Optical Applications; *2008 Cooperative Research Activity Report of International Research Center for Nuclear Materials Science*, Institute of Materials Research, Tohoku University, (July, 2009).

T. Yano and K. Yoshida: Ceramic Materials to Sustain Nuclear Fusion Reactors and Its Crtical Issues; *Expected materials for the Future*, **9**[8], 22-32 (2009).

T. Yano: Radiation Damage; in Advanced Silicon Nitride Ceramics, Ed. by Japan Society for Promotion of Science, 124 Committee, Uchida-Rokakuho Publishing, pp.392-400 (2009).

H. Hyuga, N. Kondo, H. Kita, K. Yoshida: Influence of Zr Compounds Addition on NItridation Behavior of Silicon Powder; *Abst. 2009. Ann. Meeting of the Ceram. Soc. Jpn.*, 1E33, pp.28 (2009).

K. Yoshida, C.-C. See, T. Yano, H. Hyuga, H. Kita: Fabrication of Porous Mullite Ceramics with Spinel Addition; *Abst. 2009. Ann. Meeting of the Ceram. Soc. Jpn*., 2E31, pp.108 (2009).

S. Kajikawa, M. Imai, K. Yoshida and T. Yano: Interfacial Control of SiC_f/SiC Composite using Electrophoretic Deposition Method and its Mechanical Properties; *Abst. 2009. Ann. Meeting of the Ceram. Soc. Jpn*., 2P003, pp.161 (2009).

Y. Sekimoto, K. Katayama, T. Wasanapiarnpong, M. Imai, K. Yoshida and T. Yano: Fabrication of Silicon Nitride Ceramics Containing Large Sized Powder to Improve its Thermal Property by Heat-Treatment; *Abst. 2009. Ann. Meeting of the Ceram. Soc. Jpn*., 2P009, pp.164 (2009).

N. Matsumoto, K. Yoshida, K. Hashimoto, Y. Toda: Reaction Behavior of β-Tricalcium Phosphate Doped with Several Monovalent Metal Ions in Simulated Body Fluid; *Abst. 2009. Ann. Meeting of the Ceram. Soc. Jpn.*, 3G01, pp.286 (2009).

H. Shiraishi, N. Matsumoto, K. Yoshida, K. Yoshida, K. Hashimoto, Y. Toda: Preparation and Mechanical Properties of β-Tricalcium Phosphate Ceramics Doped with Vanadate Ions; *Abst. 2009. Ann. Meeting of the Ceram. Soc. Jpn*., 3G02, pp.286 (2009).

R. Miyamoto, T. Oaragaki, A. Ozawa, K. Ohashi, T. Yamada, K. Yoshida, O. Yamamuro, K. Hashimoto, Y. Toda, S. Udagawa, T. Kanazawa: Cellular Response on Na^+ and Mg^{2+} Ions Co-doped β-Tricalcium Phosphate Ceramics; *Abst. 2009. Ann. Meeting of the Ceram. Soc. Jpn.*, 3G25, pp.296 (2009).

H. Yokota, M. Yoshida, H. Ishibashi, T. Yano, H. Yamamoto and S. Kikkawa: Investigation of the Site Occupancy of Ce ions in Y_2SiO_5:Ce blue Phosphor; *Abst. 26th Annual Meeting on the Rare Earth Elements*. (2009).

Y. Ikeda, N. Matumoto, K. Yoshida, K. Hashimoto, Y. Toda, S. Udagawa, T. Kanazawa: Effect of Substituting Monovalent Metal Ion with β-Tricalcium Phosphate on Bioadsorbability; *Abst. The 118th Academic Conference of The Society of Inorganic Materials*, (13), pp.26-27 (2009).

D. Sasaki, Y. Ikeda, N. Matumoto, K. Yoshida, K. Hashimoto, Y. Toda, S. Udagawa, T. Kanazawa: Effect of Electrophoretic Condition on Properties of Aluminum Anodic Oxide Film Impregnated with Iodine; *Abst. The 118th Academic Conference of The Society of Inorganic Materials*, (17) pp.34-35 (2009).

R. Miyamoto, K. Ohashi, A. Ozawa, K. Yoshida, K. Hashimoto, Y. Toda, S. Udagawa, T. Kanazawa: Cellular Evaluation of ST2 / C7 Cells Co-Culture on Bioelectrolyte Ion Doped β-Tricalcium Phosphate; *Abst. The 118th Academic Conference of The Society of Inorganic Materials*, (25) pp.50-51(2009).

K. Ohashi, R. Miyamoto, A. Ozawa, K. Yoshida, K. Hashimoto, Y. Toda, S. Udagawa, T. Kanazawa: Evaluation of Cellular Response and Characterization of V^{3+} Ion Doped β-Tricalcium Phosphate Ceramics; *Abst. The 118th Academic Conference of The Society of Inorganic Materials*, (26) pp.52-53 (2009).

A. Ozawa, R. Miyamoto, K. Yoshida, K. Hashimoto, Y. Toda, S. Udagawa, T. Kanazawa: Evaluation of Mechanical property and Dissolution Ca^{2+} Ion on Mn^{2+} Ion Doped β-Tricalcium Phosphate Ceramics; *Abst. The 118th Academic Conference of The Society of Inorganic Materials,* (27) pp.54-55 (2009).

W. Khongwong, K. Yoshida, M. Imai and T. Yano: Preparation of SiC/SiO_2 Composite Nanowires through Evaporation of Si Solid Reactants and Their Oxygen Resistance; *3rd International Conference on Science and Technology for Advanced Ceramics*, (2009).

K. Yoshida, H. Hyuga, N. Kondo, H. Kita: Synthesis of Precursor for Fibrous Mullite Powder by Alkoxide Hydrolysis Method; *3rd International Conference on Science and Technology for Advanced Ceramics*, June 17, (2009).

K. Yoshida, T. Yano, H. Hyuga and H. Kita: Sintering Behavior of Mullite Ceramics with Spinel Addition and Their Microstructural Change with Sintering Temperature; *The International Conference and Exhibition on Materials and AustCeram 2009*, (2009).

K Yoshida, S Kajikawa, M Imai and T Yano: Microstructural Control of Two Dimensional SiC Fiber-Reinforced SiC Composites for Improvement of Their Thermal Conductivity; *17th International Conference on Composites or Nano Engineering*, (2009).

W. Khongwong, K. Yoshida, M. Imai and T. Yano: A Simplified Method for Synthesis of SiC/SiO_2 Core-Shell Nanowires; *Abst 2009 Annual Meeting of the Ceramic Society of Japan*, 2P015, pp.167, (2009).

T. Yano, J. Yamane, K. Yoshida**,** S. Miwa and M. Ohsaka: Low temperature liquid-phase-assisted sintering of Si_3N_4 ceramics as an inert matrix for confinement of minor actinides"; *Abst. Actinides 2009*, 4P33, pp.370-371, San Francisco USA, (2009).

T. Yano, T. Yamagami, K. Yoshida and M. Akiyoshi: Neutron-Irradiation-Induced Crystalline Defects in β-Silicon Nitride and Their Thermal Stability; *Abst. 14th International Conference on Fusion Reactor Materials,* 5A-O-1, (2009).

K. Yoshida, S. Kajikawa, M. Imai and T. Yano: Interfacial Control of Two-Dimensional SiC Fiber-Reinforced SiC Composites by Electrophoretic Deposition Method and Polycarbosilane Impregnation"; *Abst. 14th International Conference on Fusion Reactor Materials*, P3-041, (2009).

T. Sawabe, K. Yoshida and T. Yano: Change in XRD peak-shift of 3C-SiC due to Neutron Irradiation and Post-Irradiation Isochronal Annealing; *Abst. 14th International Conference on Fusion Reactor Materials*, P2-109, (2009).

S. Yamazaki, K. Yoshida and T. Yano: Comparative Experimental Study on Recovery Behavior of Point Defects in Neutron-Irradiated SiC; *Abst. 14th International Conference on Fusion Reactor Materials*, P2-108, (2009).

N. Matsumoto, Y. Ikeda, K. Yoshida, K. Hashimoto, Y. Toda: Dissolution Behavior of Beta-Tricalcium Phosphate Doped with Monovalent Metal Ions in Acetic Acid Buffer; *Abst. 8th Pacific Rim Conference on Ceramic and Glass Technology (PacRim 8),* June 2, 2009, Vancouver, Canada, PACRIM8-S21-P169-2009.

R. Miyamoto, T. Yamada, K. Yoshida, O. Yamamuro, K. Hashimoto, Y. Toda: Cellular Response on Sodium and Magnesium Ions-Codoped Beta-Tricalcium Phosphate Ceramics; *Abst. 8th Pacific Rim Conference on Ceramic and Glass Technology (PacRim 8)*, June 2, 2009, Vancouver, Canada, PACRIM8-S20-P165-2009.

N. Matsumoto, K. Yoshida, Kazuaki Hashimoto, Yoshitomo Toda: Preparation and Antibacterial Mechanism of β-Tricalcium Phosphate Doped with Antibacterial Metal Ions; *3rd International Conference on Science and Technology for Advanced Ceramics (STAC3)*, June 17, 2009, Yokohama, Japan, 17pP079.

N. Matsumoto, K. Hashimoto, Y. Toda, K. Yoshida: Preparation and Mechanical Properties of β-TCP Ceramics Doped with Vanadate Ions; *The 22nd International Symposium on Ceramics in Medicine*, October 27, 2009, Daegu, Korea, P001.

N. Matsumoto, K. Yoshida, K. Hashimoto, Y. Toda: Fabrication of Porous β-Tricalcium Phosphate Ceramics using Precursor Prepared by Polymerized Complex

Method; *Special Symposium for Celebration on the 10th Anniversary of the Division of Ceramics in Medicine, Biology and Biomimetics, The Ceramic Society of Japan in conjunction with 9th Asian BioCeramics Symposium* (ABC2009), December 9, 2009, Nagoya, Japan, P-12.

R. Miyamoto, T. Yamada, K. Yoshida, O. Yamamuro, K. Hashimoto, Y. Toda: ST2/C7 Cells Behavior on Bioelectrolyte Ions Co-Doped β-Tricalcium Phosphate Ceramics; *Special Symposium for Celebration on the 10th Anniversary of the Division of Ceramics in Medicine, Biology and Biomimetics, The Ceramic Society of Japan in conjunction with 9th Asian BioCeramics Symposium* (ABC2009), December 10, 2009, Nagoya, Japan, P-31.

K. Ohashi, R. Miyamoto, K. Yoshida, K.Hashimoto, Y. Toda: Cellular Evaluation of MC3T3-E1 Cells on VO_4^{3-} Ions Doped β-Tricalcium Phosphate Ceramics; *Special Symposium for Celebration on the 10th Anniversary of the Division of Ceramics in Medicine, Biology and Biomimetics, The Ceramic Society of Japan in conjunction with 9th Asian BioCeramics Symposium* (ABC2009), December 10, 2009, Nagoya, Japan, P-33.

A. Ozawa, R. Miyamoto, K. Yoshida, K. Hashimoto, Y. Toda: Cellular Evaluation of C7 Cells on Mn^{2+} Ion Doped β-Tricalcium Phosphate Ceramics; *Special Symposium for Celebration on the 10th Anniversary of the Division of Ceramics in Medicine, Biology and Biomimetics, The Ceramic Society of Japan in conjunction with 9th Asian BioCeramics Symposium (ABC2009),* December 10, 2009, Nagoya, Japan, P-53.

C.-C. See, K. Yoshida, T. Yano and M. Imai: Influence of the Form of Aluminium System Additives on Grain Growth of Silicon Carbide Ceramics; *Abst. 22nd Fall Meeting of the Ceramic Society of Japan*, pp.315, 2M05, (2009).

W. Khongwong, K. Yoshida and T. Yano: Low-Cost Production and Characterization of SiC Nanowires; *Abst. 22nd Fall Meeting of the Ceramic Society of Japan*, pp.311, 1M26, (2009).

J. Koo, K. Yoshida and T. Yano: Prerssureless Sintering of Micron-Sized Beta-Silicon Carbide with Homogeneous Particle Size Distribution; *Abst. 22nd Fall Meeting of the Ceramic Society of Japan*, pp.324, 1PM03, (2009).

N. Matsumoto, A. Yokokawa, K. Yoshida, K. Hashimoto, Y. Toda: Preparation and Material Science Evaluation of β-Tricalcium Phosphate Doped with Vanadate Ions; *Abst. 22nd Fall Meeting of the Ceramic Society of Japan*, pp.65, 3B02, (2009).

K. Yoshida, H. Hyuga, N. Kondo, H. Kita: Formation Mechanism of Fibrous Mullite Precursor by Alkoxide Hydrolysis Method and Its Morphological Change with Heat-Treatment; *Abst. 22nd Fall Meeting of the Ceramic Society of Japan*, pp. 312, 1M28, (2009).

N. Matsumoto, D. Saito, K. Yoshida, K. Hashimoto, Y. Toda, S. Udagawa, T. Kanazawa: Preparation of Porous β-Tricalcium Phosphate Ceramics Using Calcium Phosphate Precursors by Polymerized Complex Method; *Abst. The 119th Academic Conference of The Society of Inorganic Materials*, pp.28-29, (14), (2009).

K. Sato, N. Matsumoto, K. Yoshida, K. Hashimoto, Y. Toda, S. Udagawa, T. Kanazawa: Characterization of β-Tricalcium Phosphate Co-Doped with Divalent Metal and Silicate Ions; *Abst. The 119th Academic Conference of The Society of Inorganic Materials*, pp.70-71, (35), (2009).

A. Katayama, N. Matsumoto, K. Yoshida, K. Hashimoto, Y. Toda, S. Udagawa, T. Kanazawa: *In vitro* Bioadsobability of β-Tricalcium Phosphate Co-Doped with Monovalent and Divalent Metal Ions; *Abst. The 119th Academic Conference of The Society of Inorganic Materials*, pp.72-73, (36), (2009).

Y. Ikeda, N. Matumoto, K. Yoshida, K. Hashimoto, Y. Toda, S. Udagawa, T. Kanazawa: Effect of Substituting Metal Ions Doped into β-Tricalcium Phosphate on *in vitro* Bioabsorbability; *Abst. The 119th Academic Conference of The Society of Inorganic Materials,* pp.76-77, (38), (2009).

A. Ozawa, R. Miyamoto, K. Yoshida, K. Hashimoto, Y. Toda, T. Kanazawa: Behavior of Osteoclast Cells on Manganese(II) Ion-Doped β-Tricalcium Phosphate Ceramics; *Abst. 19th Meeting of Japanese Association of Inorganic Phosphorus Chemistry*, Tokyo, Japan, pp.6-7, (1), (2009).

R. Miyamoto, T. Yamada, K. Yoshida, O. Yamamuro, K. Hashimoto, Y. Toda, T. Kanazawa: Evaluation of ST2/C7 Cells on Bioelectrolyte Doped β-Tricalcium Phosphate Ceramics; *Abst. 19th Meeting of Japanese Association of Inorganic Phosphorus Chemistry*, pp.8-9, (2), (2009).

N. Matsumoto, K. Yoshida, K. Hashimoto, Y. Toda: Effect of Vanadate Ions on Mechanical Properties of β-Tricalcium Phosphate Ceramics; *19th Meeting of Japanese Association of Inorganic Phosphorus Chemistry*, pp.28-29, (12), (2009).

K. Yoshida, H. Hyuga, N. Kondo, H. Kita: Improvement of Oxidation Resitance of Graphite Powder by Its Surface Treatment with Phosphate; *Abst. 19th Meeting of Japanese Association of Inorganic Phosphorus Chemistry*, pp.80-81, (37), (2009).

K. Ohashi, R. Miyamoto, K. Yoshida, K. Hashimoto, Y. Toda: Cellular Evaluation of MC3T3-E1 Cells on VO_4^{3-}

Ions Doped β-Tricalcium Phosphate; *Abst. The 32th Annual Meeting of the Japanese Society for Biomaterials*, pp.175, (2C14), (2009).

A. Ozawa, R. Miyamoto, K. Yoshida, K. Hashimoto, Y. Toda: Evaluation of Bone Absorption Ability on Bioessential Transition Metal Ion Doped β-Tricalcium Phosphate Ceramics; *Abst. The 32th Annual Meeting of the Japanese Society for Biomaterials*, pp.176, (2C15), (2009).

R. Miyamoto, K. Yoshida, K. Hashimoto, Y. Toda: Cellular Evaluation of ST2/C7 Cells on Monovalent and Divalent Ion Bioelectrolyte Ions Doped β-Tricalcium Phosphate Ceramics; *Abst. The 32th Annual Meeting of the Japanese Society for Biomaterials*, pp.176, (2C15), (2009).

H. Yokota, M. Yoshida, H. Ishibashi, H. Yamamoto, T. Yano and S. Kikkawa: Degradation Properties of Ce-Doped Gd_2SiO_5 Phoapher under Continuous Electron Beam Irradiation; *Abst. 22nd Fall Meeting of the Ceramic Society of Japan*, pp.349, 1O03, (2009).

W. Khongwong, M. Imai, K. Yoshida and T. Yano: Effect of Reaction Condition on Synthesis of SiC Nanowires by Simple Thermal Evaporation; *Abst. 3rd International Conference on Processing Materials for Properties*, IV-1, pp.16, (2009).

R. Miyamoto, T. Yamada, K. Yoshida, O. Yamamuro, K. Hashimoto, Y. Toda: ST2/C7 Cells Behavior on Bioelectronic Ions Co-Doped β-Tricalcium Phosphate Ceramics; *Archives of BioCeramics Research*, Vol. **9**, pp.291-294, (2009).

K. Ohashi, R. Miyamoto, K. Yoshida, K. Hashimoto, Y. Toda, S. Udagawa, T. Kanazawa: Cellular evaluation of MC3T3-E1 cells on VO_4^{3-} Ions Doped β-Tricalcium Phosphate Ceramics; *Archives of BioCeramics Research,* Vol. **9**, pp.299-302, (2009).

A. Ozawa, R. Miyamoto, K. Yoshida, K. Hashimoto, Y. Toda: Cellular Evaluation of C7 Cells on Mn^{2+} Ion Doped β-Tricalcium Phosphate Ceramics; *Archives of BioCeramics Research*, Vol. **9**, pp.375-378, (2009).

K. Yoshida, T. Yano, K. Hashimoto, Y. Toda: Fracture Behavear of Microstructural Controlled Hydroxyapatite-Zirconia Composites; *Abst. 119th Annual Meeting of Society for Inorganic Materials*, pp.33 (2009).

S. Miwa, M. Osaka, T. Ukai and T. Yano: Densification of Inert Matrix Fuels Using Naturally-Occurring Material as a Sintering Additive; *Abst. MRS Fall Meeting 2009*, (2009).

S. Miwa, M. Osaka, Y. Akutsu, T. Yano, K. Kurosaki, S. Yamanaka, S. Takano and Y. Yamane: Inert Matrix Fuel Concept for the Rapid Incineration of Minor Actinides Harmonious with a Fast Reactor Cycle System; *International Conference on Fast Reactors and Related Fuel Cycles*, IAEA-Cn-176-07-13P, (2009).

Takeshi Sakurai, Takamasa Mori, Shigeaki Okajima, Kazuhiro Tani, Takenori Suzaki and Masaki Saito: Measurement and Analysis of Reactivity Worth of ^{237}Np Sample in Cores of TCA and FCA; J. Nucl. Sci. Technol. Vol. **46**, No. 6, p. 624-640 (2009).

H. Sagara, T. Yamamoto, *et. al*,: Numerical Analysis of Am sample irradiation in experimental fast reactor Joyo; *ACTINIDES 2009*, San Francisco, July (2009).

Masaki Saito: Protected Plutonium Production (P^3) by Transmutation of Minor Actinides for Peace and Sustainable Prosperity; *2nd JAPAN-IAEA Workshop on Advanced Safeguard Technology for the Future Nuclear Fuel Cycle*, Nov. 10-13, 2009, Tokai-mura, (2009).

Sidik Permana, Mitsutoshi Suzuki and Masaki Saito: Core Performance and Isotopic Plutonium Vector Analysis in MA doped FaCT FBR; *Int. Conf. Fast Reactors Related Fuel Cycles: Challenges Opportunities (FR09)*, 7-11 Dec., 2009, Kyoto, Japan (2009).

Masaki Saito: Protected Plutonium Production (P^3) by Transmutation of Minor Actinides for Peace and Sustainable Prosperity; *Int. Conf. Fast Reactors Related Fuel Cycles: Challenges Opportunities (FR09)*, 7-11 Dec., 2009, Kyoto, Japan (2009).

S. Koyama, M. Itoh, H. Sagara and M. Saito: Protected Plutonium Production by Transmutation of Minor Actinides for Peace and Sustainable Prosperity - Irradiation Tests of Np and Np-U Samples in Experimental Fast Reactor JOYO (JAEA) and Advanced Thermal Reactor ATR (INL) -; *proc GLOBAL 2009*, 9410, p. 2356-2362 (2009).

M.Saito: Protected Plutonium Production by Transmutation of Minor Actinides for Peace and Sustainable Prosperity -Fundamentals of P3 Mechanism and Methodology Development for Plutonium Categorization-; *proc. GLOBAL 2009*, 9397, p.2363-2368 (2009).

E. Hamase, M. Saito and H. Sagara: Effects of MA doping in Fast Breeder Reactor; *proc. GLOBAL 2009,* 9063, p. 2318-2324 (2009).

Y. Meiliza, M. Saito and H. Sagara: Pu Denaturing by Transmutation of MA in FBR Multi-cycle; *proc. GLOBAL 2009,* 9062, p. 2325-2332 (2009).

Sidik Permana, Zaki Suud, Masaki Saito and Mitsutoshi Suzuki: Trans-Uranium Doping Utilization for Increasing

Protected Plutonium Proliferation of Small Long Life Reactor; *proc. GLOBAL 2009,* 9473, p. 2381-2388 (2009).

H. Sagara, T. Yamamoto, S. Koyama S. Maeda, T. Shiba,and M. Saito: Am-241 Irradiation Analysis in Experimental Fast Reactor Joyo; *Trans. Am. Nucl. Soc. Winter Mtg. 2009*, *(ISSN: 0003-018X*), vol. 101, p.765-766 (2009).

Ismailov Kairat, Nishihara Kenji, Sasa Toshinobu and Saito Masaki: Neutronic Benchmarking of Transmutation by Adiabatic Resonance Crossing Experiment; *Trans. Am. Nucl. Soc. Winter Mtg. 2009*, *(ISSN: 0003-018X*), vol. **101,** p.10-11 (2009).

H. Sagara and G. S. Chang: ATR 2A/2B As-Run Neutronics Uncertainty Analysis; *INL/EXT-09-17197, Prepared for U.S. Department of Energy Transmutation Fuels Campaign* (2009).

Y. Ikeda, K. Hiroe, N. Asanuma, M. Nogami, and A. Shirai: Electrochemical Studies on Uranyl(VI) Chloride Complexes in Ionic Liquid, 1-Butyl-3- methylimidazolium Chloride; *J. Nucl. Sci. Technol*., **46**, 158-162 (2009).

K. Takao, T. Takahashi, and Y. Ikeda: Complex Formation of Uranyl Ion with Triphenylphosphine Oxide and Its Ligand Exchange Reaction in 1-Butyl-3-methylimidazolium Nonafluorobutanesulfonate Ionic Liquid; *Inorg. Chem*., **48**, 1744-1752 (2009).

N. Koshino, Y. Kachi, T.R. Varga, A.C. Benyei, M. Shiro, K. Takao, and Y. Ikeda: Structures of of Homoleptic Eight- and Nine-coordinate Uranium(IV) Perchlorate Complexes with Sulfoxide Molecules as Ligands; *Inorg. Chim. Acta*, **362**, 3433-3439 (2009).

Y. Ohashi, N. Asanuma, M. Harada, Y. Wada, T. Matsubara, and Y. Ikeda: Application of Ionic Liquid as a Medium for Treating Wastes Contaminated with UF_4; *J. Nucl. Sci. Technol*., **46**, 771-775 (2009).

Y. Takahashi, H. Hotokezaka, K. Noda, M. Nogami, and Y. Ikeda: Extraction of Uranium(VI) from Nitric Acid Solution Using Pyrrolidone Derivatives; *J. Nucl. Sci. Technol*., **46**, 787-792 (2009).

I.A. Zaafarany, K.S. Khairou, R.M. Hassan, and Y. Ikeda: Physicochemical Studies on Cross-linked Thorium(IV)-Alginate Complex Especially the Electrical Conductivity and Chemical Equilibrium Related to the Coordination Geometry; *Arabian J. Chem*., **2**, 1-10 (2009).

K. Takao, K. Noda, M. Nogami, Y. Sugiyama, M. Harada, Y. Morita, K. Nishimura, and Y. Ikeda: Solubility of Uranyl Nitrate Precipitates with *N*-Alkyl-2-pyrrolidone Derivatives (Alkyl = *n*-Propyl, *n*-Butyl, *iso*-Nutyl, and Cyclohexyl); *J. Nucl. Sci. Technol*., **46**, 995-999 (2009).

K. Takao, S. Tsushima, S. Takao, A.C. Scheinost, G. Bernhard, Y. Ikeda, and C. Hennig: X-ray Absorption Fine Structures of Uranyl(V) Complexes in Non-aqueous Solutions; *Inorg. Chem.*,**48**, 9602-9604 (2009).

Y. Takahashi and Y. Ikeda: *trans*-Bis(*N*-cycrohexyl-2-pyrrolidone)dinitrato-palladium(II); *Acta Cryst*. **E65**, m1533-m1534 (2009).

Y. Morita, K. Takao, S.-Y. Kim, Y. Kawata, M. Harada, M. Nogami, K. Nishimura, and Y. Ikeda: Development of Advanced Reprocessing System Based on Precipitation Method Using Pyrrolidone Derivatives as Precipitants -Precipitation Behavior of U(VI), Pu(IV), and Pu(VI) by Pyrrolidone Derivatives with Low Hydrophobicity-; *J. Nucl. Sci. Technol*., **46**, 1129-1136 (2009).

Y. Tachibana, M. Nogami, Y. Sugiyama, and Y. Ikeda: Kinetic and Mechanistic Studies on Decomposition Reactions of Pyrrolidone Derivatives using O_3; *World Congress on Ozone & Ultraviolet Technologies*, Boston, Massachusetts, USA, May 4-5, 2009.

S-Y. Kim, N. Ohta, Y. Morita, N. Asanuma, K. Takao, and Y. Ikeda: Electrochemical Studies of Uranyl Nitrate Complexes in 1-Alkyl-3- methylimidazolium Nitrate Ionic Liquids; *Actinides 2009*, San Fransisco, USA, July 12-17, 2009.

K. Takao, M. Kato, S. Takao, A. Nagasawa, A.C. Scheinost, G. Bernhard, C. Hennig, and Y. Ikeda: Structural and Electrochemical Studies on Uranyl(VI) Complexes with Pentadentate Schiff Base Ligand: A Guide to Stable Uranyl(V); *Actinides 2009*, San Fransisco, USA, July 12-17, 2009.

K. Takao, S. Tsushima, S. Takao, A.C. Scheinost, G. Bernhard, Y. Ikeda, and C. Hennig: X-ray Absorption Fine Structures of Uranyl(V) Complexes in Non-aqueous Solutions; *Actinides 2009*, San Fransisco, USA, July 12-17, 2009.

Y. Morita, S.-Y. Kim, Y. Kawata, Y. Ikeda, and T. Kikuchi: Development of Advanced Reprocessing System Using Highly Selective and Controllable Precipitansts -Precipitation Behavior of Plutonium from U-Pu Solution-; *Global 2009*, Paris, France, September 6-11, 2009.

Y. Takahashi, M. Nogami, H. Hotokezaka, and Y. Ikeda: Extraction of Uranium(VI), Pd(II), and Re(VII) from Nitric Acid Solutions Using Pyrrolidone Derivatives; *12th International Conference on the Chemistry and Migration Behavior of Actinides and Fission Products in the Geosphere*, Migration 2009, Kennewick, USA, September 20-25, 2009.

Y. Ikeda: An Overview on Studies of Structures and Reactivities of Uranyl(V) Complexes; *12th International*

Conference on the Chemistry and Migration Behavior of Actinides and Fission Products in the Geosphere, Migration 2009, Kennewick, USA, Septembeer 20-25, 2009.

Y. Takahashi, N. Asanuma, Y. Ohashi, and Y. Ikeda: Extraction Behavior of Uranyl Ions by *N*-dodecyl-2-pyrrolidone Using Ionic Liquids as Extraction Media; *The 6th Reprocessing Recycle Seminar* (2009).

Y. Sano, K. Ishino, N. Asanuma, and Y. Ikeda: Redox Behavior of Metallocene in BMINfO; *The 6th Reprocessing Recycle Seminar* (2009).

K. Nagase, M. Ozaki, N. Asanuma, Y. Ohashi, and Y. Ikeda: A Study on Dissolution of Steel Materials in Choline Chloride-Urea Eutectic Mixture; *The 6th Reprocessing Recycle Seminar* (2009).

Y. Kawata, Y. Kim, M. Sato, Y. Morita, Y. Ikeda, and T. Kikuchi: Development of Advanced Reprocessing System Using Precipitants with High Selectivity and Control Ability (12) Precipitation experiments using spent nuclear fuels; *The Annual Meeting of the Atomic Energy Society of Japan* (2009).

T. Shibahara, M. Osada, T. Chikazawa, T. Kikuchi, Y. Morita, and Y. Ikeda: Development of Advanced Reprocessing System Using Precipitants with High Selectivity and Control Ability (13) Examination of thermal decomposition of U(VI)-pyrrolidone compounds and its application to the fuel preparation; *The Annual Meeting of the Atomic Energy Society of Japan* (2009).

T. Kawasaki, M. Nogami, Y. Sugiyama, M. Harada, Y. Ikeda Y. Morita, and T. KikuchiY. Ikeda, and K. Nishimura,: Development of Advanced Reprocessing System Using Precipitants with High Selectivity and Control Ability (14) Recycling of pyrrolidone derivatives of thermal decomposition of precipitates; *The Annual Meeting of the Atomic Energy Society of Japan* (2009).

Y, Sugiyama, M. Nogami, T. Kawasaki, M. Harada, Y. Ikeda, Y. Morita, and T. Kikuchi: Development of Advanced Reprocessing System Using Precipitants with High Selectivity and Control Ability (15) A study on adsorption and desorption behavior of polyvinylpolypyrrolidone; *The Annual Meeting of the Atomic Energy Society of Japan* (2009).

Y. Takahashi, H. Hotokexaka, M. Nogami, and Y. Ikeda: Extraction Behavior of Pd(II) and Re(VII) Ions in the extraction of uranyl ions using pyrrolidone derivatives as the extractant; *The Annual Meeting of the Atomic Energy Society of Japan* (2009).

Y. Takahashi, N. Asanuma, and Y. Ikeda: A Study on Extracted Species in Extraction of Uranyl Ions Using BMINfO as Extraction Media; *The Annual Meeting of the Atomic Energy Society of Japan* (2009).

Y. Takahashi, N. Asanuma, and Y. Ikeda: Mechanism for the Extraction of Uranyl Ions Using BMINfO Containing NDP; *The Fall Meeting of the Atomic Energy Society of Japan* (2009).

M. Nogami, Y. Sugiyama, T. Kawasaki, M. Harada, Y. Ikeda, Y. Morita, and T. Kikuchi: Development of Advanced Reprocessing System Using Precipitants with High Selectivity and Control Ability (16) Examination of Durability of NBP as Low Hydrophobic Precipitant; *The Fall Meeting of the Atomic Energy Society of Japan* (2009).

M. Harada, M. Nogami, Y. Sugiyama, T. Kawasaki, Y. Ikeda, Y. Morita, and T. Kikuchi: Development of Advanced Reprocessing System Using Precipitants with High Selectivity and Control Ability (17) Examination of masking effect; *The Fall Meeting of the Atomic Energy Society of Japan* (2009).

Y. Takahashi, M. Nogami, Y. Ikeda, and H. Hotokezaka: A Study on Extraction of U(VI) Using Pyrrolidone Derivatives as Extractants in Microchemical Chip Method; *The Fall Meeting of the Atomic Energy Society of Japan* (2009).

N. Miyamoto, T. Tsukahara, Y. Kachi, M. Harada, K. Yoshino, and Y. Ikeda: Effect of Solute-solvent Interactions on Solubility of Metal Complexes with Hexafluoroacetylacetonate into Supercritical CO_2; *The 59th Symposium of Coordination Chemistry of Japan* (2009).

A. Canlier, T. Kawasaki, S. Chowdhury, and Y. Ikeda; Structural and Electrochemical Studies on trans-Dioxorhenium(V) Complexes with Pyridine Derivatives; *The 59th Symposium of Coordination Chemistry of Japan* (2009).

Y. Sato, Y. Takahashi, T. Arai, and Y. Ikeda: Studies on Structure and Reactivity of Uranyl Nitrate Complexes with Pyrrolidone Derivatives as Extractant; The 31st Solution Chemistry Symposium (2009).

S. Watanabe, Y. Iida, N. Suzui, T. Katabuchi, S. Ishii, N. Kawachi, H. Hanaoka, S. Watanabe, S. Matsuhashi, K. Endo, N. Ishioka: Production of No-Carrier-Added ^{64}Cu and Applications to Molecular Imaging by PET and PETIS as a Biomedical Tracer; *Journal of Radioanalytical and Nuclear Chemistry*, **280**, pp. 199-205 (2009).

C. Guerrero, and 114 authors arranged in alphabetical order (The total number of authors is 115. M. Igashira is 46th author.): The n_TOF total absorption calorimeter for neutron capture measurement at CERN; *Nucler*

Instruments and Methods, **A608**, 424-433 (2009).

M.Calviani, J. Praena, and 120 authors in alphabetical order (The total number of authors is 122. M. Igashira is 51st aushor.): High-accuracy 233U(n,f) cross-section measurement at the white-neutron source n_TOF from near-thermal to 1 MeV neutron energy; *Physical Review*, **C 80,** 044604-1-11 (2009).

H. Makii, Y. Nagai, T. Shima, K. Mishima, H. Ueda, M. Igashira, T. Ohsaki: E1 and E2 cross sections of the $^{12}C(\alpha,\gamma 0)^{16}O$ reaction using pulsed alpha beams; *Physical Review*, **C 80**, pp. 065802-1-16 (2009).

T. Wang, M. Lee, G. Kim, Y. Oh, W. Namkung, TI. Ro, YR. Kang, M. Igashira, T. Katabuchi: Measurement of keV-Neutron Capture Cross-Sections and Capture Gamma-Ray Spectra of ^{56}Fe and ^{57}Fe; *Nuclear Instruments and Methods in Physics Research*, **B268,** 440-449 (2010).

K. Kino, F. Hiraga, M. Furusaka, Y. Kiyanagi, M. Igashira, M. Mizumoto, T. Katabuchi: Design of a Collimator System of a Neutron Beam Line for Neutron-Nucleus Reaction Measurements; *Proc 11th International Conference on Radiation Shielding and the 15th Topical Meeting of the Radiation Protection and Shielding* Division, Callaway Gardens, USA, 2008, ed. R. M. Howell and N. E. Hertel, Nuclear Technology, **168**, pp. 317-321 (2009).

K. Kino, T. Kamiyama, Y. Kiyanagi, F. Hiraga, M. Furusaka, M. Ohta, M. Oshima, F. Kitatani, A. Kimura, T. Kin, M. Koizumi, S. Goko, Y. Toh, S. Nakamura, H. Harada, K. Furutaka, M. Igashira, T. Katabuchi, M. Mizumoto: Measurement of spatial and energy distributions and pulse shape of neutron beam at J-PARC/MLF BL04; *2009 Fall Meeting of the Atomic Energy Society of Japan*, pp. 438 (2009).

M. Mizumoto, M. Igashira, T. Katabuchi, J. Hori, K. Kino, Y. Kiyanagi, T. Kamiyama, F. Hiraga, M. Furusaka, A. Kimura, Y. Toh, S. Nakamura, S. Goko, T. Kin, M. Ohta, F. Kitatani, K. Furutaka, M. Koizumi, H. Harada, M. Oshima: The characteristic experiments of neutron flux and neutron and gamma-ray fields with gamma-ray detectors at the BL04 of J-PARC MLF; *2009 Fall Meeting of the Atomic Energy Society of Japan*, pp. 464 (2009).

M. Ohta, M. Oshima, F. Kitatani, A. Kimura, T. Kin, M. Koizumi, S. Goko, Y. Toh, S. Nakamura, H. Harada, K. Furutaka, M. Igashira, T. Katabuchi, M. Mizumoto, T. Kamiyama, K. Kino, Y. Kiyanagi, F. Hiraga, M. Furusaka: Measurement of Neutron Spectrum at BL04 of J-PARC/MLF; *2009 Fall Meeting of the Atomic Energy Society of Japan*, pp. 465 (2009).

T. Katabuchi, M. Mizumoto, M. Igashira, A. Kimura, Y. Toh, S. Nakamura, S. Goko, T. Kin, M. Ohta, F. Kitatani, K. Furutaka, M. Koizumi, H. Harada, M. Oshima, J. Hori, K. Kino, T. Kamiyama, F. Hiraga, M. Furusaka, Y. Kiyanagi: Neutron capture gamma-ray measurement with NaI(Tl) detector at BL04 of J-PARC/MLF; *2009 Fall Meeting of the Atomic Energy Society of Japan*, pp. 466 (2009).

A. Kimura, M. Oshima, M. Ohta, F. Kitatani, T. Kin, M. Koizumi, S. Goko, Y. Toh, S. Nakamura, H. Harada, K. Furutaka, M. Igashira, T. Katabuchi, M. Mizumoto, T. Kamiyama, K. Kino, Y. Kiyanagi: Test experiment for neutron capture cross section measurement with a Ge detector; *2009 Fall Meeting of the Atomic Energy Society of Japan*, pp. 467 (2009).

S. Goko, M. Oshima, F. Kitatani, A. Kimura, T. Kin, M. Koizumi, Y. Toh, S. Nakamura, H. Harada, K. Furutaka, M. Igashira, T. Katabuchi, M. Mizumoto, J. Hori: Measurement of neutron capture reaction for ^{238}U at KURRI LINAC; *2009 Fall Meeting of the Atomic Energy Society of Japan*, pp. 468 (2009).

S. Kamada, M. Igashira, T. Katabuchi, M. Mizumoto: Measurement of neutron capture cross sections and capture gamma-ray spectra of Se-74, 76 at 550 keV; *2009 Fall Meeting of the Atomic Energy Society of Japan*, pp. 469 (2009).

T. Kobayashi, T. Hattori, N. Hayashizaki, M. Takahashi, T. Katabuchi: Boron neutron capture Therapy using neutrons produced by proton accelerators; *2009 Fall Meeting of the Atomic Energy Society of Japan*, pp.937-940 (2009).

H. Harada, K. Furutaka, S. Goko, A. Kimura, T. Kin, F. Kitatani, M. Koizumi, S. Nakamura, M. Ohta, M. Oshima, Y. Toh, M. Igashira, T. Katabuchi, M. Mizumoto, M. Furusaka, F. Hiraga, T. Kamiyama, K. Kino, Y. Kiyanagi, T. Fujii, J. Hori, K. Takamiya: Measurements of Neutron Capture Cross Sections using a 4□Ge Spectrometer at the J-PARC/MLF/NNRI; *Third Joint Meeting of the Nuclear Physics Divisions of the APS and JPS, Bulletin of American Physical Society*, 54, p.190 (2009).

T. Katabuchi, M. Igashira, M. Mizumoto, K. Furutaka, S. Goko, H. Harada, A. Kimura, T. Kin, F. Kitatani, M. Koizumi, S. Nakamura, M. Ohta, M. Oshima, Y. Toh, M. Furusaka, F. Hiraga, T. Kamiyama, Koich Kino, Y. Kiyanagi, T. Fujii, J. Hori, K. Takamiya: Measurements of Neutron Capture Cross Sections Using a NaI(Tl) Spectrometer at the J-PARC MLF Neutron Nucleus Reaction Instrument; *Third Joint Meeting of the Nuclear Physics Divisions of the APS and JPS, Bulletin of American Physical Society*, 54, p. 190 (2009).

K. Kino, M. Furusaka, F. Hiraga, T. Kamiyama, Y. Kiyanagi, K. Furutaka, S. Goko, H. Harada, A. Kimura, T. Kin, F. Kitatani, M. Koizumi, S. Nakamura, M. Ohta, M. Oshima, Y. Toh, M. Igashira, T. Katabuchi, M. Mizumoto, T. Fujii, J. Hori, K. Takamiya, Neutron Beam Provided by

the Neutron Nucleus Reaction Instrument at the J-PARC MLF; *Third Joint Meeting of the Nuclear Physics Divisions of the APS and JPS, Bulletin of American Physical Society*, 54, p. 190 (2009).

K. Kino, T. Kamiyama, Y. Kiyanagi, F. Hiraga, M. Furusaka, M. Ohta, M. Oshima, F. Kitatani, A. Kimura, T. Kin, M. Koizumi, S. Goko, Y. Toh, S. Nakamura, H. Harada, K. Furutaka, M. Igashira, T. Katabuchi, M. Mizumoto: Study on nuclear data by using a high intensity pulsed neutron source for advanced nuclear system (2) J-PARC beam line for capture cross-section; *2010 Annual Meeting of the Atomic Energy Society of Japan*, pp. 93 (2010).

M. Oshima, M. Ohta, F. Kitatani, A. Kimura, T. Kin, M. Koizumi, S. Goko, Y. Toh, S. Nakamura, H. Harada, K. Furutaka, T. Kamiyama, K. Kino, Y. Kiyanagi, M. Furusaka, M. Igashira, T. Katabuchi, M. Mizumoto: Study on nuclear data by using a high intensity pulsed neutron source for advanced nuclear system (3) Performance of 4π Ge spectrometer for neutron capture cross section measurements; *2010 Annual Meeting of the Atomic Energy Society of Japan*, pp. 94 (2010).

A. Kimura, M. Ohta, M. Oshima, F. Kitatani, T. Kin, M. Koizumi, S. Goko, Y. Toh, S. Nakamura, H. Harada, K. Furutaka, M. Igashira, T. Katabuchi, M. Mizumoto, T. Kamiyama, Y. Kiyanagi, K. Kino, F. Hiraga, M. Furusaka, J. Hori: nuclear system (5) Measurements of neutron capture cross sections using a 4πGe spectrometer at the J-PARC; *2010 Annual Meeting of the Atomic Energy Society of Japan*, pp. 96 (2010).

T. Katabuchi, M. Mizumoto, M. Igashira, A. Kimura, Y. Toh, S. Nakamura, S. Goko, T. Kin, M. Ohta, F. Kitatani, K. Furutaka, M. Koizumi, H. Harada, M. Oshima, J. Hori, K. Kino, T. Kamiyama, F. Hiraga, M. Furusaka, Y. Kiyanagi: Study on nuclear data by using a high intensity pulsed neutron source for advanced nuclear system (6) Measurements of neutron capture cross sections using an NaI spectrometer at J-PARC; *2010 Annual Meeting of the Atomic Energy Society of Japan*, pp. 97 (2010).

J. Hori, M. Oshima, F. Kitatani, A. Kimura, T. Kin, M. Koizumi, S. Goko, Y. Toh, S. Nakamura, H. Harada, K. Furutaka, M. Igashira, T. Katabuchi, M. Mizumoto, K. Kino, Y. Kiyanagi: Study on nuclear data by using a high intensity pulsed neutron source for advanced nuclear system (7) Measurements of neutron capture cross sections of the related nuclei using a LINAC at the KURRI; *2010 Annual Meeting of the Atomic Energy Society of Japan*, pp. 98 (2010).

S. Kamada, T. Katabuchi, M. Igashira, M. Mizumoto: Measurement of 550-keV neutron capture cross sections and gamma-ray spectra of Se-78,80,82; *2010 Annual Meeting of the Atomic Energy Society of Japan*, pp. 106 (2010).

N.Hayashizaki, T. Hattori, Yoshihisa Matsumoto, T. Katabuchi, Takahiko Tsukahara, T. Kobayashi, Development of BNCT Irradiation System using Compact Linac; *2010 Annual Meeting of the Atomic Energy Society of Japan*, pp. 155 (2010).

H. Akatsuka: Excited Level Populations and Excitation Kinetics of Nonequilibrium Ionizing Argon Discharge Plasma of Atmospheric Pressure; *Physics of Plasmas*, **16**, [4], 043502 (1-16) (2009).

K. Yoshida, T. Kanuma, H. Ichii, A. Nezu, H. Matsuura, H. Akatsuka: Flow Characteristics of a Cold Helium Arc-Jet Plasma along Open Field Lines; *IEEJ Trans. Elec. and Electron. Eng*., **4**, [3], 416-421 (2009).

T. Yuji, S. Fujii, N. Mungkung and H. Akatsuka: Optical Emission Characteristics of Atmospheric-Pressure Nonequilibrium Microwave Discharge and High-Frequency DC Pulse Discharge Plasma Jets; *IEEE Trans. Plasma Sci*., **37**, [6], 839-845 (2009).

K. Yoshida, T. Shibata, A. Nezu, H. Matsuura and H. Akatsuka: Ion Acceleration in Arc Jet Plasma along Open Field Lines; *IEEE Trans. Plasma Sci*., **37**, [8], 1414-1418 (2009).

T. Ichiki, T. Sakamoto, H. Matsuura and H. Akatsuka: Numerical Study on the Gas Temperature of Microwave Discharge Rare Gas Plasmas as a Rarified Gas Dynamic System; *J. Plasma Fusion Res. Series*, **8**, 768-772 (2009).

K. Yoshida, T. Shibata, A. Nezu, H. Matsuura, H. Akatsuka: Flowing Characteristics of Cold Arc Jet Plamsa along Open Field Lines; *J. Plasma Fusion Res. Series*, **8**, 923-927 (2009).

J. Mizuochi, T. Sakamoto, H. Matsuura and H. Akatsuka: Evaluation of Electron Energy Distribution Function in Microwave Discharge Plasmas by Spectroscopic Diagnostics with Collisional Radiative Model; *Jpn. J. Appl. Phys*., **49**, [3], 036001 (1-14) (2010).

H. Akatsuka: "*Atmospheric Pressure Plasma — Basics and Applications —", Chapter 4.4.1, Optical Emission Spectroscopy,* 164-169, Ohm-Sha, Tokyo (2009).

H. Akatsuka: Population Distribution and Excitation Kinetics of Non-Equilibrium Argon Plasma of Atmospheric Pressure; *Proc. the 6th Asia-Pacific International Symposium on the Basic and Application of Plasma Technology (APSPT-6)*, 43-46 (2009).

W. Takai, A. Nezu, H. Matsuura and H. Akatsuka: Diagnostics of oxygen-rare gas mixed plasmas excited by microwave discharge; *Proc. the 6th Asia-Pacific International Symposium on the Basic and Application of Plasma Technology (APSPT-6)*, 63-66 (2009).

K. Kuwano, A. Nezu, H. Matsuura and H. Akatsuka: Fundamental Study on Discharge Characteristics of Nitrogen-Rare Gas Microwave Plasma; *Proc. the 6th Asia-Pacific International Symposium on the Basic and Application of Plasma Technology (APSPT-6)*, 207-210 (2009).

K. Yoshida, T. Shibata, A. Nezu and H. Akatsuka: Supersonic Ion Acceleration and Potential Formation of Arc Plasma Flow at Open Field Lines; *The Papers of Technical Meeting on Plasma Science and Technology, IEE Japan*, #PST09-9, 43-47 (2009).

W. Takai, A. Nezu, H. Matsuura and H. Akatsuka: Measurement of Oxygen-Rare Gas Mixed Microwave-Discharge Plasmas; *The Papers of Technical Meeting on Plasma Science and Technology, IEE Japan*, #PST09-25, 19-23 (2009).

Y. Ohno, A. Nezu, H. Matsuura and H. Akatsuka: *The Papers of Technical Meeting on Plasma Science and Technology, IEE Japan*, #PST09-33, 65-69 (2009).

T. Yuji, H. Kawano, N. Tatsuguchi, S. Satoh and H.Akatsuka: Development of Cleaning Technology on Semiconductor Equipment Process for Atmospheric-Pressure Non-Equilibrium DC Pulse Plasma Jet; *The Papers of Technical Meeting on Plasma Science and Technology, IEE Japan*, #PST09-36, 81-86 (2009).

K. Kuwano, A. Nezu, H. Matsuura and H. Akatsuka: Optical Emission Spectroscopy and Double Probe Measurement of Microwave Nitrogen-Rare Gas Discharge Plasma; *The Papers of Technical Meeting on Plasma Science and Technology, IEE Japan*, #PST09-54, 7-12 (2009).

K. Yoshida, A. Nezu and H. Akatsuka: Supersonic Acceleration and Potential Formation of Helium Arc Plasma Flow at Open Field Lines; *Meeting Abstracts of the Physical Society of Japan*, **64** [2] p. 143 (2009).

Y. Kittaka, A. Nezu, H. Matsuura and H. Akatsuka: Fundamental Study of Interfacial Heat Transfer by Low-Pressure Non-Equilibrium Discharge Plasmas with OES Experiment and MD Simulation; *The Papers of Technical Meeting on Plasma Science and Technology, IEE Japan*, #PST09-136, 51-55 (2009).

H. Akatsuka: Population Distribution of Excited States of Cold Atmospheric Pressure Plasma; *Proc. 26th Annual Meeting, The Japan Society of Plasma Science and Nuclear Fusion Research*, 1pD25P (2009).

T. Shibata, A. Nezu and H. Akatsuka: Diagnostics of Electron Temperature of Low-Pressure Discharge Nitrogen Plasma by Optical Emission Spectroscopy; *Proceedings 27th Symposium on Plasma Processing (SPP27)*, 141-142 (2010).

W. Takai, A. Nezu, H. Matsuura and H. Akatsuka: Diagnostics of Oxygen-Rare Gas Mixed Plasmas Excited by Microwave Discharge; *Proceedings 27th Symposium on Plasma Processing (SPP27)*, 175-176 (2010).

K. Kuwano, A. Nezu, H. Matsuura and H. Akatsuka: Fundamental Study on Discharge Characteristics of Nitrogen-Rare Gas Microwave Plasma; *Proceedings 27th Symposium on Plasma Processing (SPP27)*, 177-178 (2010).

K. Kuwano, A. Nezu, H. Matsuura and H. Akatsuka: Actinometry Measurement of Dissociation Degree of N_2 Molecule in Nitrogen Discharge Plasma and Effect of Inert Gas Admixture; *Meeting Abstracts of the Physical Society of Japan*, **65** [1] p. 224 (2010).

W. Takai, A. Nezu, H. Matsuura and H. Akatsuka: Actinometry Measurement of Rare-Gas Mixture Effect on the Dissociation Degree of Microwave Discharge Oxygen Plasma; *The 2010 Annual Meeting Record, I.E.E. Japan*, p. 220 (2010).

T. Yuji, S. Aoki, Y. Kohno and H. Akatsuka: Space Charge Measurements of Surface Cleaning Sample Using Atmospheric-Pressure Non-equilibrium Discharge Plasma Jet; *The 2010 Annual Meeting Record, I.E.E. Japan*, p. 243 (2010).

H. Akatsuka: Fundamentals of Plasma Measurement and Diagnostics; Capter 2 of "*Textbook of the 3rd Plasma Electronics Incubation Hall*" (ISBN: 978-4-86348-035-3), Division of Plasma Electronics, Japan Society of Applied Physics, pp. 16-41 (2009).

H. Akatsuka: Collisional Radiative Model of Ar Plasma and Estimation of Electron Temperature Measurement of Atmospheric Pressure by OES Measurement; *Research Reports on Human Environmental Preservation Technology by Atmospheric-Pressure Plasma Flow, (P-SCD360)*, pp. 13-17, Environmental Engineering Division of The Japan Society of Mechanical Engineers, Tokyo (2009).

J. Hasegawa, H. Ikagawa, S. Nishinomiya, T. Watahiki, Y. Oguri: Beam-Plasma Interaction Experiments Using Electromagnetically Driven Shock Waves; *Nuclear Instruments and Methods in Physics Research A*, **606**, 205-211 (2009).

K. Horioka, T. Kawamura, M. Nakajima, K. Kondo, M. Ogawa, Y. Oguri, J. Hasegawa, S. Kawata, T. Kikuchi, T. Sasaki, M. Murakami, K. Takayama: Activities on Heavy Ion Inertial Fusion and Beam-Driven High Energy Density Science in Japan; *Nuclear Instruments and Methods in Physics Research A*, **606**, 1-5 (2009).

S. Thomyasirigul, H. Gukuda, J. Hasegawa, Y. Oguri: Determination of Chromium (VI) in Water by PIXE

Analysis Using Ion Exchange Paper – Limit of Detection and Interference by Coexisting Anions; *International J. of PIXE*, **19**, 1-2, 1-8 (2009).

T. Tada, H. Fukuda, J. Hasegawa, Y. Oguri: In-situ Observation of Chemical State Change of Sulfur in Solid Targets During MeV Proton Irradiation; *X-ray Spectrometry*, **38**, 3, 200-204 (2009).

T. Tada, H. Fukuda, J. Hasegawa, Y. Oguri, M. Tsuji: Chemical Speciation of Sulfur in Activated Carbon by Wavelength-Dispersive PIXE Technique; *X-ray Spectrometry*, **38**, 3, 239-243 (2009).

T. Tada, S. Wonglee, H. Fukuda, J. Hasegawa, Y. Oguri: Measurement of Chemical State Change of Phosphorus During MeV-Proton Irradiation by a High-Resolution Wavelength-Dispersive PIXE System; *International J. of PIXE*, **19**, 1-2, 9-15 (2009).

J. Hasegawa, C. Polee, H. Fukuda, Y. Oguri: A Micro-PIXE Analysis System Based on Taper Capillary Optics; *20th International Congress on X-ray Optics and Microanalysis*, 15-17 Sep. 2009, Karlsruhe, Germany (2009).

T. Tada, H. Fukuda, J. Hasegawa, Y. Oguri: Temperature rise and gas emission during chemical state analysis by WD-PIXE measurement; *20th International Congress on X-ray Optics and Microanalysis,* 15-17 Sep. 2009, Karlsruhe, Germany (2009).

J. Hasegawa, Y. Oguri, K. Horioka, T. Kikuchi, T. Sasaki, S. Kawata, K. Takayama: A beam-driven warm-dense-matter experiment using quasi-isentropically compressed targets; *The Sixth International Conference on Inertial Fusion Sciences and Applications*, 6-11 Sep. 2009, Intercontinental San Francisco, San Francisco, USA (2009).

Y. Oguri, J. Hasegawa: Bragg Curve of Heavy Ion Beams in Dissociated Hydrogen Gas Targets; *The Sixth International Conference on Inertial Fusion Sciences and Applications*, 6-11 Sep. 2009, Intercontinental San Francisco, San Francisco, USA (2009).

J. Hasegawa, Y. Oguri, K. Horioka, T. Kikuchi, T. Sasaki, S. Kawata, K. Takayama: A Plan of Warm-Dene-Matter Experiment Using Precompressed Hydrogen Target; *The 12th U.S.-Japan Workshop on Heavy Ion Fusion and High Energy Density Physics*, 7-8 Sep. 2009, Intercontinental San Francisco, San Francisco, USA (2009).

J. Hasegawa, S. Jaiyen, Y. Oguri: Dependence of Ion Transport through Glass Capillaries on Projectile and Target Atomic Numbers; *Meeting Abstracts of the Physical Society of Japan*, **65**, 1, 161 (2010).

J. Hasegawa, H. Fukuda, Y. Oguri: Numerical Analysis of MeV Ion Transportation in Glass Capillary II; *Meeting Abstracts of the Physical Society of Japan*, **64,** 2, 64 (2009).

Y. Oguri, J. Hasegawa: Macroscopic Stopping Power of Aluminum Foam Targets Heated by Pulsed Ion Beams; *Meeting Abstracts of the Physical Society of Japan*, **64**, 2, 49 (2009).

E. Yamaki, M. Takahashi: Corrosion Resistance of Fe-Al Alloy-Coated Steel under Bending Stress in High Temperature Lead-Bismuth Eutectic; *2009 International Congress on Advances in Nuclear Power Plants (ICAPP09)*, Tokyo, Japan, May 10-14, 2009, Paper 9021.

Rongyuan Sa, Minoru Takahashi: Experimental Study on Self-triggering of Vapor Explosion with Droplet of Lead-Bismuth Eutectic in Water; *The 13th International Topical Meeting on Nuclear Reactor Thermal Hydraulics (NURETH-13) N13P1220*, Kanazawa, Japan, September 27-October 2, 2009.

Teddy Ardiansyah, Minoru Takahashi, Masamichi Nakagawa, Kuniaki Miura, Makoto Asaba: Effect of Argon Gas Injection on Acoustics Noise and Onset of Sodium Cavitation in Venturi; *The 13th International Topical Meeting on Nuclear Reactor Thermal Hydraulics (NURETH-13) N13P1217* Kanazawa, Japan, September 27-October 2, 2009.

Eriko Yamaki, Minoru Takahashi: Corrosion Test of Fe-Al Alloy-coated Steels under Loading in LBE; *2009 Annual Meeting of Atomic Energy Society of Japan*, Tokyo, March 23-25, 2009, A421.

Xinghua Zhou, Minoru Takahashi, Masatoshi Kondo, Takeo Muroga: Study on Corrosion Characteristics of JLF-1 in Liquid LiPb; *2009 Fall Meeting of Atomic Energy Society of Japan*, Sendai, September 17, 2009, P19.

Asril Pramutadi Andi Mustari, Minoru Takahashi: Effect of Welding on Corrosion Properties of Ferritic-Martensitic Steels in Liquid Pb-Bi; *2009 Fall Meeting of Atomic Energy Society of Japan*, Sendai, September 17, 2009, N28.

Masashi Nakatsuka, Teddy Ardiansyah, Minoru Takahashi, Tooru Kobayashi: Development of Liquid Lithium Target for Neutron Capture Therapy Using Accelerator (1) Water Film Flow Simulation Test; *2009 Fall Meeting of Atomic Energy Society of Japan*, Sendai, September 17, 2009, C13.

Masamichi Nakagawa, Toru Kobayashi, Minoru Takahashi, Masanori Aritomi: Flow Scheme of Liquid Lithium for the Target and Coolant of BNCT using Accelerators; *2009*

Annual Meeting of The Japanese Society for Multiphase Flow (JSMF), Kumamoto, B332, pp.234-235.

Masamichi Nakagawa, Toru Kobayashi, Minoru Takahashi, Masanori Aritomi: Fundamental Stability on A Sheet Jet of Liquid Lithium for the Target and Coolant of BNCT using Accelerators; *2009 Annual Meeting of Japan Society of Mechanical Engineers*, Morioka, September 13-16, S504-2-5, pp.185-186.

Masamichi Nakagawa, Toru Kobayashi, Minoru Takahashi, Masanori Aritomi: Boundary Layer Structure in a Liquid Lithium Film Flowing down a Flat Plate for the Target and Coolant of BNCT using Accelerators; *Meeting of JSME Fluids Engineering Division*, Nagoya, November 7-8, O138, pp.77-78.

Masamichi Nakagawa, Toru Kobayashi, Minoru Takahashi, Masanori Aritomi: Centrifugal Instability on a Liquid Lithium Film Flowing down a Concave Plate for the Target and Coolant of BNCT using Accelerators; *Meeting of JSME Fluids Engineering Division*, Nagoya, November 7-8, O138, pp.79-80.

Y. Kato: Carbon recycling for reduction of carbon dioxide emission from iron-making process; *ISIJ Int*., **50**(1), pp. 181-185 (2010).

Y. Kato: Development of Chemical Heat Pumps for Utilization of Low-temperature Waste Heats; (Review Paper), *J. Jpn. Inst. Energy*, **88**(11), pp.986-993 (2009) (in Japanese).

Y. Kato, K. Otsuka, J. Ryu: Experimental Study on Fuel Reforming with Carbon Dioxide Recovery for Vehicle Use; *J. Chem. Eng. Japan*, **42**, Supplement 1, pp. s10–s16 (2009). Special Issue for International Symposium on Chemical Reaction Engineering 20 (ISCRE 20).

Y. Kato, R. Takahashi, T. Sekiguchi, J. Ryu: Study on medium-temperature chemical heat storage using mixed hydroxides; *J. Intn'l J of Refrigeration*, **32**(4), pp. 661-666 (2009).

Y. Kato: THERMAL ENERGY STORAGES IN VEHICLES FOR FUEL EFFICIENCY IMPROVEMENT; *Proc. of The 11th Intl Conference on Thermal Energy Storage (Effstock 2009)*(in CD), No. 150, 14 – 17 June (presented on 15 June), 2009, Stockholm, Sweden.

Y. Kato: Production method of hydrogen permeation membrane; *Japan patent* No. 4411409, Registered on 27 November, 2009.

Y. Kato, Y. Ujisawa: Iron making method; *Japan patent* 2010-006238, submitted of 14 January, 2010.

Y. Kato, J. Ryu: Chemical heat pump: A thermal energy utilization technology by using chemical reactions; *Chemical Engineering of Japan,* **73**(9), pp. 2-5 (2009).

J. Ryu: Fundamental principle and application of materials for chemical heat storage; *Parity*, **25** (3), 22-30 (2009) (in Japanese).

J. Ryu: Development of materials of heat storage with chemical modification; *Fine Chemical*, **38** (9), 67-72 (2009) (in Japanese).

Y. Kato, T. Obara, J. Ryu, I. Yamanaka, S. Mori, M. Suzuki: Study for carbon recycling performance in carbon recycling iron making process; *159th ISIJ Spring Meeting*, 29 March, 2010, Tsukuba.

H. Ishitobi, J. Ryu, Y. Kato: Dehydration behavior of metal salt added magnesium hydroxide; *75th SCEJ Annual Meeting,* P104, 18 March, 2010, Kagoshima.

H. Ishitobi, N. Hirao, J. Ryu, Y. Kato: Hydration behavior of metal salt added magnesium hydroxide for chemical heat pump; *41st SCEJ Autumn Meeting*, V206, 17 September, 2009, Hiroshima.

Y. Toda, K. Shimatake, S. Tanda and J. Onoe: Femtosecond carrier dynamics in quasi-one-dimensional topological compounds; (Invited paper), *Proc. SPIE* **7214**, 72141G (2009).

H.J. Kim, I.C. Bang and J. Onoe: Characteristic stability of bare Au-water nanofluids fabricated by pulsed laser ablation in liquids; *Opt. Laser Eng.* **47**, 532-538 (2009).

H. Shima, H. Yoshioka and J. Onoe: Geometry-driven shift in the Tomonaga-Luttinger exponent of deformed cylinders; *Phys. Rev. B* **79**, 201401(R) (2009).

S. Ryuzaki, T. Hasegawa and J. Onoe: X-ray diffraction and infrared multiple-angle incidence resolution spectroscopic studies on the crystal structure and molecular orientation of Zinc-porphyrin thin films on a SiO_2/Si substrate; *J. Appl. Phys.* **105**, 113529 (2009).

A. Takashima, T. Nishii and J. Onoe: DV-Xa study on the electronic structure of C_{120} isomers derived from the general Stone-Wales rearrangement; *Int. J. Quantum Chem.* **109**, 2773-2779 (2009).

S. Ryuzaki and J. Onoe: X-ray diffraction and scanning electron microscopic studies on the crystal structure and surface/interface morphology of Zinc-octaethylporphyrin films on an ITO substrate spin-coated with PEDOT:PSS; *J. Appl. Phys.* **106**, 023526 (2009).

K. Yamamoto, R. Nakajima, Y. Ochi, M. Tsuruta, M. Higuchi, A. Hida and J. Onoe: Formation of ($FeCl_3$)@phenylazomethine dendrimer (DPA): Fine control of the release and encapsulation of Fe ions in

dendrimers; *Pure and Appl. Chem*. **81**, 2253-2263 (2009).

J. Onoe: One-dimensional metallic peanut-shaped nanocarbon with positive and negative Gaussian curvatures: Toward a new science of quantum electronic systems on Riemannian surface; *J. Surf. Sci. Soc. Jpn.* **30**, 659-666 (2009).

H. Shima, H. Yoshioka and J. Onoe: Curvature effects on collective excitations in dumbbell-shaped hollow nanotubes; *Physica E* **42**, 1151-1154 (2010).

A. Takashima, J. Onoe and T. Nishii: *In situ* infrared spectroscopic and density-functional studies on the cross-linked structure of one-dimensional C_{60} polymer; *J. Appl. Phys.* **108**, 033514 (2010).

J. Onoe: Exotic-nanocarbons: Toward the development of new Riemannian space quantum systems; *Proc. Optical-electronic device committee of the electronic society of Japan*, OQD-10-001 (2010).

J. Onoe: Exotic-nanocarbons: the development of new quantum electronic systems in a curved space; *SCAT Tech. J.* **66**, 16-32 (2010).

J. Onoe: A new allotrope of π-electron conjugated nanocarbons with positive and negative Gaussian curvatures; (Invited lecture), *Institut de Physique et Chimie des Mate'riaux*, UMR 7504 CNRS-Universite' Louis Pasteur, Strasbourg, June 22 (2009).

J. Onoe: One-dimensional metallic peanut--shaped nanocarbons with positive and negative Gaussian curvatures: Toward a new science of quantum electronic systems on curved surfaces; (Invited), *9th Biennial International Workshop on Fullerenes and Atomic Clusters (IWFAC 2009)*, St Petersburg, Russia, July 6-10 (2009).

J. Onoe, T. Ito, H. Shima, Y. Toda, H. Yoshioka, and S. Kimura: One-dimensional peanut-shaped C_{60} polymer as a new quantum system; (selected paper), *5th International Conference on Diffusion in Solids and Liquids - Mass Transfer, Heat Transfer, Microstructure and Properties, Nanodiffusion and Nanostructured Materials* -, Roma (Italy), June 24-26 (2009).

H. Shima, H. Yoshioka, and J. Onoe: Tomonaga-Luttinger exponent of peanut-shaped hollow nanocylinders; *The 18th International Conference on Electronic Properties of Two-Dimensional Systems* (EP2DS-18), Kobe, July 19 - 24 (2009).

J. Onoe, T. Ito, H. Shima, Y. Toda, H. Yoshioka, and S. Kimura: Electronic and optical properties of one-dimensional C_{60} polymer with positive and negative Gaussian curvatures: a new quantum system; *20th European Conference on Diamond, Diamond-Like Materials, Carbon Nanotubes, and Nitrides*, Athens (Greece), Sept. 6-10 (2009).

S. Ryuzaki, T. Kai, T. Nishii, and J. Onoe: Improvement of the external quantum efficiency of Zn(OEP)/C_{60} layered-structure photovoltaic cells by controlling the crystal structure of Zn(OEP) films; *ECME*, Copenhagen, Denmark, Sept. 9-12 (2009).

J. Onoe, T. Ito, S. Kimura, H. Shima and H. Yoshioka: In situ photoelectron spectra of an electron-beam irradiated C_{60} film; *2nd UVSOR Workshop on Low-Energy Photoemission of Solids using Synchrotron Radiation (LEPES 09)* [A Satellite Meeting of ICESS 11, Nara, Japan] ,Okazaki, Oct.3-4 (2009).

S. Ryuzaki, T. Kai, and J. Onoe: The dependence of open circuit voltage on incident light wavelength for organic photovoltaic cells consisting of Zinc-pophyrin and fullerene films; *4th Asian Consortium on Computational Materials Science-Virtual Organization, Sendai*, Jan. 12-14 (2010).

A. Takashima, T. Nishii, and J. Onoe: Structural properties of an electron-beam irradiated C_{60} film studied by vibrational spectroscopy and density-functional calculations; *4th Asian Consortium on Computational Materials Science-Virtual Organization*, Sendai, Jan. 12-14 (2010).

T. Kai, S. Ryuzaki, and J. Onoe: An impedance spectroscopic study on the carrier dynamics in Zinc-porphyrin / fullerene photovoltaic cells; *4th Asian Consortium on Computational Materials Science-Virtual Organization*, Sendai, Jan. 12-14 (2010).

J. Onoe, T. Ito, S. Kimura, H. Shima and H. Yoshioka: One-dimensional metallic peanut-shaped C_{60} polymer from a viewpoint of curved quantum electronic systems; (Selected paper), *7th Annual Meeting of Nano Society*, Tokyo, May 9-11 (2009).

S. Ryuzaki, T. Kai, T. Nishii and J. Onoe: Structural effects of Zn(OEP) films on the external quantum efficiency of Zn(OEP)/C_{60} organic photovoltaic cells; (Selected paper), *7th Annual Meeting of Nano Society*, Tokyo, May 9-11 (2009).

A. Takashima, T. Nishii and J. Onoe: On the roles of 7- and 8-membered rings in the energy gap of C_{120} stable isomers derived from the general Stone-Wales rearrangement; *7th Annual Meeting of Nano Society*, Tokyo, May 9-11 (2009).

T. Kai, S. Ryuzaki, T. Nishii and J. Onoe: Impedance characteristics of Zn(OEP)/C_{60} organic photovoltaic cells; *7th Annual Meeting of Nano Society*, Tokyo, May 9-11 (2009).

J. Onoe: Old but new carbons: Toward the development of new quantum systems in a curved space; (Invited), *22th Annual meeting of the DV-Xα Society*, Takamatsu, Aug. 5-7 (2009).

J. Onoe: Relativistic density-functional study of nuclear materials; (Awarded talk), *22th Annual meeting of the DV-Xα Society*, Takamatsu, Aug. 5-7 (2009).

S. Ryuzaki, T. Kai, Y. Toda, S. Adachi and J. Onoe: An improvement of the generation of the inter-molecular excitons for Zn(OEP)/C_{60} layered organic photovoltaic cells by controlling the molecular orientation in Zn(OEP) films; (Selected paper), *19th Annual meeting of MRS of Japan*, Yokohama, Dec. 7-9 (2009).

A. Takashima, T. Nishii and J. Onoe: Density-functional and in situ infrared spectroscopic studies of an electron-beam irradiated C_{60} film; (Selected paper), *19th Annual meeting of MRS of Japan*, Yokohama, Dec. 7-9 (2009).

T. Kai, S. Ryuzaki and J. Onoe: Impedance spectra of Zn(OEP)/C_{60} layered photovoltaic cells; (Selected paper), *19th Annual meeting of MRS of Japan*, Yokohama, Dec. 7-9 (2009).

J. Onoe: Low-dimensional exotic-nanocarbon fabricated using photo- and electron-beam-induced excitation of C_{60}; *A workshop on advanced quantum beams and their application to nanomaterials*, Tokyo, Feb. 15 (2010).

S. Ryuzaki, T. Kai and J. Onoe: The capacitance-voltage characteristics and open-circuit voltage of Zn(OEP)/C_{60} layered photovoltaic cells; (Selected paper), *57th spring meeting of the Applied Physic Society of Japan*, Kanagawa, March 17-20 (2010).

T. Kai, S. Ryuzaki and J. Onoe: Impedance characteristics of Zn(OEP)/C_{60} layered photovoltaic cells; (Selected paper), *57th spring meeting of the Applied Physic Society of Japan*, Kanagawa, March 17-20 (2010).

A. Takashima, Y. Toda and J. Onoe: *In situ* low-temperature infrared spectra of one-dimensional metallic peanut-shaped C_{60} polymers; (selected as a B-type oral paper), 90th spring meeting of the Chemical Society of Japan, Osaka, March 26-29 (2010).

Kamdar,R.P. and Matsumoto,Y.: Radiation-induced XRCC4 Association with Chromatin DNA Analyzed by Biochemical Fractionation; *J.Radiat.Res.*, **51**, 303-313 (2010).

Sasano,N., Enomoto,A., Hosoi,Y., Katsumura,Y., Matsumoto,Y., Morita,A., Shiraishi,K., Miyagawa,K., Igaki,H. and Nakagawa,K.: Edaravone, a known free radical scavenger, enhances X-ray-induced apoptosis at low concentrations; *Cancer Lett.*, **293**, 521-527 (2010).

Morita,A., Yamamoto,S., Wang,B., Tanaka,K., Suzuki,N., Aoki,S., Ito,A., Nanao,T., Ohya,S., Yoshino,M., Zhu,J., Enomoto,A., Matsumoto,Y., Funatsu,O., Hosoi,Y. and Ikekita,M.: Sodium orthovanadate inhibits p53-mediated apoptosis; *Cancer Res.*, **70**, 257-265 (2010).

Sharma, M.K., Kamdar, R.P. and Matsumoto, Y.: Missing link in the DNA double-strand break repair process through non-homologous end joining. International Conference on Medical Physics; *Radiation Protection & Radiobiology 2009,* Jaipur (SMS Medical College & Hospital), India, 11-13 February, 2009, P-36.

Sharma, M.K., Kamdar R.P. and Matsumoto, Y.: Phosphorylation-mediated regulation of XRCC4 and XLF by DNA-PK in DNA double-strand break repair through non-homologous end-joining; *2nd Asian Congress of Radiation Research*, Seoul (COEX), Korea, 17-20 May 2009, P-RB-026.

Matsumoto, Y. XRCC4: A bona fide substrate of DNA-PK in DNA double-strand break repair; *2nd Asian Congress of Radiation Research,* Seoul (COEX), Korea, 17-20 May 2009, P-RB-032 (Also Oral Talk).

Kamdar, R.P. and Matsumoto, Y.: Assembly of XRCC4-DNA ligase IV-XLF complex on DNA double-strand breaks in situ revealed by biochemical fractionation analysis; *2nd Asian Congress of Radiation Research*, Seoul (COEX), Korea, 17-20 May 2009, P-RB-054 <Best Poster Award>.

Imamichi, S., Aonuma, T., Fukuda, K., Okubayashi, M., Shiraishi, T., Tokai, A., Ito, T., Nohtomi, A., Sugiura, N. and Matsumoto, Y.: Role of DNA-PK and ATM in the phosphorylation-mediated regulation of XRCC4 in DNA double-strand break repair; *2nd Asian Congress of Radiation Research*, Seoul (COEX), Korea, 17-20 May 2009, P-RB-076 <Best Poster Award>.

Sharma, M.K. and Matsumoto, Y.: Elucidation of DNA Damage Recognition/Repair Mechanism and Its Application to Cancer Therapy – The True Substrates of DNA-PK and the Significance of Phosphorylation.

Kamdar, R.K. and Matsumoto, Y.: Assembly of XRCC4-DNA ligase IV-XLF complex on radiation damaged chromatin in situ revealed by biochemical fractionation analysis.

Sharma, M.K. and Matsumoto, Y.: The true substrate of DNA-dependent protein kinase (DNA-PK) and the significance of phosphorylation.

D. Kuwahara, S. Tsuji-Iio, Y. Nagayama, T. Yoshinaga, M. Sugito, Z. Shi, S. Yamaguchi, Y. Kogi, A. Mase: Development of 2-D Antenna Array for Microwave Imaging Reflectometry in LHD; *J. Plasma Fusion Res. SERIES*, Vol. **8**, 649 - 654 (2009).

S. Nomura, N. Tanaka, K. Tsuboi, H. Tsutsui, S. Tsuji-Iio, R. Shimada: Design Considerations for SMES Systems Applied to HVDC Links; *EPE 2009* , Barcelona, Spain, Sep. 8-10, 2009.

S. Tsuji-Iio, Y. Maruyama, T. Miyazaki, H. Tsutsui, R. Shimada: Thermostatic control of optical isolator for long-term stability of magneto-optic sensing with orthogonally polarized two-frequency laser; *14th Int. Symp*. Laser-Aided Plasma Diagnostics, Treviso, Ialy, Sep. 21st - 24th 2009.

T. Habuchi, H. Tsutsui, S. Tsuji-Iio, R. Shimada: 3-Dimesional Stress Analysis of Virial-Limit Coils; *21st Inter. Conf. on Magnet Technology*, Hefei, China, Oct. 18-23, 2009.

S. Maeyama, A. Ishizawa, T.-H. Watanabe, M. M. Skoric, N. Nakajima, S. Tsuji-Iio, and H. Tsutsui: Effects of unsteady sheared E x B flow on slab ITG turbulence; *The 51st Annual Meeting of APS-DPP*, Atlanta, GA, U.S., Nov. 5, 2009.

D. Kuwahara, S. Tsuji-Iio, Y. Nagayama, T. Yoshinaga, Z. Shi, S. Yamaguchi, Y. Kogi, A. Mase: Microwave Imaging Diagnostics in LHD (2); *26th Annual Meeting of the Japan Soc. of Plasma Sci. and Nucl. Fusion Res.*, 1pE19P, Kyoto, Dec. 1 - 4, 2009.

T. Habuchi, H. Tsutsui, S. Tsuji-Iio, R. Shimada: 3-Dimensional Stress Analysis of Virial-Limit Coils with Finite Element Method; *26th Annual Meeting of the Japan Soc. of Plasma Sci. and Nucl. Fusion Res.*, 3pD35P Kyoto, Dec. 1 - 4, 2009.

S. Maeyama, A. Ishizawa, T.-H. Watanabe, M. Skoric, N. Nakajima, S. Tsuji-Iio, H. Tsutsui: Effects of unsteady E×B flows on ITG turbulence and its model; *Meeting Abs. Phys. Soc. Japan*, Vol. **64**, Issue 1, Part 2, 21aTE-8, 236, Okayama, March 20 - 23, 2010.

Hiroki Takezawa and Toru Obara: Calculation of the Integral Kinetic Model Transient Parameters by the Monte Carlo Method for Space-Dependent Kinetic Analysis; *Nuclear Science and Engineering*, **164,** 1-7 (2010).

Toru Obara and Liem Peng Hong: Small Reactor For Semiconductor Production By Neutron Transmutation Doping; *Proc. of The 2'nd International Conference on Advances in Nuclear Science and Engineering 2009-ICANSE2009, Bandung, Indonesia, November 3-4, 2009, pp.15-18, (2010).*

Dwi Irwanto, Yukikata Kato, Ichiro Yamanaka, Toru Obara: Preliminary Study of Burnup Characteristics for a Simplified Small Pebble Bed Reactor; *Proc. of The 2'nd International Conference on Advances in Nuclear Science and Engineering 2009-ICANSE2009, Bandung, Indonesia, November 3-4, 2009, pp.27-30, (2010).*

Toru Obara, Liem Peng Hong, Hideki Yagi: Concept of Small Reactor for Neutron Transmutation Doping using PWR Type Fuel Elements; *Proc. of 2009 International Congress on Advances in Nuclear Power Plants (ICAPP'09), Tokyo, Japan, May 10-14, 2009*, Paper 9039 (2009).

Toru Obara, Junichiro Otani: Fundamental Analysis of Graphite Moderated Reactor for Laser Propulsion by Nuclear-Pumped Laser; *14th Intenational Conference on Emerging Nuclear Energy Systems (ICENES-2009),* Erieira, Portugal, June 29 - July 3, 2009.

Byambajav Munkhbat, Toru Obara: Design study on small reactor for semiconductor production using LWR fuel ; (1) Reactor Concept; *2010 Atomic Energy Society of Japan Annual Meeting*, H01 (2010).

Hiroki Takezawa, Toru Obara: Study on Experimental Reactor for Nuclear Pumped Laser; (XI) Space Dependent Kinetic Analysis for Coupled Reactor with Low Enriched Uranium; *2010 Atomic Energy Society of Japan Annual Meeting,* H31 (2010).

Dwi Irwanto, Toru Obara: Design Study of Innovative Simplified Small Pebble Bed Reactor; (1) Design Concept and Sample Design Analysis; *2009 Atomic Energy Society of Japan Fall Meeting*, F34 (2009).

Hiroki Takezawa, Toru Obara: Study on Experimental Reactor for Nuclear Pumped Laser; (X) Validation of Space Dependent Kinetic Analysis Based on Integral Kinetic Model; *2010 Atomic Energy Society of Japan Fall Meeting*, F36 (2009).

Y. Sato, A. Funakoshi, K. Okada, M. Akiyoshi, T. Matsunaga, S. Koyama, M. Ozawa, T. Suzuki: Study on thermal stability of tertiary pyridine resin; *J. Them Anal Calorim. Journal of Thermal Analysis and Calorimetry*, **97** (2009) 297-302.

Tatsuya Suzuki, Yasuhiko Fujii, Wu Yan, Hitoshi Mimura, Shin-ichi Koyama, Masaki Ozawa: Adsorption behavior of VII group elements on tertiary pyridine resin in hydrochloric acid solution; *J. Radioanal. Nucl, Chem.* **282** (2009) 641-643.

Masaki Ozawa, Shinichi Koyama, Tatsuya Suzuki, Reiko Fujita and Yasuhiko Fujii: From Waste to Resource, Nuclear Rare Metals as a Dream of Modern Alchemists; *Proc. ICENES 2009 (14th International Conference on Emerging Nuclear Energy Systems*, pp.85, 29th June-3rd July, Ericeira, Portugal(2009).

Masaki Ozawa, Tatsuya Suzuki, Shinichi koyama, Isao Yamagishi, Reiko Fujita , Ken Okada, Katsuyoshi Tatenuma, Hitoshi Mimura and Yasuhiko Fujii: Adv.-ORIENT Cycle, Its Scientific Progress and the Engineering Feasibility; *Proc.Global2009*(CD),

pp.1117-1126, 6th -11th September, Paris, France(2009).

Yoshihiko Sato, Ken Okada, Miyako Akiyoshi, Takehiro Matsunaga, Tatsuya Suzuki, Shinichi koyama, Masaki Ozawa: The Thermal Stability of Tertiary Pyridine Resin for the Application to Multi-functional Reprocessing Process-Adv.-ORIENT Cycle development; *Proc.Global 2009*(CD), pp.962-969, 6th -11th September, Paris, France (2009).

Masaki Ozawa, Shinichi Koyama and Tatsuya Suzuki; Potentiality and Reality on Recycle of Nuclear Rare Metals as a New Resource for the Next Generation; Abstracts, pp.37, CD, *R'09 World Congress Resource Management and Technology for Material and Energy Efficiency*, Davos, Switzerland, September 14-16(2009).

T. Suzuki, K. Otake, M. Sato, M. Ozawa, M. Hara, T. Mitsugashira, Y. Fujii: Adsorption behaviors of f-elements on tertiary pyridine and quaternary pyridinium resins; *4th Asia-Pacific Symposium on Radiochemistry*, Napa Valley, CA, USA, Nov.29-Dec.4, (2009) p. 220.

Tatsuya Suzuki, Maiko Tanaka and Shinichi Koyama: Research and development on removal and recovery of minor-actinides from spent molten salt waste of pyrochemical reprocessing(4)Recovory of minor actinides by using pyridine resin and purification of salt waste by cation exchange; *2009 fall meetings of atomic energy society of Japan*, (2009) p.626.

Masayuki Iwata, Kosuke Shimokawa, Tsuyoshi Arai, Katsuhisa Nagayama, Tatsuya Suzuki, Kenichi Horiguchi and Atsushi Sugaya: A Basic Study for Stabilization Treatment of Low Level Liquid Waste Including Phosphoric Ion; *2009 fall meetings of atomic energy society of Japan*, (2009) p.637.

Yoshihiko Sato, Ken Okada, Miyako Akiyoshi, Takehiro Matsunaga, Tatsuya SUzuki, Shin-ichi Koyama and Masaki Ozawa: Study on thermal stability of tertiary pyridine resin (3) evaluation of effects by coexistent elements to the reaction of resin/methanol/nitric acid, hydrochloric acid systems; *2009 fall meetings of atomic energy society of Japan*, (2009) p.597.

Ken Okada, Yoshihiko Sato, Miyako Akiyoshi, Takehiro Matsunaga, Tatsuya Suzuki, Shin-ichi Koyama and Masaki Ozawa: Study on thermal stability of tertiary pyridine resin (4) Gram scale thermal analysis using glass vessel; *2009 fall meetings of atomic energy society of Japan*, (2009) p.598.

Tatsuya Suzuki, Yasuhiko Fujii, Shin-ichi Koyama, Masaki Ozawa: Adsorption Behavior of Light Platinum Group Elements on Tertiary Pyridine Resin; *The 25th symposium for Japan Association of Ion Exchange*, (2009) I-102.

H. Kikunaga,T. Mitsugashira, T. Suzuki, M. Nomura, A. Shinohara: Measurement of the half-life of Th-229g; *2009 annual meeting of the Japan society of nuclear and radiochemical sciences* (2009)3B05.

Saori Umehara, Tadafumi Kishimoto, Hidekazu Kakubata, Masao Nomura, Toshitaka Kaneshiki, Tatsuya Suzuki, Youichi Sakuma, Yasuhiko Fujii, Shigeki Nemoto and Takao Oi: Calcium Isotope Separation by Using Crown Ether Resins (5)A long-distance migration experiment by the chromatography; *2010 annual meetings of atomic energy society of Japan*, (2010) p.445.

Shin-ici Koyama, Masaki Ozawa, Kiyoko Kurosawa, Yukio Hanamoto, Katsuyoshi Tatenuma, Tatsuya Suzuki and Yasuhiko Fujii: Metal corrosion evaluation in hydrochloric acid media on tertiary pyridine-type resin applying to fuel reprocessing system (4)Metal corrosion evaluation in simulated high-level waste based on hydrochloric acid media; *2010 annual meetings of atomic energy society of Japan*, (2010) p.497.

Kazuhiro Otaka, Toshihiko Okazaki, Takashi Hoshi, Tatsuya Suzuki, Toshitaka Kaneshiki, Masao Nomura, Yasuhiko Fujii and Yasuyuki Ikeda: Carbon isotope separation technology development; *2010 annual meetings of atomic energy society of Japan*, (2010)p.447.

Masao Nomura, Toshitaka Kaneshiki, Tatsuya Suzuki, Yasuyuki Ikeda, Yasuhiko Fujii, Takashi Hoshi, Kazuhiro Otaka and Toshihiko Okazaki: Carbon isotope isotope effects in the adsorption of the carbon monoxide by the zeolite; *2010 annual meetings of atomic energy society of Japan*, (2010)p.448.

H. Matsuura, S. Watanabe, H. Akatsuka, Y. Okamoto, A. K. Adya: XAFS analyses of molten metal fluorides; *J. Fluor, Chem*. **130**, 53-60, (2009).

Y. Iwadate, H. Matsuura, A. Kajinami, K. Takase, N. Ohtori, N. Umesaki, R. Fujita, K. Mizuguchi, H. Kofuji, M. Myochin: Local structure analyses of molten lanthanum trichloride – alkali chloride ternary systems: approaches from fundamentals to pyrochemical reprocessing; *Electrochemistry*, **77**, 736-740, (2009).

H. Matsuura, A. Nezu, H. Akatsuka, T. Nagai, A. Uehara, T. Fujii, O. Shirai, H. Yamana, M. Myochin and Y. Okamoto: XAFS analysis on the molten chlorides containing uranyl ions; *Nuclear Science*, NEA/NSC/DOC, 15, 19-26 (2009).

C. Bessada, A. –L. Rollet, D. Zanghi, P. Melin, E. Labrude, S. Brassamin, O. Pauvert, C. Thefany, H. Matsuura, D. Thiaudiere, B. Sitaud, P. –L. Solari: A Double Barrier Cell for High Temperature EXAFS Experiments in Molten Actinides Fluorides Mixtures; *Nuclear Science,* NEA/NSC/DOC, 15, 117-122 (2009).

A. Uehara, Y. Okamoto, T. Fujii, H. Matsuura, N. Sato, H. Yamana: EXAFS studies of uranium ions in calcium chloride hydrate melts; *Nuclear Science*, NEA/NSC/DOC, 15, 197-203 (2009).

Takehiko Tsukahara, Wataru Mizutani, Kazuma Mawatari, and Takehiko Kitamori: NMR Studies of Structure and Dynamics of Liquid Molecules Confined in Extended Nanospaces; *Journal of Physical Chem*istry *B*, **113**, 10808-10816 (2009).

Takehiko Tsukahara, Takuya Kuwahata, Akihide Hibara, Haeng-Boo Kim, Kazuma Mawatari, and Takehiko Kitamori: Electrochemical Studies on Liquid Properties in Extended Nanospaces Using Mercury Microelectrodes; *Electrophoresis*, **30**, 1-7 (2009).

Björn Renberg, Kae Sato, Takehiko Tsukahara, Kazuma Mawatari, and Takehiko Kitamori: Thermal bonding of nano- and microfluidic chips; *Microchimica Acta*, **166**, 177-181 (2009).

Björn Renberg, Kae Sato, Kazuma Mawatari, Naokazu Idota, Takehiko Tsukahara, and Takehiko Kitamori: Serial DNA immobilization in micro and extended nanospace channels; *Lab on a Chip*, **9**, 1517-1523 (2009).

Naokazu Idota, Takahiko Tsukahara, Kae Sato, Teruo Okano, and Takehiko Kitamori: The use of electron beam lithographic graft-polymerization on thermoresponsive polymers for regulating the directionality of cell attachment and detachment; *Biomaterials*, **30**, 2095-2101 (2009).

Ryu Kojima, Kazuma Mawatari, Björn Renberg, Takehiko Tsukahara, and Takehiko Kitamori: Integration of immunoassay into extended nanospace; *Microchimica Acta*, **164**, 307-310 (2009).

Takehiko Tsukahara: Investigation on Physicochemical Properties of Nanofluidics and Its Application to Separation and Analysis; *J. Visual. Soc. Japan*, **29** (2), 243-244 (2009).

Akihide Hibara, Takehiko Tsukahara, Takehiko Kitamori: Integrated fluidic systems on a nanometer scale and the study on behavior of liquids in small confinement; *Journal of Chromatography A*, **1216**, 673-683 (2009).

A. Kogo, K. Mawatari, T. Tsukahara, T. Kitamori: Capillary Condensation and Vapor-Liquid Coexisting Process in Extended Nanospace; *Proceedings of µTAS 2009* Chemical and Biological Microsystems Society Publishing, (2009).

K. Morikawa, M. Kato, T. Tsukahara, K. Mawatari, A. Hibara, T. Kitamori: Evaluation of Glass Surfice State Using Streaming Potential Measurement in Extended-Nano Space; *Proceedings of µTAS 2009*, Chemical and Biological Microsystems Society Publishing, (2009).

M. Inaba, M. Kato, T. Tsukahara, K. Mawatari, A. Hibara, T. Kitamori: Nanochromatography, Separation of Solutes in Extended-Nano Spaces Using Pressure-Driven Flow; *Proceedings of µTAS 2009*, Chemical and Biological Microsystems Society Publishing, (2009).

H. Emon, K. Mawatari, T. Tsukahara, T. Kitamori: Surface Modification of Lipid Bilayers in Extended-nano Space for Making Artificial Intercellular Structures; *Proceedings of µTAS 2009*, Chemical and Biological Microsystems Society Publishing, (2009).